The Interactions of Halogens

Andrew Mark London West

Thesis presented for the degree of

Doctor of Philosophy

The University of Edinburgh

2022

Declaration

I declare that this thesis has been composed entirely by myself.

I confirm that all research, unless otherwise stated, has been performed by myself, and any contributions from other researchers have been outlined at the beginning of each chapter and indicated in relevant figure captions.

I declare that this work has not been submitted for any other degree or professional qualification.

Signature: Date: 07/01/2022

Andrew Mark London West

Table of Contents

Acknowledgments

I would like to extend my thanks to my supervisor Prof. Scott L. Cockroft for not only his providing me with the opportunity to conduct my PhD endeavours within his group but also for his guidance and support over my four years of study. Though my leaving the group is to be stayed by my being accepted for a post-doctoral research position within the group, I will do so having grown both academically and as a person as a result of his supervision.

I would like to express my gratitude to both the EPSRC and ERC for providing funding for the work documented here.

I would like to offer thanks to my family for doing their best to understand what I'm saying when the topic of conversation has turned to my research and for their endless emotional support. I also thank my good friends Marco Persichillo and James Mellor for the more than many hours we have spent gaming over these years and for being my reprieve away from academic life.

Though there are far too many people at the University of Edinburgh that I would like to thank; a small selection is as follows. I would like to thank all members of the Cockroft group, both past and present for creating an excellent working environment that has allowed me to prosper. Special thanks to Dr Stefan Borsley for his excellent guidance and advice (in matters both academic and alcoholic) and with my settling into the group. I would like to thank, Alex *shuffles* Elmi, *Big D* Pascoe, Antoine *chucky* Bader, Qingshu *power-play* Zheng and the rest of the Cockroft Group Official Trumps League, for all the *slightly less than productive time* we spend playing cards. And would also like to thank/apologise to the rest of the group for putting up with our seemingly endless rounds of cards in the office. The deck of the bespoke cards will be a prized possession and source of fond memories.

I would like to thank Rebecca Burns and Dominic Cairns-Gibson for all their support over these years, for enjoying my *sass* and for their keeping me entertained. It is with their help that I have managed to keep myself together over the years. I thank Ivan Smoliar for being quite possibly the nicest person I have ever met, as well as Dan

Edwards, Louis Gravillier and Tim Spankie for their support during my writing up period. The COVID19 pandemic with its resultant lockdowns and restrictions have been hard on everyone, but it would be the height of greed to ask for a better group to help me through it.

Finally I would like to thank Dr Juraj Bella for all of his help with and training in NMR spectrometry. His help with my obtaining more than 2000 NMR spectra is highly appreciated. If I leave no other mark, I at least leave the mark of my soles on the NMR facility floor.

Lay Summary

Common knowledge of atoms and molecules extends to notion of *balls* connected by *sticks*. A secondary school education should imbue one with an understanding that those *sticks* correspond to bonds that are either covalent or ionic. Additionally, the same chemistry education should introduce the idea of van der Waals forces and electrostatic interactions; an understanding of viscosity and how geckos work. Between these two sits the hydrogen bond, alone; belonging to neither category.

What might come as a surprise to those without a higher level chemistry education is that the hydrogen bond is not so alone and belongs alongside an entire cohort of interaction. Referred to as either weak non-covalent interactions or σ-hole interactions. While an understanding of these interactions has not peculated into the boarder public knowledge, these interactions are by no means irrelevant. Far from it in fact. As we continue to demand more from chemistry across its multitude of faculties we need more complex tools. Halogen bonds (group 17) offer an analogous alternative to hydrogen bonds but have to potential to be much more tuneable; by virtue of there being four readily usable bond donor halogen atoms; rather than just the one for hydrogen bonds. The larger halogen atoms are more polarizable meaning that they are more readily tuned by their neighbouring atoms.

In this thesis **chapter 1** consists of an explanation of the both halogen bonding and the concept of the σ-hole. This is followed by a review of a number of studies that discuss the nuances of halogen bonds and other σ-hole interactions; primarily chalcogen (group 16) and pnictogen bonds (group 15). This review discusses the multifaceted nature of the forces responsible for driving these interactions.

Chapter 2 focuses of the interactions of halogen atoms with aromatic moieties; employing a class of molecule referred to as a molecular torsion balance. This allows for the measurement of interaction strength by measuring its effect on the conformational equilibrium. Measurements are taken in 17 different solvent systems to assess the effects that the interactions between the solvent molecules have on the halogen···arene interactions.

Chapter 3 focuses the idea of splitting the linear interaction between donor and acceptor atoms into a fork. A process referred to as bifurcation. This much allowing for either a single bond donor to simultaneously interact with two acceptors or a single acceptor to interact with two donors. The chapter focusses on measuring the strength of bifurcated halogen bonds by ^{1}H NMR titration and reports an extremely rare example of a trifurcated halogen bond (A single halogen atom bonding to three bond acceptors at the same time). Study is also extended to include bifurcated hydrogen bonds, allowing for comparison between halogen bonds and a comparatively better understood interaction.

Thesis Abstract

As an analogue of the ubiquitous hydrogen bond, interest in halogen bonding has garnered interest since the turn of the twenty-first century. The orthogonal nature and occasionally surprising characteristics of halogen bonds (compared to better-understood hydrogen bonds) has seen them find useful application in a wide range of disciplines.

Chapter 1 summarises key literature characterising the halogen bond, including the identification of the σ-hole. The novel character of halogen bonds and the role played by a verity of physiochemical forces are discussed; with an in-depth review of recreant advances pertaining to anti-electrostatic halogen bonds. Other closely related σ-hole interactions such as chalcogen and pnictogen bonding are also introduced with key similarities and novel characteristics being highlighted.

Chapter 2 presents an experimental and theoretical investigation of halogen-arene interactions using molecular torsion balances. Thermodynamic double mutant cycles are used to future dissect the energetics halogen-arene from the background noise. A broad solvent screen reveals the solvent-dependent nature of such dispersion-driven contacts. This is supported by a number of computational experiments that further characterise the various energetic contributions and used to study their angular and geometric dependencies.

Chapter 3 examines bifurcated halogen bonds and hydrogen bonds using a combined solution-phase and computational approach. The binding properties of a series of halogen bonded host-guest complexes are compared with hydrogen-bonded analogues. Experimental changes in free energy for the host-guest complexes were determined by ^{1}H NMR titration. Bi- and trifurcated interactions were found to be energetically cooperative, but the nature of said cooperativity differs between hydrogen and halogen bonds. Computational methodologies including SAPT and NBO calculations were used to partition energetic contributions and to rationalise the experimentally observed experimental trends and rationalize the differences between the interaction types.

Abbreviations

ΔE	Change in energy (calculated)
ΔG	Change in free energy (Experimental)
$\Delta\Delta G$	Change in change in free energy (Experimental)
ΔH	Change in enthalpy
σ*	Antibonding orbital
ωB97X	Chai, Head-Gordon long-range corrected hybrid density functional
ωB97X-D	Chai and Head-Gordon long-range corrected hybrid density functional with D2 dispersion correction
A	σ-hole interaction acceptor
AIM	Bader's theory of atoms in molecules
ALMO	Absolute localized molecular orbital method
B3LYP	Beke, three-parameter, Lee-Yang-Parr functional
B3LYP-D3	Grimme D3 dispersion corrected B3LYP
B97D	Becke's 97 functional with dispersion correction
BCP	Bond critical point
BH_3	Borane
BLW	Block localized wave function
BLW-ED	Block localized wave function energy decomposition
$(BPin)_2$	Bis(pinacolato)diboron
Br	Bromine
BSSE	Basis set superposition error
C_6F_5I	Iodopentafluorobenzene
CCl_4	Carbon tetrachloride
$CDCl_3$	Deuterated chloroform
$CDCl_2$	Deuterated dichloromethane

ced	Cohesive energy density
Ch	Chalcogen atom (group 16)
ChB	Chalcogen bond
$CHCl_3$	Chloroform
Cl	Chlorine
CS_2	Carbon disulphide
CSD	Cambridge structural database
CX_3	Methyl trihalide group
d	Doublet (NMR spectroscopy)
D	σ-hole interaction donor
D•A2	One donor, two acceptor bifurcated system
D2•A	Two donor, one acceptor bifurcated system
D2	D2 Grimme dispersion correction
D3	D3 Grimme dispersion correction
D4	D4 Grimme dispersion correction
DCM	Dichloromethane
dd	Doublet of doublets (NMR spectroscopy)
DFT	Density functional theory
DFT-D	Dispersion corrected density functional theory
DMC	Double mutant cycle
DMSO	Dimethylsulfoxide
dt	Doublet of triplets (NMR spectroscopy)
EDA	Energy decomposition analysis
ELF	Electron localization function
ESI	Electrospray ionisation mass spectrometry
ESP	Electrostatic surface potential
Eq	Molar equivalents
F	Fluorine
H	Hydrogen

H_2O	Dihydrogen oxide (water)
HB	Hydrogen bond
HG	Host-Guest complex
|HH	Host-Host complex
HF	Hartree Fock
HOMO	Highest occupied molecular orbital
I	Iodine
IQA	Interacting quantum atoms method
IUPAC	International Union of Pure and Applied Chemistry
LiB	Lithium bond
LiOH	Lithium hydroxide
LMO-EDA	Localized Molecular Orbital Energy Decomposition Analysis
LP	Lone pair of electrons
LUMO	Lowest unoccupied molecular orbital
m	Multiplet (NMR spectroscopy)
M06	Minnesota 06 functional
Me	Methyl group
$MgSO_4$	Magnesium sulphate
MO	Molecular orbital
NaOH	Sodium Hydroxide
NBO	Natural Bond Orbital
NCI	Non-covalent interaction index
Ng	Nobel gas
NMR	Nuclear Magnetic Resonance Spectroscopy
PDB	Protein data base
$Pd_2(dba)_3$	Tris(dibenzylideneacetone)dipalladium(0)
$Pd(dppf)Cl_2$.DCM	[1,1′-Bis(diphenylphosphino)ferrocene]dichloropalladium(II)
$Pd(OAc)_2$	Palladium(II) acetate

Pn	Pnictogen atom (group 15)
PnB	Pnictogen bond
ppm	Parts per million
PyBOP	Benzotriazol-1-yloxytripyrrolidinophosphonium hexafluorophosphate
q	Quartet (NMR spectroscopy)
QTAIM	Bader's quantum theory of atoms in molecules
RCP	Ring critical point
RDC	Residual dipolar coupling NMR spectroscopy
rt	Room temperature (25^{o}C)
s	Singlet (NMR spectroscopy)
SAPT	Symmetry Adapted Perturbation Theory
SAPT0	Symmetry Adapted Perturbation Theory with Hartree Fock treatment of molecules
SAPT2	SAPT0 mythology with second order treatment of intramolecular electron correlation
SAPT2+ccd	SAPT2 methodology with coupled-cluster doublet treatment of dispersion term
SAPT2-ct	SAPT2 methodology with additional charge-transfer module
SAPT(DFT)	Symmetry Adapted Perturbation Theory with density functional treatment of molecules
SPhos	2-Dicyclohexylphosphino-2',6'-dimethoxybiphenyl
t	Triplet (NMR spectroscopy)
TBACl	Tetrabutylammonium chloride
TEA	Triethylamine
TFA	Trifluoroacetic acid
THF	Tetrahydrofuran
TLC	Thin layer chromatography
TMEDA	Tetramethylethylenediamine
UV-Vis	Ultraviolet–visible spectroscopy

VB	Valance bond theory
VDD	Voronoi deformation density
vdW	Van der Waals
$V_{s,max}$	Maxima on electrostatic potential surface
	(0.001 a.u unless stated otherwise)
$V_{s,min}$	Minima on electrostatic potential surface
	(0.001 a.u unless stated otherwise)
X	Halogen atom (group 17)(Including Me groups where appropriate)
XB	Halogen bond
Y	Halogen bond acceptor

Chapter 1

The nuances of halogen bonds and other σ-hole interactions

Abstract

Halogen bonds and analogous σ-hole interactions represent powerful tools for a broad cohort of fields, ranging from small molecule catalysis to bimolecular engineering. However, while widely used and studied there is much contention surrounding their physiochemical origin. This chapter constitutes a summary of key literature pertaining to the characterisation of the halogen bond and the identification of the σ-hole. It highlights several recent developments in the field of halogen bonding with an in-depth look into *anti-electrostatic* or *counter intuitive* halogen bonding. Reviewed in the chapter are also several literature examples of halogen bonds of novel character to demonstrate the role played by forces other than the commonly discussed electrostatic driving forces. Furthermore, review is extended to other σ-hole type interaction such as chalcogen and pnictogen bonding; highlighting key similarities and novel character examples.

Contributions: This chapter is a literature review compiled by Andrew Mark London West (AMLW). All work has been conducted by the discussed authors and referenced accordingly.

1.1 Introduction to Halogen Bonds

The term halogen bonding references the attractive interaction between halogen atoms and electron donating species such as Lewis bases.[1,2] Though the term halogen bond was not coined until the 1970's,[3] the first observations of such attractive forces date back to the nineteenth century with attractive associations between I_2 and NH_3 being noted.[4] These interactions between two seemingly electron rich moieties at first appeared paradoxical and it wasn't until the mid-to-late-twentieth century that a proper understanding of them started to be cultivated. The 1950's saw the development of Mulliken charge transfer theory,[5] which provided a basis for work conducted by Hassel studying various halogen bonded complexes using X-ray and electron diffraction techniques.[6] Rationalisation of these complexes through purely charge transfer means was challenged in the 1990's when the modelling of electrostatic surface potentials as pioneered by Scrocco, Tomasi and co-workers,[7,8] was applied to the case of halogen bonds by Politzer and others.[9-11] Equation 1.1 shows the basis of this methodology for the calculation of the electrostatic potential surfaces, V(r) at location R_A (Z_A being the charge on nucleus A and $\rho(r)$ being the electronic density function of the studied molecule). This approach allows for the identification of electrophilic and nucleophilic regions on a molecule of interest. Modelling of the electrostatic potential surfaces of halogenated species reveals an anisotropic electron distribution in covalently bound halogen atoms (Figure 1.1). Such surfaces show depletion of the electron density at the extension of the R-X covalent bond (R = any suitable atom for covalent bonding, X = halogen atom), often culminating in a localized region of positive potential that has since been termed the σ-hole.[12-21] As described in Politzer's 1994 paper, this arrangement affords interactions "head-on with nucleophiles, side-on with electrophiles" allowing for a wide variety of interaction possibilities.[9] The same paper also described the interactions as "hydrogen bond breakers" due to the early indication of the comparable interaction energies of halogen bonds. Critically, electrostatic surface potential is not just a computationally derived term, and Steward and co-workers demonstrated several experimental measurements of it using diffraction methods.[22-24] Furthermore, recent study by Hobza, Jelinek and co-workers demonstrated real-space imaging of σ-holes using Kelvin probe force microscopy; adding further strength to the σ-hole model.[25]

$$V(r) = \sum_{A} \frac{Z_A}{|R_A - r|} - \int \frac{\rho(r')dr'}{|r' - r|'} \qquad \text{(Equation 1.1)}$$

Correlation of σ-hole electrostatic surface potential maxima at 0.001 a.u ($V_{s,max}$) with calculated gas phase interaction strengths has yielded some strong correlations.[14,15,26,27] Reassuringly, the expansion of this approach to other interactions involving donor species with anisotropic electron distributions has seen similar levels of success.[14] Accordingly, the overarching term, *σ-hole interaction*, is now in common usage.

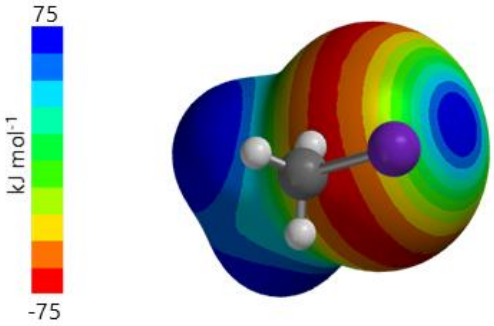

Figure 1.1: Electrostatic surface potential calculated for methyl iodide. Note the comparable electrostatic potentials over the σ-hole and hydrogen atoms.

Initial studies of σ-holes in halogenated species in the 2000's found that σ-holes are not present on fluorine atoms, which was attributed to the degree of *sp* orbital hybridization within the halogen atom. A much greater degree of *p* orbital hybridisation is observed in fluorine, leading to greater electron density over the extension of the R-X bond compared to the other halogens.[19] However in 2011, Metrangolo demonstrated that while fluorine-centred XBs tend to be weaker than those involving heavier halogens, they can still occur.[28] Drawing attention to several previous gas-phase[29] and solid-state examples,[30,31] the authors note that while positive σ-holes in fluorine are only observed as a result of adjacent strong electron withdrawing groups; the σ-hole is still present in all R-X moieties even if the $V_{s,max}$ remains negative.[28] A 2011 paper by Frontera and co-workers, presented an in-depth computational study of substituent effects on halogen bonds, and found a good

correlation with established Hammett constants on both halogen bond donors and acceptors.[32] The field of halogen bonding has seen rapid development, which continues to be seen. The IUPAC definition of halogen bonding states that they occur "*when there is evidence of a net attractive interaction between an electrophilic region associated with a halogen atom in a molecular entity and a nucleophilic region in another, or the same, molecular entity.*"[1] The detailed 2013 IUPAC recommendations draw attention to the notion that electrostatics, polarisation, charge transfer, and dispersive forces all pay important roles in the interaction.[1]

1.2 The role of electrostatics and anti-electrostatic halogen bonds

The often-assumed pre-eminence of electrostatic forces in halogen bonding has been challenged by so called anti-electrostatic or counter intuitive halogen bonds. Such systems are characterised by attraction between a typical halogen bond acceptor and a halogen bond donor with a negatively charged extension of the X-R bond axis. Mo and co-workers drew attention to such systems in 2018[33] following theoretical reports of anti-electrostatic hydrogen bonding by Weinhold.[34] Such reports prompted debate,[35,36] during the course of which, several anti-electrostatic hydrogen bonds in previously reported protein structures were retrospectively identified.[37-42] Indeed, even though the recent bout of interest in such halogen bonding systems can be attributed to the work of Mo and co-workers, attractive halogen bonds featuring negative surface potential σ-holes are not a new phenomenon.[43-48]

The Mo 2018 study[33] looked at both anti-electrostatic hydrogen bonds and halogen bonds and attributed the dominant attractive force in such systems to polarisation. Significant delocalisation of electron density from the donor to the acceptor was identified using computational electron density difference maps. Though not the dominant attractive force, the authors noted the important role played by charge transfer. Calculations revealed reduced interaction well depth on plots of relative ΔE against interaction distance when charge transfer was artificially quenched using the block-localised waveform methodology.[49-52] The authors noted that this effect was more pronounced in halogen bonds compared to hydrogen bonds.

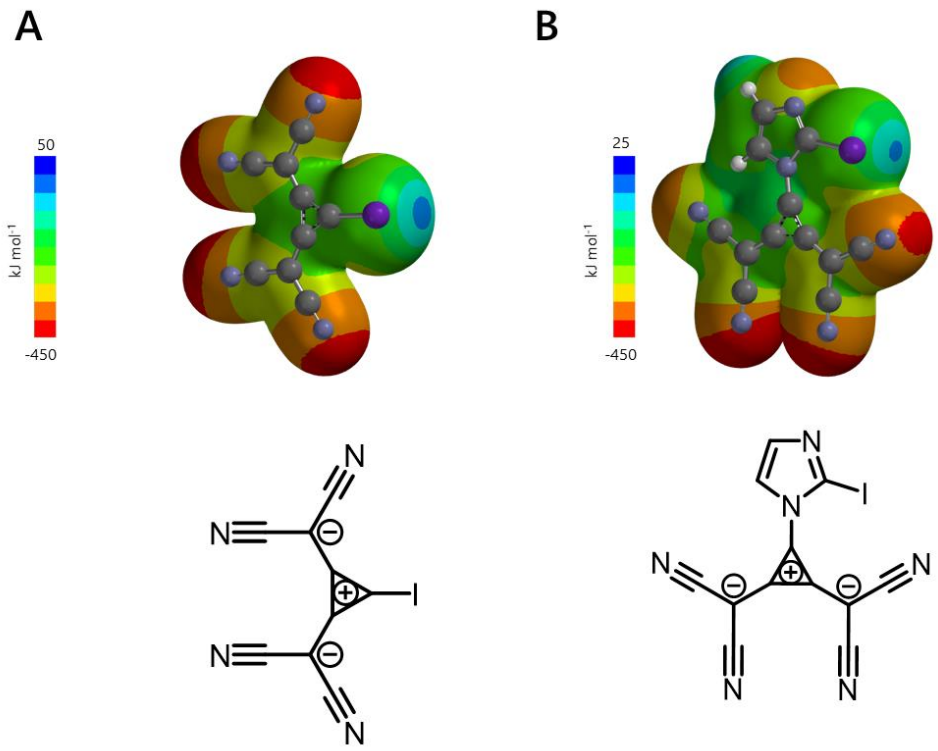

Figure 1.2: A) ESP of 1,2-bis(dicyanomethylene)-3-iodo-cyclopropanid anion $V_{s,max}$ = –80.4 kJ mol^{-} [153] B) 1,2-bis(dicyanomethylene)-3-iodoimidazolyl-cyclopropanid anion $V_{s,max}$ = –127.9 kJ mol^{-1}.[53]

Anti-electrostatic halogen bonds were also studied computationally in 2020 by Huber and co-workers[53] using the anions shown in Figure 1.2. Calculated interaction-distance plots revealed attractive kinetic stabilities and negative Δ*G* values for complexes of these anions with halide ions. The interactions remained favourable even when an SMD18 solvent model[54] for acetonitrile was applied, suggesting that some anti-electrostatic halogen bonds may be stable in solution. Huber and co-workers later demonstrated that bond critical points (BCPs) existed along the halogen bond path using QTAIM analysis,[55,56] while non-covalent interaction index (NCI) treatments also confirmed an attractive interaction.[57,58] As part of the 2020 paper[53] the relevant donor species were synthesised and shown to produce clearly recognisable halogen bonds in crystals. The structure of a complex formed with the donor shown in Figure 1.2A possessed C-I···N angles of 178.9^{o} and intermolecular distances of 2.97 Å (16% shorter than the sum of the van der Waals radii), resulting in linear chains (Figure 1.3A). The high degree of linearity is worth drawing attention to, but it is also worth noting that Stone and co-workers, demonstrated that much of the linearity of halogen bonds stems from exchange repulsion considerations,[59] which are assumed to be unchanged in anti-

electrostatic systems. The complexes in Figure 1.2B assembled as halogen-bonded dimers and trimers rather than linear chains, which to led to less-linear halogen bond geometries, with C-I···N angles of 170-173º and bond lengths approximating the sum of the respective van der Waals radii Figure 1.3B.

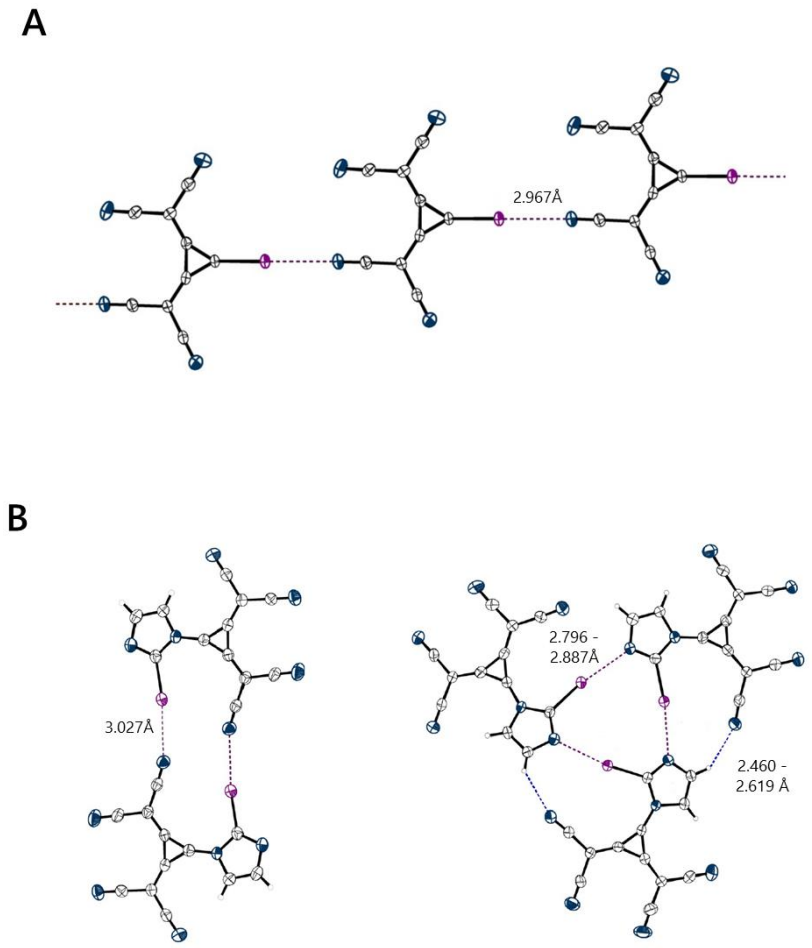

Figure 1.3: A) Halogen bonded chains in crystals of the 1,2-bis(dicyanomethylene)-3-iodo-cyclopropanid anion. B) Dimer (left) and trimer (right) structures found in the crystals produced by the 1,2-bis(dicyanomethylene)-3-iodoimidazolyl-cyclopropanid anion.[53]

Emphasis is often placed on the role of polarisation in halogen bonding, which can be examined using the point charge approach.[60,61] It was found by Huber and co-workers that positioning –1.0 and –0.5 single point charges at halogen bond-relevant distances (3.5 Å and 3.0 Å) on the complexes shown in Figure 1.2, flipped the $V_{s,max}$ from a negative electrostatic potential to a positive one. Polarisation to such a degree would be in line with other studies and presents an explanation for the viability of anti-electrostatic halogen bonds.[33] However, using atomic charges (as determined by

natural bond orbital (NBO)[62,63] and Mulliken[64,65] calculations) and distances determined from the crystal structures provides a more realistic model of the polarisation effects. When such modelling was performed, the observed polarisation resulted in less negative $V_{s,max}$ values, and critically, did not involve sign switching.[53] This means that the electrostatic interactions within these halogen bonds are still repulsive in nature. Indeed, complexes of these specific halogen bond donors were modelled in the gas phase and gave repulsive kinetic and energetic terms. Huber notes that the large electrostatic repulsion between the anions may be alleviated by the inclusion of counter ions, the dielectric environment of the polar solvent, and solvophobic effects (solvent-solvent interactions outcompeting solvent-solute interactions).[53] Such medium effects are not dissimilar from packing forces increasing the viability of particularly weak interactions in the solid state.

The results of these calculations do not diminish the importance of polarisation in such halogen bonds; a change in $V_{s,max}$ from –80 kJ mol^{-1} to –16 kJ mol^{-1} or –9.6 kJ mol^{-1} (for NBO or Mulliken charges respectively) are very substantial. Indeed, modelling of polarisation in other anti-electrostatic halogen bonds has been shown to be sufficient to overcome an otherwise repulsive electrostatic term.[45,66] The findings allow the authors to draw attention to the importance of lone pair (LP) to σ* orbital interactions in enabling the occurrence of these and other anti-electrostatic halogen bonds.[48] Moreover, the cyclopropenylium-based anti-electrostatic halogen bonds (Figure 1.2) were proven to occur in solution.[55] These experiments agreed with the computational findings that pointed to the importance of solvation; anti-electrostatic halogen bonding was found to be strongest in polar solvents. The use of UV-Vis spectroscopy showed strong increases in absorption bands in the 290-350 nm range in response to increasing concentrations of anionic halogen bond donor in a Bu_4NI solution (Figure 1.4A). Absorption in this range indicative of increasing iodine concentration, which is consistent I^- anion dissociating from the $Bu4N^+$; a product of halogen bonding. Furthermore, significantly different behaviour was seen when measurements were repeated with an analogous non-halogenated donor species (X = H, Figure 1.4B).

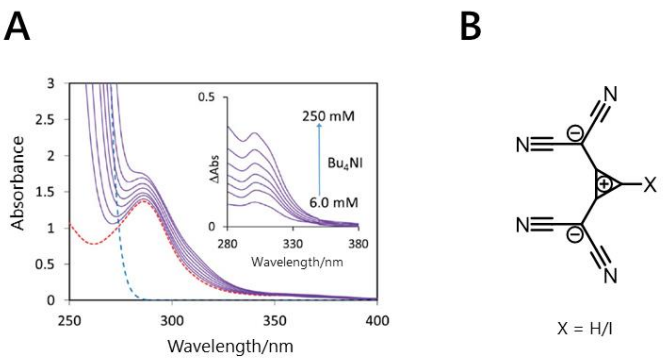

Figure 1.4: A) Superimposed UV-Vis spectra for titrations of Bu_4NI against 2-bis(dicyanomethylene)-3-iodo-cyclopropenylium. Dashed red line is uncomplexed 2-bis(dicyanomethylene)-3-iodo-cyclopropenylium, dashed blue line is uncomplexed Bu_4NI. B) Cyclopropenylium-derivatives employed by Huber *et al.*[55]

Calculations on complexes between the 1,2-bis(dicyanomethylene)-3-iodo-cyclopropanid anion and Br^-, Cl^- and I^- anions[53,55] found a trend of increasingly strong complexation with decreasing halide size; though the omission of F^- from the series is noted. Despite their anti-electrostatic nature, this mirrors previously reported free energy trends in neutral XB complexes.[2,67,68] The UV-Vis spectra of anti-electrostatic XBs show interesting departures from conventional halogen bonds. Typically, a trend of increasing red shift is observed as halide acceptors descend the group.[69-71] Such a trend is not seen in the anti-electrostatic halogen bonds, and the wavelengths of the absorption peaks remain static. Employing Mulliken charge-transfer theory,[64,65] the trend observed with neutral halogen bond donors can be explained by increases in the HOMO-LUMO gap as the halide HOMO energies increase from Cl^- to I^-.[69] This is predicated on the fact that the complex-wide HOMO is located on the halide in conventional XB complexes, but this is no longer the case in complexes formed with the 1,2-bis(dicyanomethylene)-3-iodo-cyclopropanide donor. The anti-electrostatic halogen bond donor possesses a HOMO that is higher in energy than those of the individual halides. Accordingly, the lowest-energy electron excitations occur almost exclusively within the donor species and are independent of the halide.[55] This does not mean that charge transfer is not occurring within these systems. Instead, halogen bond donor-acceptor transitions no longer correspond to the lowest energy absorption band,[69] and any such processes are masked by absorption transitions occurring within the 1,2-bis(dicyanomethylene)-3-iodo-cyclopropanide donor species[55]

2021 also saw commentary on anti-electrostatic halogen bonds by some of the authors behind the initial identification of the σ-hole in the context of halogen bonding. Politzer and co-workers, looked at a broader scope of 20 anti-electrostatic halogen bonded systems in a comparative study with more traditional analogues.[72] A good correlations (R^2 = 0.97) was obtained for fits of the calculated Δ*E* values for the 20 anti-electrostatic halogen bonds using a regression based on the electrostatic potentials and the average polarizability of the nitrogen base (Equation 1.2).

$$\Delta E = -a\left[V_{s,max}\right] - b[\alpha] + c \qquad \text{(Equation 1.2)}$$

$V_{s,max}$ as defined by Equation 1.1. α is the average polarisability of the nitrogen base.[73] *a*, *b*, and *c* are coefficients derived by multiple linear regression analysis.[72] For anti-electrostatic halogen bonded systems; *a*, *b*, and *c* are 0.06849, 0.6052 and 0.7442, respectively. For additional weak halogen bonded systems; *a*, *b*, and *c* are 0.1633, 0.7488 and 0.8550, respectively. For additionally included strong halogen bonded systems; *a*, *b*, and *c* are 0.3437, 1.193 and 2.625, respectively.

Compellingly, extending the same approach to analogous weak-to-intermediate strength conventional halogen bonds also gave a good correlation (R^2 = 0.95). However, when stronger halogen bonds were considered with Δ*E* = >40 kJ mol^{-1}, the regression based values were found to be consistently less negative than the calculated Δ*E* values. This is not unsurprising as previous studies have shown greater polarisation contributions in stronger halogen bonds, which cannot be effectively accounted for using a simple regression model like this which only accounts for the polarisation of the acceptor.[74]

The authors stress that polarisation is an intrinsic part of any intermolecular interaction and note that while many previous studies have been able to correlate Δ*E* values with the $V_{s,max}$ values for the σ-holes,[15,45,75] this is predicated on the fact that polarisation plays a minor role in most weak-to-intermediate strength halogen bonds (Δ*E* = 0-40 kJ mol^{-1}) and its omission was not detrimental to the correlations. The occurrence of anti-electrostatic halogen bonds has led to sweeping and provocative statements being made, such as *"the essential irrelevance of electrostatic contributions"*[34] and *"electrostatics and polarization determine the strength of the halogen bond: a red*

card for charge transfer".[76] Given the small number of anti-electrostatic halogen bonding systems that have been studied in detail; a more reasoned assessment would place the relative importance of different contributions being dependent upon the nature of the individual system, rather than being hallmarks of halogen bonding as a whole. Indeed, the very definition of charge transfer is controversial in its own right, since it is easily argued that charge transfer and polarisation are inherently indistinguishable.[15] One accepted distinction is that charge transfer refers to a discrete intermolecular exchange of electrons, while polarisation corresponds to electron redistribution within the confines of the individual components of the complex.[77]

1.3 The role of charge transfer and polarisation in halogen bonds

We do not need to just consider such extreme examples as anti-electrostatic halogen bonding to see the role played by non-coulombic forces in halogen bonding. Indeed, examples of the importance of such forces can be seen in relatively simple systems, even where electrostatics constitute the primary attractive force. Like Legon and Hill,[78] we would like to draw attention to Shaik's theoretical examinations of 1:1 solvent-dihalogen complexes[77] similar to those that sparked interest in halogen bonding in the 1940's.[5] Shaik's works employed both bottom-up valence bond theory (VB)[79-82] and the top-down block-localised wave (BLW) methodology.[49-52,83,84] Both methods indicated a consistent and strong role for charge transfer in all but the weakest halogen bonds.

The bottom-up approach of valence bond theory allowed the authors to consider the frozen state. This can be described as the complex of the donor and acceptor species at optimal distances, but without allowing any changes in the wave functions. This state thus consists of the Pauli repulsion and deformation energies, which are associated with the cost of transitioning from the free monomers to the minimised complex. The vast majority of the energies for these frozen states are repulsive, showing that electrostatics alone are not sufficient to overcome the inherent repulsive forces incurred upon complexation. Charge transfer terms were found to be the most significant energies not present in the frozen states of the 24 complexes representative of the solvent-dihalogen complexes. The VB and BLW methods gave consistent

energies, and good correlations were also found between the calculated charge transfer terms and the total energies (R^2 >0.83).[77]

Shaik and co-workers also noted strong correlations between the lengthening of the X-X bond and the charge transfer energies (and by extension, the total interaction energies) determined using the VB and BLW methods. Such bond lengthening occurs when the formation of a halogen bond results in electron density being accepted into the σ* orbital of the X-X bond of the, counterintuitively named, halogen bond donor.

Internal polarisation of the individual complex components was also quantified in the methodologies employed by Shaik and co-workers.[77] While all of the energies were negative, and contributed to stabilising the complexes, in all but a handful of cases, the polarisation terms were not sufficient to invert the sign of the frozen energies. Previous studies see good correlations between interaction energies and the BLW polarisation term alone.[85] However, mirroring Huber's examination of anti-electrostatic halogen bonds, the favourable role of polarisation is not sufficient enough to produce a stable complex without other favourable interaction contributions.[53,55] Shaik helpfully points out that both the polarisation and charge transfer terms can be effectively absorbed into the electrostatic energy term in the parameterisation of computationally efficient force fields.[77]

Interestingly, charge transfer has been identified as the main contributor to putative halogen bonds involving F_2 (Figure 1.5). Since F_2 lacks a positively charged σ-hole, this effectively make such complexes anti-electrostatic in nature. This reinforces the position that anti-electrostatic halogen bond may be more ubiquitous than might be assumed based on the prevalence conception of halogen bonds being electrostatically dominated.

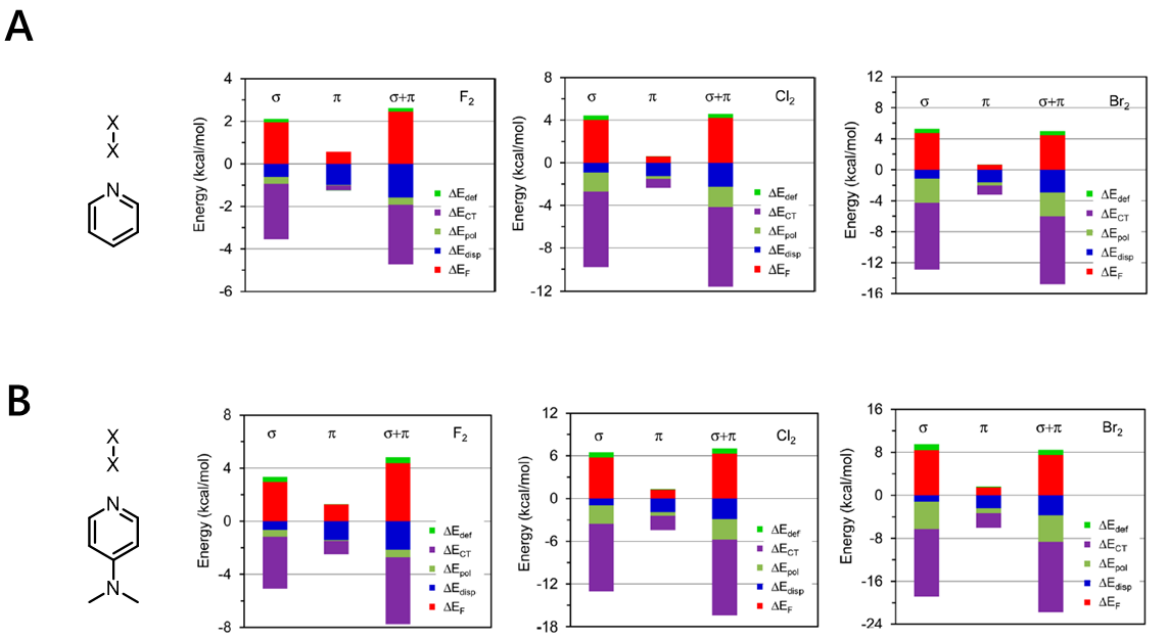

Figure 1.5: Breakdown of BLW energy contributions to the binding energies of dihalogens, F_2, Cl_2 and Br_2 (left to right) with A) pyridine and B) dimethylaminopyridine. σ, π and σ+π refer to conformations pertaining to dihalogen approaching the heteroaromatic nitrogen on the aromatic plane, interactions with the aromatic π system, and interactions with both respectively.[77]

Mo and co-workers has also employed block-localised wave function theory to study charge transfer in halogen bonds.[86] Comparison of the BLW function to DFT-D calculations allows charge transfer components to be excluded, or included, respectively; an approach referred to as BLW energy decomposition (BLW-ED). The authors noted the similarity of this approach to the absolute localised molecular orbital (ALMO) method[87] that has also been applied to halogen bonded systems.[88] Minimised geometries produced using the two methodologies yielded some immediately apparent differences; most notably the dispersion-excluded BLW produced much longer halogen bonds than the dispersion included DFT-D calculations. The results of this much can be seen in the frozen energy terms, which were all attractive in the longer, charge-transfer excluded complexes, but predominantly repulsive in the shorter charge-transfer included complexes.[86]

The complexes that retain attractive frozen energies in both methodologies all featured F_3C-X halogen bond donors, which contain the most electron withdrawing substituent and thus possessing the deepest σ-holes and largest electrostatic terms.[12-19,75] The frozen energies for DFT-D calculations were larger in magnitude than the BLW

calculations as a result the shorter bonds incurring larger steric repulsion energies. The DFT-D complexation energies were more stable than their BLW counterparts (average enhancement of 81%), in spite of the universally less negative frozen energies; a result of the inclusion of large charge transfer terms. The shorter halogen bonds also had more negative polarisation terms, as anticipated. This is reflected in the strong correlation between the change in bond distance (ΔR_{CX}) with both the BLW-ED charge transfer energy (ΔE_{CT}) and the amount of charge transferred as determined by natural population analysis (ρ_{CT}) (Figure 1.6). The authors also note the more pronounced effect that substituents have on the systems where charge transfer is allowed. Indeed, a change of < 4 kJ mol^{-1} is seen moving from F_3C-X···A to Br_3C-X···A for the BLW calculations compared to the DFT calculations which yielded consistently greater changes. Previous studies have determined the effects of substituents on halogen bonds via correlations with Hammett substituent constants,[32] but Mo and co-workers[86] also identify substituent-modulated charge transfer interactions as playing an additional role.

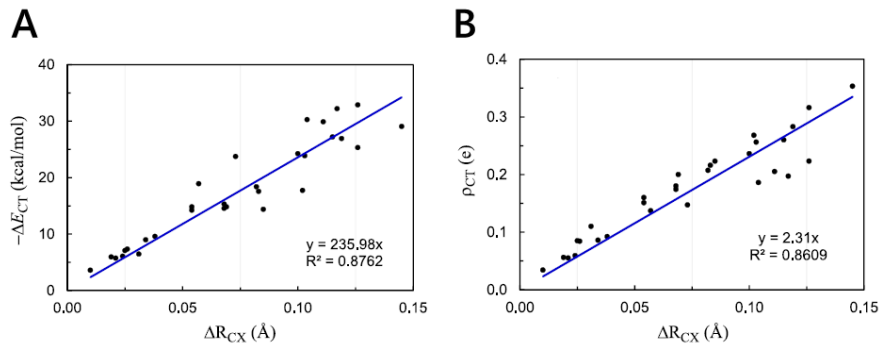

Figure 1.6: A) Plot of change in C-X bond length (ΔR_{CX}) against BLW-ED charge transfer term (ΔE_{CT}). B) Plot of change in C-X bond length (ΔR_{CX}) against charge transferred as determined by natural population analysis (ρ_{CT}).[86]

Computational studies showing the importance of charge transfer to halogen bonds are supported by Taylor and co-workers.[89] They compared computational energies of halogen bonded complexes with ΔG values obtained experimentally using ^{19}F NMR titrations. Given the prevalence of heavily fluorinated species in studies pertaining to halogen bonding, ^{19}F NMR spectroscopy is a well-established technique for study of halogen bonds.[90,91] Taylor's study employed substituted iodoperfluoroarenes (Figure

1.7) as halogen bond donors. Iodopentafluorobenzene (Figure 1.7A) was found to bind to tributylphosphine oxide with a binding constant (K_a) that was ten times higher than its amine-substituted analogue (Figure 1.7B) in cyclohexane solution. A strong correlation between the experimental measurements and σ-hole electrostatic surface potentials was determined using B3LYP/6-31G**-LANdp (R^2 = 0.97).

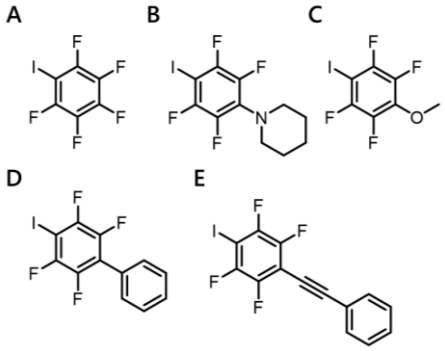

Figure 1.7: Iodoperfluoroarene species employed by Taylor and co-workersr in an ^{19}F NMR study of halogen bonding.[89]

The above is in line with computational studies conducted by Politzer and co-workers.[75] Although, the small datasets of experimental halogen bond energies measured in solution initially appeared reasonably consistent with a simple electrostatic model,[92] both Hunter[93] and Taylor[89] later found that experimental data could not be rationalised using simple electrostatic models. For example, Taylor found in his 2010 study, that halogen bond acceptor ability ranked using electrostatic potentials should follow the order Bu_3PO>Bu_2SO~quinuclidine>Et_3N, but the order was instead experimentally determined to be quinuclidine>Bu_3PO>Me_2SO>Et_3N.

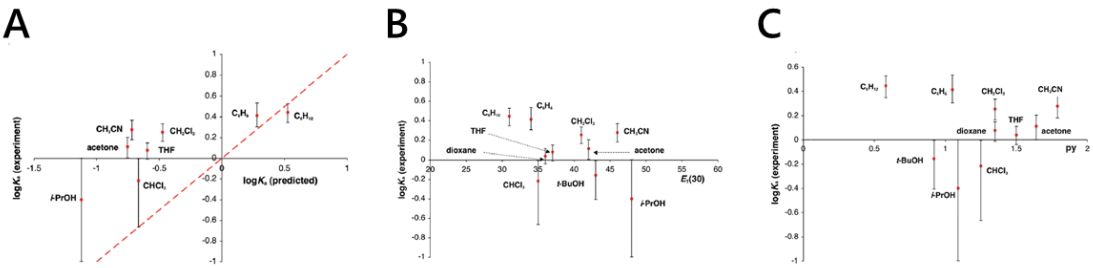

Figure 1.8: A) Plot of logK_a for $C_8F_{17}I$:TEA complexes determined using ^{19}F NMR titrations against logK_a predicted using the Hunter solvation model for the same system. Red dashed line corresponds to y = x. B) and C) Fits of experimental the same experimental logK_a values as a function of the $E_T(30)$ and py solvent polarity scales respectively.[89]

Further inadequacies of a purely electrostatic model were revealed when solvent effects were considered (Figure 1.8A).[89] The most significant deviations from the experimentally measured values were for the Lewis basic solvents. The experimental values were significantly more favourable than predicted based on electrostatics alone, indicating the presence of additional attractive components. Furthermore, no correlations were seen against solvent polarity as encoded using the $E_T(30)$ and py scales, respectively (Figure 1.8B-C).[94] The most notable outliers correspond to the strongest hydrogen bond donor solvents, which the py scale has been shown to effectively separate from polarisability.[95] Such deviations were suggested to result from competition between hydrogen and halogen bond donor sites.[96-98]

In stark contrast with the poor correlations involving empirical scales, the experimental halogen bond energies were instead found to correlate strongly ($R^2 = 0.97$) with DFT gas-phase complexation energies that were corrected for basis set superposition errors (BSSE) using counterpoise correction.[99] While the magnitude of the calculated and experimental energies differed significantly due to the lack of a solvent model in the calculations, the ability of the DFT calculations to modelling charge transfer yielded a very notable benefit. Indeed, Hunter and co-workers have also noted the limitations of electrostatic models in predicting the energies of halogen bonds with strong acceptors where charge transfer is expected to play a larger role.[92]

1.4 The role of exchange repulsion in halogen bonds

While the role played by charge transfer in halogen bonds can be described as somewhat contentious, the role played by exchange repulsion is less so. Stone's 2013 paper constitutes the seminal paper on this matter.[59] Stone employed a symmetry adapted perturbation theory DFT (SAPT(DFT))[100,101] energy dissection to several simple halogen bonding systems (Figure 1.9 and 1.10). Like numerous other works, he found the primary attractive component to be electrostatic, but with non-negligible contributions from induction and dispersion. He concluded that it is acceptable to describe halogen bonds as being electrostatically driven. However, exchange repulsion was observed to be the most important term governing the linearity of halogen bonds. Due to their similarities to hydrogen bonds, there is often temptation to employ the

hard sphere repulsion models to halogen bonds. However, covalently bound halogens have an oblate shape[29] since the extension of the R-X bond axis is shorter than the equatorial radii due to the same anisotropic distribution of electron density that gives rise to σ-holes.[102,103]

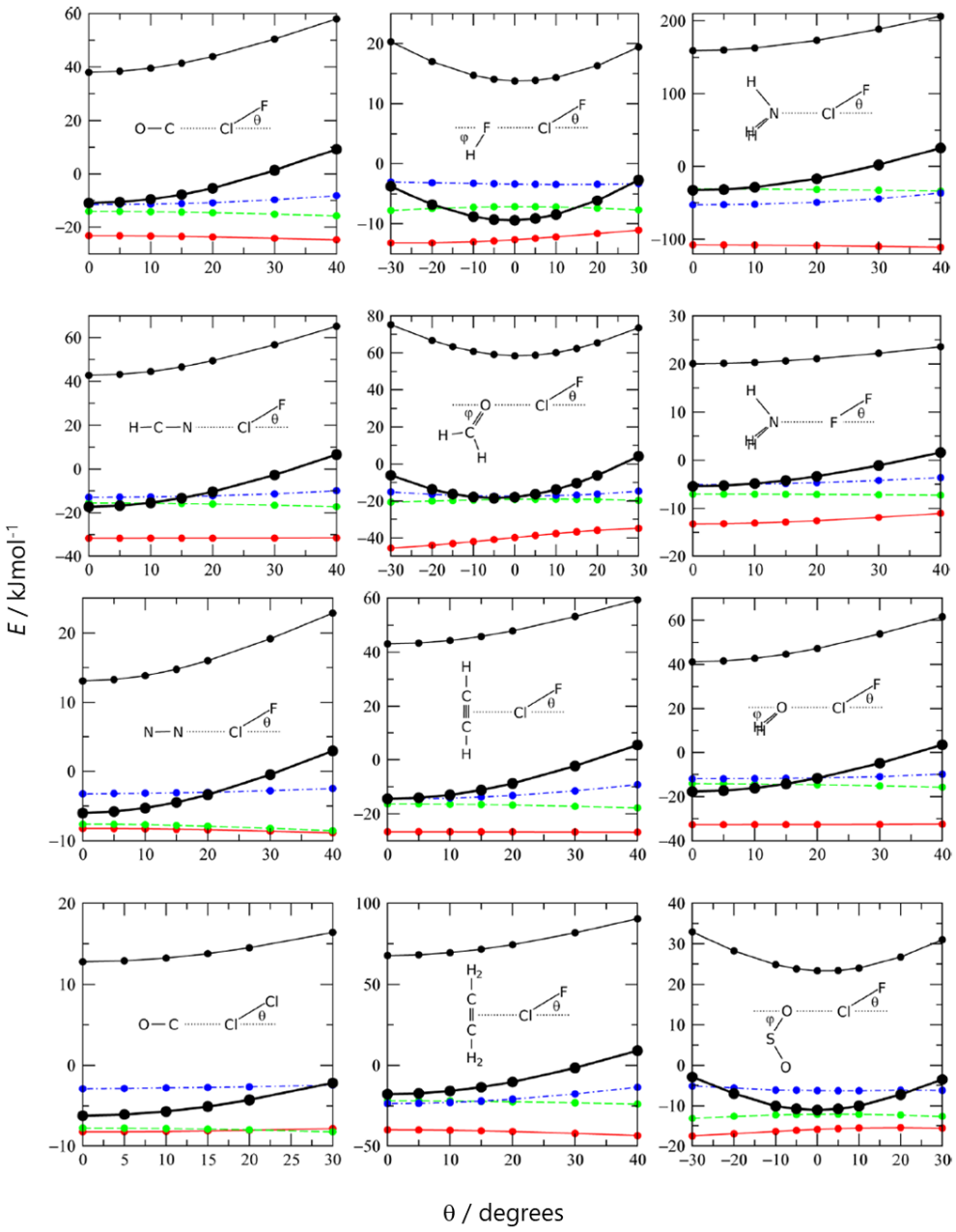

Figure 1.9: SAPT dissection of the halogen bonding systems studied by Stone. Components correspond accordingly; thick black lines to SAPT total; red to electrostatic term; green to dispersion term; blue to induction; thin black to exchange repulsion. Terms are plotted with variations in angle θ that corresponds to changes in the orientation of the σ-hole relative to the halogen-bond axis.[59]

This characteristic was first noted by Legion[29] when considering abnormally short halogen bonds,[29] in which there is increased overlap of the donor and acceptor electron densities as the bond deviates from linearity. Correspondingly, the lines corresponding to exchange repulsion (thin black lines in Figure 1.9) show a noticeable increase in energy due to deviations in angle θ away from co-linearity with the halogen bond axis. Stone[59] draws much attention to the fact that the total interaction energies (thick black lines) shadow the exchange repulsion energies (thin black lines) closely in terms of angular dependencies. The SAPT(DFT) calculations show very little change the attractive components in response to angle θ (Figure 1.9; red, blue, and green lines), meaning that the larger changes in the exchange repulsion dominate the changes in the total energy. Stone[59] acknowledges that this correlation of energies with exchange repulsion had previously been noted by Adhikari and Scheiner.[104] In contrast, Shields and co-workers[105] attributed the linearity of base···BrCN complexes to repulsive electrostatic interactions originating from the non-bonding electron pairs located around the equator of the bromine atom; though neither of the earlier studies were as comprehensive as Stone's.[59]

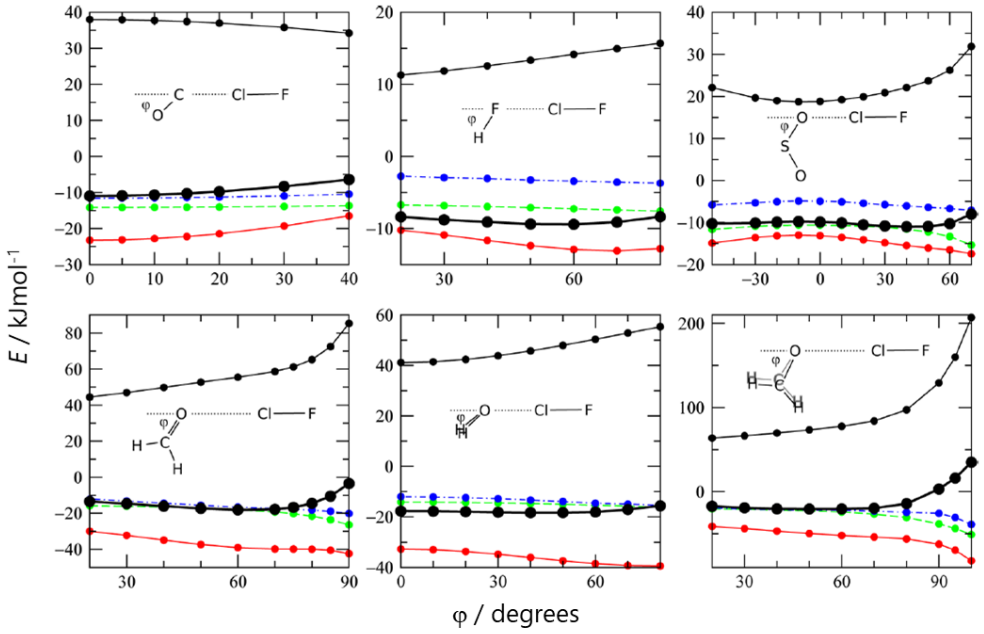

Figure 1.10: SAPT dissection of the halogen bonding systems studied by Stone. Variations in angle φ corresponds to changes in the orientation of the halogen bond acceptor relative to the halogen bond axis. Components correspond accordingly; thick black lines to SAPT total; red to electrostatic term; green to dispersion term; blue to induction; thin black to exchange repulsion.[59]

Stone's study is also extended to variations in angle φ, which is defined as the deviation from collinearity with the halogen bond, and is a measure of alignment of the halogen bond axis with the lone pair of the halogen bond acceptor (Figure 1.10).[59] Figure 1.10 shows a more complex relationship that should be considered on a case by case basis; perhaps unsurprisingly, given the more varied nature of the acceptors considered. Reassuringly, the effects of polar flattening can be seen here as well in the case of the H-F acceptor system (Figure 1.10, top centre) which adds weight to prior conclusions. However, the curvature is less pronounced due to the more spherical nature of the fluorine atom relative to the heavier halogens.[102] In this system, the exchange repulsion term steadily increase as the halogen bond and the extension of the F-H axis move away from collinearity. Even with a completely negative electrostatic surface potential, the manifestation of the fluorine σ-hole can be seen in the electrostatic term here, which becomes more negative as the halogen bond acceptor site moves towards the electron rich equator.[59]

Further study into the effects of polar flattening on the stabilities of halogen bonded complexes was conducted by Hobza and co-workers in 2015.[102] They note that polar flattening has been known since the 1960's and exists in all covalently bonded atoms.[106,107] The prominence of polar flattening in halogens can be attributed to their predominant monovalency, which exposes the flattened extension of the covalent bond rather than being masked by other covalent bonds.[102] Hobza and co-workers considered a simplistic hard-sphere model to a more realistic flattened one to assess the effects of polar flattening on halogen bonds. They applied such a comparison to 32 complexes and decomposed the interaction energies using the SAPT methodology.[100,101]

As might be expected, polar flattening allows for shorter halogen bond distances due to a reduction in exchange repulsion.[102] The extent of this reduction can be measured by the differences between the equatorial (Figure 1.11, $r_{\perp}$) and axial (Figure 1.11, r_{II}) radii of the calculated standard 0.001 bohrs/A^3 isodensity surfaces.[108,109] Energetic changes due to polar flattening can be ascertained by comparing equilibrium geometry energies to those of geometries adjusted by the elongation of halogen bond. Shorter

bonds increased the magnitude of electrostatic, dispersion, and orbital mixing interactions when polar flattening was modelled.[110]

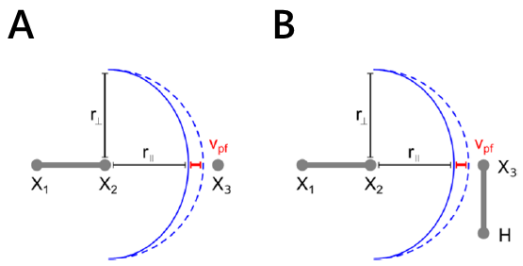

Figure 1.11: Graphical representation of the model employed by Hobza *et al*, to assess the energetic effects of polar flattening. A) representing systems with single atom anion acceptors, B) representing systems with equatorial XH acceptor species.[102]

Using the above approach, the dihalogens FBr, ClBr, Br_2 and IBr were found to exhibit polar flatting representing 15%, 12%, 11% and 10% of the isodensity.[102] Polar flattening in halogen bonded complexes of these dihalide species showed a tight range spread for the minimum electron-density (ρ_{min}) locations as determined using QTAIM for a variety of acceptors ($\Delta \leq 0.07$ Å). The range was even tighter within specific classes of acceptors, such as for halide anions, hydrogen halides, and noble gases. The authors noted that the relative degree of polar flattening observed in these complexes maintained the same FBr > ClBr > Br_2 > IBr trend, and that variations in the magnitude of polar flattening observed after complexation did not exceed 2%. This demonstrates that the degree of polar flattening is a property of the uncomplexed donor species and is in turn, predominantly dependent on the electronegativity of the adjacent halogen moiety.

Energies for the minimised complexes and those elongated by the polar flatting equivalent distance as determined by either the absolute monomer radial distance difference or the ρ_{min} locations, are shown in Figure 1.12. As might be expected, the absolute values for the anionic F^- acceptor systems are much more negative than their neutral analogues. However, the trends in energetic changes are consistent with the elongated halogen bonds both being weaker than those found in the complexes at equilibrium geometries. The slightly more severe monomer radii based flattening

model resulted in the less negative ΔE values than the ρ_{min} location based flattening model. The stronger anionic halogen bond complexes see smaller relative changes due to the absence of polar flattening as defined by ρ_{min}. This can be attributed to their relatively wide association energy well that make such interaction relative resistant to minor changes in distance.[102]

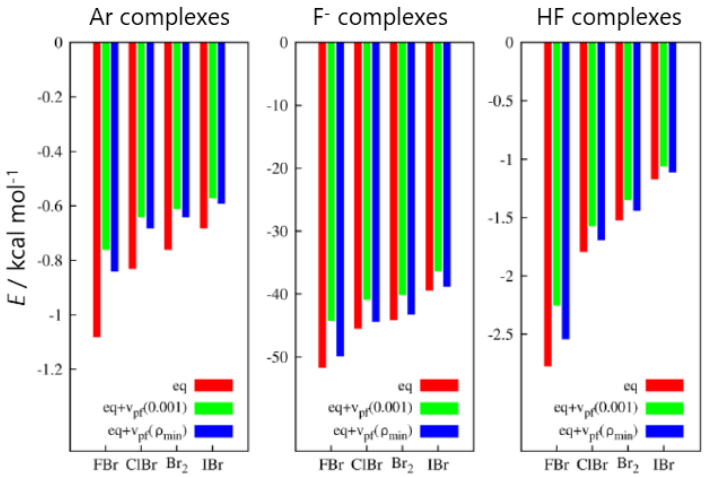

Figure 1.12: CCSD(T)/CBS energies calculated for dihalogen complexes with Ar, F^- and HF acceptors (left to right). Corresponding to; equilibrium geometry, red; elongated by magnitude of polar flattening as determined by differences in atomic radii, green; elongated by magnitude of polar flattening as determined by ρ_{min} location; green.[102]

DFT-SAPT calculations can rationalise the high strength of the F^- acceptor interactions, and large roles are played by electrostatic and charge transfer terms (Figure 1.13 centre). For all of the three donor types the changes in the individual terms are much greater than the changes in the total term. This is due to the counter play of the three attractive terms against the exchange-repulsion term; with the latter seeing the most significant changes, thus holding the greatest degree of influence on the interaction. The relative importance of the attractive SAPT terms changes significantly for each acceptor class. The need to consider the relative importance of the attractive forces behind halogen bonds on case-by-case basis is a central theme of this review, which is very much typified by these SAPT results. This also highlights the importance of the type of acceptor present in the halogen bond and many previous studies into the nature of such interactions only considered one type of acceptor; typically either halide anions or Lewis bases.

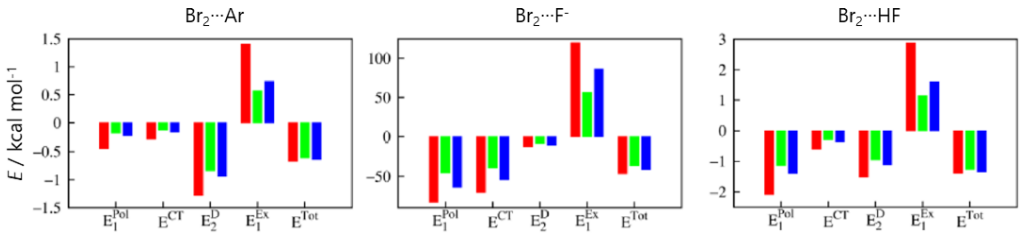

Figure 1.13: SAPT component breakdowns for halogen bonding complexes with three distinct category acceptor species. Colours correspond to; equilibrium geometry, red; elongated by magnitude of polar flattening as determined by differences in atomic radii, green; elongated by magnitude of polar flattening as determined by ρ_{min} location; green.[102]

1.5 The role of London dispersion in halogen bonds

Though it has been found to be non-negligible in the vast majority of halogen bonds, London dispersion (the attractive component of van der Waals (vdW) forces) has been shown to be increasingly important when weaker acceptors are involved.[2] The noble-gas acceptors considered in the above-discussed study by Hobza and co-workers[102] is a prime example of this, with many authors pointing out the usefulness of such systems that lack strong interactions between permanent multipoles for the study of non-electrostatic forces in halogen bonded systems.[102,111-115] Similarly, a series of 2019 papers by Pirani and co-workers studied halogen-noble gas interactions and employed an integrated experimental/theoretical approach based on the parametrisation of data obtained from molecular beam scattering techniques. [111,112,116,117] These studies found dispersion to be the most significant force in the systems. However, comparison of dihalogen-noble gas complexes to other diatom-noble gas complexes that are purely driven by dispersion, found that purely vdW-dependent calculations were unable to reproduce the experimental ground-state dihalogen-noble gas results. This suggests that these halogen bonding interactions are primarily, rather than purely dispersive.

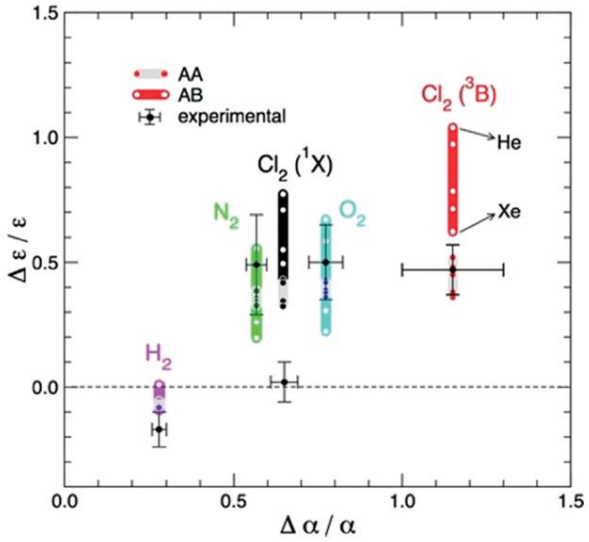

Figure 1.14: Plot of relative conformational stability of T-shaped and co-linear conformations (Δε/ε) against the polarisability of the diatom (Δ α/α). AA and AB refer to two distinct computational models for the diatom; the former employing a two-interaction site model (each contributing half the polarisability) and the latter a single unique anisotropic interaction site. ^{1}X and ^{3}B refer to the ground and triplet excited states respectively.[112]

Figure 1.14 shows that the conformational preferences of dihydrogen, dinitrogen and dioxygen noble gas adducts all favour perpendicular T-shaped complexes (positiveΔ ε/ε). This can be rationalised by the directional anisotropy of polarisability in such electron acceptors. Dihydrogen shows little conformational preference, but the much more anisotropic (60-80%) dinitrogen and dioxygen express a clear energetic preference for interactions away from the less polarisable polar-regions. The polarisation anisotropy of dichloride sits between dihydrogen and dioxygen, but the experimental results show significant deviation from the calculations and show a much weaker conformational preference.

Charge transfer from the noble gas atom to the halogen in the collinear geometry is found to be the cause of this discordance between the experimental and vdW models. A more detailed computation model that employed a three-body term accounting for molecular orbital formation within the Cl_2 molecule, and an additional charge-transfer model alongside the vdW forces (improved Lennard-Jones function model)[118] was able to reproduce the experimental potential energy surfaces quantitatively (Figure 1.15). Indeed, the authors note that they are not the first to draw attention to the role

of charge transfer in such systems. Analogous studies of noble gas complexes with CCl_4 and weak hydrogen bonded helium adducts also possessed charge-transfer characteristics. Interestingly, Figure 1.14 shows that in the triplet excited state the conformational preference of the dichloride complex can, like the other diatoms, be predicted based on the polarisation anisotropy. This can be seen again for the more complex computational model in Figure 1.15, with the energy well for the collinear conformation being much shallower.

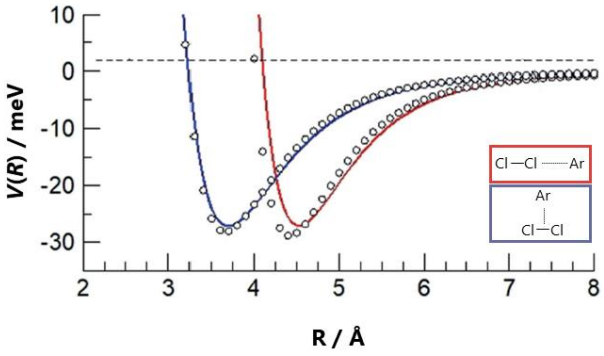

Figure 1.15: Plot of interaction potential against intermolecular distance. Solid lines refer to experimentally derived potential energy surfaces, and white circles to *ab initio* calculated energies. Red, linear geometry; blue, T-shaped geometry. [112]

In the follow-up paper,[111] the authors extend this analysis to a broader set of dihalogens, considering Br_2-Ng and I_2-Ng complexes as well as the previously discussed Cl_2-Ng[112] and find good agreement between experimental and charge-transfer-included analytical models. For all dihalogen-noble gas systems considered, the movement from ground to triplet excited state was accompanied by the switching of geometric preference from collinear to T-shaped in response to the disappearance of charge transfer interactions in the latter state.[111,112] As might be expected of predominantly dispersive interactions, there is a general increase in interaction stability in response to increases in the size and polarisability of the atoms involved. These systems are a powerful example of how a term that is secondary in magnitude can still exhibit a strong influence on the halogen bond.

A 2015 study by Frontera and co-workers[119] strikes similar chords, demonstrating the need for the inclusion of dispersion corrections in the modelling more traditional electrostatically driven σ- and π-hole systems. They found that, even though

dispersion corrections often result in overestimations in stability, their inclusion was necessary for accurate predictions. The study focuses on the geometric preferences of the halogen bonds and π-hole interactions shown in Figure 1.16B. The authors emphasise the similarities of the physical nature of these two classes of interactions.[119-121] For the halogen bonded complexes, agreement in terms of interaction energies calculated by the MP2 and BP86 levels are significantly improved when the latter is appended with Grimme's D3 dispersion correction.[122] The same was found to be true for the π-hole complexes where fluorine acts as the electron donor, but for similar complexes involving iodine the D3 correction was found to significantly overestimate energies. This is unsurprising given that the latter is an interaction between two very large and polarisable atoms. Since this work was published, Grimme's improved D4 dispersion correction[123,124] has become available and aims to provide a better representation of polarisability, but to our knowledge this new model has not been applied to these systems.

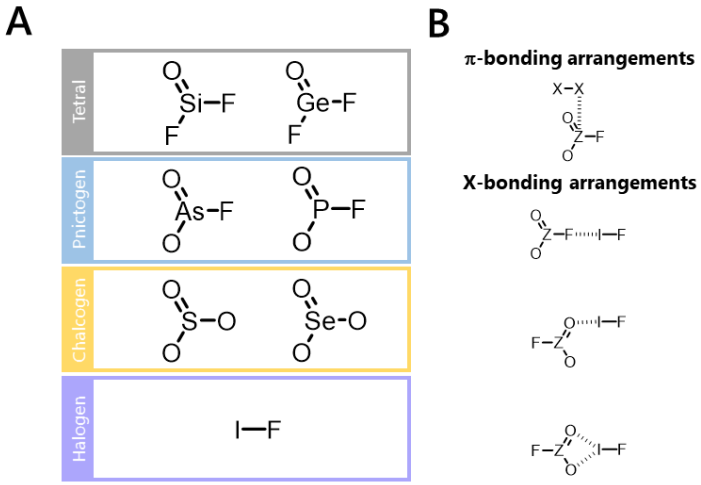

Figure 1.16: A) Model systems as employed by Frontera and co-workers. B) Arrangements employed. Examples are presented using a ZO_2F system but are applicable to ZOF_2 and ZO_3 systems where applicable.[119]

The importance of dispersion in halogen bonds was also emphasised by Riley and Hobza in their 2008 paper.[43] The authors discuss some of the issues present in earlier studies that comment on dispersion, but employ basis sets that are not large enough to describe such effects accurately, often leading to their underestimation.[125] The authors present the failure of the Hartree-Fock methodology[126] (which does not model

dispersion) to predict the strength of several Br and Cl halogen bonds that have been shown to be favourable experimentally.[2,43] In response, the authors conducted SAPT energy dissections on DFT-minimised geometries with a large basis sets (up to aug-cc-pVQZ)[127,128] on a set of $H_3CX\text{-}OCH_2$ complexes (Figure 1.17). As might be expected, the interactions are stabilised on descending the halogen series. However, the relative magnitudes of the energy components shows a more unconventional picture with the dispersion terms being more negative that the electrostatic terms for the chlorine and bromine halogen bonds in all of the three aug-cc-pVxZ basis sets and in the extrapolated complete basis set limit.[129] Minimised geometries also support the dominance of dispersion in chlorine-oxygen halogen bonds, with their minimised geometries possessing a more relaxed linear dependency (~167° versus ~173° for iodine). This suggests the diminished, though far from negligible role of the σ-hole in the interaction.[43] For the iodine halogen bonds the situation is changed and electrostatics are now the most significant term with this being seen in the relative predictive success of Hartree-Fock methods that lack dispersion correction. It is worth noting that the magnitude of all SAPT energy terms increased on descending the halogen series and it is only the relative weighting of the terms that changes.

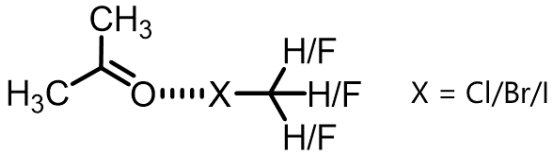

Figure 1.17: Model system employed by Riley and Hobza. Models include all variations in the number of fluorine atoms on the halogen bond donor.[43]

Riley and co-workers also extend SAPT calculations to fluorinated analogues of the halogen bond donors (Figure 1.17).[43] As has been extensively documented, the increase in the electronegativity of atoms adjacent to a halogen bond donor increases the depth of the halogen's σ-hole,[32] typically resulting in increased halogen bond strengths. This is manifested in the larger magnitude of the SAPT interaction totals in all three halogen systems in response to increasing number of fluorine substituents (Figure 1.18). The increased strength of the σ-hole is expressed in the same increases being observed in the electrostatic terms. However, the expansion of the σ-hole is accompanied by a relocation of electron density away from the halogen, as expressed

in the reduced dispersion term accompanying increasing fluorination. This results in the flipping of the dominant term from dispersion to electrostatics in the trifluoro chlorine complex and in the difluoro bromine complex. The effect that fluorination has on the larger halogen atoms is unsurprising,[130] but the prevalence of highly fluorinated, heavy halogen donors may contribute to the colloquial description of halogen bonds as predominantly electrostatic interactions.

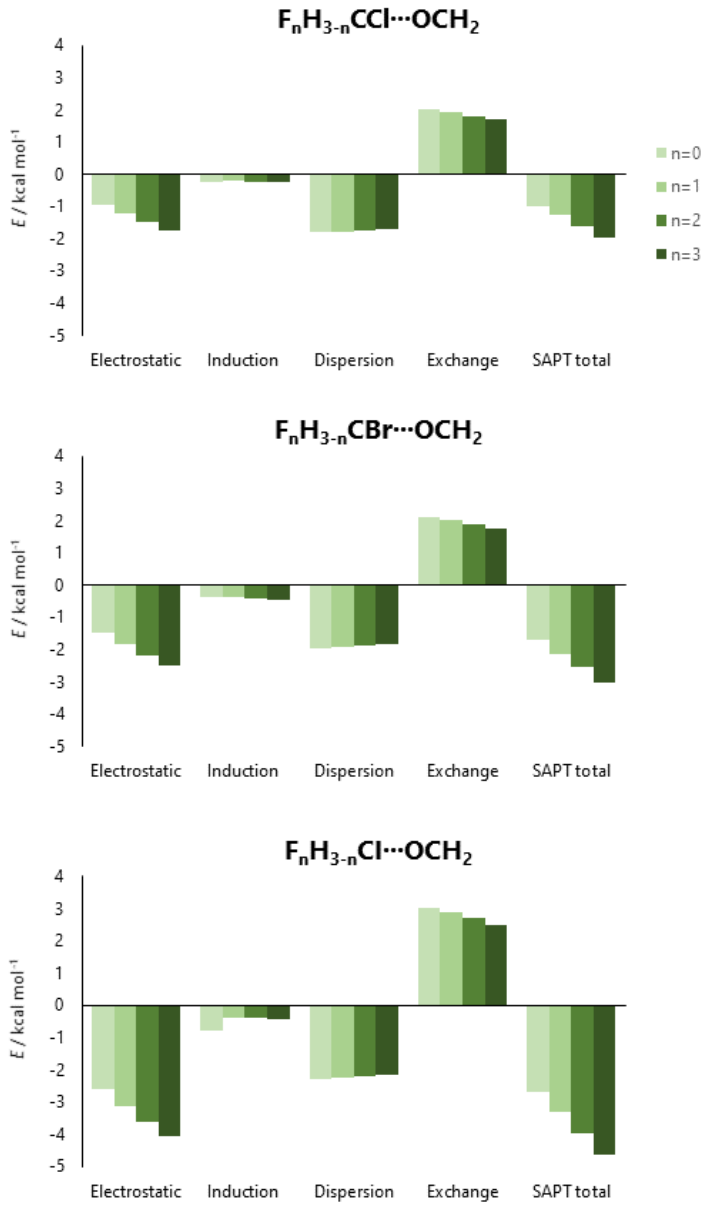

Figure 1.18: Graphical depiction of the terms of SAPT energy dissection conducted by Riley and Hobza.[43]

1.6 Chalcogen bonds

Unsurprisingly, the phenomena responsible for the emergence of σ-holes in halogenated species are not unique, and halogen bonding analogues have been noted throughout the main group. Perhaps the second most widely recognised of these interactions (after halogen bonding) are chalcogen bonds, which feature σ-hole interactions involving group 16 elements as electron acceptors.[131] Like halogen bonds, the earliest observations of what we now understand to be chalcogen bonds date back to the nineteenth century,[132,133] but it was the comparatively recent rationalisation of the σ-hole that has led to contemporary interest in them.[19] Indeed, both halogen and chalcogen bonds can be justified by the same orbital mixing arguments.[12,16,19] Chalcogen bonds also exhibit remarkably similar behaviours to halogen bonds being often being characterised by linearity and proportionality to the electrostatic surface potential.[18,19,134-136] However, in contrast to the monovalent halogens, the divalency of group 16 elements means that they can furnish two σ-holes at the extension of covalent bonds. Nonetheless, comparison can be drawn to halogen bonding systems involving hypervalent iodine donors (Figure 1.19).[137-140]

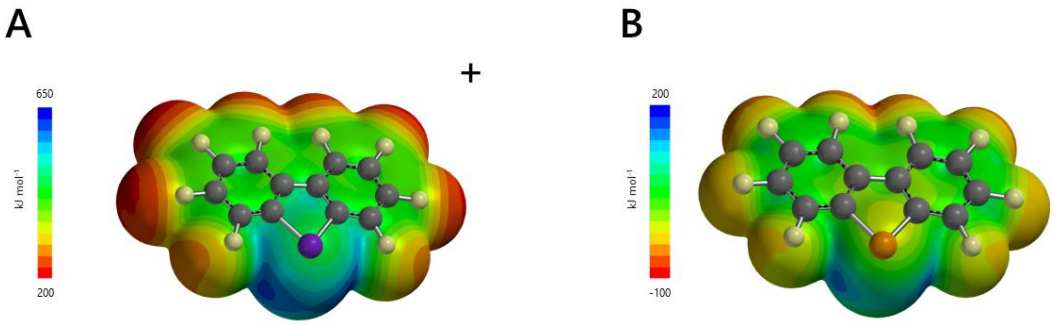

Figure 1.19: A) electrostatic surface potential for hypervalent iodine$^{(III)}$ showing dual σ-holes, B) Electrostatic surface potential for a typical chalcogen bond donor species.

The relatively well-established nature of chalcogen bonds yielded an IUPAC definition in 2019,[131] and we expect that the next decade will see definitions for other σ-hole type interactions. Unlike the definition of the halogen bond,[1] the chalcogen bond definition makes no mention of specific intermolecular forces responsible for the bond, which can be seen as a sign of the more contested nature of such forces that has

arisen in recent years. Discussion concerning the role of orbital interactions and dispersive forces has spilled over from halogen bonds to their analogous interactions.

In 2017, the original documenters of the σ-hole phenomena, Politzer and co-workers[9,10] revisited the subject and provided extended insight into its relevance to group 15, 16 and 17 elements.[18] The authors comment on the relative simplicity of univalent halogen bond donors that point away from the molecule to which they are bound compared to the more complicated environment of analogous σ-hole donors. By comparison, the group 14, 15, 16 and 17 atoms are more deeply embedded into the frame work, which often deflects σ-hole interactions away from the extensions of the covalent bond axis.[18,134,141-145] Indeed, many different examples are highlighted in Politzer's review,[18] which discusses geometric aspects primarily from an electrostatic potential perspective. While others have corroborated such observations, they are typically rationalised as being the result of anisotropic exchange repulsion forces. Both Politzer[18,19] and Haberhauer[146] note much closer boundaries of the electron densities of the chalcogen atoms in the equatorial plane of the Ch-R bonds as compared to the perpendicular plane. SAPT studies by the latter showed significantly greater exchange repulsion penalties for deviations out of the equatorial plain (Figure 1.20). In a similar vein to Stone's findings for halogen bonds,[59] Haberhauer and co-workers found electrostatics to be the driving force of the chalcogen bonds, but exchange repulsion showed the strongest response to changes in geometry in all directions (Figure 1.20B and C). All of these studies were performed computationally in the gas phase. However, σ-hole interactions observed in the crystalline phase have been commonly been found to deviate unexpectedly from geometries anticipated from gas-phase calculations.[136,142-144,147,148]

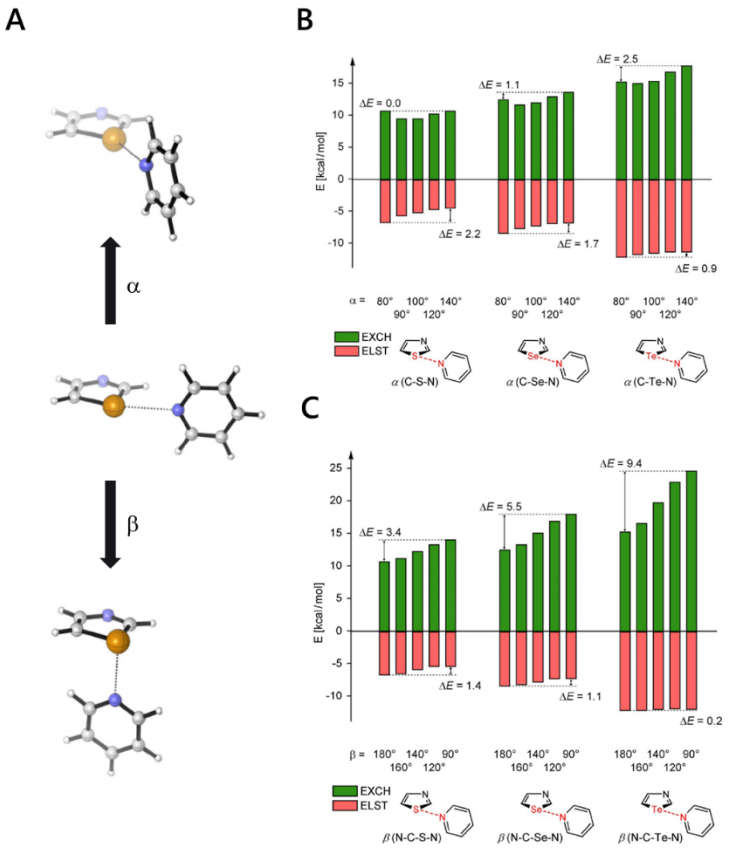

Figure 1.20: A) Angular variation model employed by Haberhauer, α corresponding to variations within the aromatic plane, β to variations out of the aromatic plane. B) Plot of SAPT electrostatic and exchange terms for three chalcogen bonding systems as a product of variations in angle α. C) Plot of SAPT electrostatic and exchange terms for three chalcogen bonding systems as a product of variations in angle β.[146]

Politzer and co-workers, as well as several other authors, extend their conclusions advocating for the purely Coulombic (electrostatic and polarisation) model of halogen bonds to chalcogen bonds[19] and to the other σ-hole interactions.[13,18,149,150] A 2017 study by Cockroft and co-workers underscored the potential importance of polarisation in chalcogen bonding.[151] Compellingly, this study centred around solution-phase studies with interaction strengths being determined from the conformational preferences of molecular balance systems (Figure 1.21A). A 13-solvent screen of the conformational preferences of these molecular balances was conducted. Remarkable solvent-independence of the conformational preferences was observed (Figure 1.21B). Most of the energies for each balance were within error, except in the very strong

hydrogen-bond donor solvent perfluoro-*tert*-butyl alcohol, which competed for hydrogen bonding to the carbonyl group.

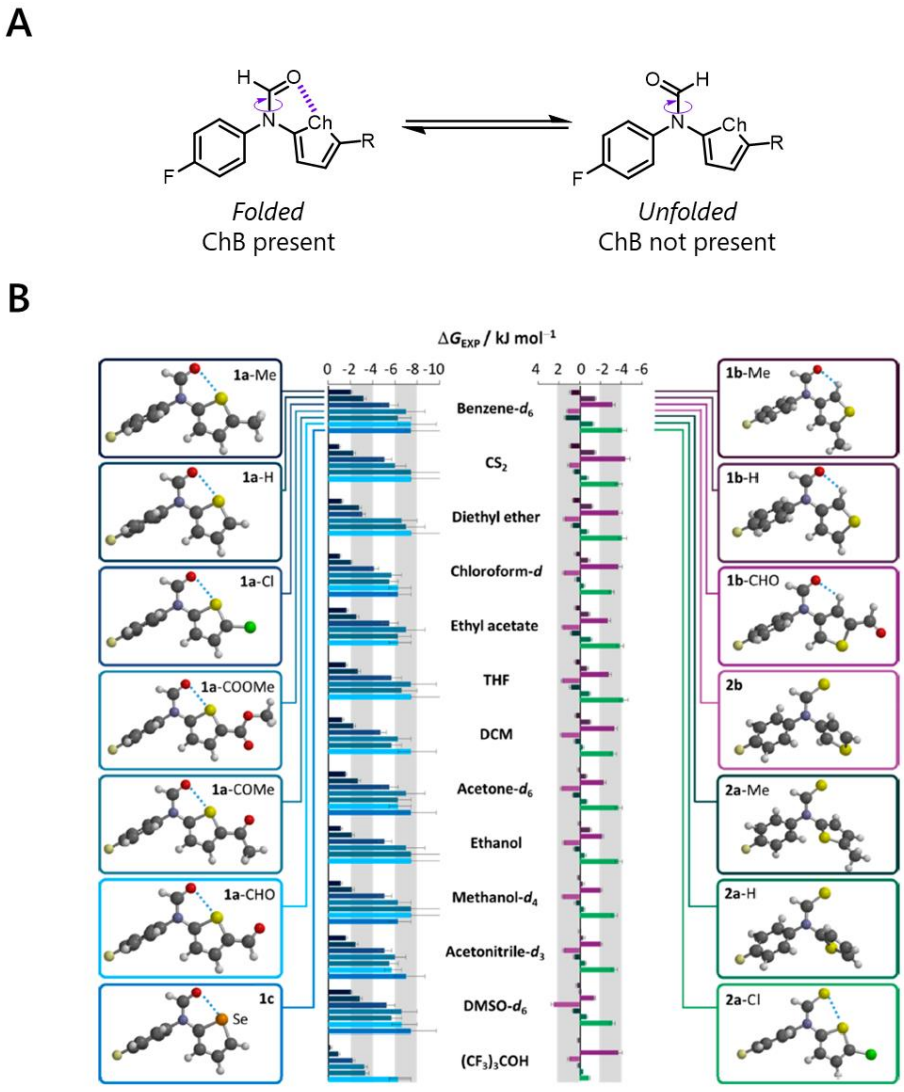

Figure 1.21 A) Molecular torsion balance system as employed by to measure ChB strengths **B)** Experimentally measured conformational free energies for molecular torsion balance systems studied by Cockroft and co-workers in a verity of solvents.[151]

A multitude of studies have demonstrated the ability of solvents to exert pressures on the conformational preferences of molecular balances though both electrostatic and solvophobic influences.[152-160] The fact that interaction strengths are seemingly unaffected by the presence of competing hydrogen donors and acceptors constitutes a considerable rebuttal to electrostatic forces being a primary determinant of chalcogen bond interactions. However, the observation is in line with previous solution phase

chalcogen bonding studies that noted only modest variations in response to solvent changes.[161] The authors also considered the role of London dispersive forces based on the relationship between the measured interaction energies and the bulk polarisability of the solvents used. If the chalcogen bonds present in these balances were significantly dispersive in nature, then highly polarisable solvents such as carbon disulfide would be expected to offer significant attenuation, but this was not seen. The negligible role of dispersion in these systems is further reinforced by there being no significant change in the correlation between experimental and computational results when dispersion corrections are added (B3LYP/6-311G* $R^2 = 0.94$ and ωB97X-D/6-311G* $R^2 = 0.84$).[151] A lack of a strong solvent dependency has been previously noted in several studies for other σ-hole type interactions,[89,92,93,161] but examples counter to this have also been seen.[55,162,163] Such context dependency is perhaps unsurprising, given that we have already shown such interactions to be rather resistant to generalisations about their behaviour.

Cockroft and co-workers[151] find a much more conclusive result when considering the chalcogen bonds as a product of induction effects. Molecular orbitals energies for the open and closed conformers of the balances were determined using DFT calculations. The majority of orbitals saw little change between the conformers in which the chalcogen bond was present or broken. However, some orbitals saw noticeable conformer-dependent changes in energy. They could be divided into two categories; though-bond resonance effects resultant from the delocalisation of amide lone pairs into the aromatic ring (orange points, Figure 1.22), and lone pair to $\sigma^*_{Ch\text{-}C}$ orbital mixing from the O/S chalcogen bond acceptor to the S/Se chalcogen bond donor (teal points, Figure 1.22). It is interesting to note that this orbital mixing was also seen in the β-thiophene balances, but with the delocalization going into the $\sigma^*_{H\text{-}C}$ orbital instead. This demonstrates not only the similarity between chalcogen bonds and hydrogen bonds, but also the presence of orbital interactions to both.

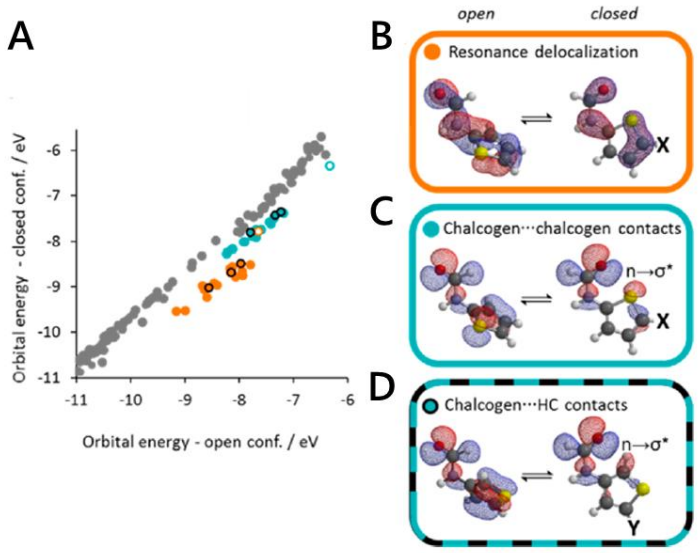

Figure 1.22: A) Plot of DFT-calculated orbital energies for the open and closed geometries of the molecular balances shown in Figure 21. Grey points denote orbitals where no significant change is observed between the conformers. B) Visualisation of electron delocalisation though conformer-dependent resonance effects. C) Visualisation of LP to σ* orbital mixing between oxygen and heteroaromatic chalcogen atoms. D) Visualisation of LP to σ* orbital mixing between oxygen and the C-H bond.

Orbital interactions where electrons are accepted into an anti-bonding orbital are characterised by an accompanying lengthening of the acceptor bond, and accordingly this was seen in the calculated minimised structures. Correlation of this elongation to the experimental energies was poor, but the chalcogen adjacent bond length is also modulated by the adjacent substituent groups (Figure 1.21B). Reassuringly, a good correlation ($R^2 = 0.99$) between the thiophene balance experimental energies and the energies of the orbitals identified to contain the LP to σ* orbital mixing in both the chalcogen and hydrogen bond examples was found (Figure 1.23). This combined with the lack of solvent dependencies provides a compelling for argument that the energetic trends (but not necessarily the absolute energies) of the chalcogen bonds were dominated by orbital interactions. Nonetheless, Cockroft and co-workers raise the important point that the preference for the chalogen bonded conformer for the selenophene balance was more favourable than the trend observed for the thiophene balances (Figure 1.23). They pointed out that the relative chalcogen bond donor and acceptor abilities of these systems are heavily influenced by the intramolecular geometric constraints imposed by the molecular balance design.

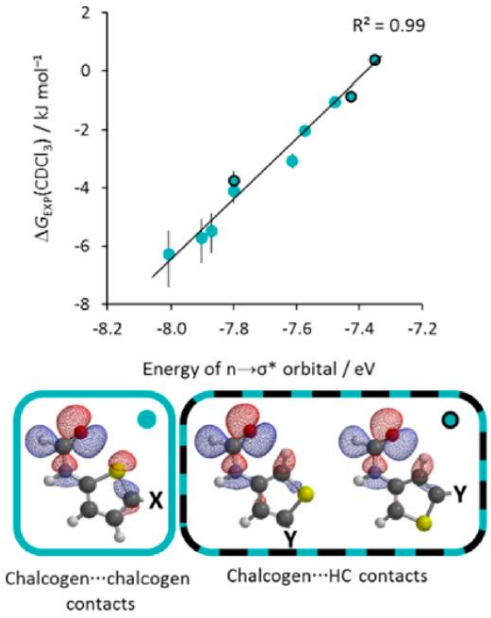

Figure 1.23: Plot of experimentally measured conformational free energies for molecular torsion balance systems against LP to σ* orbital energies. LP to $\sigma^*_{Ch\text{-}C}$, teal; LP to $\sigma^*_{H\text{-}C}$, teal and black striped.[151]

The previously mentioned, study by Haberhauer and co-workers also identified orbital interaction as playing a role in chalcogen bonds; especially when the larger tellurium is acting as the chalcogen bond donor atom.[146] NBO calculations conducted as part of their studies into angular dependencies of chalcogen bonds deemphasised the role of specific LP to σ* mixing and noted the relatively minor change in the sum of intermolecular orbital energies in response to both axial and equatorial changes in chalcogen bond geometries relative to the plane of the aromatic donor.[146] The expected diminishing magnitude of LP to σ* mixing was predicted to be compensated by other mixing events (hollow bars in Figure 1.24). However, it should be noted that all of these calculations still involve contact between the chalcogen atoms, hence the limited change in polarisation aspects is somewhat different to the case where a chalcogen bond is either completely broken or formed.

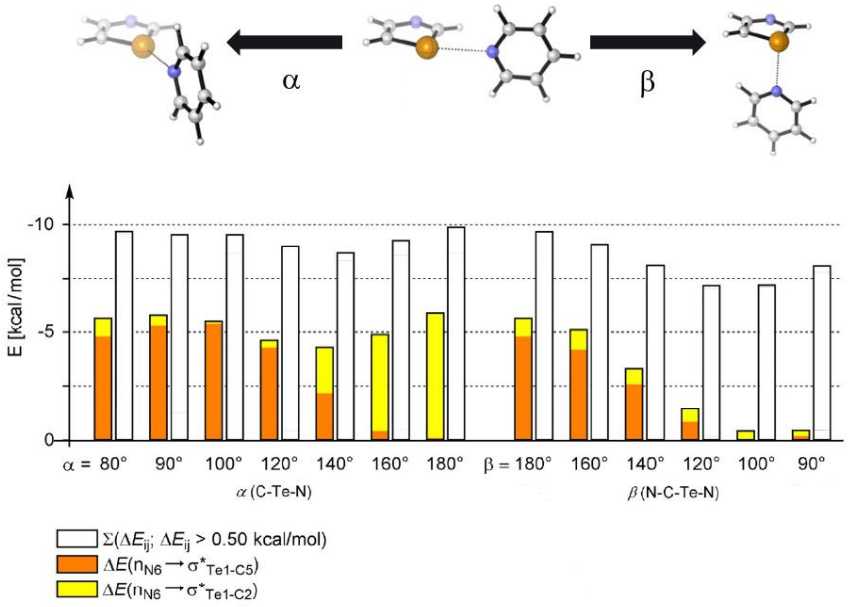

Figure 1.24: Energy transfer between donor NBOs and acceptor NBOs in the model systems employed by Haberhauer and co-workers. In aromatic plane angular variations (α) left; out of aromatic plane (β).[146]

While Politzer[18] and Cockroft[151] deemphasise the role of dispersion in chalcogen bonds, dispersion can play a larger role in the absence of a solvent that competes for dispersion.[164-166] For example, Chopra examined diphenylselenide and diphenyltelluride synthons, which upon crystallisation yielded double chalcogen bonds with π system acceptor moieties (Figure 1.25).[164] Such systems are comparatively rare for chalcogen bonds, but crystal database analysis showed that there is a general preference for bonding to lone pair acceptors over π systems.[167-169]

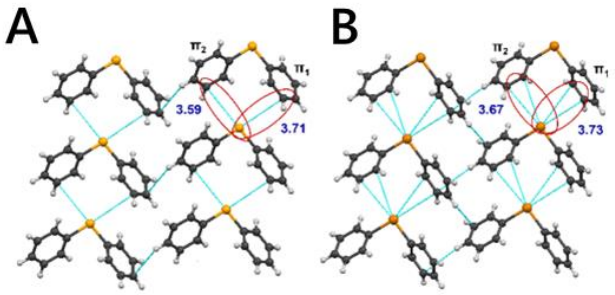

Figure 1.25: Crystal structures for A) Ph_2Se and B) Ph_2Te highlighting putative Ch···π chalcogen bonds.[164]

The authors noted the high degree of similarity between the two analogues.[164] QTAIM analysis of the two crystal structures also showed similarities with both of them possessing chalcogen bond typical bond critical points with positive Laplacian values indicating a degree of covalency to the otherwise closed-shell chalcogen bonds present. This is reinforced by NBO modelling that showed overlap between two σ^*_{ch} antibonding orbitals and occupied π orbitals in both species. The more positive Laplacian values for the tellurium bond critical points, their shorter lengths relative to the sum of their van der Waals radii, and the shallower σ-holes of the selenium systems all point towards Te-π chalcogen bonds being stronger than their selenium analogues. This trend may also offer an explanation for the failure of diphenylsulphide to produce crystals via the same methodology.[164]

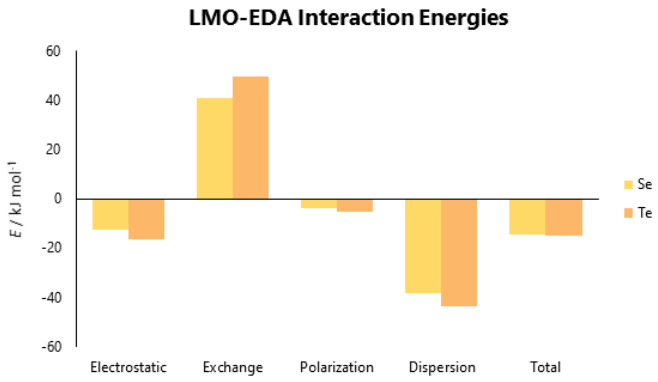

Figure 1.26: Graphical depiction of the LMO-EDA energy dissection terms conducted by D. Chopra *et al.*[164]

Figure 1.26 shows the results of LMO-EDA calculations[170] conducted on the obtained crystal structures using M06-2X/6-31G**, but with a much larger cc-pVDZ-PP pseudo potential being applied to the selenium and tellurium atoms.[164] The total energies of these calculations confirms the predicted strength of the Te···π bond over the Se···π. The most striking results of these calculations are the very large dispersion terms that represent 70% and 67% of the stabilisation terms for the selenium and tellurium dimers, respectively. This finding draws parallels to the X-Ng halogen bond SAPT calculations reported by Hobza and co-workers.[102] Chopra and co-workers acknowledge the limitations inherent to using a simple dimer to provided commentary on the real-space behaviour of systems.[164] Analysis of the energy frameworks[171] yields

similar results; the radii of the green cylinders shown in Figure 1.27 corresponding to dispersion are noticeably greater than the red ones corresponding to electrostatics. The observation of horizonal cylinders also revealed weak C-H···π interactions (Figure 1.28), which by contrast, are the most stabilising interaction in crystals of the analogous compound diphenyloxide (which lacks the ability to form chalcogen bonds).[172]

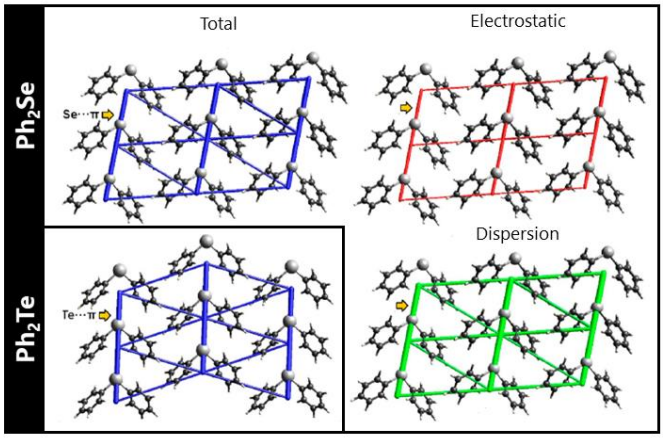

Figure 1.27: Energy frameworks for Ph_2Se and Ph_2Te (insert) blue. Frameworks dissected into electrostatic (red) and dispersive (green) components. The diameter of the cylinders is proportional to the strength of the interaction forces along the indicated axis.[164]

Though demoted to a secondary role in these systems, the effects of electrostatics can still be clearly seen. Electrostatic potentials for the diphenylchalcogenide series show some asymmetry in the two σ-holes on each chalcogen atom (60.4 kJ mol^{-1} and 55.1 kJ mol^{-1} for Se and 94.5 kJ mol^{-1} and 91.9 kJ mol^{-1}),[164] which is a product of the different phenyl orientations. This asymmetry is clearly reflected in the slight asymmetry of the chalcogen bond lengths see in the crystalised structures (Figure 1.25). Studies on analogous perfluorophenyl derivatives demonstrated deeper σ-holes on both the tellurium and selenium atoms that would produce chalcogen bonds with a more prominent electrostatic terms.[173] However, the stability demonstrated by the phenyl-substituted species demonstrated that maximising the amount of electron withdrawing substituents is not a prerequisite for forming stable σ-hole interactions.

Comparison of the work of Chopra to other studies should also be prefaced with an acknowledgment that comparing packed crystal structures to solution or gas phase systems is inherently imperfect due to the to the large cost of breaking dispersive

interactions without a solvent to fill in the resultant space. Previous studies have demonstrated this, with energetically favourable interactions that predominantly dispersive interactions being heavily attenuated by competition by the solvent.[152-154]

1.7 Pnictogen bonds

The term pnictogen bonds is used to describe σ-hole interactions featuring group 15 electrophiles by comparison with halogen and chalcogen bonds. Though comparatively understudied, pnictogen bonding systems have proved useful in furthering our collective understanding of σ-hole interactions. At the time of writing, there is no formal IUPAC definition for pnictogen bonding. However, the terms pnictogen bond and tetrel bond (group 14 analogue) are mentioned in Resnati and colleagues' preface of the recommendation to the IUPAC on the definition of the chalcogen bond.[131] Politzer and co-workers' identification of σ-holes and associated secondary bonding interactions again provided a fresh perspective of otherwise counterintuitive behaviours observed in solution and crystals over the previous century.[149,174-177] In the original 2007 paper, it was noted how smoothly the σ-hole concept may be transferred to pnictogen bonding; σ-holes can again be rationalised by depleted of *p* orbitals at the extension of σ bonds.[149] The higher degree of *sp* hybridisation seen in the lighter pnictogens explains their shallower σ-holes. Like chalcogen bonds, pnictogen bonds tend to be less linearly aligned along the covalent bonding axis than halogen bonds. Indeed, Politzer determined that electrostatic $V_{s,max}$ location deviated by around 20° from the from the bonding axis.[149] Like halogen[125,178-181] and chalcogen bonds,[133,147,148] pnictogen bonds are also influenced by surrounding atoms and substituents.

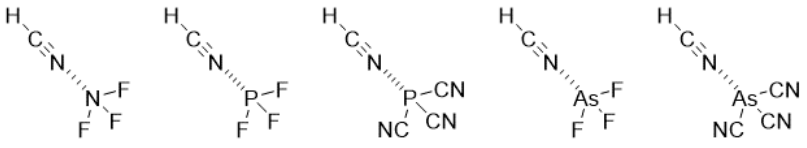

Figure 1.28: Pnictogen bonding systems studied by Politzer et.al.[149]

In addition to characterising the σ-holes of pnictogen atoms, Politzer also examined the complexes shown in Figure 1.28.[149] A strong relationship between complex

stability and σ-hole depth was readily established, and corroborated by subsequent studies. For example, Matile and co-workers have examined the catalytic potential of σ-hole interactions in pentafluorophenyl-substituted halogen, chalcogen, and pnictogen bond donors.[173]

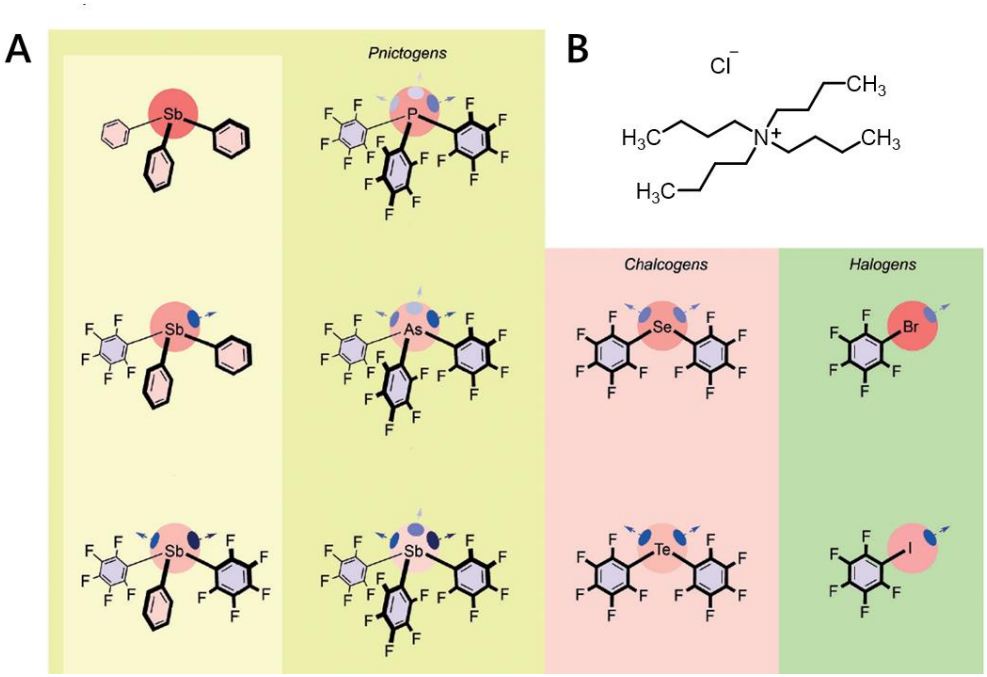

Figure 1.29: A) σ-hole interaction donor species studied by Matile *et al.* B) Tetrabutylammonium chloride (TBACl) employed as a σ-hole interaction acceptor in ^{19}F NMR titrations.[173]

^{19}F NMR titrations of the σ-hole donors shown in Figure 1.29 against TBACl were used to determine the dissociation constants of the resultant chloride complexes. The strength of these complexes followed the trend of increasing strength descending from row 3 to 4 and increasing from group 17 to 16 to 15.[173] The inter-row trend can be attributed to the decrease in electronegativity and the increase in polarisability with the same trend being reported by several previous studies.[2,12,19,149] The strength of the pnictogen bonds and weakness of the halogen bonds compared to the chalcogen bonds showed increasing binding strength with increasing number of electron-withdrawing species. One might also reasonably consider this increased binding strength to be due to an increasing number of σ-hole binding sites.[182] However, the computationally minimised structures of tris(pentafluorophenyl)arsine and tris(pentafluorophenyl)stibane reject this suggestion, since the bulky aromatic substituents afford the central pnictogen atom with only one solvent/substrate-

accessible σ-hole (Figure 1.30). In addition, replacing one of the pentafluorophenyl groups with a non-fluorinated, less-electron withdrawing substituents was found to increase the desiccation constant of the interaction from 19 μM to 570 μM respectively, demonstrating a significant reduction in binding strength. This is supported by accompanying DFT (M06-2X/6–311G**/aug-cc-pVTZ-pp) calculations for the chloride binding energies, which see the same decrease in halogen bond strength; –216.7 kJ mol^{-1} to –185.8 kJ mol^{-1}.

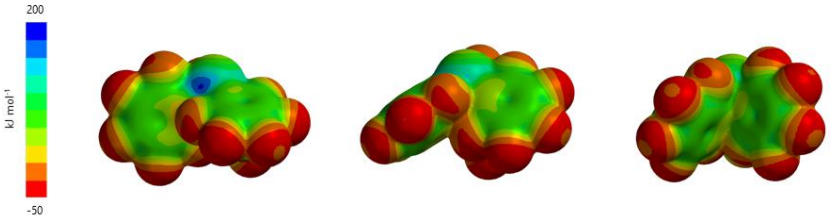

Figure 1.30: Electrostatic surface potentials for the three faces of tris(pentafluorophenyl)stibane as employed by Matile *et al.* The σ-hole is only viable on one of the faces, left.[173]

Compellingly, the results of both the non-fluorinated substitution experiment and the comparison of the halogen, chalcogen, and pnictogen species translated well into catalytic activity in the two chloride extraction experiment shown in Figure 1.31.[173] However, the tellurium and iodine catalysts had very similar catalytic activity, both of which were orders of magnitude weaker than the antimony catalyst. Catalytic turnover was not observed with any of the row 4 element catalysts, which was in accord with the dissociation constants measured in NMR titrations noted above. Indeed, the catalytic role of the σ-hole interactions was confirmed by the addition of 1.1 equivalents of the competitive binder TBACl, which completely quenched catalytic activity. The authors note the remarkable effectiveness of these relatively simple, monodentate, and neutrally charged species in this catalytic context. By comparison, hydrogen, halogen, and chalcogen catalysts required multidentate binding sites and/or charges to achieve the same catalytic activity as tris(pentafluorophenyl)stibane.[183-187] Hence, there is strong impetus for the consideration and study pnictogen bonds, despite the present lack of a formal IUPAC definition.

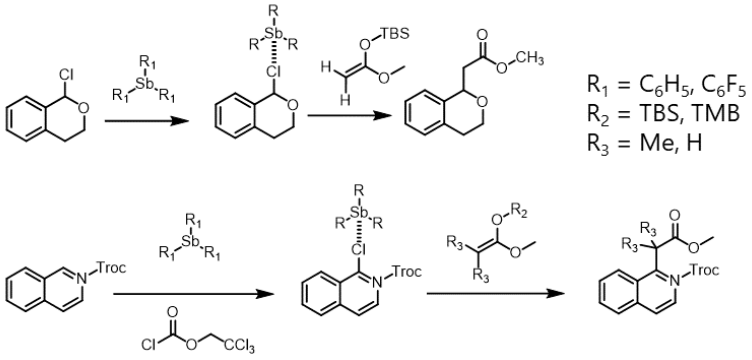

Figure 1.31: Chloride extraction experiments employed by Matile *et al*. to test the catalytic activity of the σ-hole interaction donors shown in Figure 1.30.[173]

Though electrostatics are undeniably a very important component in pnictogen bonding, several computational techniques have identified important roles played by other forces in pnictogen bonded systems. Sánchez-Sanz and co-workers applied AIM, NBO and SAPT calculations to XNO_2 (X = F, Cl, Br, I) homodimers (Figure 1.32A).[188] A variety of σ-hole interactions, including pnictogen bonds, were formed that depended on the relative geometry of the interacting monomers. Molecular electrostatic surface potentials revealed σ-holes following the expected trends; halogen atom σ-holes increased in depth with increasing halogen size/polarisability, while the pnictogen σ-holes increased in depth with increasing halogen electronegativity. The authors employed Bader's AIM methodology[189] to classify the interactions within the multitude of arrangements, all of which contained bond critical points with relatively small electron density values and small positive Laplacians; both of which are characteristic of the mostly closed shell σ-hole interactions.

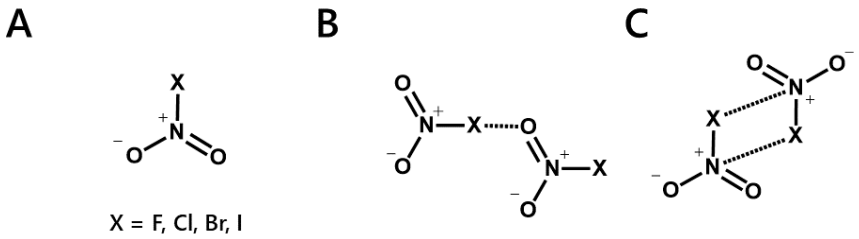

Figure 1.32: A) XNO_2 species as employed by Sanchez-Sanz et.al. B) Halogen (left) and C) pnictogen (right) bonding examples of the multitude of arrangements possible for the XNO_2 homodimers.[188]

Mirroring earlier discussion of anti-electrostatic halogen bonds, it is interesting to note that the FNO_2 halogen σ-hole is not positively charged, yet the calculations suggested the formation of favourable halogen bonded dimers. However, SAPT-DFT calculations showed dispersion to be the largest attractive term regardless of the specific bonding interaction in all but a few complexes; accounting for up to 71% of the interaction.[188] Accordingly, most of these interactions may not be manifested in the presence of solvent. Only the systems with the deepest σ-holes were found not dominated by dispersion; iodine systems where halogen bonding occurred and fluorine systems where pnictogen bonding is occurred.

The SAPT-DFT calculations generally showed the induction term to be the least important of the attractive terms in these systems, accounting for around 10% of the total.[188] NBO calculations were in agreement with this finding. Electronegativity was found to govern the magnitude of orbital interactions, but the extent of delocalisation was generally small. This is unsurprising as the majority of the interactions within these systems could be described as longer range interactions that are often dispersive in nature.[188,190]

The exceptions to this trend were the situations where iodine acted as either a halogen bond donor or acceptor. In these cases, the induction term was found to be slightly smaller than the electrostatic term while also involving short interaction distances relative to the sum of the component van der Waals radii (~3.4 Å). The only pnictogen atom included in this study was the nitrogen,[188] so we are unable to see if induction dominated short range interactions occur for other heavier pnictogens.

SAPT calculations have been used to examine pnictogen bonding systems involving phosphorus donors. Sanchez-Sanz and co-workers studied pnictogen bonds within the proton sponge systems shown in Figure 1.33A.[191] In these cases, the phosphorus centre provides the σ-hole, while the nitrogen centre serves as a lone pair donor. As might be predicted, the addition of electron-donating substituents (CH_3 moieties) to the nitrogen atom increased its ability to form pnictogen bonds (Figure 1.33, blue). Similarly, the addition of electron-withdrawing substituents to the phosphorus atom also strengthened the interaction, but by deepening the phosphorus σ-hole (Figure 1.33, red). The interaction strength was found to increase in proportion to the

electronegativity of the substituent. Substitution of the pnictogen bond donor yielded stronger effects on the interaction strength and bond length. This can be attributed to the higher polarisability of phosphorus compared to nitrogen. The SAPT data showed that the electrostatic term was the largest, typically twice that of the second largest term, dispersion. Two exceptional cases were seen where electrostatics was eclipsed by the dispersion; these were the situations where strong electron-withdrawing groups were positioned on the pnictogen bond acceptor, reducing its nucleophilicity. Consequently, these two exceptions were the most repulsive studied, demonstrating the importance of electrostatics.

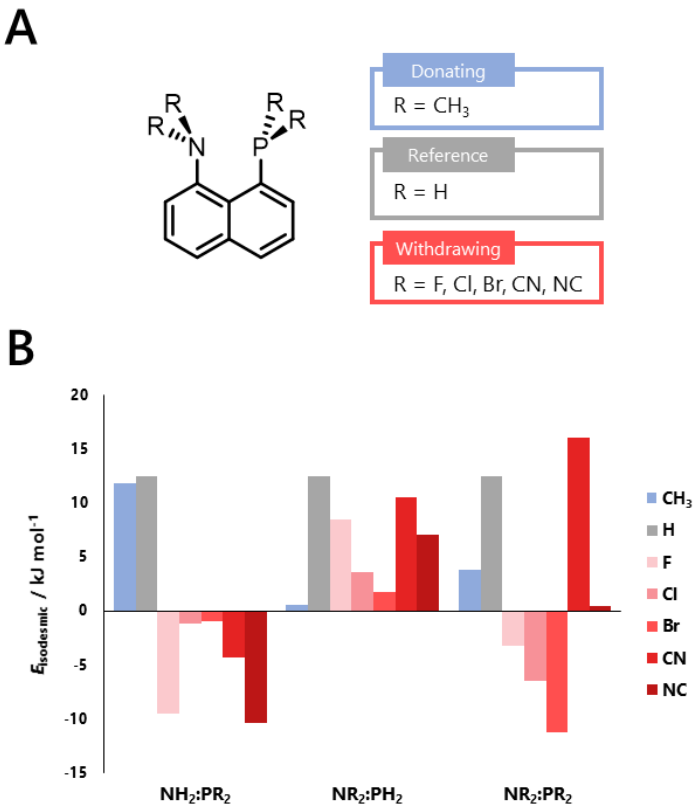

Figure 1.33: A) 8-phosphinonaphthalen-1-amine derivatives as employed by Sanchez-Sanz *et al.* and B) corresponding isodesmic energies calculate at CCSD(T)/aug0-cc-pVDZ.[191]

The addition of electron-withdrawing groups to the pnictogen bond acceptor yielded interaction strengths that were inversely proportional to the electronegativity of the substituent appended. Curiously, however, the unsubstituted -NH_2 acceptor was the most repulsive (Figure 1.33, grey). From an electrostatics standpoint, this observation does not make sense given the modest electronegativity of hydrogen substituents.

However, this is only part of the story, as the role of the pnictogen bond donor/acceptor may be reversed in this system; nitrogen may act as a pnictogen bond donor, while phosphorus possesses lone pairs subtle for pnictogen bond accepting. Such a situation was confirmed using NBO calculations, which found P_{LP} to σ^*_{N-X} transfer being observed alongside the expected N_{LP} to σ^*_{P-X} in many systems. The situation was most clearly demonstrated with the case of NH_2:$P(CH_3)_2$ where N_{LP} to σ^*_{P-X} was effectively quenched and supplanted by P_{LP} to σ^*_{N-X} transfer with more than two-fold relative magnitude.[191]

NBO calculations also showed increased orbital interactions upon the addition of electron withdrawing groups to either, or both, of the pnictogens. With the substitution on phosphorus again, being markedly more effective. Curiously, the trends within the substituted systems run counter to the substituent electronegativity trend and in the case of phosphorus substitution, and counter to the calculated interaction energies. This is especially noteworthy in the substituted nitrogen systems, as while this is expected for N_{LP} to σ^*_{P-X} interactions, this also extends to the P_{LP} to σ^*_{N-X} transfer. The first of these oddities can be rationalised by the fact that the pnictogen bond distance follows the observed NBO trends, so it can be argued that the degree of orbital overlap results from the proximities of the interacting moieties, rather than that interaction being the driving force behind the association.[191] This is supported by the results of AIM calculations where the relevant bond critical points have very modest electron densities and Laplacians, which is indicative of predominantly closed shell interactions. The trend of the NBO energies for the substituted phosphorus species running counter to the trend in the isodesmic interaction energies is more complicated however. DFT minimised geometries (MP2/aug0-cc-pVDZ) and electron localisation function (ELF) calculations conducted on them, show that the nitrogen lone pair consistently faces the phosphorus σ-hole, rather than the other way around (Figure 1.34). This was also verified via a crystal structure database search of related structures,[192] which found that the average C-N···P angle was significantly wider than the average C-P···N angle.[191,193]

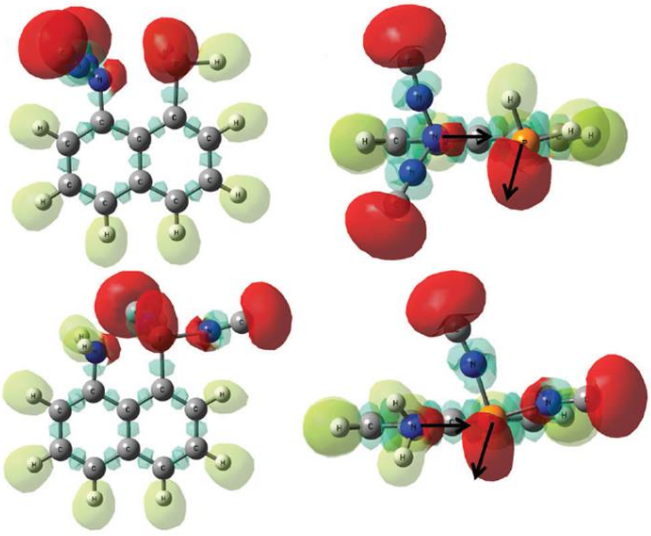

Figure 1.34: ELF isosurfaces for $N(NC)_2$:PH_2 (top) and NH_2:$P(NC)_2$ (bottom). Yellow, monosynaptic (hydrogenoid) basins; teal, disynaptic (double bond) basins; red, monosynaptic (lone pair) basins. Arrows denote the approximate locations of lone pairs.[191]

Some sense can be made of the observed discord between the trends by considering the dispersion interactions arising from the close contact between the polarisable halogen atoms to the donor species. Indeed, the chalcogen bond interaction energies also correlated with dispersion interaction coefficients.[194,195] The addition of Grime's D3 dispersion correction[122] revealed a trend of increasing interaction strength with increasing dispersion interaction coefficient. This relationship between dispersion and orbital interactions is unsurprising given the relative SAPT weightings and is very much in line with the findings of Sánchez-Sanz's homodimer studies discussed above.[188]

More recently, other dissection methodologies have been applied to pnictogen bonds. In 2021, Bickelhaupt and co-workers[196] applied canonical energy decomposition analysis and other computational methods to a $X_3Pn\cdots A^-$ model system. As might be expected using a hard electrostatics model, pnictogen bond strength increased with increasing pnictogen size, while increasing the halide ion size decreased pnictogen bond strength accompanying. The energy decomposition analysis revealed both attractive Coulombic and orbital interactions, while the Pauli exclusion was repulsive.[197-199] Interestingly, significant orbital interactions were observed, even for the lighter pnictogens; with the term making up between 34% to 64% of the total

attractive energy. The authors also employed Voronoi deformation density (VDD) analysis[200,201], which is a novel method for studying atomic charges, which rather than calculating specific atomic charges, tracks the movement of charge into or out of a defined Voronoi cell, which in this case was defined around the pnictogen atom. The VDD analysis revealed an increasing atomic charge associated with the heavier pnictogens. For example, a +0.21 change was observed for the F_3N donor *vs.* +0.57 for the F_3Sb donor. Whilst such changes obviously augment the electrostatic terms, the authors also point out the corresponding benefit to the orbital interaction, since the delocalisation results in the $\sigma^*_{Pn\text{-}X}$ acceptor orbital possessing a higher amplitude that allows for better HOMO-LUMO overlap, though it can also be argued that this can be seen as orbital interactions being strengthened by electrostatics. Figure 1.35 illustrates the relatively high degree of parallelism between the trends observed for the attractive electrostatic and orbital interaction energy terms in the energy decomposition analysis. The authors note that the same type of analysis yielded similar results for halogen and chalcogen bonds.[196,202-204]

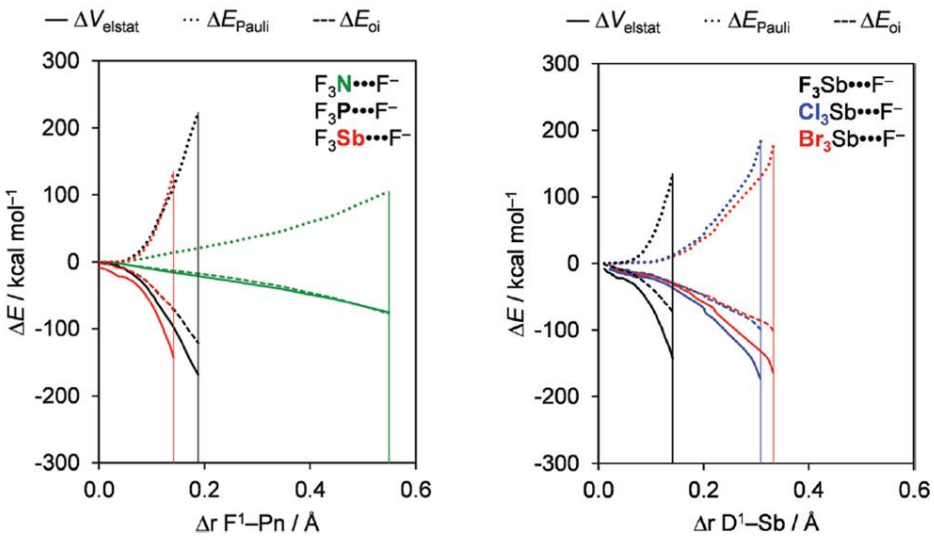

Figure 1.35: Energy decomposition analysis of to $X_3Pn\cdots A^-$ model systems. Left, on varying the pnictogen atom; right, on varying the X_3 substituents.[196]

The above findings contrast with Sanchez-Sanz's previously discussed work that found only small orbital interactions in some pnictogen bonds.[188,191] The pnictogen bonds examined by Bickelhaupt here were much stronger; employing charged acceptors. The fact that they differ from the longer range dispersive nitrogen

interactions should not be considered especially noteworthy. However, the different trends observed in the two studies from changing the halogen covalently bonded to the pnictogen atom is surprising. A σ-hole model based on substituent electronegativity would predict F_3Pn complexes to yield stronger pnictogen bonds than analogous Br_3Pn complexes. However, the inverse is reported by Bickelhaupt and co-workers in their 2021 paper,[196] as shown in Figure 1.36. This discrepancy can be resolved by considering the role of strain in these systems.[205-207] The same changes in electronegativity that change the strength of the X-Pn bond also influence the deepness of the σ-holes. Accordingly, the weaker Pn-Br covalent bonds can stretch more easily than the stronger Pn-F covalent bonds when adopting equilibrium geometries.

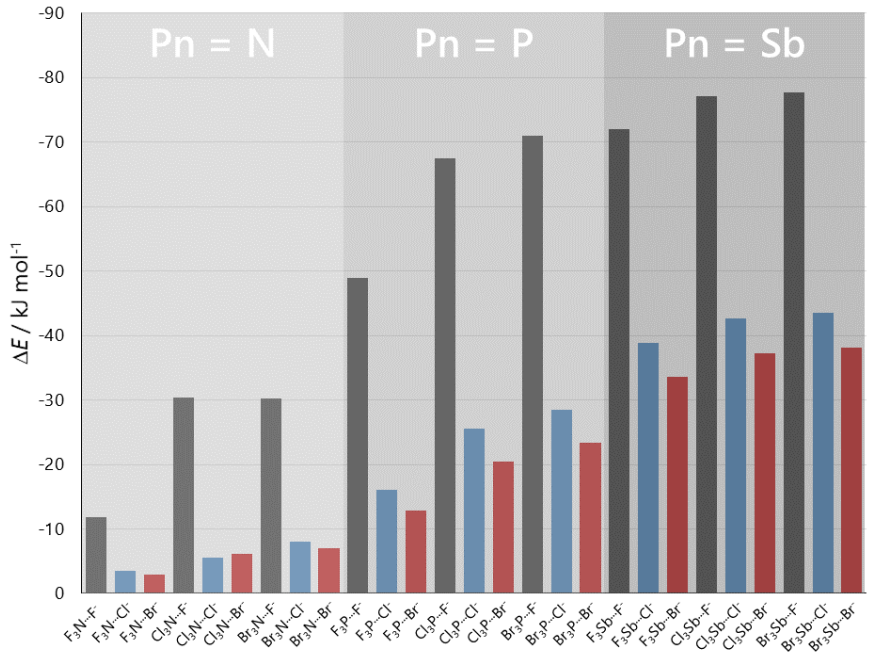

Figure 1.36: Graphical depiction of M06/QZ4P energies calculated for the $X_3Pn\cdots A^-$ model systems. $A^- = F^-$ (grey), Cl^- (blue); Br^- (red).[196]

Consequently, the proportionally greatest changes in pnictogen bond strength can be seen in the Pn = N complexes as the X-N covalent bonds are the weakest. Voronoi deformation density reveals that the atomic charges associated with the pnictogen cell can be seen to increase in positivity in response to X-Pn bond expansions; this has a greater effect on the depth of the σ-hole than the substituent electronegativity. Interestingly, the relative weakness of the fluorine-substituted pnictogen bond donors can be seen to be partially result from the limited capacity of strong F-Pn covalent

bonds to extend. Indeed, Figure 1.35 (right) shows that the fluorinated example reaches the zenith of its electrostatic and orbital enhancements upon changing the X^- pnictogen bond distance much earlier than the heavier halogen analogues.

Throughout, Bickelhaupt and co-workers comment on the many similarities between pnictogen,[196] halogen,[202] chalcogen,[203] and hydrogen bonds.[202,204] They note that the interaction energies fall in a broadly similar range, and that strong orbital components occur in all of them, and contributing up to 65% 97%, 76% and 66% of the attractive terms, respectively.[202-204] Indeed, the authors describe the results of this paper as consolidating earlier works. Furthermore, the model presented here is also very similar to what has been observed for interactions between anions and alkali or coinage metals.[204] Interestingly, this portfolio of work suggests that halogen, chalcogen, and pnictogen bonds have the potential to be noticeably stronger than hydrogen bonds; not only due to their stronger orbital interactions, but in the enhanced electrostatic forces resultant from these interactions.[196] Such a conclusion contradicts what might be expected based on examining the electrostatic potentials of the isolated pnictogen bond donor; $V_{s,max}$ values would place hydrogen bonds as typically being stronger.[14,20,21,208]

1.8 σ-hole interaction comparisons

Comparison between σ-hole interactions and hydrogen bonds are often made and with good reason. Arunan and co-workers have compared halogen bonds and hydrogen bonds to lithium bonds.[209] Employing Bader's atoms in molecules (AIM) theory,[189] strong correlations between the electron density at the bond critical points (BCPs) and the bond strengths were observed for all three interactions (Figure 1.37). However, the authors note that while the slopes for hydrogen and halogen bonds are very comparable, lithium bonds see significantly steeper slopes. The positive Laplacian values for all three interactions are indicative of predominantly closed-shell interactions, but the far more positive values for the lithium bond suggest a near purely ionic interaction. The close to zero Laplacian vales for the halogen bonds and hydrogen bonds indicate only a slight covalent character, which is supported by NBO calculations.

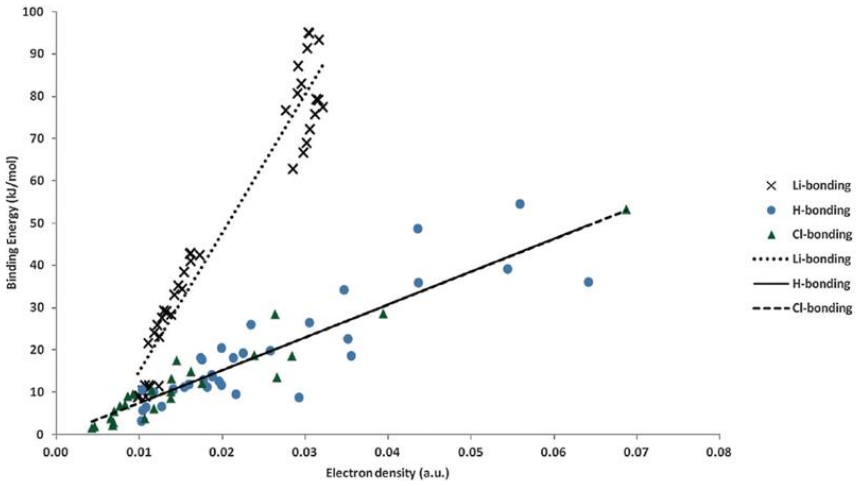

Figure 1.37: Plot of BSSE-corrected MP2/aug-cc-PVTZ energies and BCP electron densities for HB, LiB and XB (Cl only) complexes studied by Arunan *et al.*[209]

In addition to highlighting similarities, the supporting NBO calculations also reveal subtle differences between the hydrogen and halogen bonds. While hydrogen-bond formation results in a loss of covalent character and proportional increase in iconicity in the H-R bond, halogen-bond formation only sees an accompanying loss of covalence in the X-R bond. Bickelhaupt and co-workers also point out orbital interaction differences between hydrogen and halogen/chalcogen/pnictogen bonds; noting that the small size of hydrogen results in less Pauli repulsion due to the absence of overlap between the HOMO of the bond acceptor and the filled high-energy atomic orbitals of the bond donor.[196,202,203] Indeed, differences between halogen bonds and hydrogen bonds have been described by many authors, often with an emphasis being placed on the role that dispersion plays in halogen bonding due the inherently higher polarisabilty of heavier atoms.[98,202,210-212] A 2019 study by Frontera and co-workers[213] investigated halogen and hydrogen bonds involving hypohalous acid donors, and found remarkable similarities between the two in terms of electrostatic and orbital interactions. They noted that the dispersion terms were dependent upon the size of the halogens in the halogen bonds, but this term was of course, approximately constant for the hydrogen bonded complexes (due to the constant hydrogen bond donor atom).

As has been discussed above, the relative weightings and behaviours of the attractive and repulsive forces that drive σ-hole interactions are highly dependent on the identities of both the acceptor and donor species. As originally outlined by Politzer

and co-workers,[12-21] σ-hole depth is encoded by the electrostatic surface potential and this serves as useful first approximation for predicting interaction strength. However, numerous examples of this identifier falling short have been identified and presented above. Critically, examples of these cases have been demonstrated not only by calculation, but by empirical measurements of various bonding systems.[53,55,89,111,112,151] Furthermore, energetic dissections have demonstrated that stable halogen bonded systems can be dominated by either dispersive forces or electron sharing interactions as well as the commonly discussed electrostatic forces. In light of this, it is not accurate to reference only one of the partially motivating forces driving the interaction. The situation is baked into the IUPAC definition of the halogen bond, which clearly references the multitude of forces involved.[1] Given the high degree of similarity in the nature of halogen, chalcogen, and pnictogen bonds, but also hydrogen bonds,[60,75,105,209] tetrel bonds,[14,18,214], triel bonds,[215-218] beryllium bonds,[219,220] aerogen bonds,[221,222] lithium bonds,[223-225] alkali metal interactions[226] and coinage/other metal interactions[204,227-229] several authors have argued the need for a broad definition for this collection of interactions.[14,229] Throughout this chapter the term σ-hole interaction has been used, but as initially prefaced, this is used due to a lack of a better alternative. The σ-hole is indeed a common theme in these interactions; even in anti-electrostatic interactions the σ-hole is still present, meaning that positive electrostatic potential is a common, but not a defining characteristic.[53,55,72] The issue with such a term is that it invites neglect of dispersion and electron delocalisation forces that can often play important, if not primary roles. The same issue exists with the term *weak non-covalent interaction* that is also in common parlance, as it is not uncommon for these interactions to possess at least some covalent character. A zenith case can be provided by halogen bond examples, such as the IF···F^- reported by Bickelhaupt and Wolters, that are nearly entirely driven by orbital interactions (97%).[202] A more inclusive term that is representative of the multifaceted forces behind these interactions is needed.

1.9 References

1 Desiraju, G. R., Ho, P. S., Kloo, L., Legon, A. C., Marquardt, R., Metrangolo, P., Politzer, P., Resnati, G. & Rissanen, K. Definition of the halogen bond. *Pure Appl. Chem.* **85**, 1711-1713 (2013).

2 Cavallo, G., Metrangolo, P., Milani, R., Pilati, T., Priimagi, A., Resnati, G. & Terraneo, G. The Halogen Bond. *Chem. Rev.* **116**, 2478-2601 (2016).

3 Dumas, J.-M., Kern, M. & Janier-Dubry, J. L. Cryoscopic and Calorimetric Study of MX4-Polar Organic Base Interactions (M = C, Si, X = Cl, Br)—Influence of Element and of Halogen. *Bull. Soc. Chim. Fr.* **11**, 1785–1790 (1976).

4 Guthrie, F. XXVIII.—On the iodide of iodammonium. *J. Chem. Soc.* **16**, 239-244 (1863).

5 Mulliken, R. S. Structures of Complexes Formed by Halogen Molecules with Aromatic and with Oxygenated Solvents. *J. Am. Chem. Soc.* **72**, 600–608 (1950).

6 Hassel, O. Structural Aspects of Interatomic Charge-Transfer Bonding. *Science* **170**, 497-502 (1970).

7 Bonaccorsi, R., Scrocco, E. & Tomasi, J. Molecular SCF Calculations for the Ground State of Some Three-Membered Ring Molecules: $(CH_2)_3$, $(CH_2)_2NH$, $(CH_2)_2NH_2$+, $(CH_2)_2O$, $(CH_2)_2S$, $(CH)_2CH_2$, and N_2CH_2. *J. Chem. Phys.* **52**, 5270-5284 (1970).

8 Scrocco, E. & Tomasi, J. The electrostatic molecular potential as a tool for the interpretation of molecular properties. In: New Concepts II. Topics in Current Chemistry Fortschritte der Chemischen Forschung. *Springer, Berlin, Heidelberg.* **42** (1973).

9 Murray, J. S., Paulsen, K. & Politzer, P. Molecular surface electrostatic potentials in the analysis of non-hydrogen-bonding noncovalent interactions. *Proc. Indian Acad. Sci. (Chem. Sci.)* **106**, 267-275 (1994).

10 Murray, J. S. & Politzer, P. Correlations between the solvent hydrogen-bond-donating parameter .alpha. and the calculated molecular surface electrostatic potential. *J. Org. Chem.* **56**, 6715–6717 (1991).

11 Tomasi, J., Bonaccorsi, R. & Cammi, R. Theoretical models of chemical bonding. *Springer-Verlag, Berlin.* (1991).

12 Clark, T., Hennemann, M., Murray, J. S. & Politzer, P. Halogen bonding: the σ-hole. *J. Mol. Model.* **13**, 291–296 (2007).

13 Politzer, P., Murray, J. S. & Clark, T. Halogen bonding: an electrostatically-driven highly directional noncovalent interaction. *Phys. Chem. Chem. Phys.* **12**, 7748-7757 (2010).

14 Politzer, P., Murray, J. S. & Clark, T. Halogen bonding and other σ-hole interactions: a perspective. *Phys. Chem. Chem. Phys.* **15**, 11178--11189 (2013).

15 Politzer, P. & Murray, J. S. Halogen Bonding: An Interim Discussion. *ChemPhysChem* **14**, 278 – 294 (2013).

16 Clark, T. σ -Holes. *WIREs Comput. Mol. Sci.* **3**, 13−20 (2013).

17 Clark, T., Politzer, P. & Murray, J. S. Correct electrostatic treatment of noncovalent interactions: the importance of polarization. *WIREs Comput. Mol. Sci.* **5**, 169-177 (2015).

18 Politzer, P., Murray, J. S., Clark, T. & Resnati, G. The σ-hole revisited. *Phys.Chem.Chem.Phys.* **19**, 32166-32178 (2017).

19 Murray, J. S., Lane, P., Clark, T. & Politzer, P. σ-hole bonding: molecules containing group VI atoms. *J. Mol. Model.* **13**, 1033–1038 (2007).

20 Riley, K. E., Murray, J. S., Fanfrlik, J., Rezac, J., Sola, R. J., Concha, M. C., Ramos, F. M. & Politzer, P. Halogen bond tunability II: the varying roles of electrostatic and

dispersion contributions to attraction in halogen bonds. *J. Mol. Model* **19**, 4651-4659 (2013).

21 Politzer, P., Murray, J. S. & Clark, T. Explicit Inclusion of Polarizing Electric Fields in σ- and π-Hole Interactions. *J. Phys. Chem. A* **123**, 10123−10130 (2019).

22 Stewart, R. F. On the mapping of electrostatic properties from bragg diffraction data. *Chem. Phys. Lett.* **65**, 335-342 (1979).

23 Politzer, P. & Truhlar, D. G. *Chemical Applications of Atomic and Molecular Electrostatic Potentials*. 1 edn, (Springer, 1981).

24 Klein, C. L. & Stevens, E. D. *Structure and Reactivity*. 25-64 (VCH, 1988).

25 Mallada, B., Gallardo, A., Lamanec, M., Torre, B. D. L., Spirko, V., Hobza, P. & Jelinek, P. Real-space imaging of anisotropic charge of σ-hole by means of Kelvin probe force microscopy. *Science* **374**, 863-867 (2021).

26 Bundhun, A., Ramasami, P., Murray, J. S. & Politzer, P. Trends in σ-hole strengths and interactions of F3MX molecules (M = C, Si, Ge and X = F, Cl, Br, I). *J. Mol. Model.* **19**, 2739–2746 (2013).

27 Riley, K. E., Murray, J. S., Fanfrlik, J., Rezac, J., Sola, R. J., Concha, M. C., Ramos, F. M. & Politzer, P. Halogen bond tunability I: the effects of aromatic fluorine substitution on the strengths of halogen-bonding interactions involving chlorine, bromine, and iodine. *J. Mol. Model.* **17**, 3309-3318 (2011).

28 Metrangolo, P., Murray, J. S., Pilati, T., Politzer, P., Resnati, G. & Terraneo, G. Fluorine-Centered Halogen Bonding: A Factor in Recognition Phenomena and Reactivity. *Cryst. Growth. Des* **11**, 4238-4246 (2011).

29 Legon, A. C. Prereactive complexes of dihalogens XY with Lewis Bases B in the gas phase: a systematic case for the halogen analogue B···XY of the hydrogen bond B···HX. *Angew. Chem. Int. Ed* **38**, 2686-2714 (1999).

30 Chopra, D. & Row, T. N. G. Role of organic fluorine in crystal engineering. *CrystEngComm* **13**, 2175--2186 (2011).

31 Metrangolo, P., Murray, J. S., Pilati, T., Politzer, P., Resnati, G. & Terraneo, G. The fluorine atom as a halogen bond donor, viz. a positive site. *CrystEngComm* **13**, 6593–6596 (2011).

32 Bauza, A., Quinonero, D., Frontera, A. & Deya, P. M. Substituent effects in halogen bonding complexes between aromatic donors and acceptors: a comprehensive ab initio study. *Phys. Chem. Chem. Phys.* **13**, 20371-20379 (2011).

33 Wang, C., Fu, Y., Zhang, L., Danovich, D., Shaik, S. & Mo, Y. Hydrogen- and Halogen-Bonds between Ions of like Charges: Are They Anti-Electrostatic in Nature? *J. Comput. Chem* **39**, 481–487 (2018).

34 Weinhold, F. & Klein, R. A. Anti-Electrostatic Hydrogen Bonds. *Angew. Chem. Int. Ed.* **53**, 11214 –11217 (2014).

35 Weinhold, F. & Klein, R. A. Improved General Understanding of the Hydrogen-Bonding Phenomena: A Reply. *Angew. Chem.* **127**, 2636 – 2638 (2015).

36 Frenking, G. & Caramori, G. F. No Need for a Re-examination of the Electrostatic Notation of the Hydrogen Bonding: A Comment *Angew. Chem. Int. Ed.* **54**, 2596 – 2599 (2015).

37 Weinhold, F. & Klein, R. A. Addendum: Anti-Electrostatic Hydrogen Bonds. *Angew. Chem. Int. Ed* **54**, 12992-12992 (2014).

38 Lee, S. & Beauchamp, J. L. Fourier transform ion cyclotron resonance study of multiply charged aggregates of small singly charged peptides formed by electrospray ionization. *J. Am. Soc. Mass Spectrom.* **10**, 347–351 (1990).

39 Feketeova, L. & O'Hair, R. A. J. Multiply protonated betaine clusters are stable in the gas phase. *Chem. Commun.*, 4942–4944 (2008).

40 Kass, S. R. Zwitterion-Dianion Complexes and Anion-Anion Clusters with Negative Dissociation Energies. *J. AM. CHEM. SOC.* **127**, 13098-13099 (2005).

41 Shokri, A., Ramezani, M., Fattahi, A. & Kass, S. R. Electrostatically Defying Cation–Cation Clusters: Can Likes Attract in a Low-Polarity Environment? *J. Phys. Chem. A* **117**, 9252–9258 (2013).

42 Mata, I., Alkorta, I., Monlins, E. & Espinosa, E. Electrostatics at the Origin of the Stability of Phosphate-Phosphate Complexes Locked by Hydrogen Bonds. *CHEMPHYSCHEM* **13**, 1421-1424 (2012).

43 Riley, K. E. & Hobza, P. Investigations into the Nature of Halogen Bonding Including Symmetry Adapted Perturbation Theory Analyses. *J. Chem. Theory Comput.* **4**, 232-242 (2008).

44 Frontera, A., Gamez, P., Mascal, M., Mooibroek, T. J. & Reedijk, J. Putting Anion–π Interactions Into Perspective. *Angew. Chem. Int. Ed* **50**, 9564-9583 (2011).

45 Murray, J. S., Shields, Z. P.-I., Seybold, P. G. & Politzer, P. Intuitive and counterintuitive noncovalent interactions of aromatic regions with the hydrogen and the nitrogen of HCN. *J. Comput. Sci.* **10**, 209–216 (2015).

46 Bauza, A., Frontera, A., Mooibroek, T. J. & Reedijk, J. The N-atom in $[N(PR_3)_2]$+ cations (R = Ph, Me) can act as electron donor for (pseudo) antielectrostatic interactions. *CrystEngComm* **17**, 3768–3771 (2015).

47 Mooibroek, T. J. Coordinated nitrate anions can be directional π-hole donors in the solid state: a CSD study. *CrystEngComm* **19**, 4485–4488 (2017).

48 Novak, M., Marek, R. & Foroutan-Nejad, C. Anti-Electrostatic CH–Ion Bonding in Decorated Graphanes. *Chem. Eur. J.* **23**, 14931 –14936 (2017).

49 Mo, Y. Geometrical optimization for strictly localized structures. *J. Chem. Phys.* **119**, 1300-1306 (2003).

50 Mo, Y., Song, L. & Lin, Y. Block-Localized Wavefunction (BLW) Method at the Density Functional Theory (DFT) Level. *J. Phys. Chem. A* **111**, 8291–8301 (2007).

51 Mo, Y., Song, L., Wu, W., Cao, Z. & Zhang, Q. Electronic Delocalization: A Quantitative Study From Modern Ab Initio Valence Bond Theory. *J Theor Comput Chem* **1**, 137 (2002).

52 Mo, Y. & Peyerimhoff, S. D. Theoretical analysis of electronic delocalization. *J. Chem. Phys.* **109**, 1687-1697 (1998).

53 Holthoff, J. M., Engelage, E., Weiss, R. & Huber, S. M. "Anti-Electrostatic" Halogen Bonding. *Angew. Chem. Int. Ed* **59**, 11150–11157 (2020).

54 Engelage, E., Schulz, N., Heinen, F., Huber, S. M., Truhlar, D. G. & Cramer, C. J. Refined SMD Parameters for Bromine and Iodine Accurately Model Halogen-Bonding Interactions in Solution. *Chem. Eur. J.* **24**, 15983 –15987 (2018).

55 Loy, C., Holthoff, J. M., Weiss, R., Huber, S. M. & Rosokha, S. V. "Anti-electrostatic" halogen bonding in solution. *Chem. Sci.* **12**, 8246–8251 (2021).

56 Bader, R. F. W. A Quantum Theory of Molecular Structure and Its Applications. *Chem. Rev.* **91**, 893-928 (1991).

57 Johnson, E. R., Keinan, S., Mori-Sanchez, P., Contreras-Garcia, J., Cohen, A. J. & Yang, W. Revealing Noncovalent Interactions. *J. Am. Chem. Soc.* **132**, 6498–6506 (2010).

58 Contreras-Garcia, J., Johnson, E. R., Keinan, S., Chaudret, R., Piquemal, J.-P., Beratan, D. N. & Yang, W. NCIPLOT: A Program for Plotting Noncovalent Interaction Regions. *J. Chem. Theory Comput.* **7**, 625–632 (2010).

59 Stone, A. J. Are Halogen Bonded Structures Electrostatically Driven? *J. Am. Chem. Soc.* **135**, 7005-7009 (2013).

60 Hennemann, M., Murray, J. S., Politzer, P., Riley, K. E. & Clark, T. Polarization-induced σ-holes and hydrogen bonding. *J. Mol. Model* **18**, 2461–2469 (2012).

61 Huber, S. M., Jimenez-Izal, E., Ugalde, J. M. & Infante, I. Unexpected trends in halogen-bond based noncovalent adducts. *Chem. Commun.* **48**, 7708–7710 (2012).

62 Foster, J. P. & Weinhold, F. Natural Hybrid Orbitals. *J. Am. Chem. Soc.* **102**, 7211-7218 (1980).

63 Reed, A. E., Weinstock, R. B. & Weinhold, F. Natural population analysis. *J. Chem. Phys.* **83**, 735-746 (1985).

64 J.A. Montgomery, J., Frisch, M. J., Ochterski, J. W. & Petersson, G. A. A complete basis set model chemistry. VI. Use of density functional geometries and frequencies. *J. Chem. Phys.* **110**, 2822-2827 (1999).

65 J.A. Montgomery, J., Frisch, M. J., Ochterski, J. W. & Petersson, G. A. A complete basis set model chemistry. VII. Use of the minimum population localization method. *J. Chem. Phys.* **112**, 6532-6542 (2000).

66 Maxson, T., Jalilov, A. S., Zeller, M. & Rosokha, S. V. Halogen Bonding Between Anions: Association of Anion Radicals of Tetraiodo-p-benzoquinone with Iodide Anions. *Angew. Chem. Int. Ed.* **59**, 17197–17201 (2020).

67 Sawar, M. G., Dragisic, B., Sagoo, S. & Taylor, M. S. A Tridentate Halogen-Bonding Receptor for Tight Binding of Halide Anions. *Angew. Chem. Int. Ed* **49**, 1674 –1677 (2010).

68 Tepper, R., Schulze, B., Jager, M., Friebe, C., Scharf, D. H., Gorls, H. & Schbert, U. S. Anion Receptors Based on Halogen Bonding with Halo-1,2,3-triazoliums. *J. Org. Chem.* **80**, 3139−3150 (2015).

69 Rosokha, S. V. & Traversa, A. From charge transfer to electron transfer in halogen-bonded complexes of electrophilic bromocarbons with halide anions. *Phys. Chem. Chem. Phys.* **17**, 4989--4999 (2015).

70 Watson, B., Grounds, O., Borley, W. & Rosokha, S. V. Resolving the halogen vs. hydrogen bonding dichotomy in solutions: intermolecular complexes of trihalomethanes with halide and pseudohalide anions. *Phys.Chem.Chem.Phys.* **20**, 21999--22007 (2018).

71 Kepler, S., Zeller, M. & Rosokha, S. V. Anion−π Complexes of Halides with p-Benzoquinones: Structures, Thermodynamics, and Criteria of Charge Transfer to Electron Transfer Transition. *J. Am. Chem. Soc.* **141**, 9338–9348 (2019).

72 Murray, J. S. & Politzer, P. Can Counter-Intuitive Halogen Bonding Be Coulombic? *CHEMPHYSCHEM* **22**, 1201– 1207 (2021).

73 III, R. D. J. in *NIST Computational Chemistry Comparison and Benchmark Data Base* Vol. 101 (2018).

74 Murray, J. S. & Politzer, P. Interaction and Polarization Energy Relationships in σ-Hole and π-Hole Bonding. *Crystals* **10**, 76(71-16) (2020).

75 Murray, J. S. & Politzer, P. Hydrogen Bonding: A Coulombic σ-Hole Interaction. *J. Indian Inst. Sci.* **100**, 21–30 (2020).

76 Brinck, T. & Borrfors, A. N. Electrostatics and polarization determine the strength of the halogen bond: a red card for charge transfer. *J. Mol. Model.* **25**, 125- (2019).

77 Wang, C., Danovich, D., Mo, Y. & Shaik, S. On The Nature of the Halogen Bond. *J. Chem. Theory Comput.* **10**, 3726−3737 (2014).

78 Hill, J. G. & Legon, A. C. On the directionality and non-linearity of halogen and hydrogen bonds. *Phys. Chem. Chem. Phys.* **17**, 858-867 (2015).

79 Cooper, D. L. *Valance Bond Theory*. (Elsevier, 2002).

80 Gallup, G. A. *Valence Bond Methods: Theory and Applications*. (Cambridge University Press, 2002).

81 Shaik, S. & Hiberty, P. C. *A Chemist's Guide to Valence Bond Theory*. Vol. Hoboken N.J. (Wiley-Interscience, 2008).

82 Wu, W., Su, P., Shaik, S. & Hiberty, P. C. Classical Valence Bond Approach by Modern Methods. *Chem. Rev.* **111**, 7557–7593 (2011).

83 Mo, Y., Bao, P. & Gao, J. Energy decomposition analysis based on a block-localized wavefunction and multistate density functional theory. *Phys. Chem. Chem. Phys.* **13**, 6760–6775 (2011).

84 Mo, Y., Gao, J. & Peyerimhoff, S. D. Energy decomposition analysis of intermolecular interactions using a block-localized wave function approach. *J. Chem. Phys.* **112**, 5530-5538 (2000).

85 Mo, Y., Subramanian, G., Gao, J. & Ferguson, D. M. Cation−π Interactions: An Energy Decomposition Analysis and Its Implication in δ-Opioid Receptor−Ligand Binding. *J. Am. Chem. Soc.* **124**, 4832–4837 (2002).

86 Inscoe, B., Rathnayake, H. & Mo, Y. Role of Charge Transfer in Halogen Bonding. *J. Phys. Chem. A* **125**, 2944−2953 (2021).

87 Khaliullin, R. Z., Cobar, E. A., Lochan, R. C., Bell, A. T. & Head-Gordon, M. Unravelling the Origin of Intermolecular Interactions Using Absolutely Localized Molecular Orbitals. *J. Phys. Chem. A* **111**, 8753-8765 (2007).

88 Thirman, J., Engelage, E., Huber, S. M. & Head-Gordon, M. Characterizing the interplay of Pauli repulsion, electrostatics, dispersion and charge transfer in halogen bonding with energy decomposition analysis. *Phys. Chem. Chem. Phys.* **20**, 905--915 (2018).

89 Sarwar, M. G., Dragisic, B., Salsberg, L. J., Gouliaras, C. & Taylor, M. S. Thermodynamics of Halogen Bonding in Solution: Substituent, Structural, and Solvent Effects. *J. Am. Chem. Soc.* **132**, 1646–1653 (2010).

90 Messina, M. T., Metrangolo, P., Panzeri, W., Ragg, E. & Resnati, G. Perfluorocarbon-hydrocarbon self-assembly. Part 3. Liquid phase interactions between perfluoroalkylhalides and heteroatom containing hydrocarbons. *Tetrahedron Lett* **39**, 9069–9072 (1998).

91 Lunghi, A., Cardillo, P., Messina, T., Metrangolo, P., Panzeri, W. & Resnati, G. Perfluorocarbon—hydrocarbon self assembling. Thermal and vibrational analyses of one-dimensional networks formed by α,ω-diiodoperfluoroalkanes with K.2.2. and K.2.2.2. *J. Fluorine Chem.* **97**, 191-194 (1998).

92 Cabot, R. & Hunter, C. A. Non-covalent interactions between iodo-perfluorocarbons and hydrogen bond acceptors. *Chem. Commun.*, 2005–2007 (2009).

93 Robertson, C. C., Perutz, R. N., Brammer, L. & Hunter, C. A. A solvent-resistant halogen bond. *Chem. Sci.* **5**, 4179–4183 (2014).

94 Reichardt, C. *Solvents and Solvent Effects in Organic Chemistry, 3rd, Updated and Enlarged Edition*. (Wiley-VCH, 2006).

95 Dong, D. C. & Winnik, M. A. The Py scale of solvent polarities. *Can. J. Chem.* **62**, 2560-2565 (1984).

96 Metrangolo, P. & Resnati, G. Halogen Versus Hydrogen. *Science* **321**, 918-919 (2008).

97 Corradi, E., Meille, S. V., Messina, M. T., Metrangolo, P. & Resnati, G. Halogen Bonding versus Hydrogen Bonding in Driving Self-Assembly Processes. *Angew. Chem. Int. Ed* **39**, 1782-1786 (2000).

98 Aakeroy, C. B., Fasulo, M., Schltheiss, N., Desper, J. & Moore, C. Structural Competition between Hydrogen Bonds and Halogen Bonds. *J. Am. Chem. Soc.* **129**, 13772-13773 (2007).

99 Boys, S. F. & Bernardi, F. The calculation of small molecular interactions by the differences of separate total energies. Some procedures with reduced errors. *Mol. Phys.* **19**, 553-566 (1970).

100 Parker, T. M., Burns, L. A., Parrish, R. M., Ryno, A. G. & Sherrill, C. D. Levels of symmetry adapted perturbation theory (SAPT). I. Efficiency and performance for interaction energies. *J. Chem. Phys.* **140**, 094106 (2014).

101 Hohenstein, E. G. & Sherrill, C. D. Density fitting of intramonomer correlation effects in symmetry-adapted perturbation theory. *J. Chem. Phys.* **133**, 014101 (2010).

102 Sedlak, R., Kolar, M. H. & Hobza, P. Polar Flattening and the Strength of Halogen Bonding. *J. Theor. Comput. Chem.* **11**, Polar Flattening and the Strength of Halogen Bonding (2015).

103 Kerdawy, A. E., Murray, J. S., Politzer, P., Bleiziffer, P., Heßelmann, A., Gorling, A. & Clark, T. Directional Noncovalent Interactions: Repulsion and Dispersion. *J. Chem. Theory Comput.* **9**, 2264−2275 (2013).

104 Adhikari, U. & Scheiner, S. Sensitivity of pnicogen, chalcogen, halogen and H-bonds to angular distortions. *Chem. Phys. Lett.* **532**, 31-35 (2012).

105 Shields, Z. P., Murray, J. S. & Politzer, P. Directional Tendencies of Halogen and Hydrogen Bonds. *Int. J. Quantum Chem.* **110**, 2823–2832 (2010).

106 Bondi, A. van der Waals Volumes and Radii. *J. Phys. Chem.* **68**, 441-451 (1964).

107 Nyburg, S. C. 'Polar Flattening': Non-Spherical Effective Shapes of Atoms in Crystals. *Acta. Cryst.* **A35**, 641-645 (1979).

108 Murray, J. S. & Politzer, P. Molecular Surfaces, van der Waals Radii and Electrostatic Potentials in Relation to Noncovalent Interactions. *Croat. Chem. Acta* **82**, 267-275 (2009).

109 Bader, R. F. W., Carroll, M. T., Cheeseman, J. R. & Chang, C. Properties of Atoms in Molecules: Atomic Volumes. *J. Am. Chem. Soc.* **109**, 7968-7979 (1987).

110 Riley, K. E. & Hobza, P. The relative roles of electrostatics and dispersion in the stabilization of halogen bonds. *Phys. Chem. Chem. Phys.* **15**, 17742-17751 (2013).

111 Nunzi, F., Erasmo, B. D., Tarantelli, F., Cappelletti, D. & Pirani, F. The Halogen-Bond Nature in Noble Gas–Dihalogen Complexes from Scattering Experiments and Ab Initio Calculations. *Molecules* **24**, 4274-4294 (2019).

112 Pirani, F., Cappelletti, D., Falcinelli, S., Cesario, D., Nunzi, F., Belpassi, L. & Tarantelli, F. Selective Emergence of the Halogen Bond in Ground and Excited States of Noble-Gas–Chlorine Systems. *Angew. Chem. Int. Ed* **58**, 4195 –4199 (2019).

113 Rohrbacker, A., Halberstadt, N. & Junda, K. C. The Dynamics of Noble Gas–HalogenMolecules and Clusters. *Annu. Rev. Phys. Chem.* **51**, 405-433 (2000).

114 Beswick, J. A., Halberstat, N. & Janda, K. C. Structure and dynamics of noble gas-halogen and noble gas ionic clusters: When theory meets experiment. *Chem. Phys.* **399**, 4-16 (2012).

115 Naumkin, F. Y. & McCourt, F. R. W. Contributions of the two conformers to the microwave spectrum and scattering crosssection of the He-Cl_2 van der Waals system,evaluated from an ab initio potential energy surface. *J. Chem. Phys.* **108**, 9301-9312 (1998).

116 Cappelletti, D., Cinti, A., Nicoziani, A., Falcinelli, S. & Pirani, F. Molecular Beam Scattering Experiments as a Sensitive Probe of the Interaction in Bromine–Noble Gas Complexes. *Front. Chem.* **17**, 1-10 (2019).

117 Nunzi, F., Cesario, D., Belpassi, L., Tarantelli, F., Roncaratti, L. F., Falcinelli, S., Cappelletti, D. & Pirani, F. Insight into the halogen-bond nature of noble gas-chlorine systems by molecular beam scattering experiments, ab initio calculations and charge displacement analysis. *Phys. Chem. Chem. Phys.* **21**, 7330-7340 (2019).

118 Pirani, F., Brizi, S., Roncaratti, L. F., Casavecchia, P., Cappelletti, D. & Vecchiocattivi, F. Beyond the Lennard-Jones model: a simple and accurate potential function probed by high resolution scattering data useful for molecular dynamics simulations. *Phys. Chem. Chem. Phys.* **10**, 5489–5503 (2008).

119 Bauza, A. & Frontera, A. Competition between Halogen Bonding and π-Hole Interactions Involving Various Donors: The Role of Dispersion Effects. *CHEMPHYSCHEM* **16**, 3108 – 3113 (2015).

120 Bene, J. E. D., Alkorta, I. & Elguero, J. Properties of Complexes $H_2C=(X)P:PXH_2$, for X = F, Cl, OH, CN, NC, CCH, H, CH_3, and BH_2: P···P Pnicogen Bonding at σ-Holes and π-Holes. *J. Phys. Chem. A* **117**, 11592−11604 (2013).

121 Solimannejad, M., V.Ramezani, Trujillo, C., Alkorta, I., Sanchez-Sanz, G. & Elguero, J. Competition and Interplay between σ-Hole and π-Hole Interactions: A Computational Study of 1:1 and 1:2 Complexes of Nitryl Halides (O_2NX) with Ammonia. *J. Phys. Chem. A* **116**, 5199−5206 (2012).

122 Grimme, S., Antony, J., Ehrlich, S. & Krieg, H. A consistent and accurate ab initio parametrization of density functional dispersion correction (DFT-D) for the 94 elements H-Pu. *J. Chem. Phys.* **132**, 154104 (2010).

123 Caldeweyher, E., Ehlert, S., Hansen, A., Neugebauer, H., Spicher, S., Bannwarth, C. & Grimme, S. A generally applicable atomic-charge dependent London dispersion correction. *J. Chem. Phys.* **150**, 154122 (2019).

124 Caldeweyher, E., Mewes, J.-M., Ehlert, S. & Grimme, S. Extension and evaluation of the D4 London-dispersion model for periodic systems. *Phys. Chem. Chem. Phys.* **22**, 8499-8512 (2020).

125 Lommerse, J. P. M., Stone, A. J., Taylor, R. & Allen, F. H. The Nature and Geometry of Intermolecular Interactions between Halogens and Oxygen or Nitrogen. *J. Am. Chem. Soc.* **118**, 3108-3116 (1996).

126 Fischer, C. F. General Hartree-Fock program. *Comput. Phys. Commun.* **43**, 355-365 (1987).

127 Peterson, K. A. Systematically convergent basis sets with relativistic pseudopotentials. I. Correlation consistent basis sets for the post-d group 13–15 elements. *J. Chem. Phys.* **119**, 11099 (2003).

128 Dunning, T. H. Gaussian basis sets for use in correlated molecular calculations. I. The atoms boron through neon and hydrogen. *J. Chem. Phys.* **90**, 1007 (1989).

129 Halkier, A., Helgaker, T., Jorgensen, P., Klopper, W., Koch, H., Olsen, J. & Wilson, A. K. Basis-set convergence in correlated calculations on Ne, N_2, and H_2O. *Chem. Phys. Lett.* **286**, 243–252 (1998).

130 Politzer, P., Lane, P., Concha, M. C., Ma, Y. & Murray, J. S. An overview of halogen bonding. *J. Mol. Model.* **13**, 305–311 (2007).

131 Aakeroy, C. B., Bryce, D. L., Desiraju, G. R., Frontera, A., Legon, A. C., Nicotra, F., Rissanen, K., Scheiner, S., G.Terraneo, Metrangolo, P. & Resnati, G. Definition of the chalcogen bond (IUPAC Recommendations 2019). *Pure Appl. Chem.* **91**, 1889–1892 (2019).

132 Hofmann, A. W. Chemische Untersuchung der organischen Basen im Steinkohlen-Theeröl (Chemical investigation of the organic bases in coal tar oil). *Justus Liebigs Ann. Chem.* **47**, 37-87 (1843).

133 Rosenfield, R. E., Parthasarathy, R. & Dunitz, J. D. Directional Preferences of Nonbonded Atomic Contacts with Divalent Sulfur. 1. Electrophiles and Nucleophiles. *J. Am. Chem. Soc.* **99**, 4860−4862 (1977).

134 Murray, J. S., Resnati, G. & Politzer, P. Close contacts and noncovalent interactions in crystals. *Faraday Discuss.* **203**, 113-130 (2017).

135 Clark, T., Murray, J. S. & Politzer, P. The σ-Hole Coulombic Interpretation of Trihalide Anion Formation. *ChemPhysChem* **19**, 3044–3049 (2018).

136 Iwaoka, M., Takemoto, S. & Tomoda, S. Statistical and Theoretical Investigations on the Directionality of Nonbonded S···O Interactions. Implications for Molecular Design and Protein Engineering. *J. Am. Chem. Soc.* **124**, 10613-10620 (2002).

137 Catalano, L., Cavallo, G., Metrangolo, P., Resnati, G. & Terraneo, G. in *Hypervalent Iodine Chemistry* (ed Thomas Wirth) 289-309 (Springer International Publishing, 2016).

138 Heinen, F., Engelage, E., Dreger, A., Weiss, R. & Huber, S. M. Iodine(III) Derivatives as Halogen Bonding Organocatalysts. *Angew. Chem. Int. Ed* **57**, 3830 –3833 (2018).

139 Wolf, J., Huber, F., Erochok, N., Heinen, F., Guerin, V., Legault, C. Y., Kirsch, S. F. & Huber, S. M. Activation of a Metal-Halogen Bond by Halogen Bonding. *Angew. Chem. Int. Ed* **59**, 16496 –16500 (2020).

140 Heinen, F., Engelage, E., Cramer, C. J. & Huber, S. M. Hypervalent Iodine(III) Compounds as Biaxial Halogen Bond Donors. *J. Am. Chem. Soc.* **142**, 8633–8640 (2020).

141 Kolar, M. H. & Hobza, P. Computer Modeling of Halogen Bonds and Other σ-Hole Interactions. *Chem. Rev.* **116**, 5155−5187 (2016).

142 Nayak, S. K., Kumar, V., Murray, J. S., Politzer, P., Terraneo, G., Pilati, T., Metrangolo, P. & Resnati, G. Fluorination promotes chalcogen bonding in crystalline solids. *CrystEngComm* **19**, 4955–4959 (2017).

143 Klapotke, T. M., Krumm, B. & Scherr, M. Studies on the Properties of Organoselenium(IV) Fluorides and Azides. *Inorg. Chem.* **47**, 4712-4722 (2008).

144 Klapotke, T. M., Krumm, B., Galvez-Ruiz, J. C., Noth, H. & Schwab, I. Experimental and Theoretical Studies of Homoleptic Tellurium CyanidesTe(CN)$_x$: Crystal Structure of Te(CN)$_2$. *Eur. J. Inorg. Chem.*, 4764-4769 (2004).

145 Scilabra, P., Terraneo, G. & Resnati, G. Fluorinated elements of Group 15 as pnictogen bond donor sites. *J. Fluorine Chem.* **203**, 62-74 (2017).

146 Haberhauer, G. & Gleiter, R. The Nature of Strong Chalcogen Bonds Involving Chalcogen-Containing Heterocycles. *Angew. Chem. Int. Ed* **59**, 21236–21243 (2020).

147 Row, T. N. G. & Parthasarathy, R. Directional Preferences of Nonbonded Atomic Contacts with Divalent Sulfur in Terms of Its Orbital Orientations. 2. S—S Interactions and Nonspherical Shape of Sulfur in Crystals. *J. Am. Chem. Soc.* **103**, 477–479 (1981).

148 Ramasubbu, N. & Parthasarathy, R. Stereochemistry Of Incipient Electrophilic And Nucleophilic Reactions At Divalent Selenium Center: Electrophilic-Nucleophilic Pairing And Anisotropic Shape Of Se In Se…Se Interactions. *Phosphorus Sulfur Silicon Relat. Elem.* **31**, 221-229 (1986).

149 Murray, J. S., Lane, P. & Politzer, P. A Predicted New Type of Directional Noncovalent Interaction. *Int. J. Quantum Chem.* **107**, 2286–2292 (2007).

150 Kumar, V., Scilabra, P., Politzer, P., Terraneo, G., Daolio, A., Fernandez-Palacio, F., Murray, J. S. & Resnati, G. Tetrel and Pnictogen Bonds Complement Hydrogen and Halogen Bonds in Framing the Interactional Landscape of Barbituric Acids. *Cryst. Growth Des.* **21**, 642-652 (2021).

151 Pascoe, D. J., Ling, K. B. & Cockroft, S. L. The Origin of Chalcogen-Bonding Interactions. *J. Am. Chem. Soc.* **139**, 15160−15167 (2017).

152 Adam, C., Yang, L. & Cockroft, S. L. Partitioning Solvophobic and Dispersion Forces in Alkyl and Perfluoroalkyl Cohesion. *Angew. Chem. Int. Ed* **54**, 1164-1167 (2015).

153 Yang, L., Adam, C. & Cockroft, S. L. Quantifying Solvophobic Effects in Nonpolar Cohesive Interactions. *J. Am. Chem. Soc.* **137**, 10084-10087 (2015).

154 Yang, L., Adam, C., Nichol, G. S. & Cockroft, S. L. How much do van der Waals dispersion forces contribute to molecular recognition in solution? *Nature Chemistry* **5**, 1006-1010 (2013).

155 Mati, I. K., Adam, C. & Cockroft, S. L. Seeing through solvent effects using molecular balances. *Chem. Sci.* **4**, 3965–3972 (2013).

156 Cockroft, S. L. & Hunter, C. A. Desolvation and substituent effects in edge-to-face aromatic interactions. *Chem. Commun.*, 3961–3963 (2009).

157 Cockroft, S. L. & Hunter, C. A. Desolvation tips the balance: solvent effects on aromatic interactions. *Chem. Commun.*, 3806–3808 (2006).

158 Muchowska, K. B., Adam, C., Mati, I. K. & Cockroft, S. L. Electrostatic Modulation of Aromatic Rings via Explicit Solvation of Substituents. *J. Am. Chem. Soc.* **135**, 9976−9979 (2013).

159 Emenike, B. U., Bey, S. N., Bigelow, B. C. & Chakravartula, S. V. S. Quantitative model for rationalizing solvent effect in noncovalent CH–Aryl interactions. *Chem. Sci.* **7**, 1401–1407 (2016).

160 Burns, R. J., Mati, I. K., Muchowska, K. B., Adam, C. & Cockroft, S. L. Quantifying Through-Space Substituent Effects. *Angew. Chem. Int. Ed* **59**, 16717–16724 (2020).

161 Garrett, G. E., Gibson, G. L., Straus, R. N., Seferos, D. S. & Taylor, M. S. Chalcogen Bonding in Solution: Interactions of Benzotelluradiazoles with Anionic and Uncharged Lewis Bases. *J. Am. Chem. Soc.* **137**, 4126−4133 (2015).

162 Robertson, C. C., Wright, J. S., Carrington, E. J., Perutz, R. N., Hunter, C. A. & Brammer, L. Hydrogen bonding vs. halogen bonding: the solvent decides. *Chem. Sci.*, 5392–5398 (2017).

163 Lu, Y., Li, H., Zhu, X., Liu, H. & Zhu, W. Effects of Solvent on Weak HalogenBonds: Density Functional Theory Calculations. *Int. J. Quantum Chem.* **112**, 1421–1430 (2011).

164 Bhandary, S., Sirohiwal, A., Kadu, R., Kumar, S. & Chopra, D. Dispersion Stabilized Se/Te···π Double Chalcogen Bonding Synthons in in Situ Cryocrystallized Divalent Organochalcogen Liquids. *Cryst. Growth Des.* **18**, 3734−3739 (2018).

165 Bleiholder, C., Gleiter, R., Werz, D. B. & Koppel, H. Theoretical Investigations on Heteronuclear Chalcogen−Chalcogen Interactions: On the Nature of Weak Bonds between Chalcogen Centers. *Inorg. Chem.* **46**, 2249–2260 (2007).

166 Bleiholder, C., Werz, D. B., Koppel, H. & Gleiter, R. Theoretical Investigations on Chalcogen−Chalcogen Interactions: What Makes These Nonbonded Interactions Bonding? *J. Am. Chem. Soc.* **128**, 2666–2674 (2006).

167 Bauza, A., Quinonero, D., Deya, P. M. & Frontera, A. Halogen bonding versus chalcogen and pnicogen bonding: a combined Cambridge structural database and theoretical study. *CrystEngComm* **15**, 3137–3144 (2013).

168 Groom, C. R., Bruno, I. J., Lightfoot, M. P. & Ward, S. C. The Cambridge Structural Database. *Acta Cryst.* **B72**, 171-179 (2016).

169 Sedlak, R., Eyrilmez, S. M., Hobza, P. & Nachtgallova, D. The role of the s-holes in stability of non-bonded chalcogenidebenzene interactions: the ground and excited states. *Phys. Chem. Chem. Phys.* **20**, 299-306 (2018).

170 Su, P. & Li, H. Energy decomposition analysis of covalent bonds and intermolecular interactions. *J. Chem. Phys.* **131**, 014102 (2009).

171 Mackenzie, C. F., Spackman, P. R., Jayatilaka, D. & Spackman, M. A. CrystalExplorer model energies and energy frameworks: extension to metal coordination compounds, organic salts, solvates and open-shell systems. *IUCrJ* **4**, 575–587 (2017).

172 Choudhury, A. R., Islam, K., Kirchner, M. T., Mehta, G. & Row, T. N. G. In Situ Cryocrystallization of Diphenyl Ether: C-H···π Mediated Polymorphic Forms. *J. Am. Chem. Soc.* **126**, 12274-12275 (2004).

173 Benz, S., Poblador-Bahamonde, A. I., Low-Ders, N. & Matile, S. Catalysis with Pnictogen, Chalcogen, and Halogen Bonds. *Angew. Chem. Int. Ed* **57**, 5408 –5412 (2018).

174 Wilkie, C. A. & Parry, R. W. Halocyanophosphines, $P(CN)_yX_{3-y}$, and Related Cyanophosphine Derivatives. *Inorg. Chem.* **19**, 1499-1502 (1980).

175 Deng, R. M. K., Dillon, K. & Sheldrick, W. S. Synthetic and Spectroscopic Studies of Phosphoranides [PR(CN),X]- and the Crystal and Molecular Structure of [NEt,] [PPh(CN),Cl]. *J. Chem. Soc. Dalton Trans.*, 551-554 (1990).

176 Ali, R. & Dillon, K. B. Some novel phosphoranides containing pentafluorophenyl groups. *J. Chem. Soc. Dalton Trans.*, 2593-2596 (1990).

177 Emerson, K. & Britton, D. The Crystal and Molecular Structure of Arsenic Tricyanide. *Acta Cryst.* **16**, 113-118 (1962).

178 Ouvrard, C., Questel, J.-Y. L., Berthelot, M. & Laurence, C. Halogen-bond geometry: a crystallographic database investigation of dihalogen complexes. *Acta Crystallogr., Sect. B: Struct. Sci.* **59**, 512−526 (2003).

179 Murray-Rust, P. & Motherwell, W. D. S. Computer Retrieval and Analysis of Molecular Geometry.1 4. Intermolecular Interactions. *J. Am. Chem. Soc.* **101**, 4374–4376 (1979).

180 Murray-Rust, P., Stallings, W. C., Monti, C. T., Preston, R. K. & Glusker, J. P. Intermolecular Interactions of the C-F Bond: The Crystallographic Environment of Fluorinated Carboxylic Acids and Related Structures. *J. Am. Chem. Soc.* **105**, 3206-3214 (1982).

181 Ramasubbu, N., Parthasarathy, R. & Murray-Rust, P. Angular Preferences of Intermolecular Forces around Halogen Centers: Preferred Directions of Approach of Electrophiles and Nucleophiles around the Carbon-Halogen Bond. *J. Am. Chem. Soc.* **108**, 4308–4314 (1985).

182 Hunter, C. A. & Andreson, H. L. What is Cooperativity? *Angew. Chem. Int. Ed* **48**, 7488 – 7499 (2009).

183 Reisman, S. E., Doyle, A. G. & Jacobsen, E. N. Enantioselective Thiourea-Catalyzed Additions to Oxocarbenium Ions. *J. Am. Chem. Soc.* **130**, 7198–7199 (2008).

184 Kniep, F., Jungbauer, S. H., Zhang, Q., Walter, S. M., Schindler, S., Schnapperelle, I., Herdtweck, E. & Huber, S. M. Organocatalysis by Neutral Multidentate Halogen-Bond Donors. *Angew. Chem. Int. Ed* **52**, 7028 –7032 (2013).

185 Jungbauer, S. H. & Huber, S. M. Cationic Multidentate Halogen-Bond Donors in Halide Abstraction Organocatalysis: Catalyst Optimization by Preorganization. *J. Am. Chem. Soc.* **137**, 12110−12120 (2015).

186 Berkessel, A., Das, S., Pekel, D. & Neudorfl, J.-M. Anion-Binding Catalysis by Electron-Deficient Pyridinium Cations. *Angew. Chem. Int. Ed* **53**, 11660 –11664 (2014).

187 Wonner, P., Vogel, L., Kniep, F. & Huber, S. M. Catalytic Carbon–Chlorine Bond Activation by Selenium-Based Chalcogen Bond Donors. *Chem. Eur. J.* **23**, 16972 – 16975 (2017).

188 Trujillo, C., Sanchez-Sanz, G., Alkorta, I. & Elguero, J. Halogen, chalcogen and pnictogen interactions in $(XNO_2)_2$ homodimers (X = F, Cl, Br, I). *New J. Chem.* **39**, 6791-6802 (2015).

189 Bader, R. F. W. *Atoms in Molecules: A Quantum Theory*. (Clarendon Press, 1990).

190 Otte, F., Kleinheider, J., Hiller, W., Wang, R., Englert, U. & Strohmann, C. Weak yet Decisive: Molecular Halogen Bond and Competing Weak Interactions of Iodobenzene and Quinuclidine. *J. Am. Chem. Soc.* **143**, 4133−4137 (2021).

191 Sanchez-Sanz, G., Trujillo, C., Alkorta, I. & Elguero, J. Modulating intramolecular P···N pnictogen interactions. *Phys. Chem. Chem. Phys.* **18**, 9148-9160 (2016).

192 Allen, F. H. The Cambridge Structural Database: a quarter of a million crystal structures and rising. *Acta Cryst.* **B58**, 380-388 (2002).

193 Sanchez-Sanz, G., Trujillo, C., Alkorta, I. & Elguero, J. Intramolecular pnicogen interactions in phosphorus and arsenic analogues of proton sponges. *Phys. Chem. Chem. Phys.* **16**, 15900-15909 (2014).

194 Becke, A. D. & Johnson, E. R. Exchange-hole dipole moment and the dispersion interaction: High-order dispersion coefficients. *J. Phys. Chem.* **124**, 014104 (2006).

195 Becke, A. D. & Johnson, E. R. A density-functional model of the dispersion interaction. *J. Phys. Chem.* **123**, 154101 (2005).

196 Santos, L. d. A., Hamlin, T. A., Ramalho, T. C. & Bickelhaupt, F. M. The pnictogen bond: a quantitative molecular orbital picture. *Phys. Chem. Chem. Phys.* **23**, 13842–13852 (2021).

197 Velde, G. t., Bickelhaupt, F. M., Baerends, E. J., Guerra, C. F., Gisbergen, S. J. A. v., Snijders, J. G. & Ziegler, T. Chemistry with ADF. *J. Comput. Chem* **22**, 931–967 (2001).

198 Bickelhaupt, F. M., Nibbering, N. M. M., Wezenbeek, E. M. v. & Baerends, E. J. Central Bond in the Three CN' Dimers NC-CN, CN-CN, and CN-NC: Electron Pair Bonding and Pauli Repulsion Effects. *J. Phys. Chem.* **96**, 4864-4873 (1992).

199 Guerra, C. F., Snijders, J. G., Velde, G. t. & Baerends, E. J. Towards an order-N DFT method. *Theor. Chem. Acc.* **99**, 391-403 (1998).

200 Bickelhaupt, F. M., Hommes, N. J. R. v. E., Guerra, C. F. & Baerends, E. J. The Carbon-Lithium Electron Pair Bond in (CH3Li)n (n = 1, 2, 4). *Organometallics* **15**, 2923-2931 (1996).

201 Guerra, C. F., Handgraaf, J.-W., Baerends, E. J. & Bickelhaupt, F. M. Voronoi Deformation Density (VDD) Charges: Assessmentof the Mulliken, Bader, Hirshfeld, Weinhold, and VDD Methods for Charge Analysis. *J. Comput. Chem.* **25**, 189-210 (2003).

202 Wolters, L. P. & Bickelhaupt, F. M. Halogen Bonding versus Hydrogen Bonding: A Molecular Orbital Perspective. *ChemistryOpen* **1**, 96-105 (2012).

203 Santos, L. d. A., Lubbe, S. C. C. v. d., Hamlin, T. A., Ramalho, T. C. & Bickelhaupt, F. M. A Quantitative Molecular Orbital Perspective of the Chalcogen Bond. *ChemistryOpen* **10**, 391–401 (2021).

204 Larranaga, O., Arrieta, A., Guerra, C. F., Bickelhaupt, F. M. & Cozar, A. d. Nature of Alkali- and Coinage-Metal Bonds versus Hydrogen Bonds. *Chem. Asian J.* **16**, 315 – 321 (2021).

205 Bickelhaupt, F. M. Understanding Reactivity withKohn-Sham Molecular Orbital Theory: E2-SN2 Mechanistic Spectrum and Other Concepts. *J. Comput. Chem.* **20**, 114-128 (1998).

206 Zeist, W.-J. v. & Bickelhaupt, F. M. The activation strain model of chemical reactivity. *Org. Biomol. Chem.* **8**, 3118–3127 (2010).

207 Vermeeren, P., Lubbe, S. C. C. v. d., Guerra, C. F., Bickelhaupt, F. M. & Hamlin, T. A. Understanding chemical reactivity using the activation strain model. *Nat. Protoc.* **15**, 649–667 (2020).

208 Bauza, A., Mooibroek, T. J. & Frontera, A. The Bright Future of Unconventional σ/π-Hole Interactions. *ChemPhysChem* **16**, 2496-2517 (2015).

209 Shahi, A. & Arunan, E. Hydrogen bonding, halogen bonding and lithium bonding: an atoms in molecules and natural bond orbital perspective towards conservation of total bond order, inter- and intra-molecular bonding. *Phys. Chem. Chem. Phys.* **16**, 22935-22952 (2014).

210 Romaniello, P. & Leji, F. Halogen Bond in $(CH_3)_nX$ (X = N, P, n = 3; X = S, n = 2) and $(CH_3)_nXO$ (X = N, P, n = 3; X = S, n = 2) Adducts with CF3I. Structural and Energy Analysis Including Relativistic Zero-Order Regular Approximation Approach in a Density Functional Theory Framework. *J. Phys. Chem. A* **106**, 9114-9119 (2002).

211 Li, Q., Xu, X., Liu, T., Jing, B., Li, W., Cheng, J., Gong, B. & Sun, J. Competition between hydrogen bond and halogen bond in complexes of formaldehyde with hypohalous acids. *Phys. Chem. Chem. Phys.* **12**, 6837–6843 (2010).

212 Landrum, G. A., Goldberg, N. & Hoffmann, R. Bonding in the trihalides (X_3^-), mixed trihalides (X_2Y^-) and hydrogen bihalides (X_2H^-). The connection between hypervalent, electron-rich three-center, donor–acceptor and strong hydrogen bonding. *J. Chem. Soc., Dalton Trans.*, 3605–3613 (1997).

213 Quinonero, D. & Frontera, A. Hydrogen Bond versus Halogen Bond in HXOn (X = F,Cl, Br, and I) Complexes with Lewis Bases. *Inorganics* **7** (2019).

214 Bauza, A., Mooibroek, T. J. & Frontera, A. Tetrel-Bonding Interaction: Rediscovered Supramolecular Force? *Angew. Chem. Int. Ed.* **52**, 12317 –12321 (2013).

215 Grabowski, S. J. Boron and other Triel Lewis Acid Centers: From Hypovalency to Hypervalency. *ChemPhysChem* **15**, 2985-2993 (2014).

216 Grabowski, S. J. π-Hole Bonds: Boron and Aluminum Lewis Acid Centers. *ChemPhysChem* **16**, 1470-1479 (2015).

217 Grabowski, S. J. Triel Bonds, π-Hole-π-Electrons Interactions in Complexes of Boron and Aluminium Trihalides and Trihydrides with Acetylene and Ethylene. *Molecules* **20**, 11297-11316 (2015).

218 Grabowski, S. J. The Nature of Triel Bonds, a Case of B and Al Centres Bonded with Electron Rich Sites. *Molecules* **25**, 2703 (2020).

219 Yanez, M., Sanz, P., Mo, O., Alkorta, I. & Elguero, J. Beryllium Bonds, Do They Exist? *J. Chem. Theory Comput.* **5**, 2763–2771 (2009).

220 Alikhani, M. E. Beryllium bonding: insights from the σ- and π-hole analysis. *J. Mol. Model.* **26**, 94 (2020).

221 Bauza, A. & Frontera, A. Aerogen Bonding Interaction: A New Supramolecular Force? *Angew. Chem. Int. Ed.* **54**, 7340-7343 (2015).

222 Bauza, A. & Frontera, A. σ/π-Hole noble gas bonding interactions: Insights from theory andexperiment. *Coord. Chem. Rev.* **404**, 213112 (2020).

223 Kollman, P. A., Liebman, J. F. & Allen, L. C. The Lithium Bond. *J. Am. Chem. Soc.* **92**, 1142–1150 (1970).

224 Rego, D. G. & Oliveira, B. G. The interplay and the formation ofσ-hole inthe π···LiX and pseudo-π···LiX(X =F, Cl and CN) lithium bonds involving unsaturatedand homocyclichydrocarbons. *Comput. Theor. Chem.* **1186**, 112899 (2020).

225 Ault, B. S. & Pimentel, G. C. Matrix Isolation Infrared Studies of Lithium Bonding. *J. Phys. Chem.* **79**, 621-626 (1975).

226 Fromm, K. M. Chemistry of alkaline earth metals: It is not all ionic and definitely not boring! *Coord. Chem. Rev.* **408**, 213293 (2020).

227 Stenlid, J. H., Johansson, A. J. & Brinck, T. σ-Holes and σ-lumps direct the Lewis basic and acidic interactions of noble metal nanoparticles: introducing regium bonds. *Phys. Chem. Chem. Phys.* **20**, 2676--2692 (2018).

228 Bauza, A., Alkorta, I., Elguero, J., Mooibroek, T. J. & Frontera, A. Spodium Bonds: Noncovalent Interactions Involving Group 12 Elements. *Angew. Chem. int. Ed.* **59**, 17482-17487 (2020).

229 Legon, A. C. & Walker, N. R. What's in a name? 'Coinage-metal' non-covalent bonds and their definition. *Phys. Chem. Chem. Phys.* **20**, 19332-19338 (2018).

Chapter 2

Halogen···Arene Interactions

Abstract

Crystallographic and computational studies support the occurrence of favourable interactions between polarisable arenes and halogen atoms. However, the systematic experimental quantification of halogen···arene interactions in solution has been hindered by large variance in steric demands of the halogens. Here we have employed synthetic molecular torsion balances to quantify halogen···arene contacts in solution. 204 conformational free energy differences were determined using a series of 10 molecular torsion balances in 17 solvent systems. A thermodynamic double-mutant cycle was used to dissect out the contribution of the halogen-arene interactions and the associated solvent effects. The experimental measurements found that such interactions were outcompeted by dispersion interactions with the surrounding solvent ($\Delta\Delta G$ > +1.5 kJ mol^{-1}). Halogen···arene contacts were slightly less disfavoured in solvents with higher solvophobicities and lower polarisabilities, but strikingly, were always less favoured than CH_3···arene contacts ($\Delta\Delta G \approx -1.0$ kJ mol^{-1}). A battery of computational methods was applied to the systems to dissect the various energetic contributions and to study the angular and geometric dependencies of such contacts.

Contributions: All compounds pertaining to balance series 1 were prepared and characterized by Dr Nicholas Dominelli-Whiteley. All compounds pertaining to balance series 2 were prepared and characterized by AMLW. In addition, AMLW conducted all double mutant cycle analysis and computational studies on both balance series.

2.1 Introduction to halogen···arene interactions

Halogen···arene interactions were first identified in 1940s,[1,2] and are receiving renewed attention through the broader emerging interest in secondary bonding interactions.[3-5] Indeed, halogen···arene interactions have been observed in over 20,000 crystal structures in the CCSD[6] and have been implicated in several protein-ligand binding interactions[7-10] as well as having applications in pharmaceuticals,[7-10] supramolecular assemblies[11-14] and in functional materials.[15] The comparatively large size of the phenyl binding partner provides a multitude of potential halogen-arene interaction geometries. In simplistic terms, these can be broken down into *T-shaped* and *side-on* geometries (Figure 2.1), which broadly differ in regard to the degree of involvement of the halogen σ-hole.

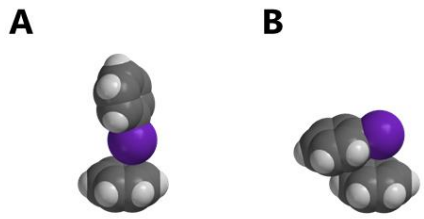

Figure 2.1: A) *T-shaped* and **B)** *side-on* geometries for halogen···arene contacts between benzene and iodobenzene.

The *T-shaped* geometry (Figure 2.1A) most closely resembles a conventional halogen bond as defined by IUPAC, which explicitly mentions the tendency for halogen bonds to form at the linear extension of the C-X bond.[4] However, as highlighted in Chapter 1 and discussed below, attractive halogen bonds are not necessarily entirely defined by attractive electrostatic interactions stemming from the σ-hole. *Side-on* geometries (Figure 2.1A) represent the most extreme deviation from a conventional halogen bonded arrangement. Indeed, there is an emerging consensus that the geometries of halogen-arene interactions tend to be less rigidly constrained than their halogen-Lewis base analogues.[3,11,16-20] For example, Jiang prepared iodine-functionalised *N*-amidothioureas that assembled into helices via tilted perpendicular iodine···arene interactions (θ = 148.1º–154.6º) (Figure 2.2A). [11] Meanwhile, tetrabromo-diquinolines prepared by Bishop were found to form side-on bromine-arene contacts within crystalline solid-state lattices (Figure 2.2B).[21]

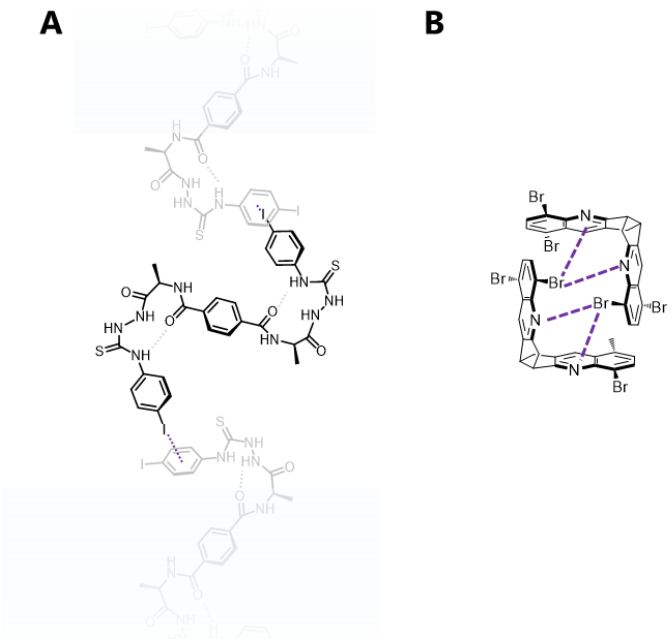

Figure 2.2: A) *N*-Amidothiourea helices held together by halogen···arene contacts as prepared by Jiang *et al*.[11] **B)** Tetrabromo-diquinoline lattice boxes held together by a combination of halogen bonding and halogen···arene contacts as prepared by Bishop *et al*.[21]

Despite their prolific nature, deep understanding of halogen-arene interactions has not permeated the scientific community, at least in part due to the multifaceted nature of halogen bonds, discussed in Chapter 1.[3,4] Moreover, solvent effects complicate the quantitative understanding of weak interactions in general.

2.2 Computational examination of halogen-arene interactions

Computational studies of halogen···arene interactions have provided insights into their nature and key energetic trends. A 2016 study by Ono *et al*. provided an in-depth examination of the geometric dependency of halogen-arene interactions. Their work demonstrated the limited role that σ-hole character plays in governing such interactions and highlighted the multiplicity of the forces at work.[17] Accordingly, side-on halogen···arene geometries similar to that depicted in Figure 2.1 are perhaps better described as interactions between two large polarisable moieties rather than as conventional halogen bonds. Indeed, the importance of dispersion has been underscored by several studies which found that dispersion must be included to reproduce experimentally observed geometries.[16-19,22,23]

More dissent in opinion is observed when considering the role of orbital effects in halogen···arene interactions. NBO analysis finds charge transfer to be both negligible[18] and non-negligible[23] in different systems. A 2018 study by Wong and co-workers[19] into interaction site preferences posits the idea of repulsive orbital overlap playing a key role. Borrowing nomenclature from inorganic chemistry, the authors discuss halogen···arene interactions in terms of hapticity; referring to the over-atom, over-bond and over-centroid binding modes as η1, η2 and η6 respective (Figure 2.3A).

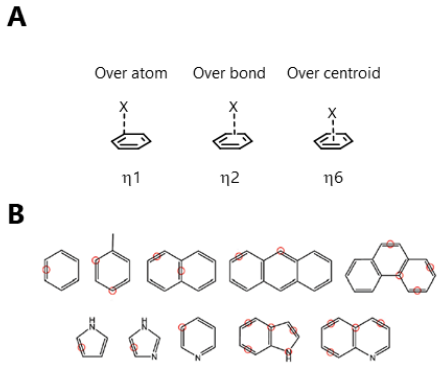

Figure 2.3: A) Interaction geometries considered for halogen···arene contacts. **B)** Aromatic and *N*-hetero-aromatic surfaces as considered by Wong *et al*. Red circles denote the locations of minimised halogen···arene interactions.[19]

For the aromatic/*N*-hetero-aromatic surfaces shown in Figure 2.3B, a search of the Cambridge Structural Database gave over 5500 hits where a halogen atom was found in close contact with one of the structures (as defined by the sum of the vdW radii). Of these hits, 3488 and 1742 were for the η1 and η2 binding modes respectively, while only 90 hits were identified for the η6 binding mode. A clear preference for interactions with the rim of the aromatic species was found, which Wong and co-workers are not alone in noting.[19] DFT calculations employing ωB97x-D/agu-cc-pVTZ geometry minimisation followed by sSAPT0/jun-cc-pVDZ energy dissection was employed to rationalise this behaviour. The η6 complex was found to be significantly less stable (for example; –14.9 kJ mol^{-1} for η6 Benzene···BrF vs. –22.5 kJ mol^{-1} for η2 Benzene···BrF). SAPT dissection scans along the purple line shown in Figure 2.4 revealed that dispersion was the most significant attractive term at all coordinates, with strength peaking over the centroid. These findings fit with the accepted literature consensus, but the lack of alignment between the trends for

dispersion and the SAPT total suggests that dispersion is not governing interaction behaviour. Instead, the SAPT total terms were most negative in the over-bond geometries, which was in line with the DFT findings. The induction and electrostatic terms also followed the same trend.

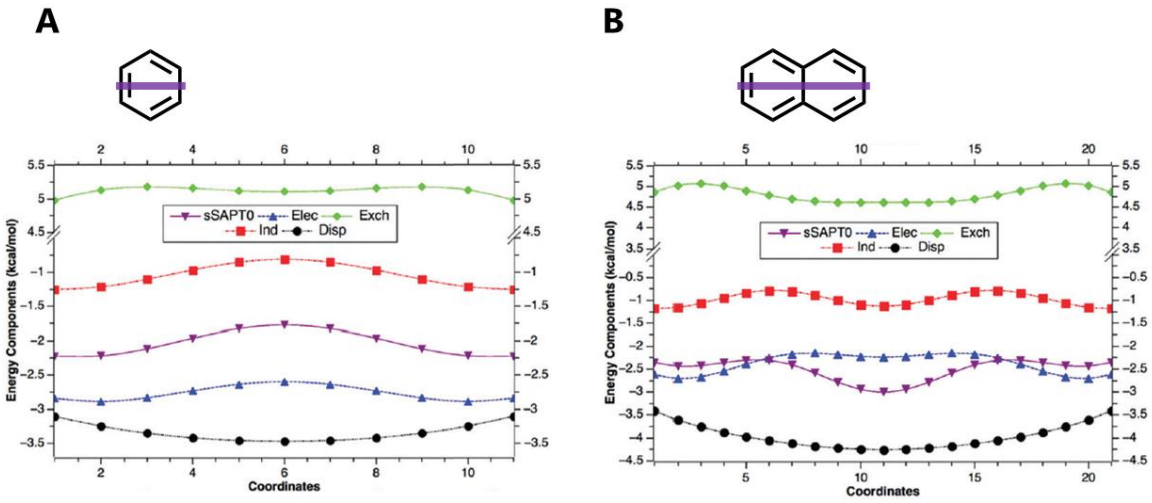

Figure 2.4: SAPT component breakdowns for scans of Cl_2, 3.2 Å over **A)** benzene and **B)** naphthalene.[19]

Wong and co-workers posit that both the induction and electrostatic terms can be rationalised by considerations of molecular orbitals, electrostatic variations being explained by lone pair···π repulsion rather than σ-hole···π attraction.[19] Though this is not a traditional description and is somewhat contentious.

Despite the insights provided by computational chemistry, calculations are currently unable to accurately account for the strongly perturbing influence of the surrounding solvent. However, crystallographic experimental investigations cannot reveal the thermodynamic nature of any putative interactions. Hence, other experiments are required to understand interaction thermodynamics in solution. Few experimental studies quantifying halogen···arene interactions have been conducted, and no studies have performed comprehensive solvent screens to study solvent effects.[24-27] The situation is underscored in the knowledge that solvents are known to exert an attenuating influence of dispersion-dominated interactions.[24-27]

2.3 Quantification of halogen-arene interactions in supramolecular complexes

The solution-phase experimental examination of halogen···arene interactions date back to the original 1940's UV-vis examinations.[1,2] A contemporary analogue of this very early work was conducted by Hansen *et al.* in 2011, who studied the complexation of C_3F_7I isomers with toluene-d_8 (Figure 2.5).[28] By employing ^{19}F NMR experiments and van't Hoff analysis to dissect out thermodynamic information, they were able to report enthalpically favourable interactions with toluene-d_8 for both C_3F_7I isomers with $\Delta H \approx -2.8$ kJ mol^{-1}. These findings were supported by DFT calculations (B3LYP-PCM/6-311++G(d,p) + LanL2DZ*) which corroborated the interaction trends, but gave interaction energies that were approximately double the magnitude of the experimental values.

1-IC_3F_7 2-IC_3F_7

Figure 2.5: C_3F_7I isomers employed by Hansen *et al.* in 2011.[29]

More complicated supramolecular complexes are have also been used to probe halogen···arene interactions. A 2004 study by Hunter *et al.*[30] employed NMR titrations to measure the binding of H-bonded complexes hosting halogen···arene interactions (Figure 2.6). Crystallographic structures of truncated singly H-bonded complexes supported the possibility of the larger complexes being able to host halogen···arene contacts. A thermodynamic double-mutant cycle approach was used to dissect out the contribution of the halogen···arene contacts to the complexation energies measured in the titrations.

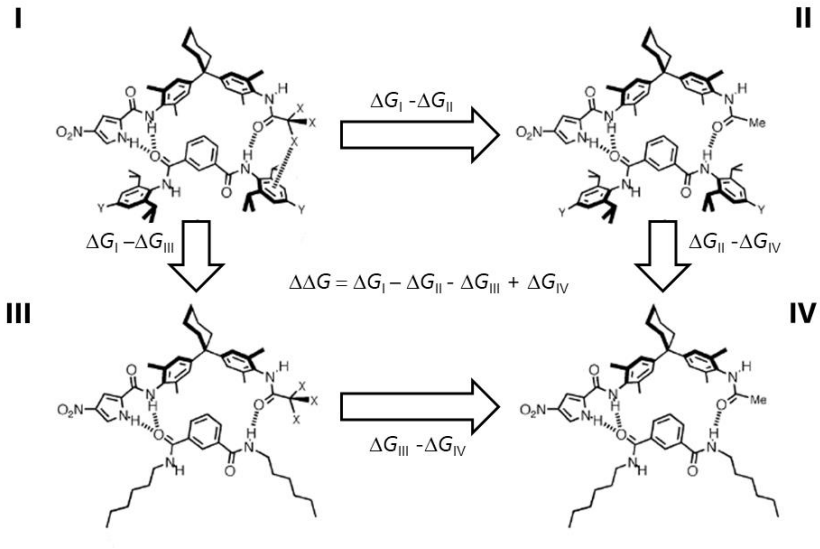

Figure 2.6: Thermodynamic double-mutant cycle employed by Hunter and co-workers to investigate halogen···arene contacts in chloroform.[30]

Double-mutant cycles were originally developed for dissecting out specific contributions in protein interactions,[31-33] but have since been widely adopted in supramolecular chemistry.[30,32,34-40] The halogen···arene interaction in Figure 2.6 could be assessed by comparing the binding energy of complex I with either of the single-mutant complexes II or III, where one of the interacting moieties has been deleted. However, doing this does not account for any secondary interactions that are changed by the single mutation. Any such secondary changes are encoded in the complexation energy change from a single mutant (II or III) to a double mutant (IV). Hence, the equation in the centre of Figure 2.6, provides a means of accounting for secondary interaction changes and isolating the contribution of the halogen···arene interaction to the overall complexation energy. Upon performing this dissection, the halogen···arene interactions examined were all found to be repulsive, but with the fluorine···arene interaction being slightly more so. However, the study was limited by solubility issues and geometric complications arising from the large changes in the size of the CX_3 moiety. There were large variations in the interaction distances; 3.07 Å (X = F, Y = NO_2) to 3.61 Å (X = Br, Y = NO_2), while iodine was not included in the study. Therefore, the authors themselves concluded that it was difficult to draw any strong conclusions.[30]

2.4 Quantification of halogen-arene interactions using molecular torsion balances

An alternative to the use of supramolecular complexes to quantify interactions is the use of molecular torsion balances.[41-44] Molecular torsion balances provide a potent tool for the investigation of weak non-covalent interactions such as halogen···arene interactions. The term molecular torsion balance was first coined by Wilcox in the mid 1990's.[45,46] Such systems rely on a conformational equilibrium serving as a reporter of the relative interactions occurring in a folded and unfolded state (Figure 2.7). Molecular balances can be designed such that an intramolecular interaction of interest is formed in the folded conformer (red line in Figure 2.2), but absent in the unfolded conformer. Hence, the relative strength of an interaction of interest can be studied by its perturbation of the equilibrium. Typically, the barrier to rotation between the states

$$\Delta G_{fold} = -RT \ln K_{fold} \qquad \text{(Equation 2.1)}$$

($\Delta G^{\ddagger}$ in Figure 2.7B) should be large enough that distinct peaks corresponding to each conformer can be resolved on the NMR time-scale. Hence, the conformational equilibrium constant between these states, K_{fold} can be readily determined by integrating the ratios of the NMR peaks corresponding to each conformer. From this, the Gibb's free energy difference between the states can then be determined using equation 2.1.

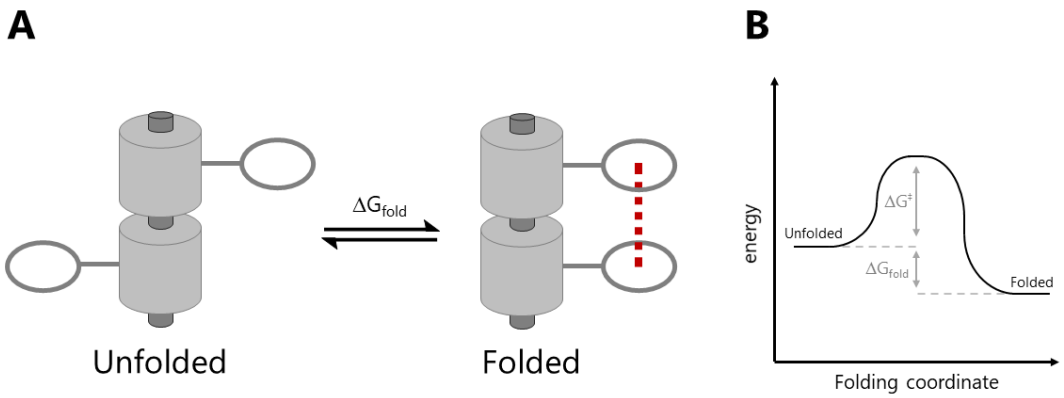

Figure 2.7 A) Cartoon depiction of a molecular torsion balance showing the unfolded and folded conformers. **B)** Energy profile for a molecular torsion balance. $\Delta G^{\ddagger}$, energy barrier to rotation; ΔG_{fold}, change in energy upon change in conformation.

Several classes of molecular torsion balances have been devised for measuring a wide range of interactions in different interaction geometries, and notable examples are presented in Figure 2.8. Indeed, one of the main advantages (and equally main limitations) of molecular balances is the well-defined geometry of the intramolecular interactions. This enables specialised geometries and interaction distances to be examined so that the designs can serve as analogues of interactions identified from protein or crystal structures. Halogen···arene interactions have seen study by several flavours of balance.

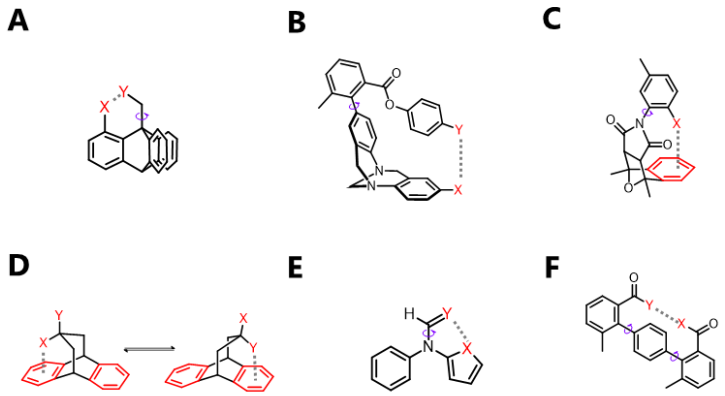

Figure 2.8: Examples of molecular torsion balance systems, interacting moieties are shown in red for clarity **A)** triptycene-derived molecular balance used by Ōki and Gung.[47] **B)** Tröger's base derived "Wilcox" balance.[45] **C)** Bicyclic *N*-arylimide molecular torsion balance designed and used by Shimizu.[48] **D)** "Motherwell" type Dibenzobicyclo[3.2.2]-nonane molecular torsion balance.[49,50] **E)** Slow rotating amide C-N bond derived balance referred to as the "Cockroft" balance.[51,52] **F)** Terphenyl molecular torsion balance.[53]

Ōki pioneered the use of molecular torsion balances in 1980s,[47,54] several years before the term had been coined.[45] As part of these studies, Ōki and co-workers used triptycene-based balances to examine a limited range of halogen···arene interactions (Figure 2.9).[47] These triptycene molecular balances are in slow exchange between the two conformers shown in Figure 2.9B at 253 K. Halogen···arene contacts are present in the two conformations shown in the bottom of Figure 2.9B, but absent in the conformer at the top. Hence, deviation away from the statistically expected 2:1 population ratio indicates the relative energies of the different interactions in the two classes of conformation. Br···arene interactions were found to be favour over Cl···arene interactions, but both were more favourable than an analogous CH_3···arene

interaction.[47,55] In contrast, a subsequent study by Gung *et al.*, employed a similar triptycene balance that could form either halogen···arene or CH_3···arene contacts, but this expressed a preference for the CH_3···arene contacts in both solid and solution states (Figure 2.9C).[56] The contrasting findings of these related studies likely arise from differences in the interaction geometries, which very much sets the tone for the geometric sensitivity of halogen···arene contacts in supramolecular structures.

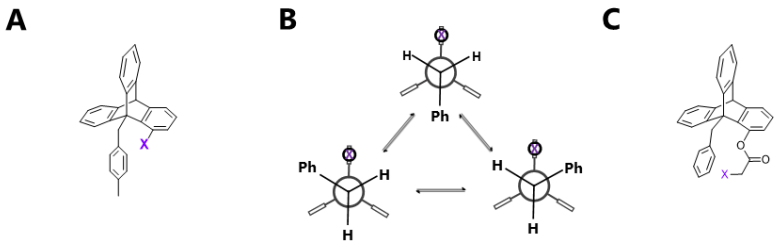

Figure 2.9: A) Triptycene type molecular torsion balance as employed by Ōki *et al.* **B)** Three-way conformational equilibrium found in triptycene molecular torsion balances. Halogen (X) arene contacts are possible in both of the lower two conformers, but not the upper one.[47,54] **C)** Derivative of the Triptycene type molecular torsion balance as employed by Gung *et al*.[56]

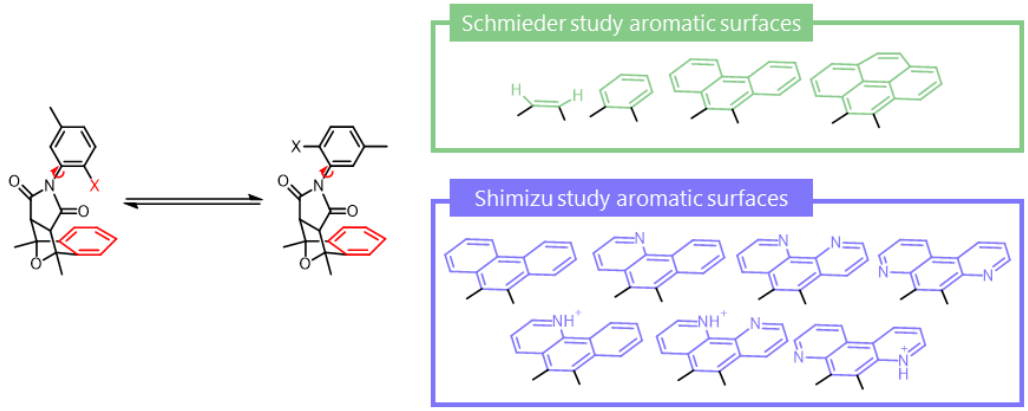

Figure 2.10: Bicyclic *N*-arylimide molecular torsion balance systems as employed by Schmieder and Shimizu showing the respective studies employed aromatic surfaces.[57,58]

More recently, the Shimizu[57] and Schmieder[58] groups have both employed bicyclic *N*-arylimide molecular torsion balance systems to examine halogen···arene interactions (Figure 2.10). Schmieder *et al.* utilised residual dipolar coupling (RDC) NMR spectroscopy to determine the open/closed conformer ratios. The authors suggested

that all the halogen···arene interactions were favourable, with magnitudes greater than –5 kJ mol^{-1}, which were comparable to the energies of biomolecular systems.[6,8] However, these energies were not direct measures of the interaction and were instead derived relative to a fluorine-substituent and extrapolated from a correlation of energies vs. the van der Waals radii of the halogens examined. While this may seem to be a potentially sound methodology, it is predicated on the fluorine···arene interaction being inert. However, examination of the raw conformational energy differences shows that the interaction trends are instead dominated by repulsion, with the largest halogens being strongly repelled from the aromatic face. Indeed, the work was completely undermined by work published in the same journal issue by Shimizu and co-workers.[57] The Shimizu group pioneered *N*-arylimide balances containing aromatic shelves;[41] they found that all halogen···arene interactions in such balances are repulsive (Figure 2.11). Contrasting with the traditional halogen bonding in which the more polarisable iodine forms the strongest bonds,[3] Shimizu found that iodine formed the most repulsive halogen···arene interactions and fluorine the least repulsive. The inflexibility of the bicyclic *N*-arylimide torsion balance means that is unable to accommodate the larger halogens. Irrespective of this steric limitation, all balances show the trend of increasing closed conformer preference as the ESP of the aromatic shelf became less negative. The introduction of increasing numbers of nitrogen atoms makes the aromatic shelf increasingly electron poor, which is manifested in their calculated ESPs. Accordingly, the least repulsive halogen···arene interactions uncovered by Shimizu are more akin to anion···π interactions than halogen bonds.[57,59-61]

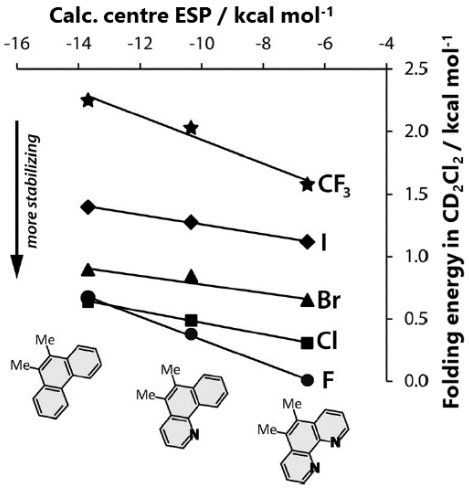

Figure 2.11: Plots of balance folding energies against calculated ESP values for the hetro-/aromatic surfaces shown.[57]

Halogen···arene interactions have also been examined in dibenzobicyclo[3.2.2]-nonane balances (Figure 2.12).[62] The study compared the halogen···arene contact against the comparatively better understood CH···arene contact. Although the CH···arene interaction is considered to be one of the weakest noncovalent interactions, it was found to consistently outcompete the halogen···arene contact when R = H. Consistent ΔG values were seen across the halogen series (7.9 kJ mol^{-1}), except the fluorine balance (ΔG = 3.9 kJ mol^{-1}) suggesting greater competition (or less repulsion) from the fluorine···arene contact compared to the other halogens. This work corroborates the prior findings of Shimizu[57] that F···arene interactions are more favourable (or less repulsive) than the other halogen contacts. These works also highlight the weakness of halogen···arene contacts, especially when there is little σ-hole involvement.

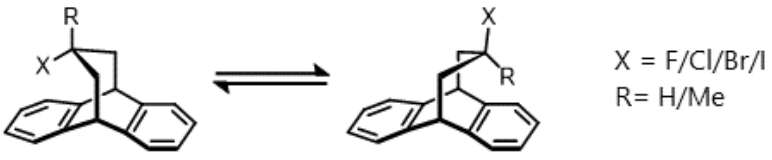

Figure 2.12: Dibenzobicyclo[3.2.2]-nonane "Motherwell" type molecular balance with conformers featuring halogen arene contacts and CH arene contacts. X = Br/I for R = H only.[62]

Replacing the R group proton with CH_3 increased the preference for the halogen···arene contact, which was attributed to the increased bulk of the CH_3 group. Indeed, the CH···arene contact was found to be favoured by –6.8 kJ mol^{-1} in the balance where X = H and R = CH_3. In the series of balances where R = CH_3, the fluorine···arene contact was favoured over the chlorine···arene contact, the latter of which was slightly more favourable than the CH_3-arene contact. Energy decomposition analysis conducted on a truncated version of the balance systems found ΔE strain to be the single largest factor in determination of which conformer was more favourable, which explains the experimental preference for the fluorine···arene contact over the chlorine, and H over CH_3. Unfortunately, the study did not include the full series of stable halogens for the R = CH_3 balances to complete the energetic comparisons.

2.5 Aims of the project

Halogen···arene contacts represent a relatively common place and useful interaction in a variety of contacts. This chapter aims to study these interactions both in the solution phase and computationally; overcoming some of the hindrances that previous studies have run into. To this end, two series of Wilcox type molecular torsion balances have been prepared and analysed to study halogen···arene contacts featuring the stable halogens (F/Cl/Br/I) and compare them to analogous CH···arene contacts (Figure 2.13A).

Interaction energies from within the balance systems have been measured across a 17 point solvent screen containing both single and mixed solvent systems with the objective of assessing the effects of solvent properties on halogen···arene contacts. In addition a combined double mutant cycle analysis of the two balance systems allows for dissection of the halogen···arene and CH···arene contacts from the background of balance system (Figure 2.13B). The principals of this approach having been outlined in Section 2.3.

In support of solution phase studies is an extensive computational study of halogen···arene contacts using DFT, DFT-D and SAPT methodologies to study both the interactions with the balance systems and the nuisances of halogen···arene contacts more generally.

2.6 Results and discussion

To facilitate study of halogen···arene interactions in solution, the Wilcox balance shown in Figure 2.13A was designed to bring the halogen and arene moieties into contact.

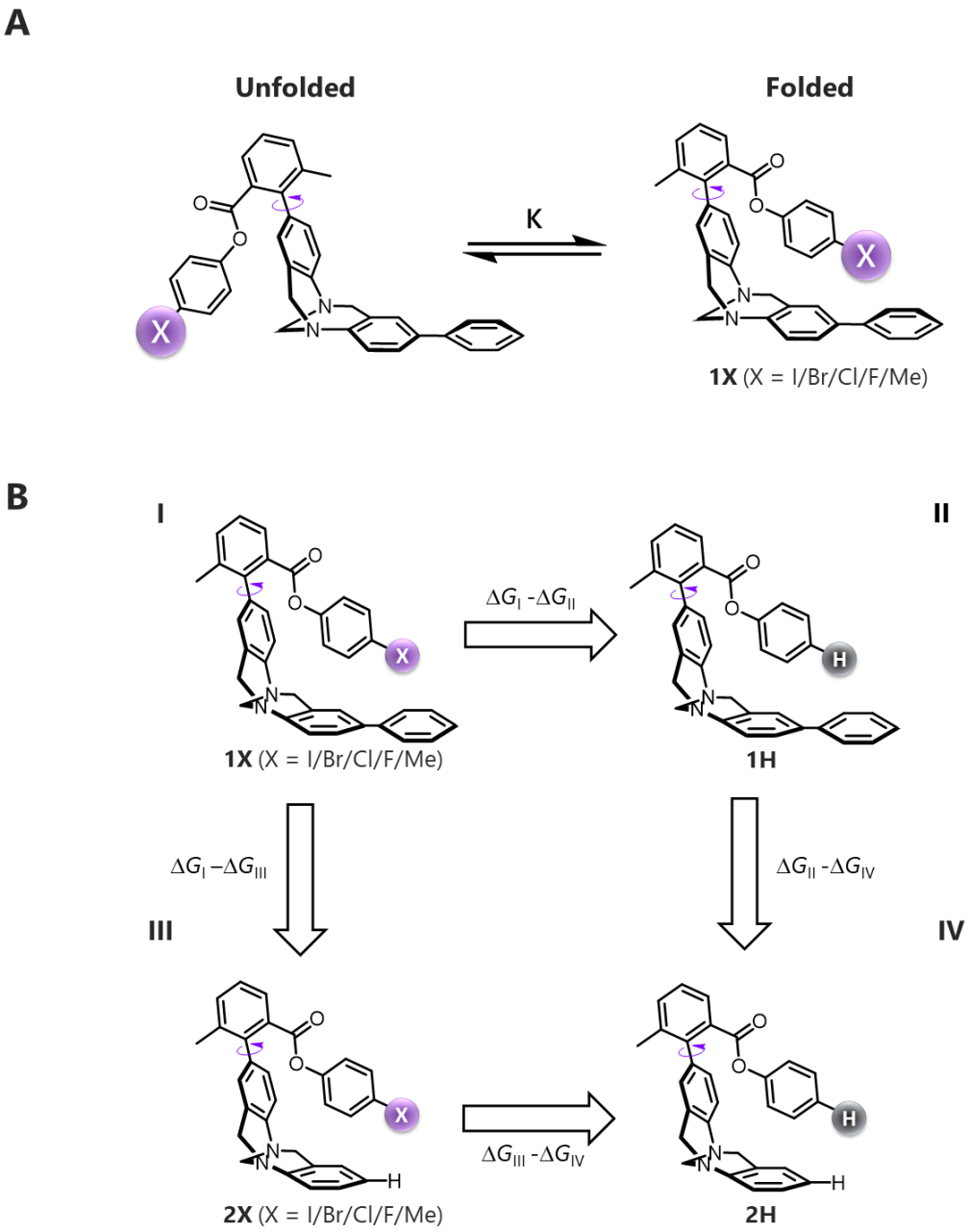

Figure 2.13: A) Wilcox molecular balance employed in this study showing the unfolded and folded conformers. **B)** Double mutant cycle employed to dissect out the energies associated with halogen···arene contacts.

The folded conformer resulting in geometries similar those that were found to be most prevalent in Schneider's crystallographic database study.[6] In contrast to rigid bicyclic *N*-arylimide balances used to examine halogen···arene interactions in previous studies,[57,58] the Wilcox balance is more flexible, which accommodates the wide range of covalent radii present within the halogen series. This flexibility should ideally mitigate issues of steric clashes that have limited previous studies.[30,58] The balance system is inherently suited to the study of dispersive contacts due to the orientation of the halogen σ-hole away from the arene moieties. Finally, the balance is small enough to allow for relatively cheap computational analysis, thus enabling comparative and energetic dissection calculations.

2.7 Synthesis of the molecular balances

The molecular torsion balances of series **1** and all relevant precursors were prepared previously by Dr Nicholas Dominelli-Whiteley in accordance with the reaction scheme presented in figure 2.14. Full synthetic details are presented in appendix A.12.

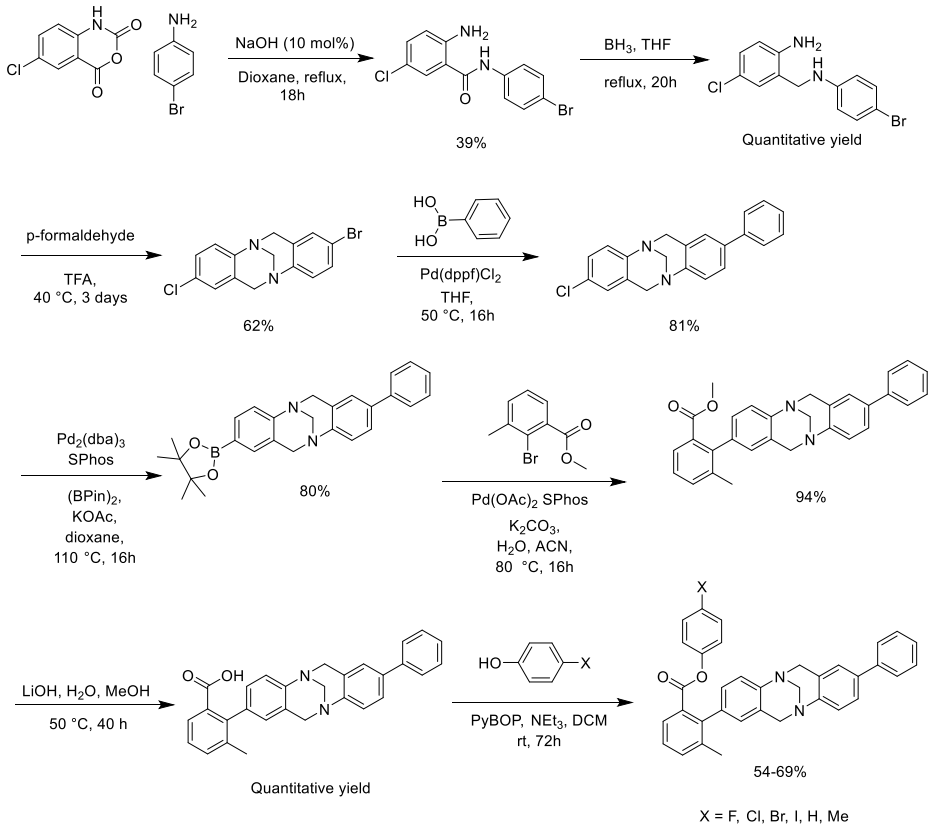

Figure 2.14: Synthetic scheme and yields for the preparation of balance series **1** and preceding intermediates.

Molecular torsion balance series **2** and all relevant precursors were prepared by AMLW and is presented in figure 2.15. Full synthetic details are presented in appendix A.13.

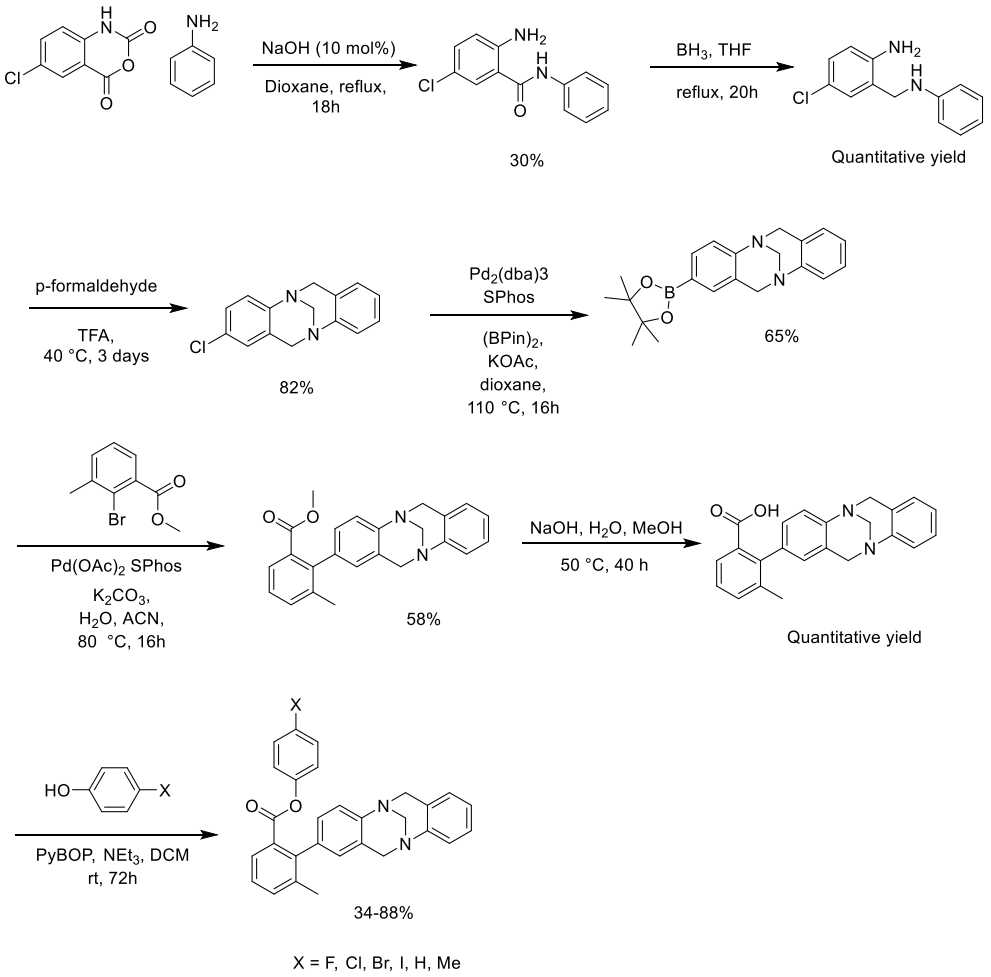

Figure 2.15: Synthetic scheme and yields for the preparation of balance series **2** and preceding intermediates.

Synthesis for both series starts with the formation of an amide from a commercially available chloroisatoic anhydride and an aniline species; brominated aniline for balance series **1**. The resultant amide is then reduced to a secondary amine using a borane-THF solution. The reduced species this then dissolved in a large volume of TFA along with paraformaldehyde and stewed at relatively low temperature for three days. This yielding a di-halogenated Tröger's base species for the synthesis of balance series **1** and a mono-halogenated Tröger's base species for the synthesis of balance series **2**.

At this point synthesis diverges. The di-halogenated Tröger's base species for the synthesis of balance series **1** is appended with an additional aromatic ring in place on its bromine atom via a [1,1′-Bis(diphenylphosphino)ferrocene]dichloropalladium^{II} mediated Suzuki-Miyaura procedure.

After this the synthetic methods reconverge for the addition of a pinacol ester to the Tröger's base species in place of the chlorine. Synthesis again employs a Suzuki-Miyaura cross-coupling reaction, this time mediated by Palladium^{II} acetate. This cross-coupling reaction sees the addition of a 1-methyl,3-methyl-benzoate to the Tröger's base that contains the reporting methyl group used to measure the equilibrium between the two conformers, with the formed C-C covalent bond rotating in slow exchange on an NMR timescale. The balance series **1** intermediate was demethylated using lithium hydroxide and the balance series **2** intermediate was demethylated using sodium hydroxide. The resultant carboxylic acids were then employed in a variety of esterification relations with 1,4 substituted phenols using PyBOP as a coupling reagent; yielding the balances of series **1** and **2** (34-88% yield).

2.8 Structural and computational analysis

X-ray crystal structures for series **1** were previously obtained by Dr Nicholas Dominelli-Whiteley.[63] The crystal structures showed contact between halogens I, Br, Cl and the terminal aromatic ring (Figure 2.16, left). The small size of the fluorine substituent meant that it did not attain contact with terminal ring in compound **1F**. Compound **1F** can therefore be considered as an electronic control since it has similar electronegativity to the other halogens. Although-the difference between the solid-state and calculated conformations were small, the gas-phase dispersion-corrected DFT-D minimised structures (M06-2X/6-311G*, ωB97X-D/6-311G* and B3LYP-D3/6-311G*(Figure 2.17) consistently placed the halogens in **1I**, **1Br** and **1Cl** above, and in closer contact with the one of the phenyl ring bonds (rather than the ring centroid). By comparison, crystal structures suggest a slightly more distant contact nearer the edge of the arene moiety, and closer to the minimised DFT structures (ωB97X/6-311G* and B3LYP/6-311G* (figure 2.16, right and centre respectively). Closer inspection of the X-ray structures revealed stacking and edge-to-face packing

contacts between the halogen-substituted aromatic rings, which perturbs the geometry in solid state.

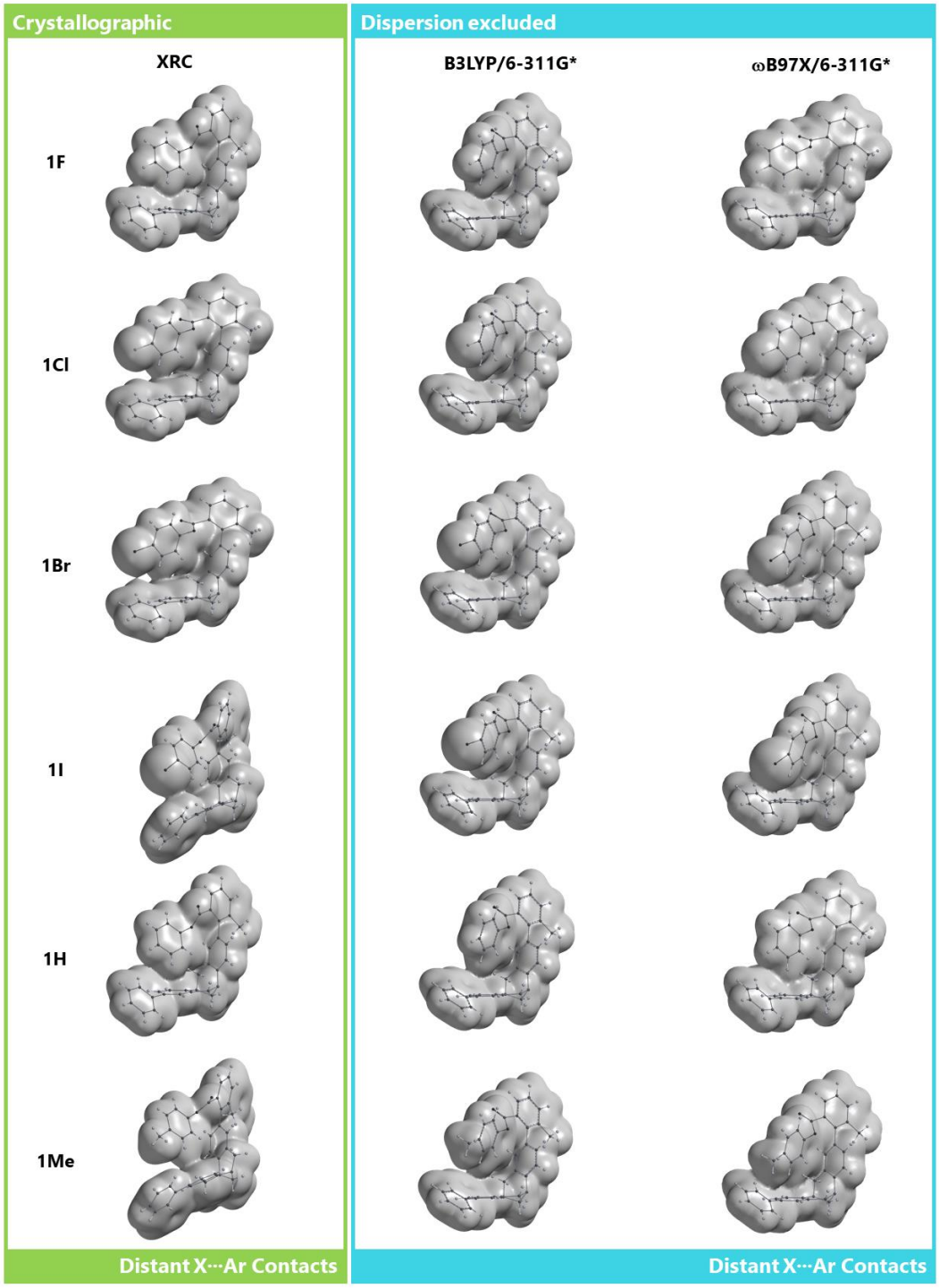

Figure 2.16: Geometries obtained from x-ray crystallography studies of balance series **1** conducted by Dr Nicholas Dominelli-Whiteley (left) and DFT minimized geometries (centre and right) of balance series **1** conducted by AMLW.

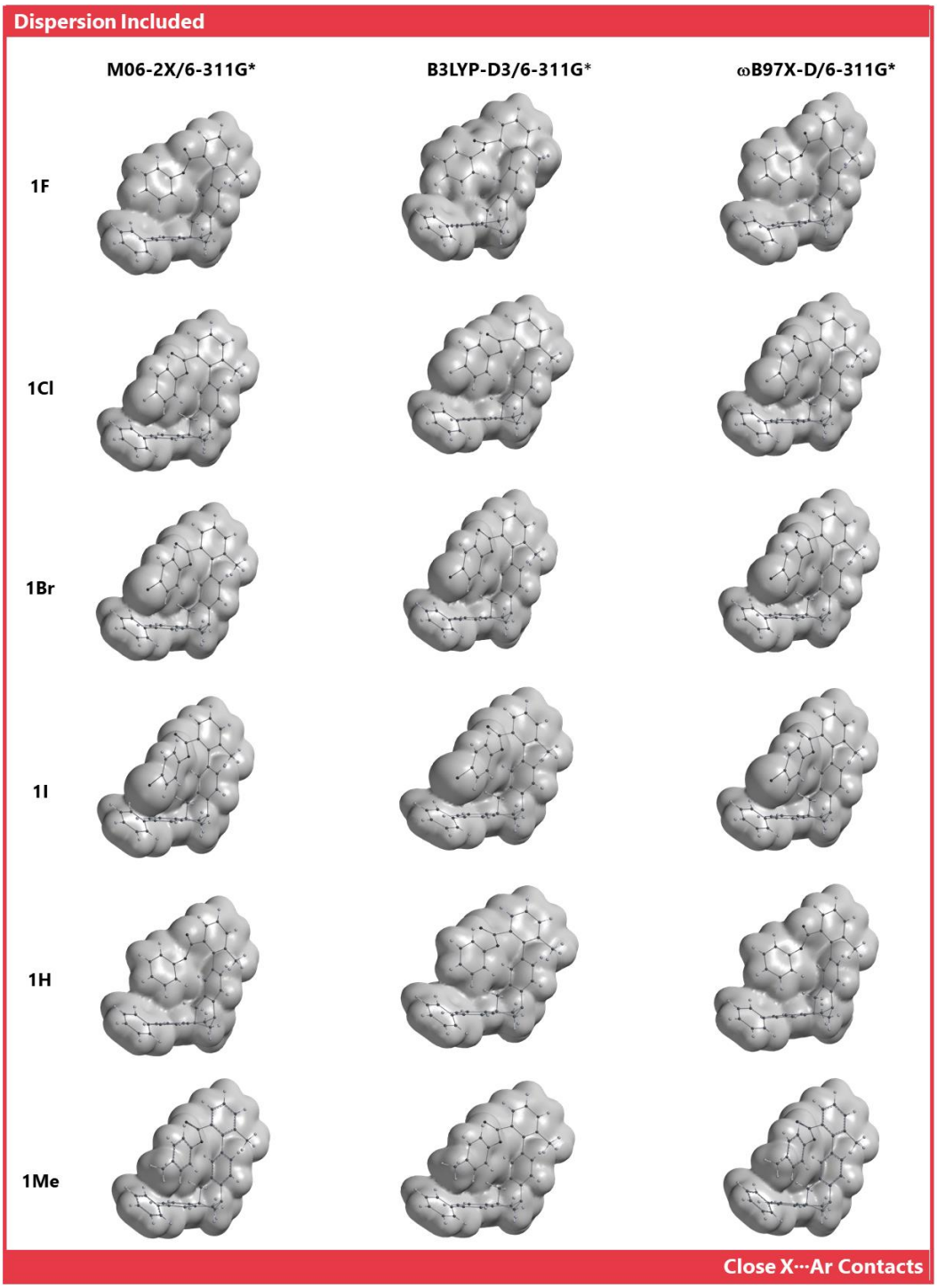

Figure 2.17: Dispersion included DFT-D minimized geometries for balance series **1**. Note consistently closer contact between the X and arene moieties.

The unfolded conformations of each of the balances were also calculated using the same DFT and DFT-D methods (Appendix A.6), allowing the gas-phase conformational energy difference between the balances, ΔE, to be determined (Appendix A.5). Figure 2.18A shows that the preference for the folded conformation decreased with increasing halogen size for the DFT methods, suggesting a strong role for sterics. However, this trend is inverted for the DFT-D functionals, due to the large contribution from stabilising dispersion interactions. Indeed, the large energetic dispersion contributions can be assessed by comparing the magnitudes of the ΔE values calculated with and without dispersion corrections for both levels of theory. The inversion of the ΔE trend within the halogen series upon the addition of a dispersion correction can be rationalized by increasing halogen polarizability accompanying an increase in size. These strong effects on not only the magnitude but also the trend suggest that dispersion plays a key role in our halogen···arene interactions.

To build upon this initial computational analysis, the ωB97X-D minimised geometries for all **1X** series balances were used to perform an energetic dissection using the SAPT2 methodology. The Wilcox balance frameworks were deleted to leave only a truncated model consisting of the terminal phenyl group and X-substituted aromatic ring in the same geometries expressed in the full balances (Figure 2.18B, inset bottom right), before SAPT2 calculations were performed on the interacting phenyl fragments. The SAPT2 calculations enabled dissection of the total interaction energy of each model complex ($SAPT_{total}$) to be dissected into the dispersion, electrostatic, induction, and exchange repulsion components (Figure 2.18B), providing insights into the relative weighting of these terms.[64,65]

Halogen···arene contacts within the balance system were found to be attractive with strength increasing with halogen size (Figure 2.18B). This is reassuring as it confirms the attractive ΔE values seen in the DFT and DFT-D calculations are not just a product of interactions within the balance backbone. Attractive components related to induction and electrostatics were identified but the largest attractive components were found to be dispersive in nature, consistent with previous studies.[16-19,22,23] This key role

of dispersion confirms initial thoughts regarding the discrepancy in trends observed between the DFT and DTF-D calculations.

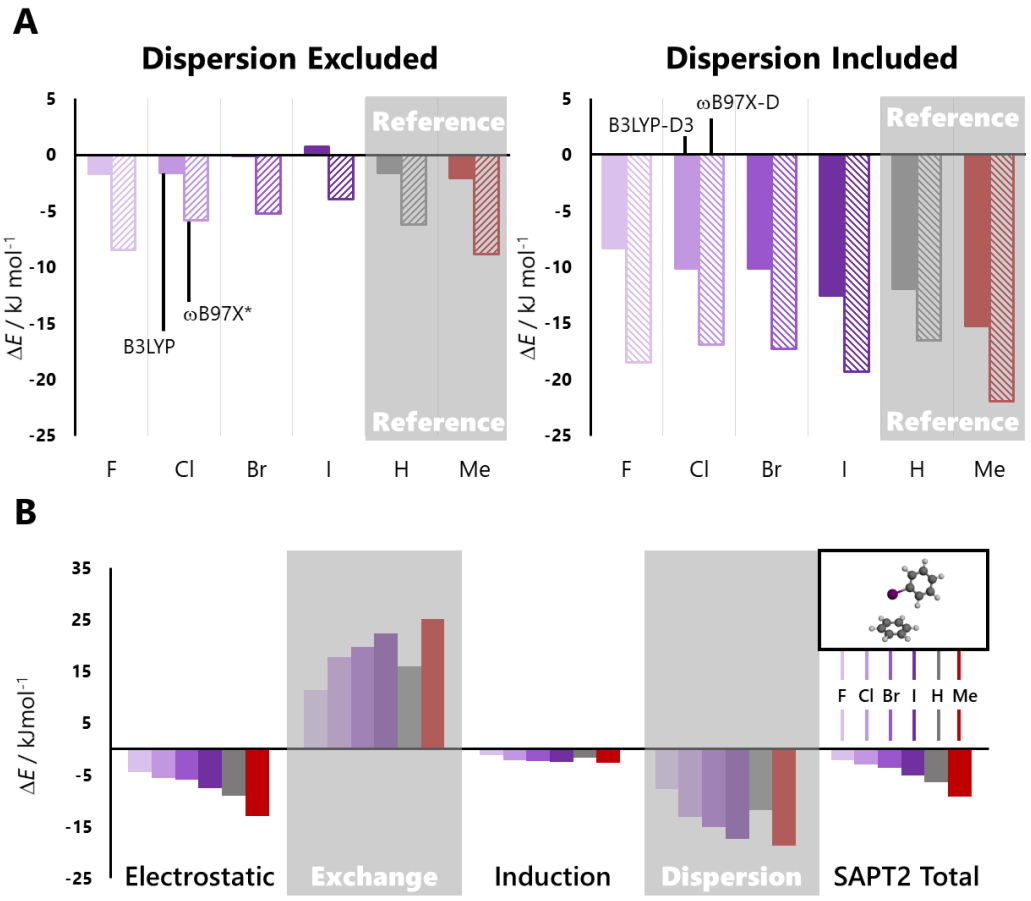

Figure 2.18 A) Δ*E* values associated with the unfolded to folded conformational change in balance series **1X** (Figure 2.13A) for DFT and DFT-D methodologies respectively. **B)** SAPT2 energy dissection for the isolated phenyl-X-phenyl interactions hosted within the series **1X** balances. Calculations conducted on a truncated version of ωB97X-D/6-311G* minimised structures (insert).

Given the inherent flexibility of the Wilcox balance, we also examined the angular dependency of the various SAPT2 energy components using a minimal model. Like the SAPT2 calculations this model, as shown in Figure 2.19, truncates the Wilcox balance into a benzene ring from the lower half of the balance and a halobenzene from the upper half. Models were varied by modulation of the bond midpoint-halogen-C1 angle whilst constraining the centroid-bond midpoint-halogen angle to 90˚. Inter-benzene ring interactions were accounted for by subtracting energies obtained for

analogous non-halogenated models from the calculated halogenated system energies. All calculations were conducted in Psi4 using the SAPT2 methodology and a 6-311G* basis set. Minimised and crystal structures suggested contact between the halogen and the phenyl ring with interaction distances being used as determined in the corresponding ωB97X-D/G-311G* minimisations. Interaction models involving over- atom and over-centroid contacts were included in the study (Figure 2.19).

The total SAPT2 energies, electrostatic, induction and exchange components were found to depend upon the angle of contact between C_{ar}-X and the aromatic ring for all three halogens and in all three arrangements. By contrast, the dispersion components were found to be consistently attractive and independent of the angle of contact, which is consistent with the non-directional nature of dispersion forces.[3,11,16-20,66,67] Corroborating with the DFT-D (Figure 2.18A, Appendix A.5) and SAPT2 energy calculations (Figure 2.18B, Appendix A.8), the magnitudes of the dispersion interactions were found to increase with increasing size and polarisability of the halogen. This consistently favourable, yet angularly independent dispersion term accounts for the loose geometric constraints that have previously been observed in X-ray crystallographic surveys of halogen···arene interactions. [3,11,16-20,66,67] Comparison of the three interaction arrangements shows very little difference between the over-bond and over-atom geometries, which is unsurprising given the relatively homogeneous nature of the interacting benzene moiety. The over-centroid arrangement is also relatively similar to the other two arrangements, though it is noticeable that the angular-dependent energies reach their zenith at greater θ angles. SAPT2 total and electrostatics terms peaking at around 100° suggests slightly more favourable contracts at these extreme angles for over-centroid contacts. This is surprising in the context of past computational studies,[19] but appears to occur because there is no significant increase in exchange cost when adopting this arrangement in our model system.

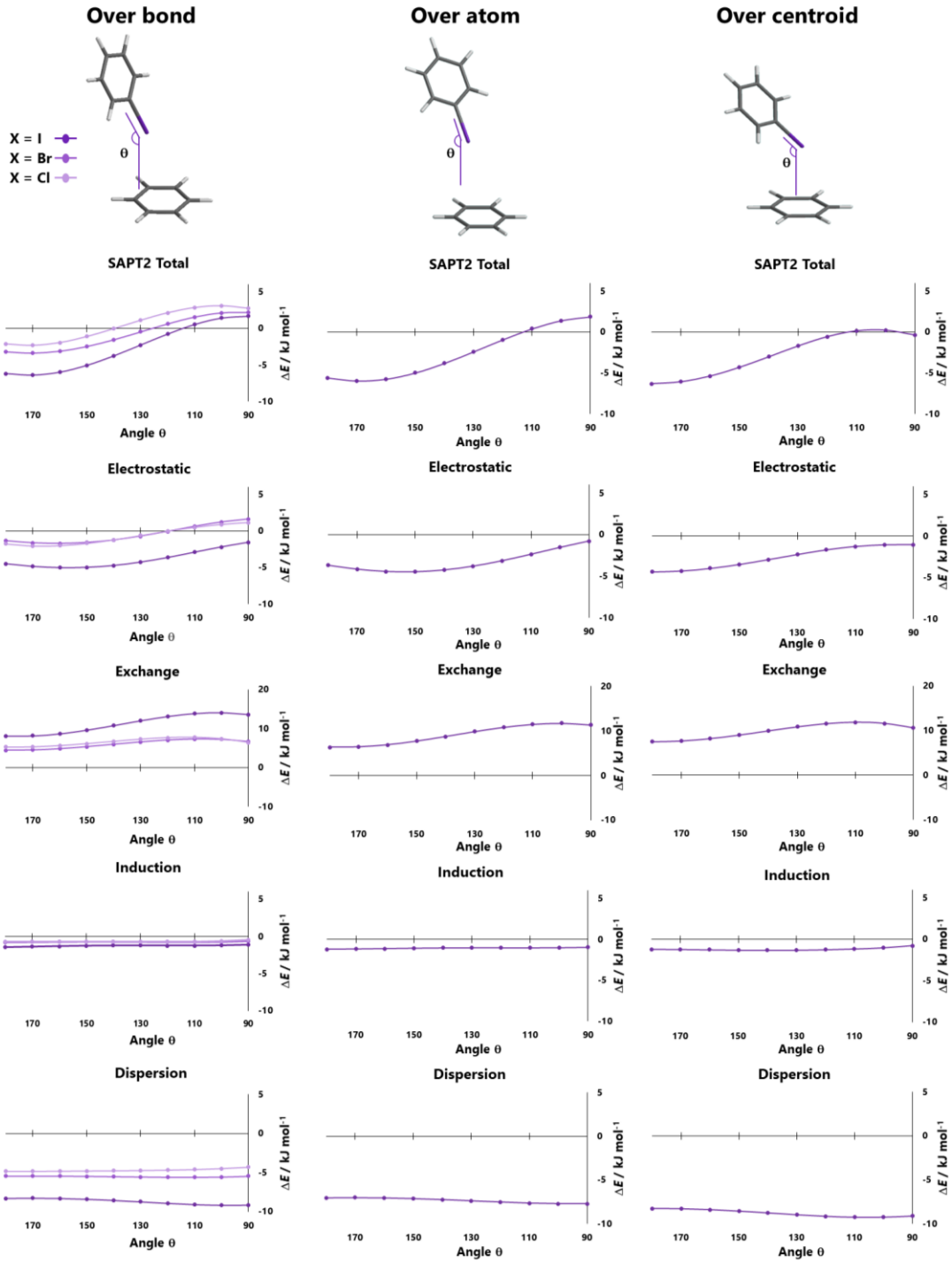

Figure 2.19: SAPT energy components as a product of variations in C-X···arene angle. Arrangement corresponding to **A)** over-bond contact, **B)** over-atom contact and **C)** over-centroid contact. All energies are normalised against non-halogenated analogues to remove contributions from arene···arene interactions.

2.9 Experimental studies

Having established the suitability of the Wilcox balance framework for investigating halogen···arene interactions and their dispersion-dominated nature in the absence of solvent, conformational free energy differences were determined in 17 solvents and solvent mixtures using ^{1}H NMR spectroscopy. The conformational equilibrium constants, *K*, were determined using the ratio of the two conformer peaks relating to the methyl group positioned *meta* to the ester moiety of the Wilcox balance (Figure 2.13A). Conformational free energies were then calculated using Equation 2.1.

The Δ*G* values obtained from ^{1}H NMR spectra by Dr Nicholas Dominelli-Whiteley of the balance series **1X** (Figure 2.20) show that the balances consistently prefer the folded conformation. However, there are only small variations in the differences between these Δ*G* values in each solvent (variation of ~1 kJ mol^{-1}). Nonetheless, a general inter-halogen trend of F>Cl=Br>I was seen across the solvents examine, which is in contradiction to the trend expected from the dispersion-corrected gas-phase calculations. The seemingly analogous trend observed in the non-dispersion corrected DFT functionals (Figure 2.18A, left) was previously characterised as being due to steric effects. However, the experimental Δ*G* values were determined in solution, and thus solvent effects must be considered. Consideration of factors other than steric constraints is especially prudent here, as inter-halogen variations of similar magnitudes are also seen in the Δ*G* values for the series **2X** balances (obtained by AMLW in a manner consistent with previous work) in which the arene moiety and its associated steric bulk have been deleted (Figure 2.20, right). Indeed, precedent exists for dispersion-driven interactions being attenuated by solvent effects.[24-26,68] Support for this precedent may be seen in the fact that the **1H** reference balance yielded similar Δ*G* values to the halogenated analogues. This suggest that solvent effects cancel out any dispersive halogen···arene contact. Interestingly, the extent of cancellation for the **1Me** balance that hosts a CH_3···π interaction is less than for the halogenated balance; this interaction is not completely dispersive in nature, and thus not as strongly attenuated by solvent effects.[46,55,69]

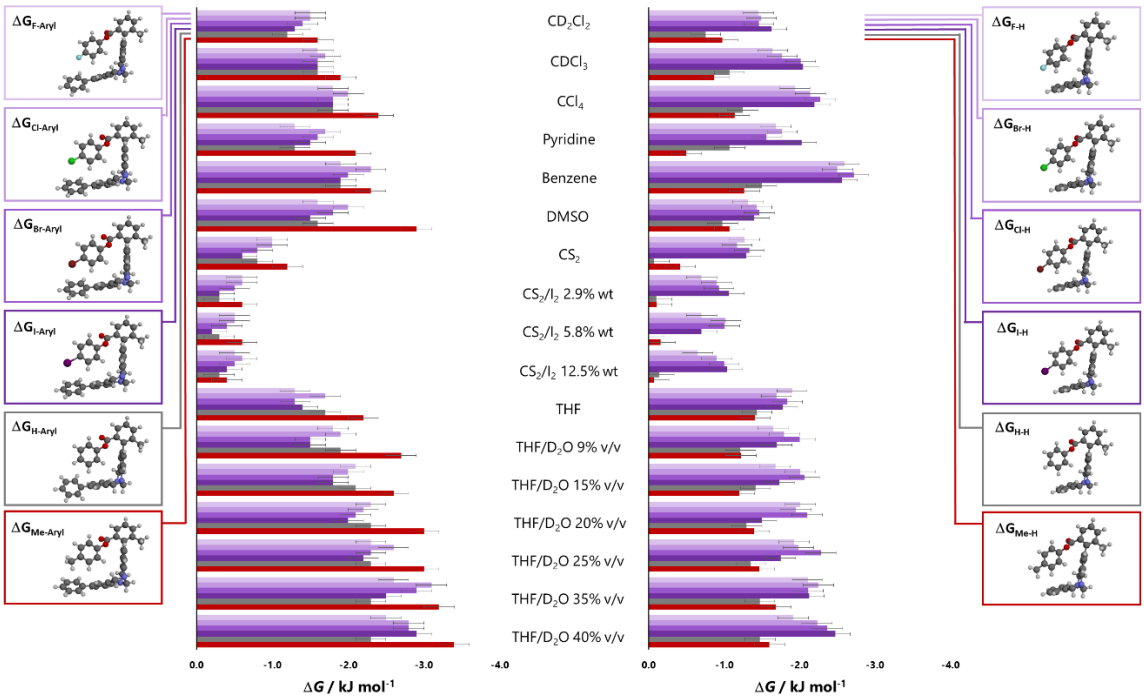

Figure 2.20: Experimental Δ*G* values for the **1X** (left) and **2X** (right) series of balances in 17 solvents and solvent mixtures.

More noteworthy is the inter-solvent variation in the Δ*G* values. Δ*G* values for series **1X** show that systematically increasing the cohesive energy density in the THF/D_2O solvent mixtures by adding more D_2O increases the favourability of halogen···arene contacts (Figure 2.20). The cohesive energy density encodes the strength of the solvent-solvent interactions, which has been show to serve as a quantitative descriptor of solvophobic effects.[24] In other words, increasing the cohesive energy density of the solvent drives the apolar groups into contact. Tellingly, the same variations in THF/D_2O mix composition do not induce such strong responses for the series **2X** balances where there is no halogen···arene contact present.

Similarly, adding the very polarisable molecule, I_2 to the most polarisable solvent, CS_2 enabled us to examine whether the favourability of the halogen···arene contact could be weakened by increasing the solvent bulk polarisability, and hence solvent competition for dispersion interactions (Figure 2.20). The Δ*G* values obtained for series **1X** show a slightly reduced preference for halogen-arene contacts (-0.6 to -0.3

kJ mol^{-1} for **1F** and -1.0 to -0.6 kJ mol^{-1} for **1I** (Appendix A.2) upon the addition of iodine to the solvent mixture.

Plots of ΔG against singular solvent properties for each balance yielded no strong correlations. Similarly, although multiple-linear regression fitting of different solvent properties to the experimental ΔG values were attempted (appendix A.9), such analyses were compounded by their small magnitudes. Multiple-linear regression analysis of just the mixed solvent systems (THF/D_2O and CS_2/I_2) did yield significantly improved correlations (R^2 = 0.81-0.96)(Appendix A.10) which adds credence to the notion of interactions within the bulk solvent playing a key role in determining halogen···arene interactions strength. Though the failure of this analysis to yield the same correlations with the entire solvent screen limits the weight of any quantitative conclusions that can be drawn.

$$\Delta\Delta G = \Delta G_{1X} - \Delta G_{1H} - \Delta G_{2X} + \Delta G_{2H} \qquad \text{(Equation 2.2)}$$

A clearer picture of the interactions present within the series **1X** balances can be ascertained via an experimental dissection of the ΔG values using the thermodynamic double mutant cycle (DMC) shown in Figure 2.13B. As outlined in Section 2.3 and 2.6, thermodynamic DMC analysis (Equation 2.2) accounts for energy changes arising from secondary interactions, enabling the contribution of the interaction of interest to the overall conformational free energy to be determined.

The use of DMC dissection in these molecular balances is vindicated by the comparable magnitudes of the ΔG values measured for the **2X** series of balances (Figure 2.20, right). Since the **2X** series of balances lacks the terminal aromatic ring, this means that the major contributor to folding is not due to halogen···arene contacts, but other secondary interactions such as the aromatic edge-to-face interactions and solvophobic effects.

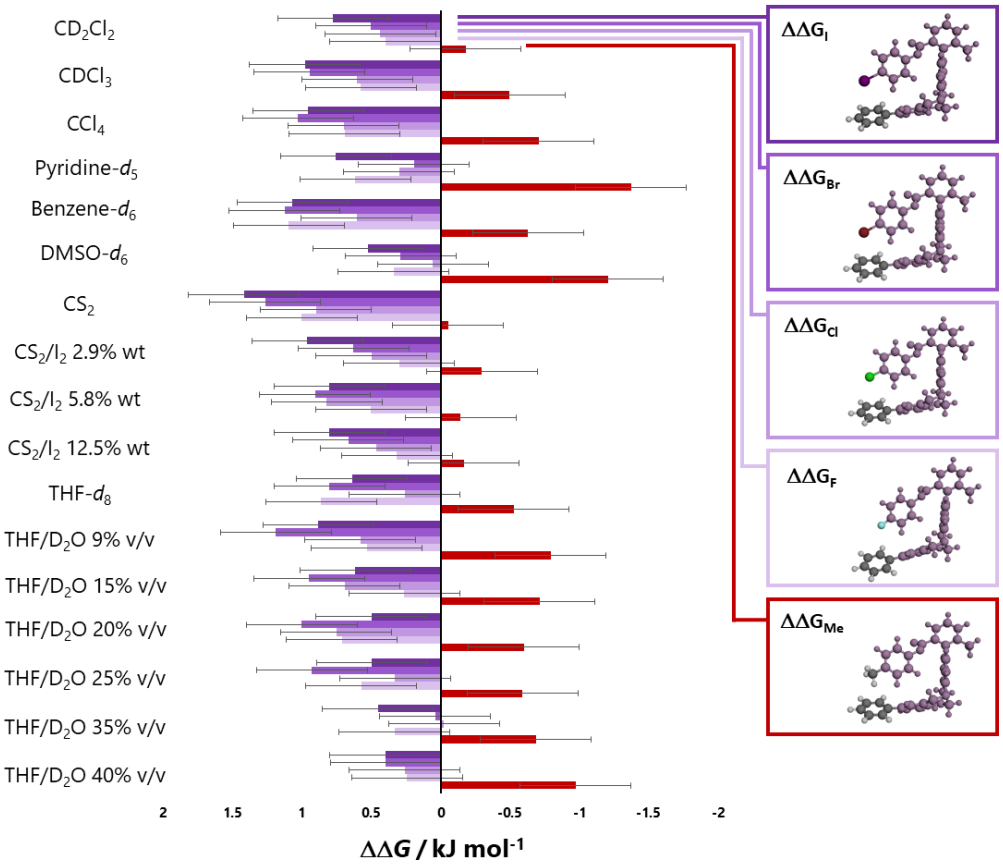

Figure 2.21: Double mutant cycle dissected ΔΔ*G* values for halogen···arene (purple) and methyl···arene (red) contacts.

The resultant DMC-dissected ΔΔ*G* values obtained for the series **1X** and **2X** balances are shown in Figure 2.21. The first observation is the very small range of the interaction energies ranging from only –1.5 kJ mol^{-1} to +1.5 kJ mol^{-1}. Nonetheless, there is stark contrast between the halogen···arene contacts and CH_3···π contacts (Figure 2.21). The consistently attractive nature of the CH_3···π contacts across all solvents examined confirms our previous assertation that an interaction exists within these balances that is not completely attenuated by solvent effects. By comparison, upon being dissected out from all other intramolecular effects, the halogen···arene contacts are all now consistently disfavoured. These dissected energies are consistent in both nature and magnitude to previous examples of dispersive interactions that have been attenuated by competitive solvent interactions.

Inter-halogen comparisons are still difficult due to the small energy differences, and are further compounded due to error propagation resulting from construction of the double mutant cycle. Despite this, it can still be seen that the larger the halogen, the less favourable the halogen···arene interaction becomes. Moreover, the change in the energetic penalty associated with varying the halogen is largest in the most polarisable solvents (CS_2/I_2 mixtures), and smallest in the solvents with the lowest polarisable solvents (THF/40% D_2O has the least variation in $\Delta\Delta G$). Solvophobic influences are also clear to see with the least disfavoured halogen···arene contacts being observed in THF/40% D_2O solution, and the most disfavoured halogen···arene contacts being found in the less cohesive organic solvents (benzene, CS_2, CCl_4).

2.10 Conclusions

Here we have used molecular torsion balances to probe the energetics of halogen···arene contacts. The adoption of the Wilcox balance framework and its inherent flexibility enabled the highly variable steric demands of the halogens to be accommodated. This enabled us to side-step steric issues that have been widely encountered in previous attempts to systematically investigate halogen interactions experimentally. The computational and experimental evidence to demonstrate that such contacts are primarily dispersive in nature. Halogen···arene contacts were shown to be weakly disfavoured in solution ($\Delta\Delta G$ = 0 to 1.5 kJ mol^{-1}), irrespective of whether the solvent had a high or low bulk polarisability (and therefore ability to engage in competitive dispersion interactions). Nonetheless, solvents that were more polarisable did compete more strongly with halogen-arene interactions. In contrast to the disfavoured halogen-arene interactions, methyl-arene interactions measured in the same class of molecular balances were found to be favoured in all solvents examined. This finding is contrary to previous findings reported by Oki and co-workers who saw Br/Cl···arene interactions stronger than the analogous CH_3···arene contact.[47,54] Our report of repulsive halogen···arene interactions is also counter to the attractive energies extrapolated by Schmieder (issues pertaining to this latter study as documented previously).[58] SAPT energy calculations support the hypothesis that the CH_3···arene interactions were favored over halogen···arene interactions due to electrostatic attraction, which are greatly diminished in the halogen···arene interactions possessed

of the studied geometries. The systems employed by Oki and Schmieder do not employ the same geometries and contain halogen···arene contacts closer to collinearity with the C-X bond. Such geometries will see a greater role played by the σ-hole, inducing greater attractive electrostatic forces and orbital effects. It is potentially here that this discrepancy can be rationalized.

Our results are however, in fair agreement with those reported by Shimizu who shows consistently repulsive halogen···arene interactions; with iodine being the most repulsive.[57] Halogen-arene interactions, particularly those involving the larger halogens, were more sensitive than CH_3-arene interactions to increasing the solvophobic effect via the addition of water (up to 40% (v/v) D_2O in THF). However, the solvophobic effect could not be increased to sufficient extent (up to 40% (v/v) D_2O in THF) to make the halogen-arene interaction favourable, suggesting that competitive interactions with the solvent still dominate the experimental behaviour.

2.11 References

1 Benesi, H. A. & Hildebrand, J. H. Ultraviolet absorption bands of iodine in aromatic hydrocarbons. *J. Am. Chem. Soc.* **70**, 2832-2833 (1948).

2 Benesi, H. A. & Hildebrand, J. H. A Spectrophotometric Investigation of the Interaction of Iodine with Aromatic Hydrocarbons. *J. Am. Chem. Soc.* **71**, 2703-2707 (1949).

3 Cavallo, G., Metrangolo, P., Milani, R., Pilati, T., Priimagi, A., Resnati, G. & Terraneo, G. The Halogen Bond. *Chem. Rev.* **116**, 2478-2601 (2016).

4 Desiraju, G. R., Ho, P. S., Kloo, L., Legon, A. C., Marquardt, R., Metrangolo, P., Politzer, P., Resnati, G. & Rissanen, K. Definition of the halogen bond. *Pure Appl. Chem.* **85**, 1711-1713 (2013).

5 Aakeroy, C. B., Bryce, D. L., Desiraju, G. R., Frontera, A., Legon, A. C., Nicotra, F., Rissanen, K., Scheiner, S., G.Terraneo, Metrangolo, P. & Resnati, G. Definition of the chalcogen bond (IUPAC Recommendations 2019). *Pure Appl. Chem.* **91**, 1889–1892 (2019).

6 Swierczynski, D., Luboradzki, R., Dolgonos, G., Lipkowski, J. & Schneider, H. J. Non-Covalent Interactions of Organic Halogen Compounds with Aromatic Systems – Analyses of Crystal Structure Data. *Eur. J. Org. Chem.*, 1172-1177 (2005).

7 Nazare, M., Will, D. W., Matter, H., Schreuder, H., Ritter, K., Urmann, M., Essrich, M., Bauer, A., Czech, J., Lorenz, M., Laux, V. & Wehner, V. Probing the Subpockets of Factor Xa Reveals Two Binding Modes for Inhibitors Based on a 2-Carboxyindole Scaffold: A Study Combining Structure-Activity Relationship and X-ray Crystallography. *J. Med. Chem* **48**, 4511-4525 (2005).

8 Matter, H., Nazare, M., Gussregen, S., Will, D. W., Schreuder, H., Bauer, A., Urmann, M., Ritter, K., Wagner, M. & Wehner, V. Evidence for C-Cl/C-Br···pi Interactions as an Important Contributionto Protein–Ligand Binding Affinity. *Angew. Chem. Int. Ed* **48**, 2911-2916 (2009).

9 Wilcken, R., Zimmermann, M. O., Lange, A., Joerger, A. C. & Boeckler, F. M. Principles and Applications of Halogen Bonding in Medicinal Chemistry and Chemical Biology. *J. Med. Chem* **56**, 1363-1388 (2013).

10 Jiang, S., Zhang, L., Cui, D., Yao, Z., Gao, B., Lin, J. & Wei, D. The Important Role of Halogen Bond in Substrate Selectivity of Enzymatic Catalysis. *Sci. Rep.* **6**, 34750 (2016).

11 Cao, J., Yan, X., He, W., Li, X., Li, Z., Mo, Y., Liu, M. & Jiang, Y. B. C–I···π Halogen Bonding Driven Supramolecular Helix of Bilateral N-Amidothioureas Bearing β-Turns. *J. Am. Chem. Soc.* **139**, 6605−6610, doi:10.1021/jacs.6b13171 (2017).

12 Mayerhçffer, U. & Wurthner, F. Halogen–Arene Interactions Assist in Self-Assembly of Dyes. *Angew. Chem.* **124**, 5713 –5717 (2012).

13 Lisac, K., Topić, F., Arhangelskis, M., Cepić, S., Julien, P. A., Nickels, C. W., Morris, A. J., Friščić, T. & Cinčić, D. Halogen-bonded cocrystallization with phosphorus, arsenic and antimony acceptors. *Nat. Commun.* **10**, 1-10 (2019).

14 Xu, Y., Huang, J., Gabidullin, B. & Bryce, D. L. A rare example of a phosphine as a halogen bond acceptor. *Chem. Commun.* **54**, 11041-11043 (2018).

15 Gullo, M. C., Baldini, L., Casnati, A. & Marchio, L. Halogen Bonds Direct the Solid State Architectures of a Multivalent Iodopropargylcalix[4]arene. *Cryst. Growth Des.* **20**, 3611−3616 (2020).

16 Wallnoefer, H. G., Fox, T., Liedl, K. R. & Tautermann, C. S. Dispersion dominated halogen–π interactions: energies and locations of minima. *Phys. Chem. Chem. Phys.* **12**, 14941–14949 (2010).

17 Tsuzuki, S., T.Uchimaru, Wakisaka, A. & Ono, T. Magnitude and Directionality of Halogen Bond of Benzene with C_6F_5X, C_6H_5X, and CF_3X (X = I, Br, Cl, and F). *J. Phys. Chem. A* **120**, 7020−7029 (2016).

18 Lu, Y., Zou, J., Wang, Y. & Yu, Q. Theoretical investigations of the C–X/π interactions between benzene and some model halocarbons. *Chem. Phys.* **334**, 1–7 (2007).

19 Ang, S. J., Mak, A. M., Sullivan, M. B. & Wong, M. W. Site specificity of halogen bonding involving aromatic acceptors. *Phys. Chem. Chem. Phys.* **20**, 8685-8694 (2018).

20 Hill, J. G. & Legon, A. C. On the directionality and non-linearity of halogen and hydrogen bonds. *Phys. Chem. Chem. Phys.* **17**, 858-867 (2015).

21 Rahman, A. N. M. M., Bishop, R., Craig, D. C. & Scudder, M. L. Pi–halogen dimer interactions and the inclusion chemistry of a new tetrahalo aryl host. *Org. Biomol. Chem.* **2**, 175-182 (2004).

22 Mebel, A. M., Lin, H. L. & Lin, S. H. Ab Initio Molecular Orbital and Density Functional Study of the C_6H_6-I_2 Complex in the Ground and Excited Electronic States. *Int. J. Quantum Chem.* **72**, 307-318 (1999).

23 Lu, Y., Zou, J., Wang, Y. & Yu, Q. Substituent Effects on Noncovalent Halogen/π Interactions: Theoretical Study. *Int. J. Quantum Chem.* **107**, 1479–1486 (2007).

24 Yang, L., Adam, C. & Cockroft, S. L. Quantifying Solvophobic Effects in Nonpolar Cohesive Interactions. *J. Am. Chem. Soc.* **137**, 10084-10087 (2015).

25 Adam, C., Yang, L. & Cockroft, S. L. Partitioning Solvophobic and Dispersion Forces in Alkyl and Perfluoroalkyl Cohesion. *Angew. Chem. Int. Ed* **54**, 1164-1167 (2015).

26 Yang, L., Adam, C., Nichol, G. S. & Cockroft, S. L. How much do van der Waals dispersion forces contribute to molecular recognition in solution? *Nature Chemistry* **5**, 1006-1010 (2013).

27 Yang, L., Brazier, J. B., Hubbard, T. A., Rogers, D. M. & Cockroft, S. L. Can Dispersion Forces Govern Aromatic Stacking in an Organic Solvent? *Angew. Chem. Int. Ed* **55**, 912 –916 (2016).

28 Hauchecorne, D., Veken, B. J. v. d., Herrebout, W. A. & Hansen, P. E. A 19F NMR study of C–I-Pi halogen bonding. *Chemical Physics* **381**, 5-10 (2011).

29 Hauchecorne, D., Veken, B. J. v. d., Herrebout, W. A. & Hansen, P. E. A ^{19}F NMR study of C–I$\cdots\pi$ halogen bonding. *Chemical Physics* **381**, 5-10 (2011).

30 Adams, H., Cockroft, S. L., Guardigli, C., Hunter, C. A., Lawson, K. R., Perkins, J., Spey, S. E., Urch, C. J. & Ford, R. Experimental Measurement of Noncovalent Interactions Between Halogens and Aromatic Rings. *ChemBioChem* **5**, 657-665 (2004).

31 Carter, P. J., Winter, G., Wilkinson, A. J. & Fersht, A. R. The Use of Double Mutants to Detect Structural Changes in the Active Site of the Tyrosyl-tRNA Synthetase (Bacillus stearothermophilus). *Cell* **38**, 835-840 (1984).

32 Horovitz, A. & Fersht, A. R. Strategy for Analysing the Co-operativity of Intramolecular Interactions in Peptides and Proteins. *J. Mol. Biol.* **214**, 613-617 (1990).

33 Serrano, L., Horovitz, A., Avron, B., Bycroft, M. & Fersht, A. R. Estimating the Contribution of Engineered Surface Electrostatic Interactions to Protein Stability by Using Double-Mutant Cycles. *Biochemistry* **29**, 9343–9352 (1990).

34 Cockroft, S. L. & Hunter, C. A. Chemical double-mutant cycles: dissecting non-covalent interactions. *Chem. Soc. Rev.* **36**, 172-188 (2007).

35 Aoyama, Y., Asakawa, M., Matsui, Y. & Ogoshi, H. Molecular Recognition of Quinones: Two-Point Hydrogen-Bonding Strategy for the Construction of Face-to-Face Porphyrin-Quinone Architectures. *J. Am. Chem. Soc.* **113**, 6233-6240 (1991).

36 Hof, F., Scofield, D. M., Schweizer, W. B. & Diederich, F. A Weak Attractive Interaction between OrganicFluorine and an Amide Group. *Angew. Chem. Int. Ed.* **43**, 5056–5059 (2004).

37 Horovitz, A. & Fersht, A. R. Co-operative Interactions during Protein Folding. *J. Mol. Biol.* **224**, 733-740 (1992).

38 Steyaert, J. & Wyns, L. Functional Interactions among the His40, Glu58 and His92 Catalysts of Ribonuclease T, as Studied by Double and Triple Mutants. *J. Mol. Biol.* **229**, 770-781 (1993).

39 Schreiber, G., Frisch, C. & Fersht, A. R. The Role of Glu73 of Barnase in Catalysis and theBinding of Barstar. *J. Mol. Biol.* **270**, 111-122 (1997).

40 Hunter, C. A., Jones, P. S., Tiger, P. & Tomas, S. Chemical Triple-Mutant Boxes for Quantifying Cooperativity in Intermolecular Interactions. *Chem. Eur. J.* **8**, 5435-5446 (2002).

41 Li, P., Vik, E. C. & Shimizu, K. D. N-Arylimide Molecular Balances: A Comprehensive Platform for Studying Aromatic Interactions in Solution. *Acc. Chem. Res.* **53**, 2705−2714 (2020).

42 Mati, I. K. & Cockroft, S. L. Molecular balances for quantifying non-covalent interactions. *Chem. Soc. Rev.* **29**, 4195-4205 (2010).

43 Elmi, A. & Cockroft, S. L. Quantifying Interactions and Solvent Effects Using Molecular Balances and Model Complexes. *Acc. Chem. Res.* **54**, 92–103 (2021).

44 Aliev, A. E. & Motherwell, W. B. Some Recent Advances in the Design and Use of Molecular Balancesfor the Experimental Quantification of Intramolecular Noncovalent Interactions of π Systems. *Chem. Eur. J.* **25**, 10516–10530 (2019).

45 Paliwal, S., Geib, S. & Wilcox, C. S. Molecular Torsion Balance for Weak Molecular Recognition Forces. Effects of "Tilted-T" Edge-to-Face Aromatic Interactions on Conformational Selection and Solid-State Structure. *J. Am. Chem. Soc.* **116**, 4497-4498 (1994).

46 Kim, E., Paliwal, S. & Wilcox, C. S. Measurements of Molecular Electrostatic Field Effects in Edge-to-Face Aromatic Interactions and CH-π Interactions with Implications for Protein Folding and Molecular Recognition. *J. Am. Chem. Soc.* **120**, 11192-11193 (1998).

47 Ooki, M. 1,9-Disubstituted Triptycenes: An Excellent Probe for Weak Molecular Interactions. *Acc. Chem. Res.* **23**, 351-356 (1990).

48 Carroll, W. R., Zhao, C., Smith, M. D., Pellechia, P. J. & Shimizu, K. D. A Molecular Balance for Measuring Aliphatic CH−π Interactions. *Org. Lett.* **13**, 4320–4323 (2011).

49 Motherwell, W. B., Moise, J., Aliev, A. E., Nic, M., Coles, S. J., Horton, P. N., Hursthouse, M. B., Chessari, G., Hunter, C. A. & Vinter, J. G. NoncovalentFunctional-Group–AreneInteractions. *Angew. Chem. Int. Ed.* **46**, 7823-7826 (2007).

50 Aliev, A. E., Moise, J., Motherwell, W. B., Nic, M., Courtier-Murias, D. & Tocher, D. A. Probing weak non-covalent interactions in solution and solid states with designed molecules. *Phys. Chem. Chem. Phys.* **11**, 97–100 (2009).

51 Muchowska, K. B., Adam, C., Mati, I. K. & Cockroft, S. L. Electrostatic Modulation of Aromatic Rings via Explicit Solvation of Substituents. *J. Am. Chem. Soc.* **135**, 9976−9979 (2013).

52 Mati, I. K., Adam, C. & Cockroft, S. L. Seeing through solvent effects using molecular balances. *Chem. Sci.* **4**, 3965–3972 (2013).

53 Elmi, A. *Aromatic Interactions in Solution* PhD Thesis thesis, University of Edinburgh, (2020).

54 Nakai, Y., Yamamoto, G. & OokI, M. Substituent effects on the populations of rotational isomers in ... Evidentce for CH_3-π interactions. *Chem. Lett.* **16**, 89-92 (1987).

55 Nakai, Y., Yamamoto, G. & OokI, M. Substituent effects on the populations of rotational isomers in ... Evidentce for CH3-pi interactions. *Chem. Lett.* **16**, 89-92 (1987).

56 Gung, B. W., Emenike, B. U., Lewis, M. & Kirschbaum, K. Quantification of CH$\cdots\pi$ Interactions: Implications on How Substituent Effects Influence Aromatic Interactions. *Chem. Eur. J.* **16**, 12357 – 12362 (2010).

57 Li, P., Maier, M., Vik, E. C., Yehl, C. J., B.E.Dial, Rickher, A. E., Smith, M. D., Pellechia, P. J. & Shimizu, K. D. Stabilizing Fluorine–pi Interactions. *Angew. Chem. Int. Ed* **56** (2017).

58 Sun, H., Horatscheck, A., Martos, V., Bartetzko, M., Uhrig, U., Lentz, D., Schmieder, P. & Nazare, M. Direct Experimental Evidence for Halogen–Aryl π Interactions in

Solution from Molecular Torsion Balances. *Angew. Chem. Int. Ed* **56**, 6454-6458 (2017).

59 Rosokha, S. V. Anion-pinteraction in metal-organic networks formed by metalhalides and tetracyanopyrazine. *J. Mol. Struct* **1138**, 129-135 (2017).

60 Mascal, M., Armstrong, A. & Bartberger, M. D. Anion-Aromatic Bonding: A Case for Anion Recognition by π-Acidic Rings. *J. Am. Chem. Soc.* **124**, 6274-6276 (2002).

61 Garau, C., Frintera, A., Quinonero, D., Ballester, P., Costa, A. & Beya, P. M. A Topological Analysis of the ElectronDensity in Anion - pi Interactions. *CHEMPHYSCHEM* **4**, 1344-1348 (2003).

62 Jian, J., Poater, J., White, P. B., McKenzie, C. J., Bickelhaupt, F. M. & Mecinovic, J. Probing Halogen−π versus CH−π Interactions in Molecular Balance. *Org. Lett.* **22**, 7870−7873 (2020).

63 Whiteley, N. D. *Hydrogen-Bonding and Halogen-Arene Interactions*, University of Edinburgh, (2017).

64 Parker, T. M., Burns, L. A., Parrish, R. M., Ryno, A. G. & Sherrill, C. D. Levels of symmetry adapted perturbation theory (SAPT). I. Efficiency and performance for interaction energies. *J. Chem. Phys.* **140**, 094106 (2014).

65 Riley, K. E. & Hobza, P. Investigations into the Nature of Halogen Bonding Including Symmetry Adapted Perturbation Theory Analyses. *J. Chem. Theory Comput.* **4**, 232-242 (2008).

66 Riley, K. E. & Hobza, P. The relative roles of electrostatics and dispersion in the stabilization of halogen bonds. *Phys. Chem. Chem. Phys.* **15**, 17742-17751 (2013).

67 Stone, A. J. Are Halogen Bonded Structures Electrostatically Driven? *J. Am. Chem. Soc.* **135**, 7005-7009 (2013).

68 Sawar, M. G., Dragisic, B., Salsberg, L. J., Gouliaras, C. & Taylor, M. S. Thermodynamics of Halogen Bonding in Solution: Substituent, Structural, and Solvent Effects. *J. Am. Chem. Soc.* **132**, 1646-1653 (2010).

69 Emenike, B. U., Spinelle, R. A., Rosario, A., Shinn, D. W. & Yoo, B. Solvent Modulation of Aromatic Substituent Effects in Molecular Balances Controlled by CH−π Interactions. *J. Phys. Chem. A* **122**, 909−915 (2018).

Chapter 3

Comparative Studies of Bifurcated Halogen Bonds and Hydrogen Bonds

Abstract

The bifurcation of non-covalent interactions presents a novel approach to tuning their strength and geometries. The bifurcation of halogen bonds is of particular interest, with many crystallographic and computational studies suggesting advantages over traditional one donor, one acceptor systems. However, in spite of this potential there is a distinct lack of systematic solution phase study of bifurcated halogen bonding arrangements. Here we attempt to address this issue by conducting such a study; measuring the strength of a series of host guest complexes via ^{1}H NMR titrations that contain single point, bifurcated and trifurcated halogen bonding arrangements. In addition to studying halogen bonds; analogous hydrogen bonding host guest systems are also studied to provide appropriate comparison. Furthermore, an array of computational methods have been employed to dissect how the underlying forces respond to bifurcation. Experimental measurement vindicated the notion of increased complexation energy in response to bi- and trifurcation in halogen bonded complexes (0.25 kJ mol^{-1} for single point XB, -4.95 kJ mol^{-1} for a bifurcated XB). SAPT calculations show that the key driving force behind the increased strength is a reduction in exchange repulsion; even if the adopted geometries result in an accompanying reduction in the attractive terms. Comparison to hydrogen bonds showed similar increases in complexation energies as a product of bifurcation with the rigid, pre-organized aromatic host series however struggled to form bifurcated complexes with the more flexible aliphatic hosts and wasn't able to form a trifurcated complex.

Contributions: All experimental and computational work was conducted by AMLW

3.1 Introduction to bifurcated halogen bonds

Halogen bonding has seen a significant rise in interest over the last two decades, with applications being found in a variety of fields.[1-7] In this chapter we expand our understanding of halogen bonding interactions beyond the more widely considered linear arrangement by considering bifurcated halogen bonds.

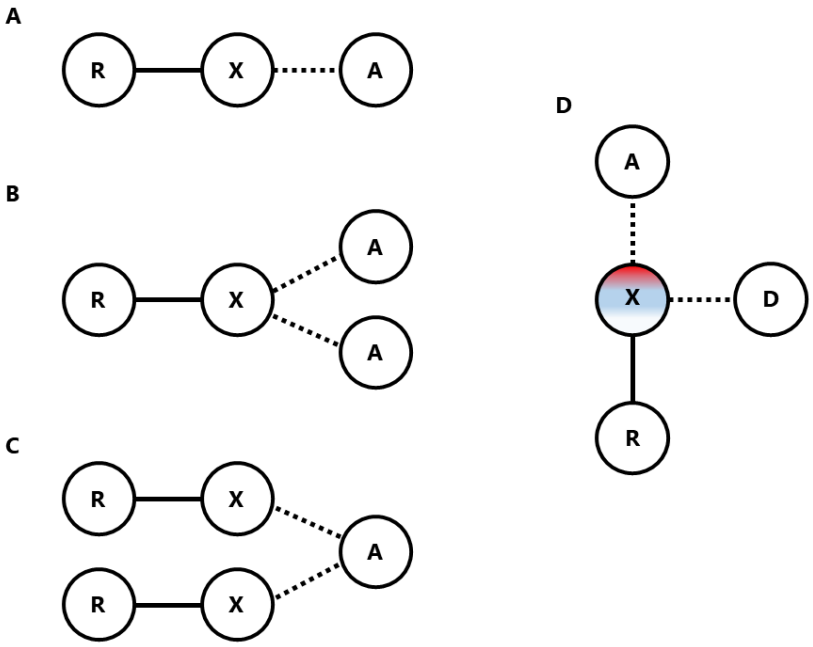

Figure 3.1: A) traditionally defined single point halogen bond. **B)** D•A_2 bifurcated halogen bonding arrangement. **C)** D_2•A bifurcated halogen bonding arrangement. **D)** Non-bifurcated bidentate halogen contain system with both axial and equatorial interactions.

Bifurcated as a term is defined as *divide into two branches or forks* and appears in a variety of contexts. Mirroring established terminology used to describe bifurcated hydrogen bonds (Figure 3.1A),[8,9] a bifurcated halogen bond involves the interaction of two bond acceptors (A) and a single bond donor (D)[8,10,11] (D•A_2, Figure 3.1B). To maintain this analogy, a bifurcated halogen bond should be defined as the interaction between two nucleophiles and one σ–hole. The anisotropic distribution of electrons that can be found in halogen bond donors[12] (chapter 1) means that halogens can act as both a donor and acceptor. A true bifurcated system should not include asymmetrical interactions involving both the σ-hole and the high equatorial electron density (Figure 3.1D). Indeed, such clarifications will prove highly useful when the concept of

bifurcation is extended to systems that feature multiple σ-holes[13] such as halogen bonding array systems and divalent iodide systems.[14,15]

It should be noted that the inverse arrangement involving one bond acceptor with two bond donors (D_2•A, Figure 3.1C), also meets the dictionary definition of bifurcation and this motif is often used interchangeably in the literature for both halogen and hydrogen bonding. Indeed, we would not be the first to highlight potential confusions that this duality of definitions may cause.[8] At time of writing there is no formal IUPAC definition for bifurcation or an alternate phrase, therefore we must specify that the term bifurcation used herein exclusively refers to the D•A_2 (Figure 3.1B) arrangement unless stated otherwise.

3.2 Donor-Acceptor-Acceptor Systems

Initial studies of bifurcated motifs in halogen bonded systems date back to the mid 1990's with much work being conducted by Desiraju.[16] Such studies employed NO_2 as a halogen bond acceptor, which produce molecular ribbons (Figure 3.2A) assembled with shorter halogen bond distances than any of the nine examples of bifurcated halogen bonds that had been identified in the CSD at the time. In contrast, the structurally similar =$C(CN)_2$ acceptor moiety did not form bifurcated bonds and assembled into a different crystal structure (Figure 3.2B). While the linear single-point halogen bonds in Figure 3.2B are shorter and more linear, only the bifurcated synthon produced well-defined sheets. Indeed, Desiraju and co-workers have since demonstrated the reliability of the bifurcated I···NO_2 synthon as a useful building block for crystal engineering.[17-20]

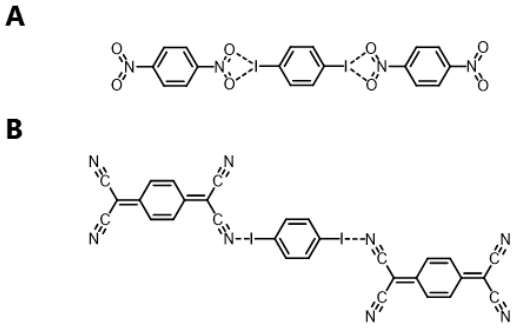

Figure 3.2: A) Bifurcated I···NO_2 discovered in Desiraju's early work, **B)** Ribbons featuring =$C(CN)_2$ halogen bond acceptor moieties did not to bifurcate.[16]

Computational studies into the physical nature of bifurcated halogen bonds have proved to be a rich vein of study. The X···NO_2 bifurcated motif as seen in Desiraju's papers were studied by Zou and co-workers in 2006[21] at MP2 level of theory using the aug-cc-PVDZ basis set. The compared bifurcated and linear halogen bonded arrangements (Figure 3.3). Contrasting with the experimental observed packing, the calculations suggested that the side-on linearly halogen bonded complexes were stronger than the bifurcated arrangement. The complexation energy of the bifurcated system when X = Cl was only 18% of the strength of the side-on system, but when X = Br the energy of the bifurcated system increased to 42% of the strength of the correspondent side-on system. This suggests that the bifurcated halogen bonding interactions are proportionally more stable with larger halogen atoms, which may explain the stability of the I···NO_2 synthon found in Desiraju's structures.[16-18]

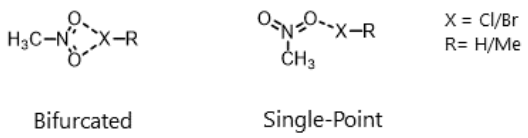

Figure 3.3: Bifurcated and single-point halogen bond interactions in the X···NO_2 system studied computationally by Zou *et al.*[21]

In addition to the MP2 calculations, the study also employed Bader's atoms in molecules (AIM) theory[22] to analyse the bifurcated arrangements. This showed two bond critical points (BCPs) and a ring critical point (RCP) demonstrating the involvement of both oxygen atoms. AIM analysis revealed modest electron density at the BCPs and their respective Laplacians, suggesting that the bifurcated interactions are predominantly closed shell. Single linear halogen bonded analogues yielded BCPs with approximately twice the electron density of those found for the individual halogen bonds in the bifurcated system. The Lapacian values followed a similar pattern, but were sufficiently small to indicate only a limited degree of covalence.

Ji and co-workers[23] expanded the exploration of bifurcated halogen bonded systems into heterocyclic aromatic species. Specifically, 1,10-phenanthroline-5,6-dione (PDONE), 4,5-diazafluoren-9-one (DAFONE) and 4,4',6,6'-tetramethyl-2,2'-bipyrimidine (TMPM) (Figure 3.4). A 2011 CSD search by the authors for the X···NO_2

bifurcated motif revealed that despite more examples being added to the database, fully symmetrical arrangements are very rare. Indeed, even asymmetrically skewed bifurcated arrangements are rare when compared to the side-on single halogen bond arrangement analogous to those studied by Zou. PDONE and TMBPM shown in Figure 3.4A aimed to produce more stable symmetrical arrangements by featuring shorter distances between the two local electrostatic potential minima ($V_{s,min}$) than present in either nitromethane or DAFONE.

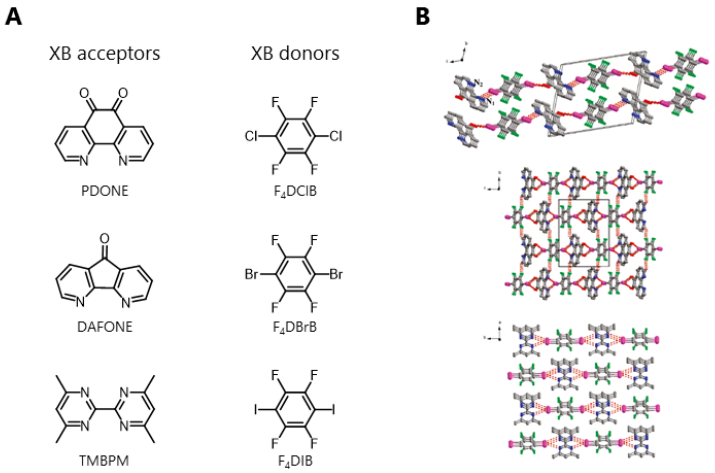

Figure 3.4: A) Designs of XB acceptors and donors employed by Ji to investigate bifurcated XBs. **B)** Crystal packing from co-crystals of F4DIB and DAFONE, top; PDONE, middle; TMBPM, bottom.[23]

Complexes formed between the heterocyclic acceptors and $C_6F_4X_2$ halogen bond donors were minimised at the B97D/TZVP level, with iodine atoms being treated with a TZVPP pseudopotential. Compellingly, Ji was able to produce several co-crystals in the laboratory by utilising these designs. Though it should be noted, in line with Ji's computational expectations, only species featuring iodine halogen bond donors readily formed co-crystals. As predicted, PDONE and TMBPM produced symmetrical bifurcated structures both computationally and in the solid state (Figure 3.4B), while the more distant lone pairs of DAFONE allowed for asymmetrically and symmetrically bifurcated arrangements to coexist computationally. In all cases, AIM analysis showed two BCPs between the halogen and both nitrogen/oxygen atoms. However, a more in-depth analysis showed a non-zero number of imaginary frequencies for all of the symmetrical structures save for those formed between PDONE/TMBPM and $C_6F_4I_2$, which suggested that all of the other symmetrical minima were actually transition states. Only the aforementioned combinations of donor and acceptor yielded

symmetrically bifurcated chains. However, there is not consistent agreement between the crystal structures and calculations; the crystals obtained from DAFONE and $C_6F_4I_2$ produced linear single halogen bonds with the second nitrogen being too far from iodine to meaningfully bifurcate. Nonetheless, this work served as a proof-of-concept for the computational design of novel bifurcated halogen bond acceptors.

Similar designs of bifurcated halogen bond acceptors are shown in Figure 3.5 as employed in a 2015 study by Bartashevich and co-workers.[24] Computational gas-phase complexes between these acceptors and dihalides produce asymmetrically bifurcated complexes, with theoretical symmetrical complexes producing a non-zero number of imaginary frequencies. Corroborating with the AIM studies of the previously discussed work, the superposition of atomic ρ- and φ-basins (as defined by the (IQA) method)[25] over electrostatic static potential maps (figure 3.5 B&C).[26-28] The former basin (ρ) defining the chemically bounded atoms and the latter (φ) defining electrically neural fragments. As much showed that interactions involving the halogen and both nitrogen atoms occurred in all cases; demonstrated by the penetration of the nitrogen atoms electron density into the halogen atoms φ-basin. Due to the asymmetrical arrangement of the complex, the shorter X···N contacts were found to be associated with significant delocalisation of electrons from the relevant nitrogen to the halogen atom. The pathways are noted to be more complex for the longer X···N' contact, but attraction is present in all cases.

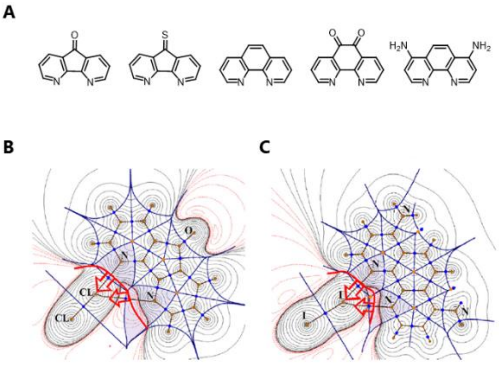

Figure 3.5: A) Expanded scope of bifurcated XB acceptors as employed by Bartashevich and co-workers. **B&C)** Superimposed images of the ρ- and φ-basins atop electrostatic surface potentials for Cl_2/4,5-diazafluoren-9-one and I_2/10-phenanthroline-4,7-diamine respectively. Red lines, ρ-basins; blue lines, φ-basins; red arrows direction of atomic attraction.[24]

Breakdown of the energetic components using the IQA methodology [29-31] shows increasing electrostatic terms with increasing halogen size and an increase in the exchange repulsion term with decreasing halogen size. While this much may appear counter intuitive this can be rationalised by the X···N' contact exerting a greater degree of influence over the heavier halogens; a product of the increased halogen size. Indeed a breakdown of the exchange energies into two-atomic terms shows counter acting trends for the X···N and X···N' contributions in response to changing halogen size. The more symmetrical and evenly distributed bonding contributions found in the heavier halogen systems highlight their greater suitability for bifurcated halogen bonding, but the results clearly demonstrated that bifurcation remains possible for Cl.

Marek and co-workers[32] drew attention to the interplay of energetic contributions in bifurcated halogen bonding. The study examined 1,2-dimethoxybenzene derivatives as bifurcated acceptors (Figure 3.6), and suggested that the stabilisation afforded by electrostatic components is comparable to the non-electrostatic terms. Furthermore, it was concluded that both the electrostatic and non-electrostatic terms increase in parallel with increasing negative charge on the electron donor.

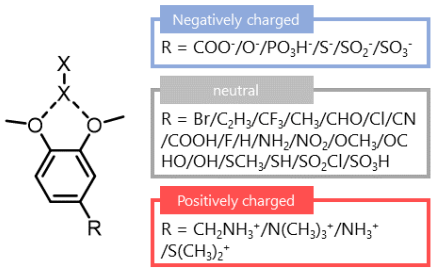

Figure 3.6: Substituted 1,2-dimethoxybenzene XB acceptors studied by Marek and co-workers.[32]

These conclusions were based on a battery of computational examinations, including Bader's quantum theory of atoms in molecules (QTAIM),[22] energy decomposition analysis (EDA)[33] and natural bond order (NBO).[34] QTAIM identified line critical points (LCP) between the donating halogen atom and both oxygen atoms in the majority of cases, a few of which will be discussed later in this section. This finding is similar to previous studies,[21,23] except for the finding that there was a reduction in the electron density at the LCP for the adjacent C-O bonds in the substituted 1,2-dimethoxybenzene derivatives. This was consistent with electron delocalisation into

the halogen bond upon complexation. NBO analysis also confirmed electron delocalisation from one lone pair on each oxygen atom into the LUMO of the halogen-carbon bond. Dissection of the interactions into their component terms *via* EDA based on M06-2X/def2-TZVPPD minimised geometries showed than in strong halogen bonds the sum of the electrostatic and Columbic terms are dominant. However, in the weaker halogen bonds this term is typically diminished and the exchange–correlation term becomes dominant. Notably, both the electron sharing terms from the EDA and the delocalisation index at the LCPs correlate well with the calculated complex energies. This emphasises the role that terms other than electrostatics play, but the relative weighting of the component terms varies significantly depending on the substituents involved. Reminiscent of the work of Riley, Hobza and others [35-37] that demonstrated increased non-electrostatic term weightings in conventional traditional halogen bonds when less electron withdrawing substituents decorate the halogen moiety.

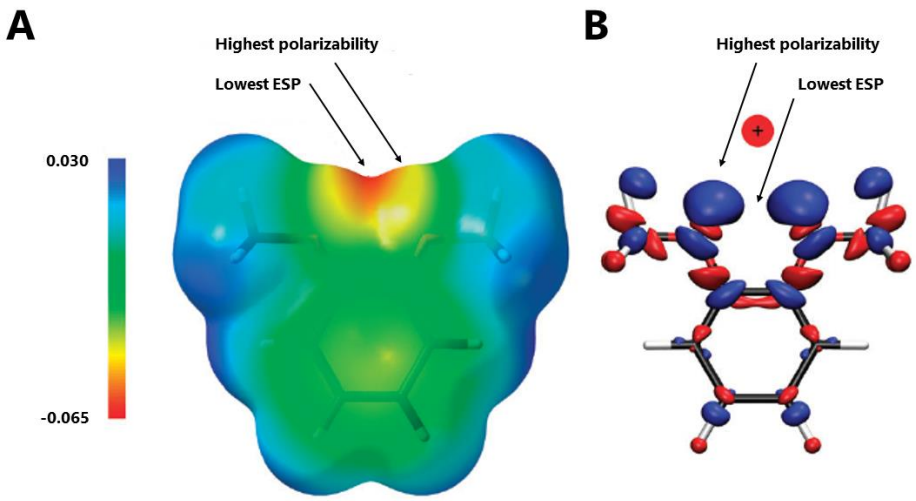

Figure 3.7: **A)** Electrostatic surface potential (kcal mol^{-1}) of 1,2-dimethoxybenzene, **B)** electron deformation density map as produced by a +0.5 a.u. point charge positioned 3 Å from the oxygen atoms. Blue and red lobes denote electron concentration and depletion respectively.[32]

Minimisation of the series of 1,2-dimethoxybenzene bifurcated halogen bond acceptors with several hetero-dihalogens yielded an interesting finding. Though the ESP $V_{s,min}$ is centred between the two oxygens, the asymmetrical arrangement of the bonding results in the halogen σ-hole coincides with region that is most polarised

(Figure 3.7) as identified by electron deformation density mapping.[38,39] The implication is that the geometry of the halogen bond favours contact associated with the best potential for polarisation (i.e. the oxygen) rather than the electrostatic minimum. Indeed, as seen in other studies, the hypothetical symmetrical arrangement is less stable.[23,24] The authors also comment on the wide range of angles that are observed between the aromatic plane and the X-X bond axis. Such deviation suggests a reduced role of electrostatics in the electron-poor donors.[35,40-42] In a few cases where minimisation rotated one of the methoxy groups out of the aromatic plane, and these geometries exhibited two-centre halogen bonds that constituted some of the most stable complexes studied. This finding again suggests that a single close-contact halogen bond (bond length 68% of Σ vdW radii) is typically stronger than a slightly more distant bifurcated arrangement (bond lengths ~90% of vdW radii).

The role of substituent effects on bifurcated halogen bonding is documented in Frontera's 2011 paper.[43] This study concluded that substituent effects affected bifurcated halogen bonds to the same extent as conventional single-point halogen bonds.[43-45] The strength of bifurcated and single halogen bonds were found to be similar in magnitude; the loss in linearity due to bifurcation being compensated by a proportional increase in donor strength. Two-acceptor one-donor ($D•A_2$) bifurcated halogen bonds were also found to be stronger than two-donor one-acceptor ($D_2•A$) cases.

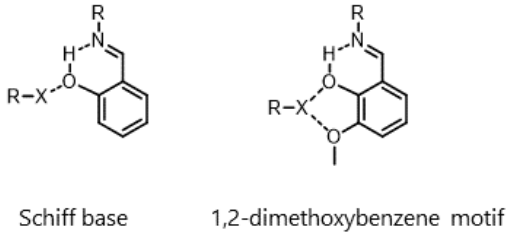

Figure 3.8: Single XB Schiff base motif and bifurcated XB 1,2-dimethoxybenzene motifs studied by Cincic and co-workers.[46]

A more recent study by Cincic and co-workers[46] considered complexes between iodopentafluorobenzene and Schiff bases (Figure 3.8). A CSD survey found that structures containing the 1,2-dihydroxyl Schiff base (Figure 3.8, right) had a 11 to 1 preference to form bifurcated bonding arrangements over single-point halogen bonds.

Of the five crystal structures included in this study, only three were found to include hydroxyl halogen bond acceptors with only two of those showing "optimal geometries". Quite tellingly, all these cases also featured an N···I halogen bond. Meanwhile, the purely homoaromatic Schiff base (figure 3.8 left) formed halogen-arene contacts in preference to HO···I halogen bonds, even though the former are expected to be very weak interactions. One limitation of such crystallographic studies is that the relative interaction strengths are not measured. However, the authors did note that the length of the single HO···I bond was similar to the shorter of the two bonds observed in the bifurcated arrangement. This led to the suggestion that the two should be reasonably comparable in strength as there is some precedent for using bond length as a predictor for strength.[12,47,48] In this case, the bond shortening of the primary halogen bond was attributed to the additional stability afforded by the formation of the secondary bifurcated interaction.

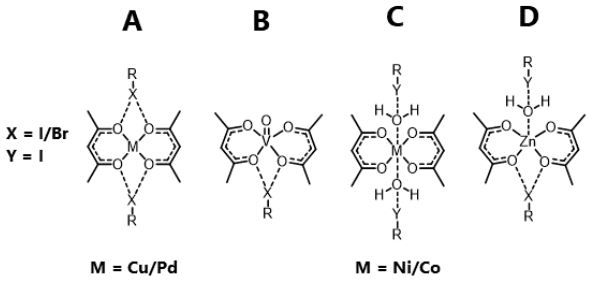

Figure 3.9: Square-planar acac metal complexes employed as bifurcated XB acceptors by Cincic et al.[49]

More recently, bifurcated halogen bond acceptors derived from metal-ligand complexes have garnered interest. Cincic and co-workers examined bifurcated halogen bonds to acetylacetonate ligands bound to square-planar metal complexes (Figure 3.9).[49] The negatively charged oxygen atoms of the anionic ligand present a particularly strong halogen bond acceptor. Co-crystallisation of $C_6F_4X_2$ with the square-planar metal complexes revealed the formation of bifurcated halogen bonds. The addition of two H_2O ligands (Figure 3.9C) showed the hydrogen bonds outcompeted the bifurcated halogen bonds from $C_6F_4X_2$, instead yielding single-point halogen bonds with the complexes H_2O ligand's oxygen atoms. However, metal complexes containing only a single H_2O ligand could still form bifurcated interactions

with $C_6F_4X_2$ on the unoccupied side of the metal complex (Figure 3.9D), suggesting a preference for bifurcation over the single-point bond.

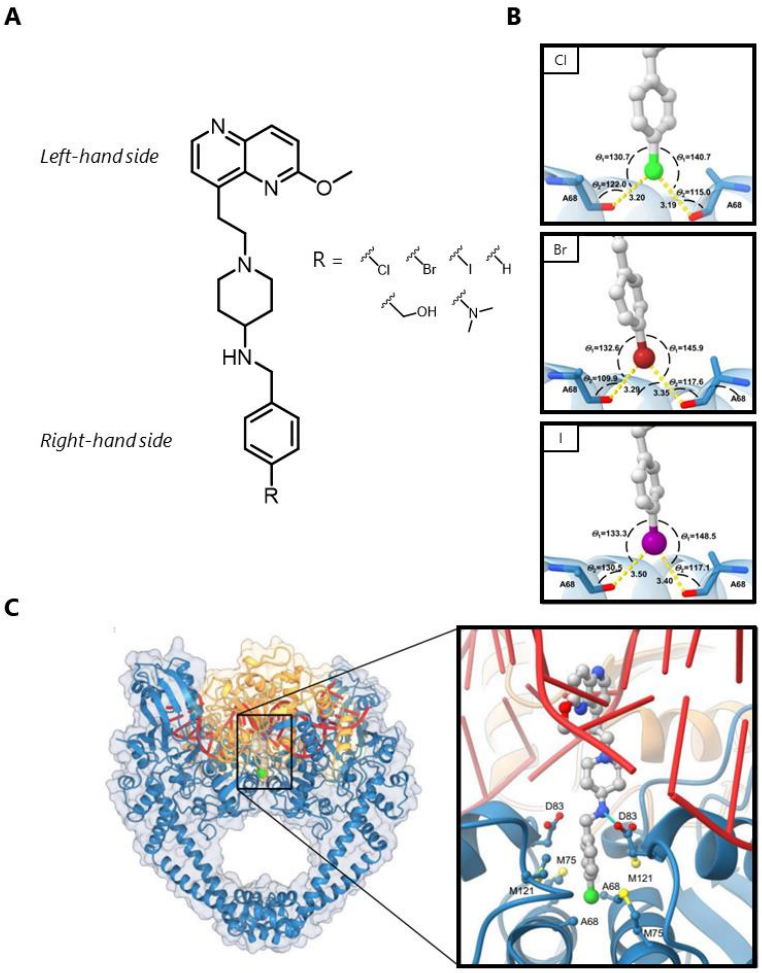

Figure 3.10: A) Novel bacterial type II topoisomerase inhibitor (NBTI) employed by Anderluh and co-workers. **B)** Molecular dynamics simulation snapshots for the three halogenated NBTIs. **C)** Hybrid cartoon representation of the Cl NBTI crystal stature in a gyrase-DNA-inhibitor complex, 2.3-Å resolution (DNA shown in red, GyrA in blue and GyrB in yellow).

The potential of bifurcated halogen bonding to be exploited in pharmaceutical design was demonstrated by Anderluh and co-workers in 2021.[50] Halogenated bacterial type II topoisomerase inhibitors (NBTIs) were shown to act as potent antibacterial DNA-gyrase inhibitors (Figure 3.10A). The authors point to such gyrase inhibitors featuring in over 200 papers in the last decade.[50] The mode of action for these species constitutes the formation of gyrase-DNA-inhibitor complexes that induces single-strand DNA cleavage (Figure 3.10C).[51] High-quality crystal structures revealed that the *left-hand*

side of the NBTIs species intercalates with the DNA,[51,52] while *right-hand side* interacts with a hydrophobic binding pocket within the GyrA protein.[51,53] This pocket is largely devoid of polar amino acid residues that might be targeted by pharmaceuticals to attain specificity and binding stability.

In the absence of traditional binding targets, the halogenated NBTIs instead form bifucated halogen bonds with the protein backbone, in this case the Ala68 residues (Figure 3.10B). As much being shown by both molecular dynamics simulations and crystal structures. Attempts were made to replicate this approach with bifurcated hydrogen bonds, but subsequent cleavage assays against *S. aureus* and *E. coli* showed a marked decrease in potency when compared to bifurcated halogen bonded compounds. The strategy of targeting backbone moieties minimises the development of bacterial resistance via single residue mutation. Tests against *S. aureus* and methicillin-resistant *S. aureus* both demonstrated the same strong antibacterial activity. The authors also make note of the relatively small size of the GyrA interaction pocket, which is less able to accommodate larger moieties and therefore making bifurcation from relatively small halogen-bond donor attractive over much larger moieties reliant on more defuse binding modes such as hydrophobicity.

3.3 Donor-Donor-Acceptor Systems

The bifurcated interactions discussed thus far all involve a single halogen atom interacting with a pair of donor species (Figure 3.1B, D•A_2). However, bifurcation may also refer to the inverse arrangement involving two halogen atoms interacting with a single acceptor (Figure 3.1C, D_2•A). A comprehensive study of nitrogen, oxygen and sulphur atoms acting as bifurcated halogen bonding acceptors was conducted in 2011.[54] A search of the CSD showed that although D_2•A hydrogen bonding is relatively common, the halogen bonded equivalent is rather rare. Instead, there is a strong preference for single-point bonding alternatives when available (Figure 3.1A). The CSD search identified five structures in which phosphine oxides acted as D_2•A bifurcated acceptors. However, attempts to co-crystalise such species with heavily fluorinated iodobenzenes (Figure 3.11) did not contain the desired arrangement. Instead of donating into the oxygen acceptor, the second halogen bond is shown to bond to the equatorial electron density of the iodine atom (figure 3.11B).

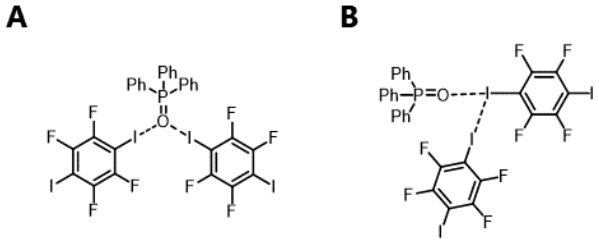

Figure 3.11: D_2•A Bifurcated XBs employing an oxygen acceptor. **A)** Structure as designed, **B)** Structure as observed in the crystal structure.[54]

Nevertheless, the authors were able to produce crystals structures featuring D_2•A bifurcated S and N centres. The sulphur containing systems are based around 1,4-dithiane, which forms a ladder complex with 1,4-$C_6F_4I_2$ (Figure 3.12A). The S···I distances observed, while shorter than the sum of the van der Waals radii, were notably longer than single halogen bonded analogues,[55,56] and the same was true for the acridine example (Figure 3.12B). The acridine example formed interlocking chains with 1,2-$C_6F_4I_2$ stabilised by aromatic stacking. In contrast, phenazine co-crystallisation with 1,2-$C_6F_4I_2$ forms only a single-point halogen bond. However, it should not be concluded that D_2•A nitrogen bifurcated halogen bonds are only accessible in the presence of aromatic stacking; a CSD search revealed several examples that were not reliant on other supporting forces.[57,58] An interesting example single short linear halogen bond between an iodine atom and a pyridine moiety that was also involved in a second longer range N···I contact at ~90° from the first was also found.[59,60] Such an arrangement further complicates the bifurcated naming dichotomy, as it could be interpreted as the combination of an I···N and an I···arene halogen bonds (Figure 3.13).

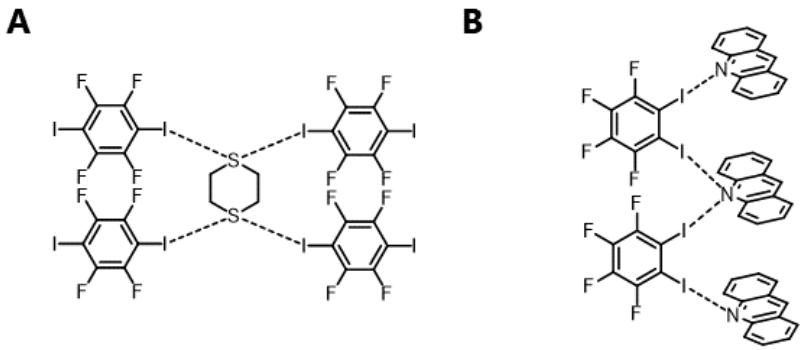

Figure 3.12: **A)** Sulphur acceptor based D_2•A bifurcated ladder complex. **B)** Nitrogen acceptor D_2•A bifurcated XB complex. Figure only shows one thread of the interlocking complex.[54]

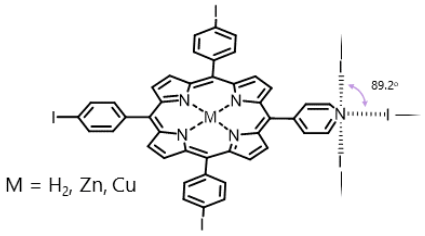

Figure 3.13: Potential trifurcated halogen bond reported by Goldberg *et al.* featuring a short 3.06 Å N···I contact in the porphyrin plane, and distant 3.48 Å N···I contacts out of the plane. [59,61]

Mirroring the examination of metal complexes in D•A_2 bifurcated halogen bonds (Figure 3.9),[49] transition metal complexes have also been used the acceptor species in D_2•A arrangements. Tetracyanonickelate $[Ni(CN)_4]^{2-}$ was found to crystallise with both bi- and trifurcated XBs upon co-crystallisation with diiodoacetylene (Figure 3.14).[61] However, attention needs to be paid to role of the counter ion with the initial co-crystallisation yielded linear tapes featuring conventional single-point halogen bonds.[62] This was attributed to the bulky $[PPh_4]^+$ counter ions, which prevented interaction between the tapes. Instead, the use of $[NBu_4]^+$ cations allowed for the inclusion of additional bridging C_2I_2 molecules between the tapes, thus creating bifurcated halogen bonds on the nitrogen atoms at the cost of slightly longer bonds (2.77-2.96 Å elongated to 2.85-3.11 Å) compared to those seen in the $[PPh_4]^+$ counter ion single-point bond only tapes. Further changes to the counter ion resulted in the

formation of a rare trifurcated halogen bond in the presence of the Bis(triphenylphosphine)iminium ($[PNP]^+$) counter ion. The crystal structures and DFT-minimised analogues indicated that the relative denticity of halogen bond centres is seemingly independent of the traditional relationship of more linear halogen bonds being shorter.[12] The trifurcated centres bear a striking resemblance to covalently bonded tetrahedral structures with 90° angles between the constituent bonds. An angle that is common to the only other known example of a single-donor trifurcated halogen bond (Figure 3.13).[59]

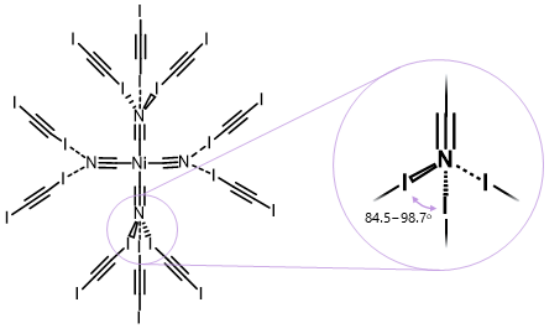

Figure 3.14: Tetracyanonickelate $[Ni(CN)^4]^{2-}/C_2I_2$ complex employed by Malichewshi *et al.*, exhibiting both D_2•A bifurcation and D_3•A trifurcation.[61]

The observed I···N···I angles for both structures (Figure 3.13 and Figure 3.14) being very similar suggests uniformity of binding motif. However, the > 0.4Å difference between the shorter and two longer halogen bonds seen in the figure 3.14 example contrasts strongly with the relatively uniform bond lengths presented by Malichewshi and co-workers. This difference is likely due to the aromatic *vs.* aliphatic character of the two nitrogen atoms, with the long-range halogen bonds, Figure 3.13 plausibly being described as halogen-arene contacts. Clearly, evidence for the significance of trifurcated halogen bonds remains scarce and as such we draw away from making strong conclusions pertaining to the geometries of such systems.

3.4 Aims of the project

Bifurcated halogen bonds have been widely studied using computational and crystallographic means, and their use as a versatile and useful synthon has been demonstrated. However, the details of their energetics and experimental significance in solution are limited. This chapter aims to quantify single-point, bifurcated, and trifurcated halogen bonds in solution using a combination of experimental and computational methods. A series of small molecules designed to facilitate a variety of halogen bonding arrangements were employed and compared to their hydrogen bonded analogues. Computational analysis of the systems employed is provided by a battery of DFT techniques including energy decomposition using symmetry adapted perturbation theory (SAPT).

3.5 Results and discussion

To facilitate study of halogen bond denticity in the solution phase, a series of host-guest NMR titration experiments involving the compounds shown in Figure 3.15 were devised.

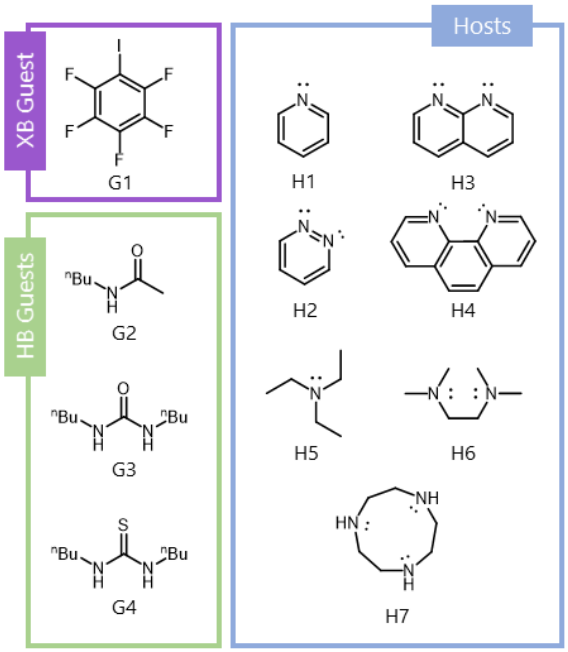

Figure 3.15: Host and guest species employed in this study to investigate halogen bonding interactions *via* host-guest ^{1}H NMR titrations.

The primary guest species selected for this study was iodopentafluorobenzene (C_6F_5I). Iodopentafluorobenzene is well suited to this study as a strong halogen bond donor and while stable enough that it does not readily dissociate into a halonium ion in solution. Furthermore, it has been used in several prior studies,[43,46,54] which facilitates comparison of solution phase experimental data with the results of published crystallographic studies.

The host species selected for investigation contain either aromatic or aliphatic nitrogen lone pair halogen bond acceptors. In the aliphatic series, triethylamine (TEA) (H5 in Figure 3.15), tetramethylethylenediamine (TMEDA) (H6 in Figure 3.15) and 1,4,7-triazacyclononane (H7 in Figure 3.15) form a series where acceptor species feature 1, 2 and 3 potential halogen bond acceptors. Pyridine is included as a single-point halogen bond acceptor, while the dinitrogen heterocyclic systems orientate the nitrogen lone pairs in different directions (Figure 3.16).

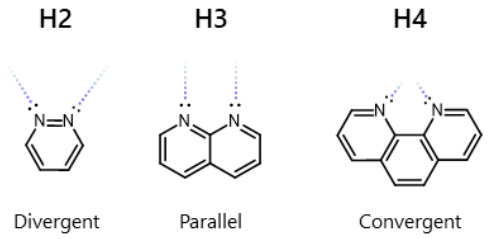

Figure 3.16: Dinitrogen aromatic hosts employed in this study, showing the relative orientations of the nitrogen lone pairs.

Additional hydrogen bonding donating guest species enable comparison between halogen bonding and hydrogen bonding analogues with equivalent numbers of donor sites (Figure 3.15, green). The solution-phase studies were supported by computational analyses. Minimised geometries and BSSE counterpoise corrected formation energies were calculated using DFT and DFT-D methodologies (B3LYP/6-311G* and ωB97x-D/6-311G*). Energetic dissections were also conducted using the SAPT2 and SAPT2+(ccd) methodologies to provide insight into the nature of the interactions involved in our host-guest complexes. Calculated natural bond orbitals (NBOs) helped to visualise the electron delocalisation contributions and add meaning to the SAPT induction terms.

3.6 Halogen bonded complexes

DFT minimisation of the complexes formed between G1 and the host series all showed the formation of favourable host-guest complexes featuring halogen bonds (Figure 3.17A). The observed geometries are consistent with the anticipated single-point, bi- and trifurcated XBs forming with the aliphatic hosts (Figure 3.17A, left). In the aromatic host series, symmetrical bifurcation is observed in G1/H4 (Figure 3.17A, bottom left), but with single-point, or asymmetric interactions involving a primary halogen bond and an additional secondary halogen bond in the other two dinitrogen-aromatic systems (Figure 3.17A, middle two, left). Expectedly a single-point halogen bond is observed with the single nitrogen acceptor species (Figure 3.17, top).

Solution-phase titrations of G1 with the host series were performed in benzene (d_6) (as described in Appendix B.1). The experimentally determined limiting changes in ^{1}H NMR chemical shift, $\Delta\delta$ are displayed alongside the minimised structures in Figure 3.17A. ΔG_{XB} values were calculated from this solution-phase data by fitting the δ values for H_A to a 1:1 binding model, fits are shown in appendix B.3.

For the aliphatic host series, all experimental data fit well to the 1:1 binding model and a clear trend in the solution-phase ΔG_{XB} values was observed (Figure 3.17B green), whereby increasing the number of halogen-bond acceptors increased stability of the complexes. This suggests that these systems may present examples of bi- and trifurcated halogen bonds in solution.

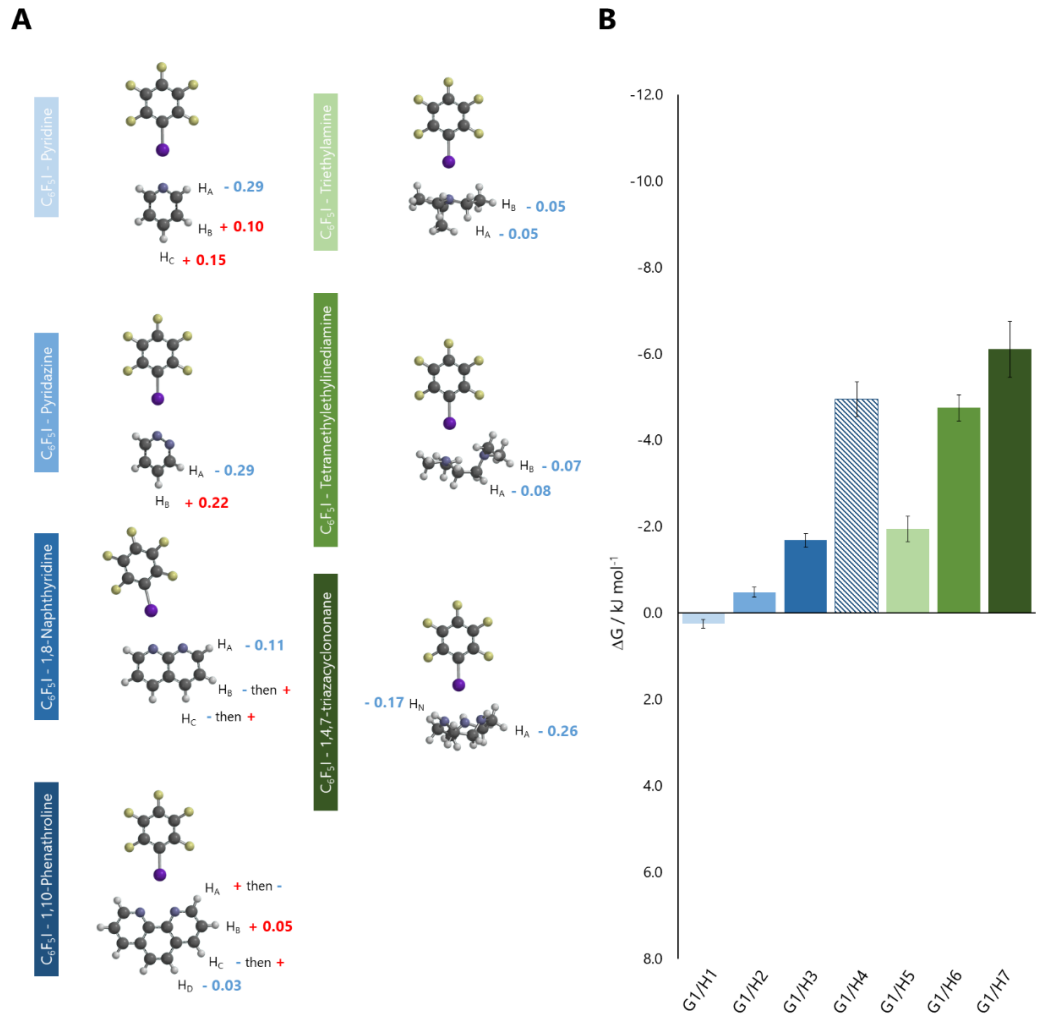

Figure 3.17: **A)** Host-guest complexes for G1 minimised using B3LYP/6-311G* and the corresponding experimentally determined limiting changes in complexation induced chemical shift for each of the respective protons (Δδ). **B)** Measured changes in Gibbs free energies for complexes formed between the two-host series and guest G1 (all in benzene-d_6 at 300 K). The hashed bar denotes less accurate data due to the observation of a secondary binding event in this complex that affects fitting of the H_A signal (see main text).

For the aromatic host series, the picture is somewhat more complex. Though fitting of the data to a 1:1 binding model was successful for the G1/H1 single halogen bond system, the calculated ΔG_{XB} value is approximately zero due to solvent competition. A slight stepwise increase in the favourability of ΔG_{XB} was observed for the H2 and H3 complexes. This trend is consistent with attractive partial bifurcation from the

proximal second nitrogen atom, mirroring the change in the electrostatic potential ($V_{s,min}$) associated with the acceptor sites of the three hosts.

Host Species	Designator	ESP $V_{s,min}$ (kJ mol^{-1})
Pyridine	H1	-191.1
1,2-pyrazine	H2	-206.5
1,8-naphthyridine	H3	-237.5
1,10-phenanthroline	H4	-284.9
Triethylamine	H5	-159.4
Tetramethylethylenediamine	H6	-187.0
1,4,7-triazacyclononane	H7	-333.1

Table 3.1: Calculated ESP $V_{s,min}$ vales for acceptor species employed.

^{1}H NMR spectra for the G1/H4 complex showed a flip between de-shielding and shielding for the H_A signal midway through the titration (Figure 3.18), suggesting the influence of a second binding mode. The same swing between de-shielding and shielding is also observed for the H_B and H_C signals in the G1/H3 complex, which also features a larger aromatic host. The increased shielding at higher concentrations for the larger aromatics is consistent with a host-guest aromatic stacking interaction, or other higher order host-guest complex. Stacking of the host was also considered as a possible explanation, but deemed unlikely as this behaviour is not observed with any of the other titrations using the same larger hosts, but with different guests. Indeed, there is strong literature precedent for the association of electron-rich aromatics with electron poor ones.[63-66] Further support for this hypothesis was obtained *via* DFT minimisations conducted with an expanded scope of starting geometries, which yielded stacked geometries (Appendix B.15) that were less stable than the desired halogen bonded arrangements. To minimise the contribution of this weaker secondary binding mode in the G1/H4 complex the obtained experimental chemical shifts were instead fitting up to the maximum observed $\Delta\delta$ (*i.e.* before dominant occurrence of the secondary binding mode at higher concentrations). Despite the increased error associated with the measurement of binding in the G1/H4 complex, the data still suggests that this complex is more stable than the complexes in the aromatic series.

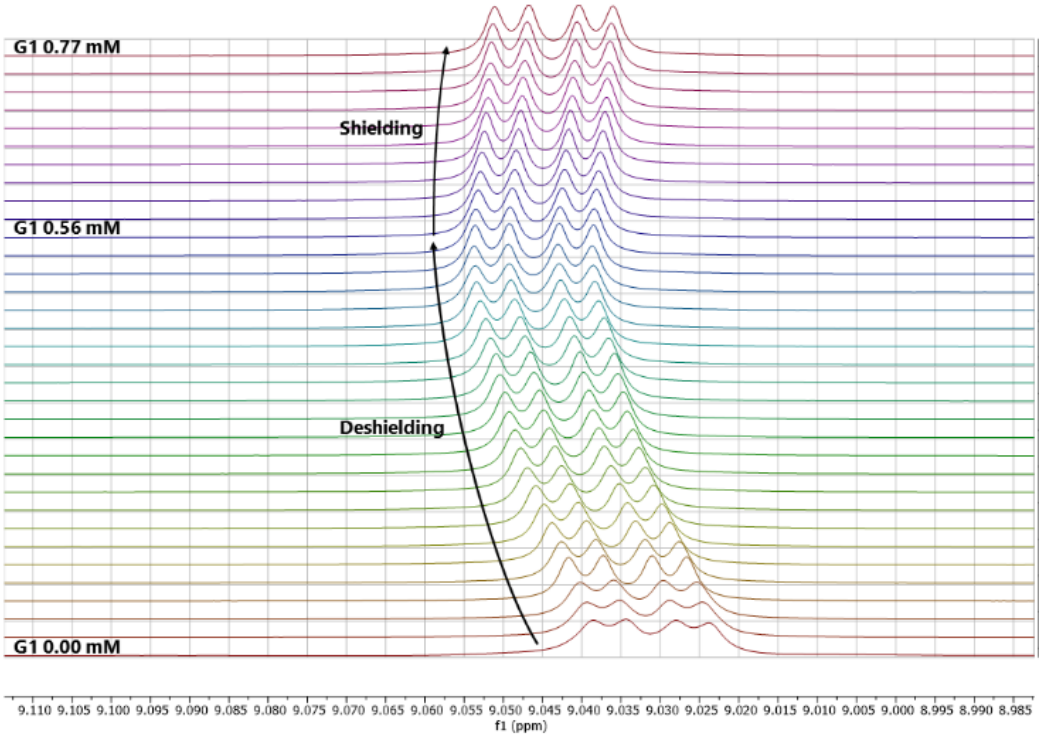

Figure 3.18: Stacked 400 MHz ^{1}H NMR spectra for the H_A signal of the titration of H4 with G1 in benzene-d_6 (300 K).

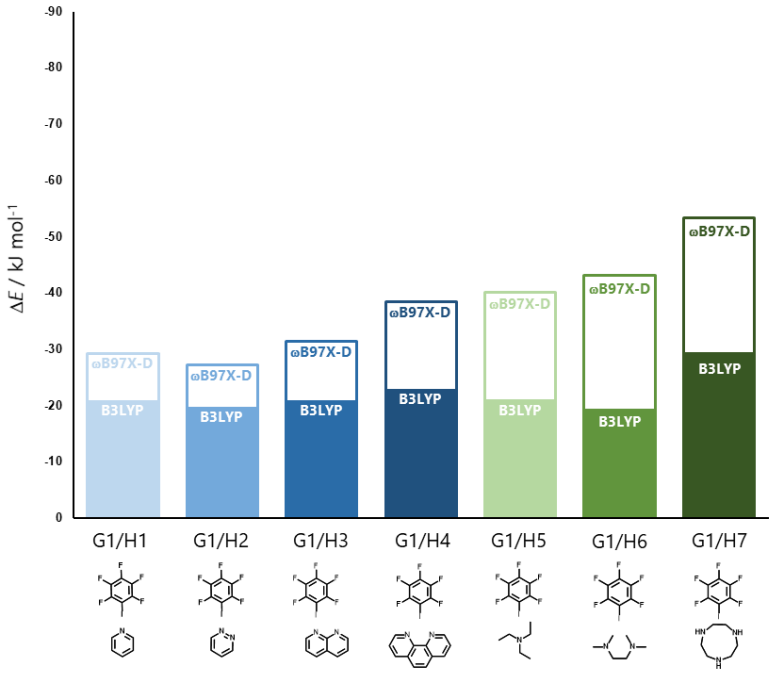

Figure 3.19: Computational BSSE counterpoise corrected formation energies for the aromatic (blue) and aliphatic (green) host series and guest G1. DFT B3LYP/6-311G* energies are shown in solid colour and the DFT-D ωB97X-D/6-311G* energies are shown as a superimposed outline.

BSSE counterpoise-corrected formation energies were calculated for complex G1/H1 to G1/H7 using the DFT and DFT-D minimised geometries (Figure 3.19).

The inclusion of a dispersion correction to the calculation has little effect on the energetic trend, but dispersion correction results in an improved, but still qualitative correlation between experimental and computational values (R^2 of ~0.77, Appendix B.7). The observation of a more stable calculated ΔE_{XB} value for the G1/H4 complex is reassuring given the uncertainty associated with our experimental measurement due to secondary complexation. Interestingly, the G1/H3 complex is predicted to be only slightly more stable than the G1/H1 and G1/H2 complexes. The DFT minimised structure of the G1/H3 complex reveals a less linear C-I···N angle than in the single ring host complexes (H1 and H2), in spite of their experimentally (Figure 3.17) and computationally (Figure 3.19) observed strength; something that is counter to the precedent of linear interactions being stronger developed for single-point XB systems.[40-42,67] As mentioned previously, the increased stability of the G1/H3 complex could be rationalised by strengthened columbic forces, with H3 possessing a $V_{s,min}$ of -237.5 kJ/mol, compared to -191.1 kJ/mol for H1 and -206.5 kJ/mol for H2. However, the closest point of contact between the host and guest species is found at a nitrogen atom rather than at the $V_{s,min}$ located midway between the two nitrogen atoms (Figure 3.20). The fact that the C-I bond axis –denoting the location of the σ-hole- and the central C-C bond axis –denoting the location of $V_{s,min}$- do not align points to a multiplicity of factors determining the arrangements of the complexes; specifically secondary electrostatic and steric repulsive forces, electron delocalisation *via* donor-acceptor interactions, and dispersion (for the dispersion-corrected calculations).

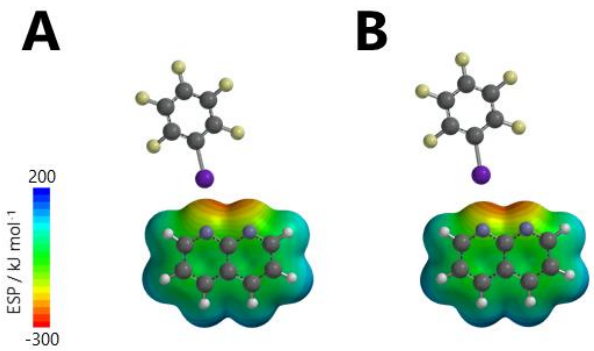

Figure 3.20: ESP of non-complexed 1,8-naphthyridine superimposed on the **A)** B3LYP/6-311G* and **B)** ωB97X-D/6-311G* minimised G1/H3 geometry. Geometries are similar with the latter seeing a slightly more linear C-I···N angle.

Similar patterns are seen for the aliphatic series, with the trifurcated G1/H7 complex possessing significantly more stabilised ΔE_{XB} and ΔG_{XB} values than the singularly halogen bonded G1/H5 complex. However, there is a significant discordance between the position of the G1/H6 complex in the experimental and DFT computational trends. A misalignment that is rectified by the addition of a dispersion correction; suggesting a significant role for dispersion in the system.

Analysis of the bond lengths and distances between atoms found in the DFT and DFT-D minimised geometries provided insights into the complexation mode of the aliphatic series with guest G1. The G1/H6 complex exhibits a clear preference for binding to one nitrogen. Electron isodensity surfaces calculated at the 0.002 bohrs/A^3 show that closest contact involves substantial electron cloud overlap between the iodine and nitrogen involved in the primary halogen bond, while the secondary iodine-nitrogen distance does not. The distance between the secondary nitrogen and iodine atoms is observed to shorten from the DFT (3.685 Å) to the DFT-D (3.501 Å) minimized structure, which can explain the increased ΔE value. However, the latter is very close to the Σ wdV radii and is significantly longer than the primary nitrogen. Indeed, the preference of halogen bonding to one nitrogen over the other in G1/H6 more closely resembles the minimised geometries for the G1/H2 or G1/H3 complexes than the *symmetrically* bifurcated G1/H4 complex. Natural bond orbitals (NBOs) calculated from the B3LYP/6-311G* geometries show nitrogen lone pair (LP) to σ^*_{I-C} donation for all nearby nitrogen atoms with second order perturbation energies >4 kJ/mol in

both the G1/H4 and G1/H7 bi- and trifurcated complexes. In contrast, all the other G1 complexes only show LP to σ^*_{I-C} donation >4 kJ/mol involving a single nitrogen atom (Figure 1.21, appendix B.12 and B.13).

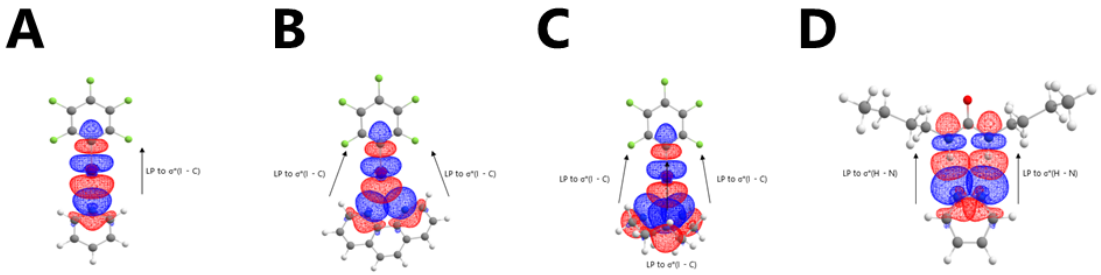

Figure 3.21: Example NBO donations for **A)** G1/H1, **B)** G1/H4, **C)** G1/H7, **D)** G3/H2. All other systems are shown in appendix B.12.

Though neither are especially convincing, the R^2 values for ΔE_{XB} against ΔG_{XB} show a marked increase in correlation going from the DFT values to DFT-D; suggesting an important role for dispersion in halogen bonded systems. The case of potentially G1/H6 typifying as much. It would be remiss not to mention that one limitation is that the DFT/DFT-D calculations only provide static snapshots of the geometries with the minimum energies and do not model the entropic advantages associated with cooperative chelate binding. Such calculations do not model the possibility of forming a second, or replacement halogen bond to a proximal nitrogen atom following formation of the initial halogen bond. In addition, the solvent was not modelled in the calculations; solvent attenuation being a significant factor in significantly dispersive interactions.[68-71]

To more deeply probe the nature of the forces responsible for the complexation energies, energetic dissection was conducted using the SAPT2 methodology using the B3LYP/6-311G* minimised geometries (Figure 3.22).[72] The SAPT2 total energy produced by these calculations mirrored the calculated DFT ΔE_{XB} formation energies shown in Figure 3.19.

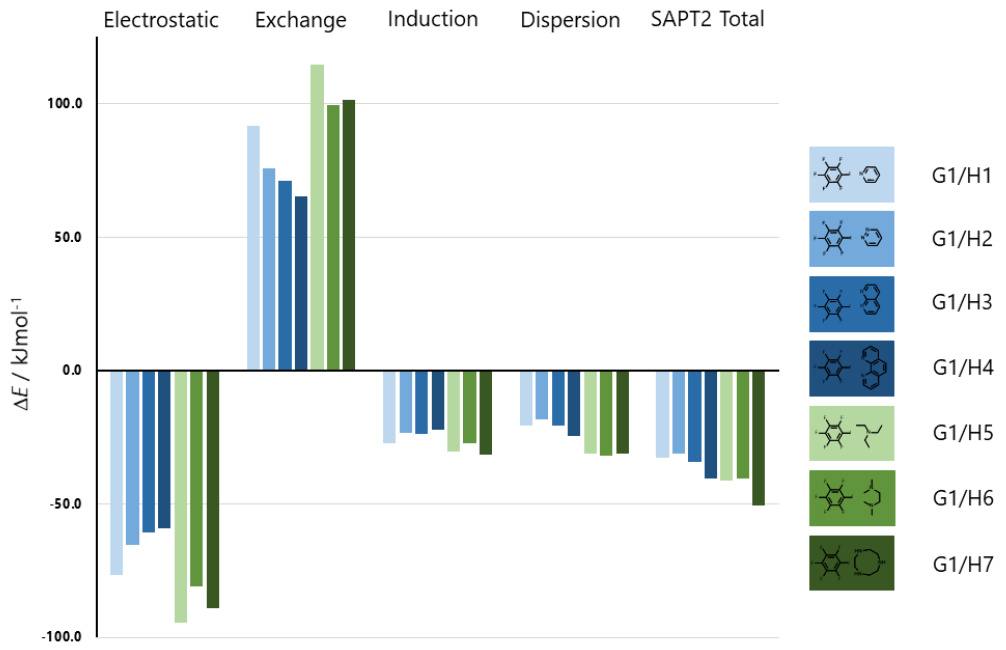

Figure 3.22: SAPT2 energy terms calculated from B3LYP/6-311G* minimised geometries of the G1/HX host-guest complexes.

As expected for halogen bonds, the most significant attractive term is the electrostatic term with its magnitude being greater than the sum of the other two attractive terms (induction and dispersion). Counterintuitively, the observed trends in the electrostatic terms oppose the trends seen in the SAPT2 total energies, the experimentally measured ΔG_{XB} values and the trends seen in the $V_{s,min}$ values for the two host series. For example, H7 possesses the most negative ESP $V_{s,min}$ in the series, which is manifested through space in the centre of the triazocyclononane ring (and along the axis of the bound C-I), but this does not result in the most favourable electrostatic SAPT term.

To understand the difference between the trends in the electrostatic terms and SAPT2 total values we must consider the other energetic terms output by SAPT calculations. The dispersion terms follow similar trends to the SAPT2 total, with dispersion becoming more favourable as the number of nitrogen acceptors and the size of the intermolecular contact area increases.

Interestingly, the dispersion terms within the aliphatic host series are very consistent and consistently more negative than their aromatic counterparts. Given the relative 2D nature of the side-on aromatic contacts compared to the 3D nature of the aliphatic contacts, this increased dispersion term should be expected. The remaining attractive

term of the SAPT2 energetic decomposition, induction, followed a similar trend to the electrostatic term, with the main difference being that the relative magnitudes of the G1/H2 and G1/H3 complex induction terms being flipped, breaking the stepwise pattern. Relative to the size of the changes in electrostatic terms however, they are close enough to each other that this difference has a negligible effect on the total energy.

Further SAPT2 energetic decomposition analysis was performed using ωB97X-D/6-311G* DFT-D minimised geometries (Appendix B.10) and SAPT2+(ccd)[72] calculations on the B3LYP/6-311G* DFT minimised geometries (Appendix B.11). However, neither of these yielded any additional findings compared to the previously discussed SAPT2 data derived from the B3LYP/6-311G* DFT minimised geometries.

Logical comparisons between the SAPT induction term and the calculated second-order perturbation energies of the associated NBOs can be drawn. With regards to the aromatic series of hosts, a comparable correlation is seen between the induction term and the sum of the second-order perturbation energies (ΣE^2) >4 kJ/mol (Appendix B.13) as is seen between the SAPT electrostatic term and ΣE^2 >4 (G1/H2 > G1/H3 for both ΣE^2>4 kJ/mol and the SAPT electrostatic term). More noteworthy differences between the SAPT2 induction terms and the Σ NBO >4 kJ/mol values can be seen in the aliphatic host series. This correlation shows a stepwise trend running inverse to the experimental ΔG_{XB} values in spite of the issues concerning the minimised geometry for G1/H6, from which the NBO's are derived. In the case of the SAPT2 induction terms for the aliphatic series, the G1/H5 and G1/H7 complexes are broadly comparable, with the latter being slightly more negative, while G1/H6 being notably less negative.

Given the number of orbitals involved it is possible that the G1/H7 SAPT2 induction term is an overestimation. Indeed, it is worth noting that the comparison between the two methodologies is not a perfect one. SAPT calculated induction terms are concerned with orbital polarisation rather that the specific transfers that are considered in NBO calculations. While higher order charge-transfer modelling SAPT (SAPT2-ct for example[73]) may produce a better correlation with ΣE^2>4 kJ/mol values, the additional computational cost of conducting another series of higher order SAPT

calculations was deemed outside of the scope of this study, given the larger issue of the solvation not being considered in these calculations.

The SAPT dispersion terms are not sufficient to explain the disparity of the electrostatic and induction trends running contrary to both the SAPT2 total energy and the experimentally measured ΔG_{XB}. Hence, attention falls upon the remaining exchange term. A stepwise reduction in the exchange-repulsion cost associated with complex formation as the number of binding sites is increased is observed within the aromatic and aliphatic host series. The complexation of G1/H6 and G1/H7 both incur lower exchange penalties than complexation of G1/H5 (issues concerning the non-bifurcated B3LYP minimization for G1/H6 as discussed previously). Hence, we can conclude that the stronger binding of the bi- and trifurcated systems over the singly bonded complexes arises from the reduction in steric clash, even if the geometries that facilitate such binding modes come at the expense of weaker electrostatic and induction contributions.

3.7 Hydrogen bonded complexes

As outlined in the aims of this project and Figure 3.15, hydrogen bonded complexes were analysed alongside the halogen bonded complexes to facilitate comparison. The experimentally determined complexation free energies (ΔG_{HB}) of the aromatic and aliphatic host series with *N*-butylacetamide (G2), *N,N'*-dibutylurea (G3) and *N,N'*-dibutylthiourea (G4) were determined in benzene d_6 (Figures 3.23 and 3.25).

3.7.1 *N*-butylacetamide (G2) complexes

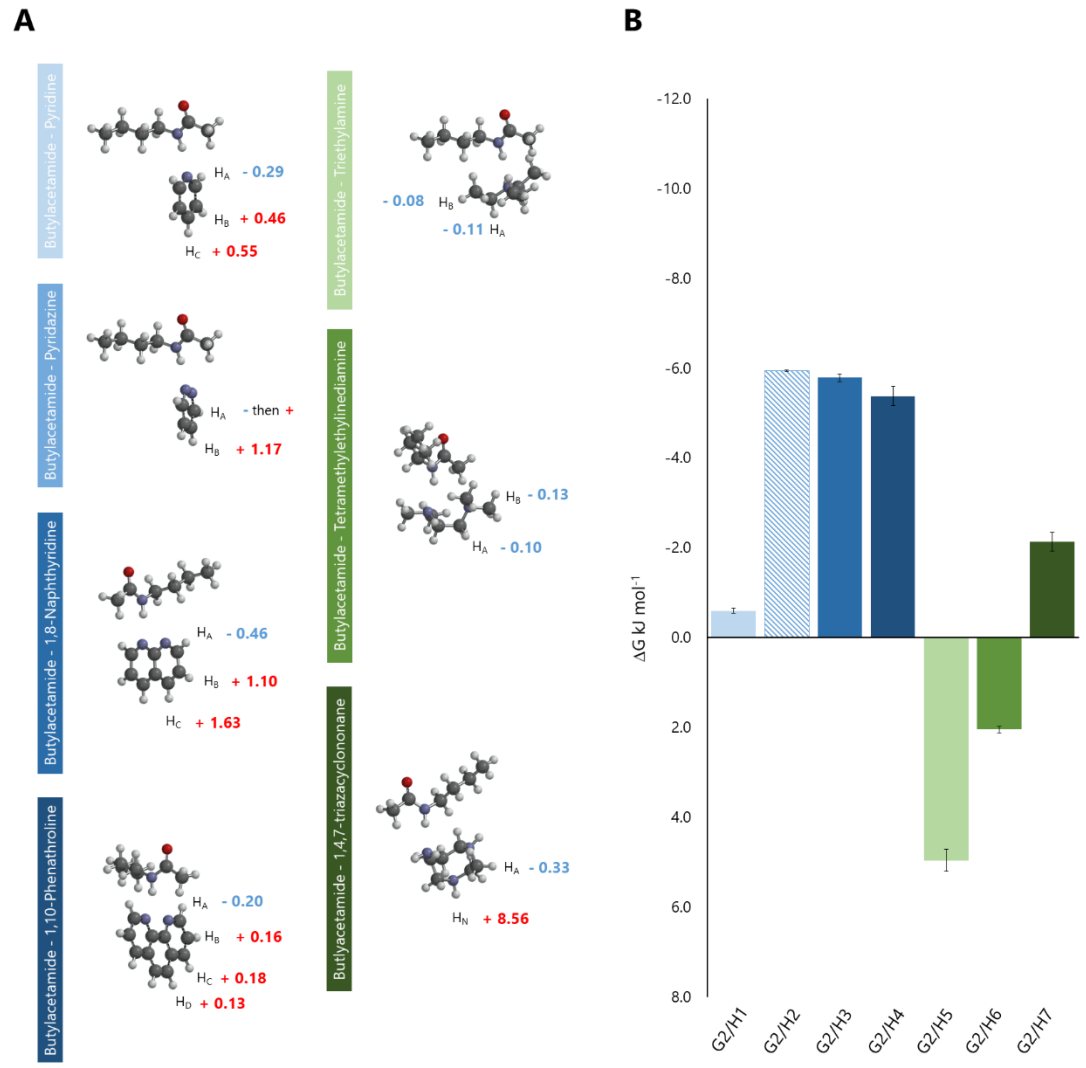

Figure 3.23: A) Host guest complexes for G2 minimised using B3LYP/6-311G* and the corresponding experimentally determined limiting changes in complexation induced chemical shift for each of the respective protons (Δδ). B) Measured changes in Gibbs free energies for complexes formed between the two host series and guest G2 (all in benzene-d_6 at 300 K). Hashed bar denotes the observation of a secondary binding effect that affects the H_A signal.

The values of ΔG_{HB} for the hydrogen bonding studies were determined by the fitting the H_a ^{1}H NMR signals to 1:1 binding models using the same method as for the G1 titrations used for the halogen bonding studies (Appendix B.3). Dimerization of G2 was observed during these titrations due to the presence of both a hydrogen bond donor and acceptor. The dimerization constant of G2 was determined in separate dilution

experiments (1.48 M^{-1}), and accounted for in the fitting of the complexation data used to determine the ΔG_{HB} values (Appendix B.3).

The ΔG_{HB} values for the G2/HX complexes shown in Figure 3.23 show interesting trends for the both the aromatic and aliphatic host series. The dinitrogen aromatic hosts bound guests with similar ΔG_{HB} values, with the singly bonded, mono-nitrogen, G2/H1 complex being significantly less stable. Given the lack of relationship between ESP $V_{s,min}$ and the ΔG_{HB} values, this trend can be attributed to the likely occurrence of bifurcation in these complexes. Caution should be observed in analysing experimental data of the G2/H2 complex as a switch from deshielding to shielding was observed in the H_A ^1H NMR signal during the titrations (similar to as seen in the G1/H4 complex). The secondary binding mode was attributed to H_A acting as a weak hydrogen bond donor, based on the similarity in the behaviour of the H_A signals during guest dimerisation dilution experiments (Appendix B.3). We expect that hydrogen bonding between G2 H_A and the oxygen atom of the guest is involved since similar behaviour is observed in the G3/H2 complex, but not in the thiourea G4/H2 complex (due to sulphur being a noticeably weaker hydrogen bond acceptor than an amide oxygen).

For the aliphatic host series, a stepwise increase in the stability of ΔG_{HB} with G2 from H5 to H7 was observed. The stepwise trend that is observed for the aromatic host series with G2, draws obvious comparison to the similar stepwise trend observed in the G1 halogen bond complexes. Notably, ΔG_{HB} values for the hydrogen bonded H5 and H6 complexes are positive, whereas all of the ΔG_{XB} values were negative (Figure 1.16B). The weaker complexation energies for the hydrogen bonded complexes compared to the halogen bonded complexes is consistent with both the hydrogen bonds being weaker than the corresponding halogen bonds, and/or the cost of desolvating the polar NH being greater than desolvation of the much less polar halogen bond donor due to hydrogen bonds with the solvent being stronger than the analogous halogen bonds.

To complement the experimental work conduced on our hydrogen bonding systems, the same computational battery employed to study our halogen bonded systems was employed here. B3LYP/6-311G* minimised geometries for the G2 host-guest complexes are shown in Figure 3.23A alongside the experimentally measured complexation-induced limiting changes in chemical shift, $\Delta\delta$. Calculated ΔE_{HB}

formation energies are shown in Figure 3.24, revealing some striking differences between the experimental and *in silico* trends.

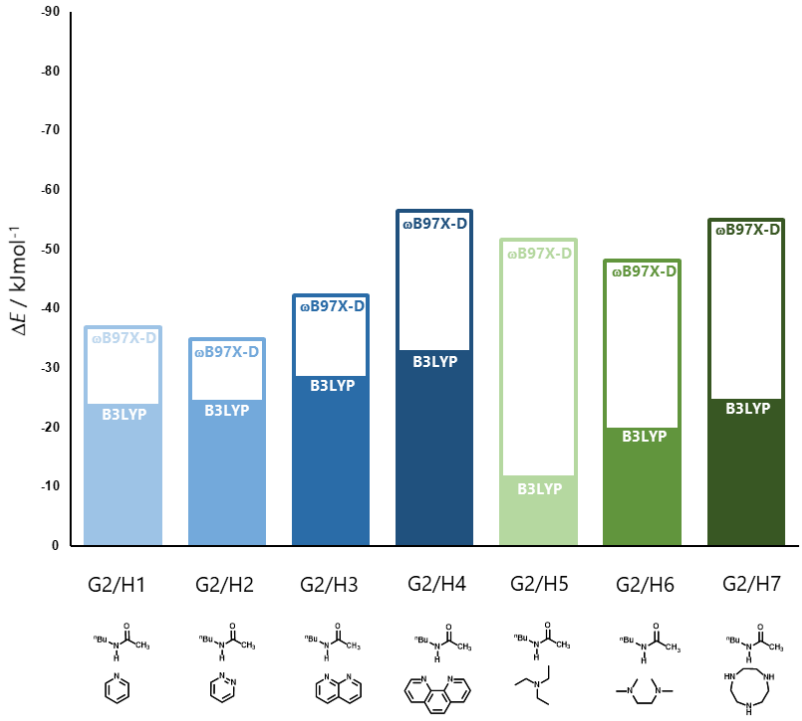

Figure 3.24: Computational BSSE counterpoise corrected formation energies for the two host series and guest G2. DFT B3LYP/6-311G* energies are shown in solid colour with the DFT-D ωB97X-D/6-311G* energies being shown as a superimposed outline

The most striking differences between the hydrogen bonding and halogen bonding systems are those observed within the aromatic host series. All these complexes minimised to form single HB complexes with G2 in both DFT and DFT-D calculations, except for the G2/H4 complex that produced a symmetrically bifurcated complex remarkably similar the G1/H4 complex. Similarly, calculated NBOs only found LP to $\sigma^*_{H\text{-}N}$ donation from more than one nitrogen atom of the host in the G2/H4 complex (Appendix B.12). These features are manifested in the ΔE_{HB} trend, which resembles that seen for the halogen bonded G1 complexes. The discord between the experimentally observed ΔG_{XB} values and the calculated ΔE_{XB} values in the G1/H6 complex that was attributed to the entropic favourability of forming a second interaction post initial association. Such chelate cooperativity also manifests in the hydrogen bonded complexes, which as before, is not modelled in the simple

computations conducted here. The retention of misalignment between the ΔG_{HB} and both the DFT and DFT-D ΔE_{HB} values pushes conclusions away from the discord being the product of a lack of dispersion modelling in B3LYP. The behaviour observed in the minimised structures can potentially be rationalised by the hydrogen atom being too small to be able to interact with both acceptor sites. However, the close proximity of the nitrogen atoms in the host series –especially in H2- should not prevent relatively close contact in solution. Indeed, given the much broader range of geometries acceptable for hydrogen bonding, it might be anticipated that higher-order multi-point interactions would be more likely to occur than more geometrically sensitive halogen bonds.[42,74,75]

The situation is more complex for the G2 complexes with the aliphatic host series, and a better correlation between the computational and the experimental results is seen compared to the aromatic series (Figures 3.23B and 3.25 green) especially for the DFT calculations. Of note is the very substantial (-51.7 kJ mol^{-1}) BSSE-corrected formation energy calculated for the G2/H5 complex calculated at the ωB97X-D level. The minimised host-guest complex revealed sizeable contact between alkyl chains, which while favourable in the gas-phase, is essentially energetically zero in organic solution (Appendix B.18).[71,76] Indeed, it is likely the overestimation of such contacts that sees the correlation between the ωB97X-D/6-311G* values and experimental data being exceptionally poor; the inverse of what is seen in the halogen bonded systems (Appendix B.7). The aliphatic host/G2 complexes are experimentally observed to form significantly less stable complexes (Figure 3.23B) relative to their aromatic bifurcated hydrogen bond counterparts, which differs from the G1 halogen bonded complexes (Figure 3.17B). Minimised geometries all show only single hydrogen bonds for the aliphatic host complexes in both the DFT and DFT-D minimizations; further supporting the notion of dispersive alkyl chain interactions being overestimated in DFT-D calculations and pushing conclusions away from hydrogen bond bi- or trifurcation in aliphatic host hydrogen bonded systems. Indeed, the minimised geometry of the triazacyclononane ring in the G2/H7 complex showed a different conformation (Figure 3.23A, bottom right) to that seen in the G1/H7 complex (Figure 3.17A, bottom right), meaning that in contrast, trifurcation cannot be accommodated in the hydrogen bonded complex.

Given the previously discussed discordance between the computational and experimental data caution should be observed regarding the SAPT2 calculations that were conducted on the both the DFT and DFT-D minimised geometries. Figure 3.25 and Appendix B.8/9 shows the energies determined from the B3LYP/6-311G* geometries, while the energies from the ωB97X-D/6-311G* geometries are tabulated in Appendix B.10. There is good qualitative correlation between the ΔE_{HB} energies and the SAPT2 total energies. The unusually similar total energies for G2/H6 and G2/H7 complexes stems from a lower-than-expected value for the dispersion term in the G2/H7 complex (Appendix B.9), potentially indicative of an upper limit on how strong dispersive interactions from the G2 hydrogen bond donor can be.

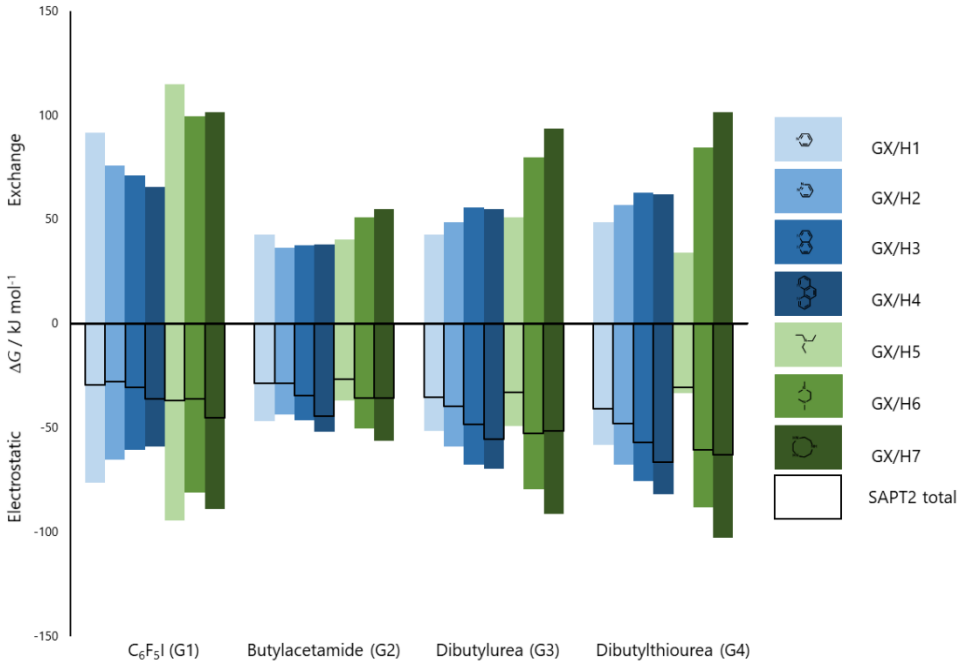

Figure 3.25: SAPT2 electrostatic and exchange terms of all host guest complexes included in this study. Energies were calculated from B3LYP/6-311G* minimised geometries with the SAPT2 total energies superimposed on top (black outlines).

Imminently obvious is the inversion of trends observed in the electrostatic and exchange terms from what was observed in the halogen bonded G1 complexes; this being especially pronounced in the aliphatic host series (Figure 3.25). A more conventional relationship was observed between the attractive and repulsive forces as the distance between the hydrogen bonded groups is varied. The aliphatic host series typified this trend, with the hydrogen bonds distances across the series being 2.320 Å,

2.214 Å, and 2.103 Å, which was correlated with increased attraction and repulsion as the distances became shorter. This is also observed in both the SAPT2 induction term and in the ΣE^2>4 kJ/mol values for the aliphatic host series (Appendix B.8/13). These observations are predicated on the single hydrogen bond model for the G2 aliphatic host complexes, and it is therefore conceivable that these observations are not relevant if bi- and trifurcation is present in these systems in solution. Insights into how bifurcated hydrogen bonds may differ from their halogen bonded analogues can be gleaned by comparison of the G2/H1 and the G2/H4 complexes; the latter being the only G2 complex to produce a bifurcated minimised geometry. Here we observe the same reduction in exchange repulsion penalty that bifurcation affords in halogen bonded systems, however the accompanying reduction in electrostatic and induction term strengths is not observed. As much may be indicative of hydrogen bonds being more suitable that halogen bonds for forming bifurcated complexes s they appear to offer the strengths afforded by the arrangement without incurring the same penalties to the attractive terms. This much can be seen in the more negative ΔG_{HB} values seen for the G2/H2-4 complexes that are suspected to be bifurcated in solution. The less negative ΔG_{HB} values seen for the aliphatic series do however, show limitations for bifurcated hydrogen bonds potentially caused by the small size of the hydrogen bond donor moiety and its difficulty in complexing with multi-dentate systems that lack preorganization.

3.7.2 *N,N'*-dibutylurea (G3) and *N,N'*-dibutylthiourea (G4) complexes

Finally we consider the remaining two guest species included in this work, G3 (*N,N'*-dibutylurea) and the analogous G4 (*N,N'*-dibutylthiourea). These two guest systems feature dual hydrogen bond donors to provide comparison between bifurcated systems and systems containing multiple distinct hydrogen bonds. G3 and G4 were found to bind well with all hosts included in this study and fitting to the 1:1 binding models was successful for all complexes when host-host dimerisation was accounted for (Appendix B.3), with the exception of H5 containing complexes where host-host dimerization significantly outcompeted the host-guest. Figure 3.26A and C show the B3LYP/6-311G* minimised geometries and complexation induced limiting changes in chemical shift $\Delta\delta$ for G3 and G4 complexes. The experimental ΔG_{HB} values are

shown in Figures 3.26B and D. The experimental ΔG_{HB} values were most favourable for these complexes, with G4 complexes generally being more stable complexes than the G3 analogues.

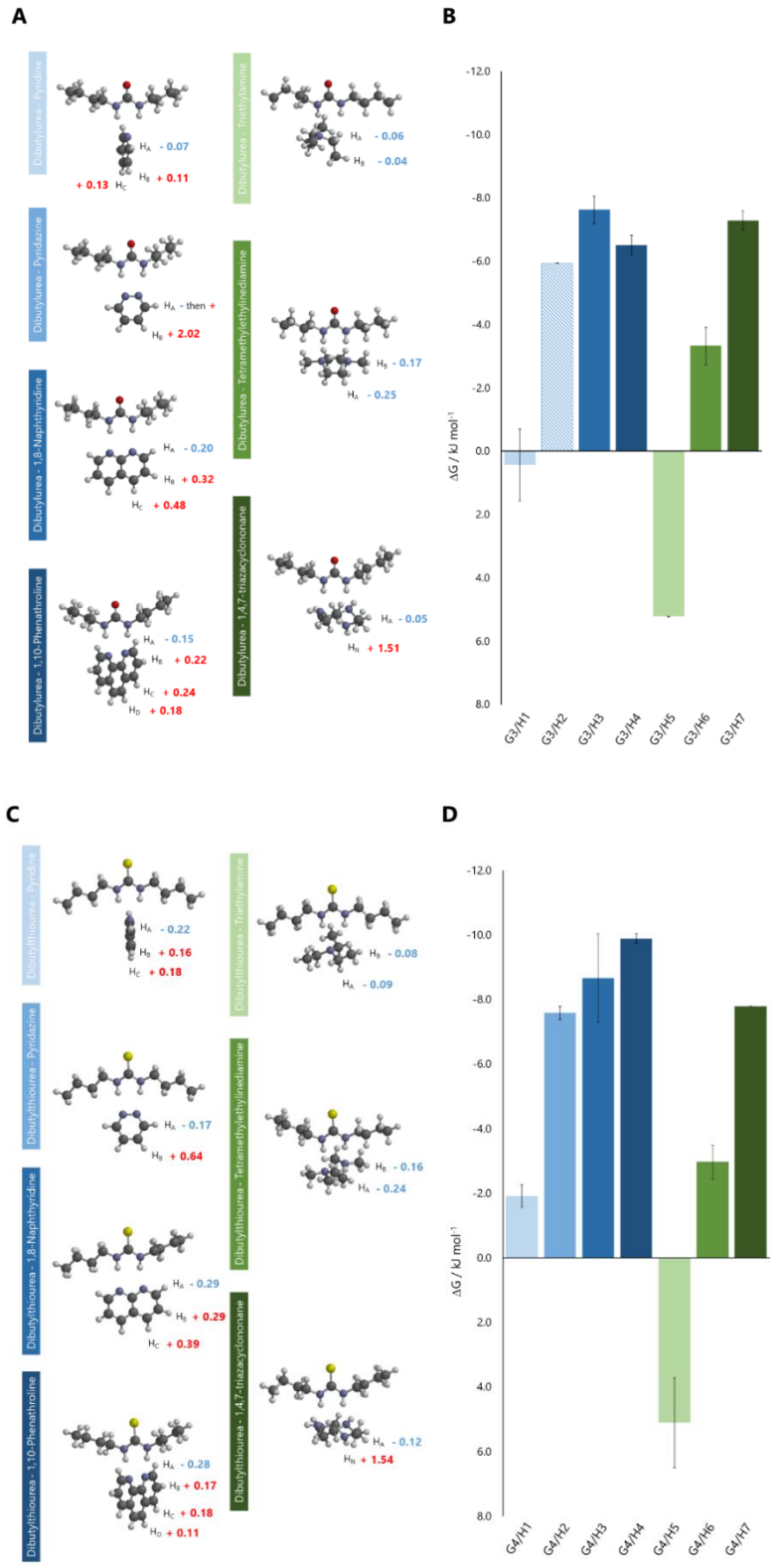

Figure 3.26: (previous page) A) Host-guest complexes for G3 minimised using B3LYP/6-311G* and the corresponding experimentally determined limiting changes in complexation induced chemical shift for each of the respective protons (Δδ). **B)** Measured changes in Gibbs free energies for complexes formed between the two host series and guest G3 (all in benzene-*d6* at 300 K). **C)** Host guest complexes for G4 minimised using B3LYP/6-311G* and the corresponding experimentally determined limiting changes in complexation induced chemical shift for each of the respective protons (Δδ). **D)** Measured changes in Gibbs free energies for complexes formed between the two host series and guest G4. Hashed bar denotes the observation of a secondary binding effect that affects the H_A signal (all in benzene-*d6* at 300 K).

There are similarities between the trends observed in the G3/G4 complexes and the G2 complexes, but with greater variance observed in the H2 through H4 complexes for both G3 and G4 guests. The similarity of the energies of the G3 and G4 host-guest complexes is not surprising as the minimised geometries support the intended dual-point hydrogen bonding is found in both complexes. The large variance observed in ΔG_{HB} may be due to the broad range of interaction geometries observed across these series; from the perpendicular arrangement of the H4 complexes to the parallel arrangement of the H2 and H3 complexes (Figure 3.26A and C).[77] Relatively little variance in ΔG_{HB} was observed for the aromatic host complexes that were able to accept two hydrogen bonds (Figure 3.23B and 3.26B/D). This adds support to the occurrence of bifurcation in the G2/H2-4 complexes, as one would expect a much more significant change in ΔG_{HB} when comparing single and dual hydrogen bonded systems (*cf.* G2/H1 complexes with G3/H2-4 or G4/H2-4 complexes).[78-82]

Interestingly, the aliphatic host series produced the same stepwise trend that was seen in the G1 and G2 guest complexes. As with the G2/H5 system, the G3/H5 and G4/H5 host-guest complexes were observed to yield positive ΔG_{HB} values suggesting the same concerns pertaining to the high cost of desolvating the polar NH. The flip of positive to negative ΔG_{HB} values in the G3/H6 and G4/H6 complexes does however imply a degree of cooperativity during the desolation of a pair of NH moieties.

The G3/H7 and G4/H7 complexes were among the most stable studied. The minimised geometries of the H7 complexes produced the same dual hydrogen bonded arrangements seen with H6 and the dinitrogen-aromatic hosts. As in the case of the

previously discussed guest species, the stronger H7 complex can be attributed to the stronger acceptor ability of the nitrogen atoms of 1,4,7-triazacyclononane (H7) over those in TMEDA (H6). However, given the proximity of the nitrogen atoms, we also considered the possibility of longer range though-space interactions involving the more distant third nitrogen atom within H7 molecule. However, any such long-range contribution is likely to be small, as like the G2/H7 complex, the lone pair of the third nitrogen points in H7 away from the interaction site in the DFT minimised geometry (Figure 3.26A and C).

Given that the calculated formation energies for the G3 and G4 host-guest complexes, ΔE_{HB}, (Figure 3.27) retain the stepwise trend seen experimentally (Figure 3.26B/D) (even with the third lone pair pointing away from the binding site), it is likely that acceptor strength is the most significant factor in determining complex stability.

More definitive conclusions can be drawn from the SAPT2 calculations, the result of this can be seen in Figure 3.25 (Appendix B.9). The trends observed in all SAPT2 terms for the hydrogen bonding complexes G2-G4 follow the same pattern; simultaneous increase of attractive and repulsive terms as total interaction strength increases. As previously described, these trends constitute the traditional relationship between attractive and repulsive terms and can be readily linked to diminishing interaction distances. Previous studies on hydrogen bonding arrays have demonstrated that the two bonds in close proximity do have an effect on each other,[78-82] but as our data shows, there is little effect on the relationship between the SAPT terms in response to increasing the number of hydrogen bonds from one to two (Figure 3.25 and Appendix B.10).

It is clear than even though the SAPT total trends and the experimentally measured trends (Figures 3.17B, 3.23B, 3.25B and 3.25D) are broadly similar for all guest series, halogen and hydrogen bonding, energetic dissection reveals that the observed increases in complex strength are the product of two distinct mechanisms. A reduced repulsive term driven mechanism as seen in bi- and trifurcated systems and an enhanced attractive term driven mechanism in the single point and duel bond systems.

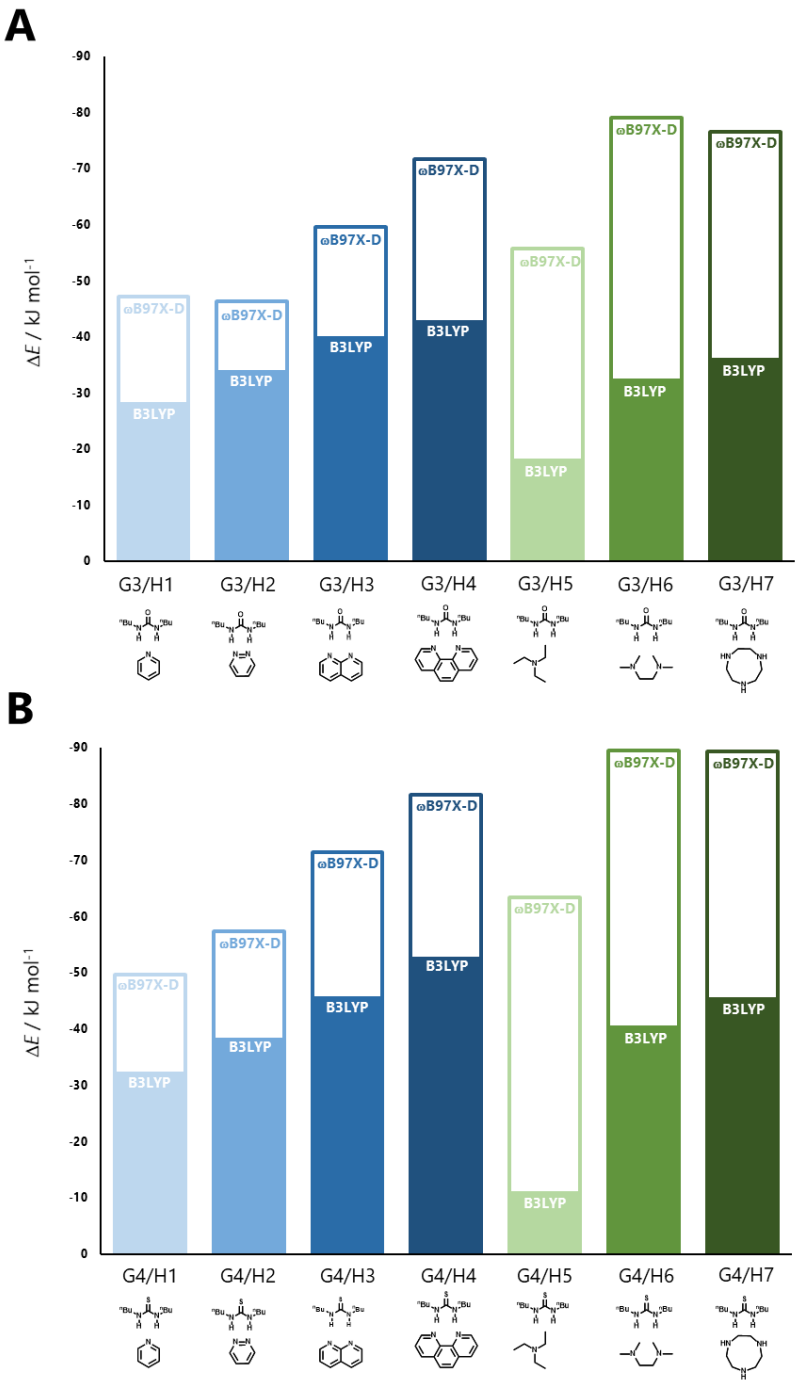

Figure 3.27: A) Computational BSSE counterpoise corrected formation energies for the two host series and guest G3. DFT B3LYP/6-311G* energies are shown in solid colour with the DFT-D ωB97X-D/6-311G* energies being shown as a superimposed outline. **B)** B3LYP/6-311G* and ωB97X-D/6-311G* energies for G4 complexes, laid out as above.

3.8 Bifurcation mode comparisons

The minimised geometries for both the G3/H1 and G4/H1 complexes show D_2•A bifurcation (Figure 3.1C). Comparing these D_2•A complexes with the D•A_2 G2/H4 complex reveals a striking difference in ΔG_{HB} and ΔE_{HB} values. Although both modes of bifurcation appear similar, our results suggest that the same increases in stability afforded by D•A_2 bifurcation (Figures 3.23B and 3.24) is not afforded by the D_2•A mode (Figures 3.25B and 3.26). As a preface it would remiss of us to not consider that this lack of additional stability being afforded by D_2•A bifurcation is simply the product of it not occurring. Indeed precedent exists for thiourea species to favour anti-conformations (figure 3.28A) over the *syn*-conformations needed to facilitate bifurcation (figure 3.28B).[83,84]

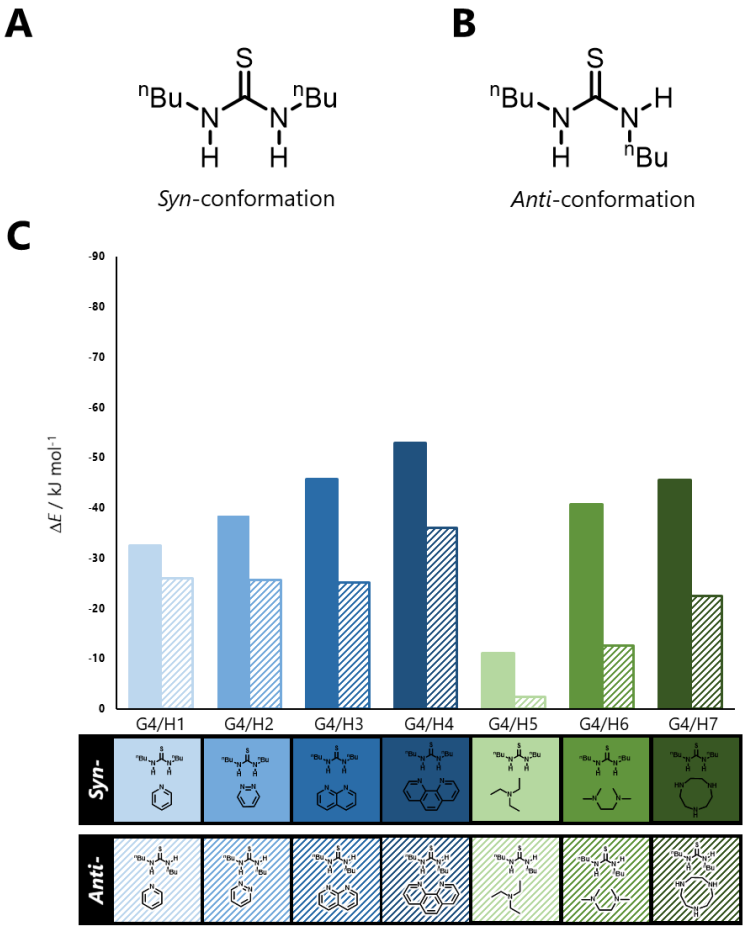

Figure 3.28: A&B) *syn*- and *anti*-conformations for dibutylthiourea respectively. **C)** Computational BSSE counterpoise corrected formation energies for G4/Hx complexes calculated at B3LYP/6-311G*. *Syn*-conformations, solid; *anti*-conformations, striped.

Concern of this notion can be somewhat alleviated by the high degree of similarity between the G3 and G4 complexes; with the same preference for anti-conformations not being seen in urea species.[83,84] Some more concrete support for the formation of can be seen D_2•A bifurcated systems can be drawn from the calculated energies for the various G4/Hx complexes in both *syn*- and *anti*-conformations. Here we see ΔE_{HB} values that are consistently more negative for the *syn*-conformations of all G4 complexes (figure 3.28C). As much suggests that the formation of additional bonds energetically outweighs the intramolecular forces that induces the previously reported *anti*-conformation preference. Appendix B.17 does however show two distinct ^{1}H NMR signals that correspond to amide hydrogens in the G3/H1 and G4/H1 titrations. This much is a sign of asymmetry in the equilibrium state of the guest species; and may be the product of both the host-guest and guest-guest complexes being present in the equilibrium system. Indeed, these signals bare striking resemblance to those seen in guest dimerization experiments (Appendix B.17) –something that, as mentioned previously, we have accounted for energetically-.

Fundamental electronic differences between the D•A_2 and D_2•A modes of bifurcation are observed in the NBOs calculated from the B3LYP/6-311G* minimised geometries (Figure 3.21 and Appendix B.12). In all of the D•A_2 complexes in this study, the magnitude of LP to $\sigma^*_{I/H-C/N}$ donation from each lone pair differed significantly, with one donation being significantly greater than the other. By comparison, for the D_2•A bifurcated complexes (G3/H1 and G4/H1) the magnitude of the two LP to σ^*_{H-N} donations are very similar (G3/H1, 2.25 and 2.61 kJ mol^{-1}; G4/H1, 3.38 and 3.38 kJ mol^{-1}). Indeed, the G3/H5 and G4/H5 host guest complexes (Figure 3.26 A and C) (H5 being the other host species with only a single bond acceptor) minimised to suggest only a single hydrogen bond, with the other donor moiety remaining unbound. The energetics of the minimised structures may be unrepresentative of the solution state complexes since the formation energies, ΔE_{HB}, from the aromatic host complexes with G3 and G4 did not produce the same distinct difference between the dual and D_2•A bifurcated bonds that is seen in the experimental results, with a more stepwise trend being predicted computationally (Figure 3.27). Counter to this, are the significantly less stable G3/H5 and G4/H5 complexes compared to the G3/H1 and G4/H1 complexes in both the DFT and experimental ΔG_{HB} values (5.1 to 5.2 kJ mol^{-1} vs. 0.4

to -1.9 kJ mol^{-1}). Such is not the case for the DFT-D formation energies, but overestimations are not uncommon for dispersion corrections especially when the solvent is not fully modelled and alkyl chains are involved.[76]

3.9 Conclusions

Bifurcation of halogen bonds is a concept that has been much discussed in computational and crystallographic studies. The present work provides an examination of halogen bonding denticity in solution using relatively simple host-guest complexes. ΔG_{XB} values obtained from fitting ^{1}H NMR titration data to 1:1 binding models showed increased stability being afforded by bi- and trifurcation. To understand the seemingly counterintuitive increases in interaction strength being afforded alongside reductions in the linearity of the C-I···N axis, we conducted additional computational studies. The most noteworthy findings came from the energetic dissection conducted using the SAPT2 methodology on DFT minimised structures. Herein, reductions in the stability of the key attractive electrostatic and induction terms were observed with increasing bifurcation, commensurate with the corresponding loss of C-I···N linearity. However, accompanying these reduced attractive forces were significant reductions in the magnitude of the repulsive exchange term. Notably, the electrostatic and induction energetic trends ran counter to the SAPT total, ΔE_{XB} and experimental ΔG_{XB} energy trends. Hence, we conclude that the reduction in repulsion is the driving force governing formation of bi- and trifurcated halogen bonds, even if this comes at the cost of weakened electrostatic and orbital interactions compared a single linear halogen bond.

To facilitate comparison of solution phase bifurcated halogen bonds with other interactions, this study also included analogous hydrogen bonded systems designed to showcase both bifurcated arrangements and two distinct bond arrangements. Trends in the obtained ΔG_{HB} values for the butylacetamide (G2) complexes suggests that hydrogen bonds may yield stronger bifurcation than equivalent halogen bonds, which can be rationalised by the much greater angular dependency inherent to halogen bonds.[12,40-42,67] D•A_2 bifurcated hydrogen bonds also possessed increased stability compared to single-point hydrogen bonds. Computational studies again provided insights, with the SAPT2 calculations showing the same reduction in exchange-

repulsion for bifurcated systems, but without the same loss in electrostatic and induction terms. Contrasting with halogen bonded systems that seek to minimise repulsion by forming bifurcated interactions, the smaller steric demands associated with hydrogen bonding were revealed by SAPT2 energy dissection; a more conventional relationship was observed in which increasingly attractive energy components are counter balanced by increases in exchange repulsion. Bifurcated and non-bifurcated analogues were compared by considering the dual hydrogen bonded systems formed with dibutylurea (G3) and dibutylthiourea (G4). G3 and G4 formed the most stable complexes of those examined, showing that while complex stability of both halogen and hydrogen bonds is increased *via* bifurcation, the SAPT calculations showed that origin of these benefits differ between the two.

The single hydrogen bond in the G2/H1 complex could also be compared with the potential D_2•A binding mode in the G4/H1 complex (as opposed to the D•A_2 and D•A_3 modes seen in other complexes). ΔG_{HB} values for these two complexes suggest that the same increase in stability afforded by D•A_2 bifurcation is not is not afforded to D_2•A binding.

3.10 References

1 Nazare, M., Will, D. W., Matter, H., Schreuder, H., Ritter, K., Urmann, M., Essrich, M., Bauer, A., Czech, J., Lorenz, M., Laux, V. & Wehner, V. Probing the Subpockets of Factor Xa Reveals Two Binding Modes for Inhibitors Based on a 2-Carboxyindole Scaffold: A Study Combining Structure-Activity Relationship and X-ray Crystallography. *J. Med. Chem* **48**, 4511-4525 (2005).

2 Matter, H., Nazare, M., Gussregen, S., Will, D. W., Schreuder, H., Bauer, A., Urmann, M., Ritter, K., Wagner, M. & Wehner, V. Evidence for C-Cl/C-Br···pi Interactions as an Important Contributionto Protein–Ligand Binding Affinity. *Angew. Chem. Int. Ed* **48**, 2911-2916 (2009).

3 Aakeroy, C. B., Bryce, D. L., Desiraju, G. R., Frontera, A., Legon, A. C., Nicotra, F., Rissanen, K., Scheiner, S., G.Terraneo, Metrangolo, P. & Resnati, G. Definition of the chalcogen bond (IUPAC Recommendations 2019). *Pure Appl. Chem.* **91**, 1889–1892 (2019).

4 Wilcken, R., Zimmermann, M. O., Lange, A., Joerger, A. C. & Boeckler, F. M. Principles and Applications of Halogen Bonding in Medicinal Chemistry and Chemical Biology. *J. Med. Chem* **56**, 1363-1388 (2013).

5 Jiang, S., Zhang, L., Cui, D., Yao, Z., Gao, B., Lin, J. & Wei, D. The Important Role of Halogen Bond in Substrate Selectivity of Enzymatic Catalysis. *Sci. Rep.* **6**, 34750 (2016).

6 Cao, J., He, X. Y. W., Li, X., Li, Z., Mo, Y., Liu, M. & Jiang, Y. B. C–I···π Halogen Bonding Driven Supramolecular Helix of Bilateral N-Amidothioureas Bearing β-Turns. *J. Am. Chem. Soc.* **139**, 6605−6610, doi:10.1021/jacs.6b13171 (2017).

7 Gullo, M. C., Baldini, L., Casnati, A. & Marchio, L. Halogen Bonds Direct the Solid State Architectures of a Multivalent Iodopropargylcalix[4]arene. *Cryst. Growth Des.* **20**, 3611−3616 (2020).

8 Rozas, I., Alkorta, I. & J.Elguero. Bifurcated Hydrogen Bonds: Three-Centered Interactions. *J. Phys. Chem. A* **102**, 9925-9932 (1998).

9 Feldblum, E. S. & Arkin, I. T. Strength of a bifurcated H bond. *PNAS* **111**, 4085–4090 (2014).

10 Albrecht, G. & Corey, R. B. The Crystal Structure of Glycine. *J. Am. Chem. Soc.* **61**, 1087-1103 (1939).

11 Desiraju, G. R. & Steiner, T. The weak hydrogen bond in structural chemistry and biology. *Acta Crystallogr. A ACTA CRYSTALLOGR A* **56** (1999).

12 Cavallo, G., Metrangolo, P., Milani, R., Pilati, T., Priimagi, A., Resnati, G. & Terraneo, G. The Halogen Bond. *Chem. Rev.* **116**, 2478-2601 (2016).

13 Bora, P. L., Novak, M., Novotny, J., Foroutan-Nejad, C. & Marek, R. Supramolecular Covalence in Bifurcated Chalcogen Bonding. *Chem. Eur. J.* **23**, 7315 –7323 (2017).

14 Catalano, L., Cavallo, G., Metrangolo, P., Resnati, G. & Terraneo, G. in *Hypervalent Iodine Chemistry* (ed Thomas Wirth) 289-309 (Springer International Publishing, 2016).

15 Wolf, J., Huber, F., Erochok, N., Heinen, F., Guerin, V., Legault, C. Y., Kirsch, S. F. & Huber, S. M. Activation of a Metal-Halogen Bond by Halogen Bonding. *Angew. Chem. Int. Ed* **59**, 16496 –16500 (2020).

16 Allen, F. H., Goud, B. S., Hoy, V. J., Howard, J. A. K. & Desiraju, G. R. Molecular Recognition via Iodo--Nitro and Iodo-Cyano Interactions: Crystal Structures of the 1 : 1 Complexes of 1,4-Diiodobenzene with l,4-Dinitrobenzene and 7,7,8,8-

Tetracyanoquinodimethane (TCNQ). *J. CHEM. SOC., CHEM. COMMUN.*, 2729-2730 (1994).

17 Thalladi, V. R., Goud, B. S., Hoy, V. J., Allen, F. H., Howard, J. A. K. & Desiraju, G. R. Supramolecular synthons in crystal engineering. Structure simplification, synthon robustness and supramolecular retrosynthesis. *Chem. Commun.*, 401-402 (1996).

18 Desiraju, G. R. Designer crystals: intermolecular interactions, network structures and supramolecular synthons. *Chem. Commun.*, 1475-1482 (1997).

19 Sarma, J. A. R. P., Allen, F. H., V.J.Hoy, Howard, J. A. K., Thaimattam, R., Biradha, K. & Desiraju, G. R. Design of an SHG-active crystal, 4-iodo-4A-nitrobiphenyl: the role of supramolecular synthons. *Chem. Commun.*, 101-102 (1997).

20 Langley, P. J., Hulliger, J., Thaimattam, R. & Desiraju, G. R. Supramolecular synthons mediated by weak hydrogen bonding: forming linear molecular arrays via C=C-H···NC and CC-H···O recognition. *New J. Chem.* **22**, 1307-1309 (1998).

21 Lu, Y. X., Zou, J. W., Wang, Y. H. & Yu, Q. S. Bifurcated halogen bonds: An ab initio study of the three-center interactions. *J. Mol. Struct* **767**, 139–142 (2006).

22 Bader, R. F. W. *Atoms in Molecules: A Quantum Theory*. (Clarendon Press, 1990).

23 Ji, B., Wang, W., Deng, D. & Zhang, Y. Symmetrical Bifurcated Halogen Bond: Design and Synthesis. *Cryst. Growth Des.* **11**, 3622–3628 (2011).

24 Bartashevich, E., Troitskaya, E., Pendas, A. M. & Tsirelson, V. Understanding the bifurcated halogen bonding N-Hal-N in bidentate diazaheterocyclic compounds. *Comput. Theor. Chem.* **1053**, 229-237 (2015).

25 Guevara-Vela, J. M., Francisco, E., Rocha-Rinza, T. & Pendas, A. M. Interacting Quantum Atoms—A Review. *Molecules* **25**, 4028 (2020).

26 Bader, R. F. W. & Beddall, P. M. Virial Field Relationship for Molecular Charge Distributions and the Spatial Partitioning of Molecular Properties. *J. Chem. Phys.* **56**, 3320 (1972).

27 Tsirelson, V. G., Avilov, A. S., Lepeshov, G. G., Kulygin, A. K., Stahn, J., Pietsch, U. & Spence, J. C. H. Quantitative Analysis of the Electrostatic Potential in Rock-Salt Crystals Using Accurate Electron Diffraction Data. *J. Phys. Chem. B* **105**, 068-5074 (2001).

28 Tsirelson, V. G., Shishkina, A. V., Stash, A. I. & Parsons, S. The experimental and theoretical QTAIMC study of the atomic and molecular interactions in dinitrogen tetroxide. *Acta Cryst.* **65**, 647–658 (2009).

29 Blanco, M. A., Pendas, A. M. & Francisco, E. Interacting Quantum Atoms: A Correlated Energy Decomposition Scheme Based on the Quantum Theory of Atoms in Molecules. *J. Chem. Theory Comput.* **1**, 1096-1109 (2005).

30 Francisco, E., Pendas, A. M. & Blanco, M. A. A Molecular Energy Decomposition Scheme for Atoms in Molecules. *J. Chem. Theory Comput.* **2**, 90-102 (2006).

31 Garcia-Revilla, M., Francisco, E., Costales, A. & Pendas, A. M. Performance of the Density Matrix Functional Theory in the Quantum Theory of Atoms in Molecules. *J. Phys. Chem. A* **116**, 1237–1250 (2012).

32 Novak, M., Foroutan-Nejad, C. & Marek, R. Asymmetric bifurcated halogen bonds. *Phys. Chem. Chem. Phys.* **17**, 6440-6450 (2015).

33 Velde, G. t., Bickelhaupt, F. M., Baerends, E. J., Guerra, C. F., Gisbergen, S. J. A. v., Snijders, J. G. & Ziegler, T. Chemistry with ADF. *J. Comput. Chem* **22**, 931–967 (2001).

34 Glendening, E. D., Reed, A. E., Carpenter, J. E. & Weinhold, F. NBO Version 3.1. (2003).

35 Riley, K. E. & Hobza, P. Investigations into the Nature of Halogen Bonding Including Symmetry Adapted Perturbation Theory Analyses. *J. Chem. Theory Comput.* **4**, 232-242 (2008).

36 Riley, K. E. & Hobza, P. The relative roles of electrostatics and dispersion in the stabilization of halogen bonds. *Phys. Chem. Chem. Phys.* **15**, 17742-17751 (2013).

37 Riley, K. E., Murray, J. S., Fanfrlik, J., Rezac, J., Sola, R. J., Concha, M. C., Ramos, F. M. & Politzer, P. Halogen bond tunability II: the varying roles of electrostatic and dispersion contributions to attraction in halogen bonds. *j. Mol. Model* **19**, 4651-4659 (2013).

38 Bouzkova, K., Babinsky, M., Novosadova, L. & Marek, R. Intermolecular Interactions in Crystalline Theobromine as Reflected in Electron Deformation Density and 13C NMR Chemical Shift Tensors. *J. Chem. Theory Comput.* **9**, 2629−2638 (2013).

39 Babinsky, M., Bouzkova, K., Pipiska, M., Novosadova, L. & Marek, R. Interpretation of Crystal Effects on NMR Chemical Shift Tensors: Electron and Shielding Deformation Densities. *J. Phys. Chem. A* **117**, 497−503 (2013).

40 Politzer, P., Murray, J. S. & Clark, T. Halogen bonding: an electrostatically-driven highly directional noncovalent interaction. *Phys. Chem. Chem. Phys.* **12**, 7748–7757 (2010).

41 Desiraju, G. R., Ho, P. S., Kloo, L., Legon, A. C., Marquardt, R., Metrangolo, P., Politzer, P., Resnati, G. & Rissanen, K. Definition of the halogen bond. *Pure Appl. Chem.* **85**, 1711-1713 (2013).

42 Metrangolo, P., Neukirch, H., Pilati, T. & Resnati, G. Halogen Bonding Based Recognition Processes: A World Parallel to Hydrogen Bonding. *Acc. Chem. Res.* **38**, 386-395 (2005).

43 Bauza, A., Quinonero, D., Frontera, A. & Deya, P. M. Substituent effects in halogen bonding complexes between aromatic donors and acceptors: a comprehensive ab initio study. *Phys. Chem. Chem. Phys.* **13**, 20371–20379 (2011).

44 Torii, H. & Yoshida, M. Properties of halogen atoms for representing intermolecular electrostatic interactions related to halogen bonding and their substituent effects. *J. Comput. Chem* **31**, 107-116 (2010).

45 Riley, K. E., Murray, J. S., Fanfrlik, J., Rezac, J., Sola, R. J., Concha, M. C., Ramos, F. M. & Politzer, P. Halogen bond tunability I: the effects of aromatic fluorine substitution on the strengths of halogen-bonding interactions involving chlorine, bromine, and iodine. *J. Mol. Model* **17**, 3309–3318 (2011).

46 Carletta, A., Zbacnik, M., Vitkovic, M., Tumanov, N., Stilinovic, V., Wouters, J. & Cincic, D. Halogen-bonded cocrystals of N-salicylidene Schiff bases and iodoperfluorinated benzenes: hydroxyl oxygen as a halogen bond acceptor. *CrystEngComm* **20**, 5332–5339 (2018).

47 Forni, A., Metrangolo, P., Pilati, T. & Resnati, G. Halogen Bond Distance as a Function of Temperature. *Cryst. Growth Des.* **4**, 291-295 (2003).

48 Clark, T., Politzer, P. & Murray, J. S. Correct electrostatic treatment of noncovalent interactions: the importance of polarization. *WIREs Comput. Mol. Sci.* **5**, 169-177 (2015).

49 Stilinovic, V., Grguric, T., Pitesa, T., Nemec, V. & Cincic, D. Bifurcated and Monocentric Halogen Bonds in Cocrystals of Metal(II) Acetylacetonates with p-Dihalotetrafluorobenzenes. *Cryst. Growth Des.* **19**, 1245−1256 (2019).

50 Kolaric, A., Germe, T., Hrast, M., Stevenson, C. E. M., Lawson, D. M., Burton, N. P., Voros, J., Maxwell, A., Minovski, N. & Anderluh, M. Potent DNA gyrase inhibitors bind asymmetrically to their target using symmetrical bifurcated halogen bonds. *Nat. Commun.* **12**, 1-13 (2021).

51 Bax, B. D., Chan, P. F., Eggleston, D. S., Fosberry, A., Gentry, D. R., Gorrec, F., Giordano, I., Hann, M. M., Hennessy, A., Hibbs, M., Huang, J., Jones, E., Jones, J., Brown, K. K., Lewis, C. J., May, E. W., Saunters, M. R., Singh, O., Spitzfaden, C. E., Shen, C., Shillinigs, A., Theobald, A. J., Wohlkonig, A., Pearson, N. D. & Gwynn, M. N. Type IIA topoisomerase inhibition by a new class of antibacterial agents. *Nature.* **466**, 935–940 (2010).

52 Gibson, E. G., Bax, B., Chan, P. F. & Osheroff, N. Mechanistic and Structural Basis for the Actions of the Antibacterial Gepotidacin against Staphylococcus aureus Gyrase. *ACS Infect. Dis.* **5**, 570−581 (2019).

53 Kolaric, A., Anderluh, M. & Minovski, N. Two Decades of Successful SAR-Grounded Stories of the Novel Bacterial Topoisomerase Inhibitors (NBTIs). *J. Med. Chem.* **63**, 5664−5674 (2020).

54 Cincic, D., Friscic, T. & Jones, W. Experimental and database studies of three-centered halogen bonds with bifurcated acceptors present in molecular crystals, cocrystals and salts. *CrystEngComm* **13**, 3224–3231 (2011).

55 Cincic, D., Friscic, T. & Jones, W. Isostructural Materials Achieved by Using Structurally Equivalent Donors and Acceptors in Halogen-Bonded Cocrystals. *Chem. Eur. J.* **14**, 747 – 753 (2008).

56 Cincic, D., Friscic, T. & Jones, W. A Stepwise Mechanism for the Mechanochemical Synthesis of Halogen-Bonded Cocrystal Architectures. *J. AM. CHEM. SOC.* **130**, 7524–7525 (2008).

57 Aakeroy, C. B., Desper, J., Fasulo, M., Hussain, I., Levin, B. & Schultheiss, N. Ten years of co-crystal synthesis; the good, the bad, and the ugly. *CrystEngComm* **10**, 1816–1821 (2008).

58 Bouchmella, K., B.Boury, Dutremez, S. G. & Lee, A. v. d. Molecular Assemblies from Imidazolyl-Containing Haloalkenes andHaloalkynes: Competition between Halogen and Hydrogen Bonding. *Chem. Eur. J.* **13**, 6130 – 6138 (2007).

59 Muniappan, S., Lipstman, S. & Goldberg, I. Rational design of supramolecular chirality in porphyrin assemblies: the halogen bond case. *Chem. Commun.* **2008**, 1777–1779 (2008).

60 Lipstman, S., Muniappan, S. & Goldberg, I. Supramolecular Reactivity of Porphyrins with Mixed Iodophenyl and Pyridyl meso-Substituents. *Cryst. Growth Des.* **8**, 1682–1688 (2008).

61 Sellin, M., Rupf, S. M., Zhang, Y. & Malischewski, M. Bi- and Trifurcated Halogen Bonding M−CN···I in 1D, 2D, and 3D Supramolecular Network Structures of Co-Crystallized Diiodoacetylene C2I2 and Tetracyanonickelate [Ni(CN)4]2−. *Cryst. Growth Des.* **20**, 7104−7110 (2020).

62 Perkins, C., Libri, S., Adams, H. & Brammer, L. Diiodoacetylene: compact, strong ditopic halogen bond donor. *CrystEngComm* **14**, 3033–3038 (2012).

63 Li, P., Vik, E. C. & Shimizu, K. D. N-Arylimide Molecular Balances: A Comprehensive Platform for Studying Aromatic Interactions in Solution. *Acc. Chem. Res.* **53**, 2705−2714 (2020).

64 Yang, L., Brazier, J. B., Hubbard, T. A., Rogers, D. M. & Cockroft, S. L. Can Dispersion Forces Govern Aromatic Stacking in an Organic Solvent? *Angew. Chem. Int. Ed* **55**, 912 –916 (2016).

65 Hwang, J. W., Li, P. & Shimizu, K. D. Synergy between experimental and computational studies of aromatic stacking interactions. *Org. Biomol. Chem.* **15**, 1554 (2017).

66 Lee, G. Y., Hu, E., Rheingold, A. L., Houk, K. N. & Sletten, E. M. Arene-Perfluoroarene Interactions in Solution. *J. Org. Chem.* (2012).

67 Stone, A. J. Are Halogen Bonded Structures Electrostatically Driven? *J. Am. Chem. Soc.* **135**, 7005-7009 (2013).

68 Yang, L., Adam, C. & Cockroft, S. L. Quantifying Solvophobic Effects in Nonpolar Cohesive Interactions. *J. Am. Chem. Soc.* **137**, 10084-10087 (2015).

69 Yang, L., Adam, C., Nichol, G. S. & Cockroft, S. L. How much do van der Waals dispersion forces contribute to molecular recognition in solution? *Nature Chemistry* **5**, 1006-1010 (2013).

70 Sawar, M. G., Dragisic, B., Salsberg, L. J., Gouliaras, C. & Taylor, M. S. Thermodynamics of Halogen Bonding in Solution: Substituent, Structural, and Solvent Effects. *J. Am. Chem. Soc.* **132**, 1646-1653 (2010).

71 Adam, C., Yang, L. & Cockroft, S. L. Partitioning Solvophobic and Dispersion Forces in Alkyl and Perfluoroalkyl Cohesion. *Angew. Chem. Int. Ed* **54**, 1164-1167 (2015).

72 Hohenstein, E. G. & Sherrill, C. D. Density fitting of intramonomer correlation effects in symmetry-adapted perturbation theory. *J. Chem. Phys.* **133**, 014101 (2010).

73 Stone, A. J. & Misquitta, A. J. Charge-transfer in Symmetry-Adapted Perturbation Theory. *Chem. Phys. Lett.* **473**, 201–205 (2009).

74 Arunan, E., Desiraju, G. R., Klein, R. A., Sadlej, J., Scheiner, S., Alkorta, I., Clary, D. C., Kjaergaard, H. G., Legon, A. C., Mennucci, B. & Nesbitt, D. J. Definition of the hydrogen bond (IUPAC Recommendations 2011). *Pure Appl. Chem.* **83**, 1637–1641 (2011).

75 Shahi, A. & Arunan, E. Why are Hydrogen Bonds Directional? *J. Chem. Sci.* **128**, 1571–1577 (2016).

76 Klimes, J. & Michaelides, A. Perspective: Advances and challenges in treating van der Waals dispersion forces in density functional theory. *J. Chem. Phys.* **137**, 120901 (2012).

77 Liao, H.-Y. & Chu, S.-Y. Hydrogen bond acceptor capability of carbonyl π-electrons—case study of the hydrogen-bonded urea dimer. *New J. Chem.* **27**, 421-424 (2003).

78 Jorgensen, W. L. & Pranata, J. Importance of Secondary Interactions in Triply Hydrogen Bonded Complexes: Guanine-Cytosine vs Uracil-2,6-Diaminopyndine. *J. Am. Chem. Soc.* **112**, 2008-2010 (1990).

79 Blight, B. A., Hunter, C. A., Leigh, D. A., McNab, H. & Thomson, P. I. T. An AAAA–DDDD quadruple hydrogen-bond array. *Nat. Chem.* **3**, 244–248 (2011).

80 Leigh, D. A., Robertson, C. C., Slawin, A. M. Z. & Thomson, P. I. T. AAAA-DDDD Quadruple Hydrogen-Bond Arrays Featuring NH···N and CH···N Hydrogen Bonds. *J. Am. Chem. Soc.* **135**, 9939–9943 (2013).

81 Dale, S. H., Elsegood, M. R. J. & Coombs, A. E. L. Hydrogen bond directed supramolecular arrays utilising hemimellitic acid: Solvent inclusion clathrates. *CrystEngComm,* **6**, 328–335 (2004).

82 Kwiatkowski, A., Grela, I. & Osmialowski, B. Conformational change in the association of a heterocyclic urea derivative forming two intramolecular hydrogen bonds in polar solvent. *New J. Chem.* **41**, 1073-1081 (2017).

83 Lenthall, J. T., Foster, J. A., Anderson, K. M., Probert, M. R., Howard, J. A. K. & Steed, J. W. Hydrogen bonding interactions with the thiocarbonyl π-system. *CrystEngComm* **13**, 3202-3212 (2010).

84 Masunov, A. & Dannenberg, J. J. Theoretical Study of Urea and Thiourea. 2. Chains and Ribbons. *J. Phys. Chem. B* **104**, 806-810 (2000).

Appendix A

Supporting information for chapter 2

Contents

A.1 Measurement of conformational free energies of molecular torsion balances

Molecular torsion balances of series 1 and 2 were prepared as 10 mM solutions in requisite solvent or solvent mixture. Spectra were obtained using Bruker Ultrashield 600 MHz equipped with a TCI cryoprobe. Assignment of the conformer peaks was conducted based on the rationale of expected shielding differences between the closed and open conformers and precedent provided by previous studies employing the Wilcox balance system. Conformational free energies were calculated from this using equation 1.

A.1.1 Determination of equilibrium constants from ^{1}H NMR spectra

Equilibrium constants were determined from the ratio of the signals associated with the methyl conformer peeks from phase and baseline corrected ^{1}H NMR spectra. Relative prevalence of conformers was determined by measurement of area under the conformer peaks using the inbuilt line fitting tool in the MestReNova software package. Example below shows fitting for **2Cl** in DCM(d_2).

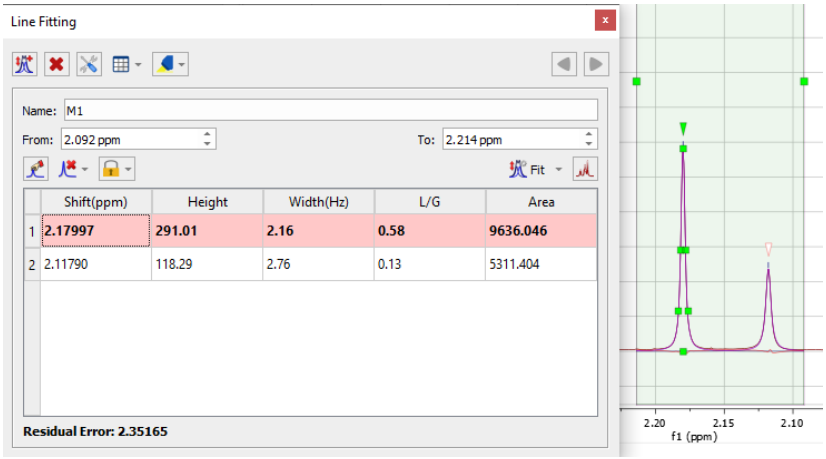

A.1.2 Estimation of errors in Δ*G* values

Errors were estimated at a conservative ±0.2 kJ mol^{-1} based for both compound series 1 and 2, in accordance with literature precedence for NMR-based studies of molecular balances.[1] Validation is based on the observation that the most extreme conformational free energy difference ΔG_{XB} reported here was -3.4 kJ mol^{-1} (approximate conformer ratio ≤ 4: 1). Integration errors associated with modern NMR spectrometers generally do not exceed 1–2%.[2] Hence, based on a 3% error in integrals, the largest expected

errors would be +0.14 kJ mol^{-1} and -0.027 kJ mol^{-1}, well within the estimate we employ.

A.1.3 Propagation of errors in $\Delta\Delta G$ values

Errors were estimated at ±0.4 kJ mol^{-1} calculated from the propagation of the conservative ±0.2 kJ mol^{-1} error estimate used for the individual ΔG values.

$$Q_{\Delta\Delta G} = \sqrt{(Q_{\Delta G_{1\mathrm{X}}})^2 + (Q_{\Delta G_{1\mathrm{H}}})^2 + (Q_{\Delta G_{2\mathrm{X}}})^2 + (Q_{\Delta G_{2\mathrm{H}}})^2} \qquad \text{(Equation 2.3)}$$

$$0.4 = \sqrt{(0.2)^2 + (0.2)^2 + (0.2)^2 + (0.2)^2}$$

A.2 Free energies of series 1 molecular torsion balances

Solvent	$\Delta G_{1\mathrm{I}}$/kJ mol^{-1}	$\Delta G_{1\mathrm{Br}}$/kJ mol^{-1}	$\Delta G_{1\mathrm{Cl}}$/kJ mol^{-1}	$\Delta G_{1\mathrm{F}}$/kJ mol^{-1}	$\Delta G_{1\mathrm{H}}$/kJ mol^{-1}	$\Delta G_{1\mathrm{Me}}$/kJ mol^{-1}
CCl_4	-1.8	-1.8	-2.0	-1.9	-1.8	-2.4
C_6D_6	-1.9	-2.0	-2.3	-2.2	-1.9	-2.3
$CDCl_3$	-1.6	-1.6	-1.7	-1.6	-1.4	-1.9
CD_2Cl_2	-1.3	-1.4	-1.5	-1.5	-1.2	-1.6
C_5D_5N	-1.5	-1.6	-1.7	-1.7	-1.3	-2.1
DMSO-d_6	-1.5	-1.8	-2.0	-1.8	-1.6	-2.9
CS_2	-0.6	-0.8	-1.0	-1.0	-0.8	-1.2
2.9% wt I_2 / CS_2	-0.3	-0.5	-0.6	-0.6	-0.3	-0.6
5.8% wt I_2 / CS_2	-0.2	-0.4	-0.5	-0.5	-0.3	-0.6
12.5% wt I_2 / CS_2	-0.4	-0.5	-0.6	-0.5	-0.3	-0.4
THF-d_8	-1.4	-1.3	-1.7	-1.3	-1.7	-2.2
9% v/v D_2O / THF	-1.5	-1.5	-1.9	-1.8	-1.9	-2.7
15% v/v D_2O / THF	-1.8	-1.8	-2.0	-2.1	-2.1	-2.6
20% v/v D_2O / THF	-2.0	-2.1	-2.2	-2.3	-2.3	-3.0
25% v/v D_2O / THF	-2.2	-2.3	-2.6	-2.3	-2.3	-3.0
35% v/v D_2O / THF	-2.5	-2.9	-3.1	-2.6	-2.3	-3.2
40% v/v D_2O / THF	-2.9	-2.8	-2.8	-2.5	-2.3	-3.4
9% v/v CD_3OD / THF	-1.4	-1.7	-1.9	-1.7	-1.7	-2.4

15% v/v CD_3OD / THF	-1.4	-1.6	-1.7	-1.5	-1.8	-2.5
20% v/v CD_3OD / THF	-1.5	-1.7	-1.7	-1.8	-1.8	-2.8
25% v/v CD_3OD / THF	-1.6	-1.6	-1.8	-1.7	-1.8	-2.7
35% v/v CD_3OD / THF	-1.6	-1.7	-1.8	-1.4	-1.6	-2.7
40% v/v CD_3OD / THF	-1.6	-1.8	-1.8	-1.6	-1.7	-2.6

In all cases THF refers to THF-d_8. Samples in CS_2 and CCl_4 were locked using a sealed internal standard of C_6D_6.

A.3 Free energies of series 2 molecular torsion balances

Solvent	**ΔG_{2I}/kJ mol^{-1}**	**ΔG_{2Br}/kJ mol^{-1}**	**ΔG_{2Cl}/kJ mol^{-1}**	**ΔG_{2F} /kJ mol^{-1}**	**ΔG_{2H} /kJ mol^{-1}**	**ΔG_{2Me} /kJ mol^{-1}**
CCl_4	-2.2	-2.3	-2.1	-1.9	-1.2	-1.1
C_6D_6	-2.6	-2.7	-2.5	-2.6	-1.5	-1.3
$CDCl_3$	-2.0	-2.0	-1.8	-1.6	-1.1	-0.9
CD_2Cl_2	-1.6	-1.5	-1.5	-1.5	-0.8	-1.0
C_5D_5N	-2.0	-1.6	-1.8	-1.7	-1.1	-0.5
DMSO-d_6	-1.4	-1.5	-1.4	-1.3	-1.0	-1.1
CS_2	-1.3	-1.3	-1.2	-1.3	-0.1	-0.4
2.9% wt I_2 / CS_2	-1.1	-0.9	-0.9	-0.7	-0.1	-0.1
5.8% wt I_2 / CS_2	-0.7	-1.0	-1.0	-0.7	0.0	-0.2
12.5% wt I_2 / CS_2	-1.0	-1.0	-0.9	-0.7	-0.1	-0.1
THF-d_8	-1.8	-1.8	-1.7	-1.9	-1.4	-1.4
9% v/v D_2O / THF	-1.7	-2.0	-1.8	-1.6	-1.2	-1.2
15% v/v D_2O / THF	-1.7	-2.1	-2.0	-1.7	-1.4	-1.2
20% v/v D_2O / THF	-1.5	-2.1	-2.0	-2.0	-1.3	-1.4
25% v/v D_2O / THF	-1.8	-2.3	-2.0	-1.9	-1.4	-1.5
35% v/v D_2O / THF	-2.1	-2.1	-2.3	-2.1	-1.5	-1.7
40% v/v D_2O / THF	-2.5	-2.4	-2.2	-1.9	-1.5	-1.6

In all cases THF refers to THF-d_8. Samples in CS_2 and CCl_4 were locked using a sealed internal standard of C_6D_6.

A.4 DFT/DFT-D computational methodologies

Initial modelling of the balance series 1 and 2 was conducted using the Spartan '14 program using either the B3LYP or ωB97X-D methods were appropriate and the 6-311G* basis set. All energies were then calculated after final geometry minimizations were conducted using the Gaussian 09 software package and the relevant level of theory (B3LYP, B3LYP-D3, ωB97X or ωB97X-D) and included 6-311G* basis set.

A.5 Computational energies

A.5.1 Computational energies for balance series 1

Solvent	ΔE_{1I} /kJ mol^{-1}	ΔE_{1Br} /kJ mol^{-1}	ΔE_{1Cl} /kJ mol^{-1}	ΔE_{1F} /kJ mol^{-1}	ΔE_{1H} /kJ mol^{-1}	ΔE_{1Me} /kJ mol^{-1}
B3LYP/6-311G*	0.7	-0.1	-1.6	-1.8	-1.6	-2.1
B3LYP-D3/6-311G*	-12.6	-7.3	-6.8	-6.4	-5.5	-0.3
ωB97X/6-311G*	-3.9	-5.8	-5.2	-8.4	-6.2	-8.8
ωB97X-D/6-311G*	-19.3	-17.3	-16.9	-18.5	-16.5	-21.9

All values reported are composite numbers obtained from comparison of "folded" and "unfolded" minimised geometries for the balance system.

A.5.2 Computational energies for balance series 2

Solvent	ΔE_{2I} /kJ mol^{-1}	ΔE_{2Br} /kJ mol^{-1}	ΔE_{2Cl} /kJ mol^{-1}	ΔE_{2F} /kJ mol^{-1}	ΔE_{2H} /kJ mol^{-1}	ΔE_{2Me} /kJ mol^{-1}
B3LYP/6-311G*	-1.3	-1.7	-1.9	-1.8	-0.9	-0.6
B3LYP-D3/6-311G*	-12.6	-7.3	-6.8	-6.4	-5.5	-0.3
ωB97X/6-311G*	-4.3	-4.9	-1.1	-5.8	-3.2	-7.8
ωB97X-D/6-311G*	-17.0	-15.5	-14.8	-13.4	-10.2	-13.1

All values reported are composite numbers obtained from comparison of "folded" and "unfolded" minimised geometries for the balance system.

A.6 DFT Minimized geometries

Folded

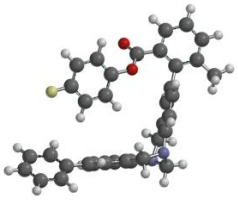

Unfolded

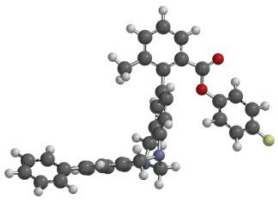

A.6.1 **1F** at B3LYP/6-311G*

Folded

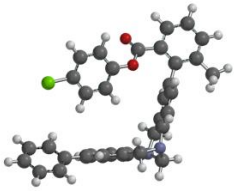

Unfolded

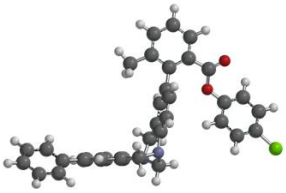

A.6.2 **1Cl** at B3LYP/6-311G*

Folded

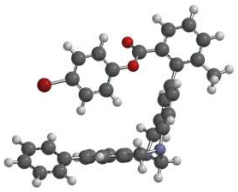

Unfolded

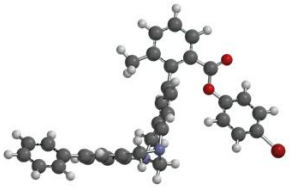

A.6.3 **1Br** at B3LYP/6-311G*

Folded

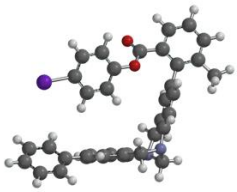

Unfolded

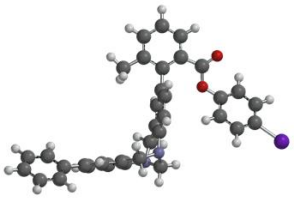

A.6.4 **1I** at B3LYP/6-311G*

Folded

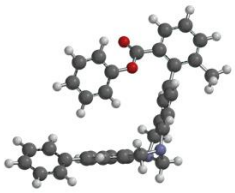

Unfolded

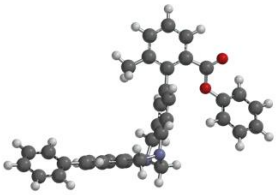

A.6.5 **1H** at B3LYP/6-311G*

Folded

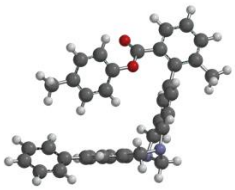

Unfolded

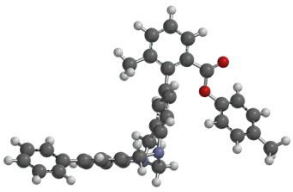

A.6.6 **1Me** at B3LYP/6-311G*

A.7 DFT-D Minimized geometries

Folded

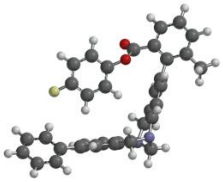

Unfolded

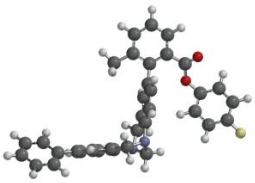

A.7.1 **1F** at ωB97X-D

Folded

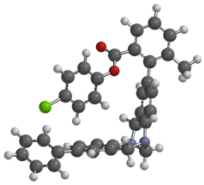

Unfolded

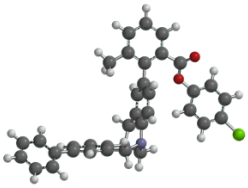

A.7.2 **1Cl** at ωB97X-D

Folded

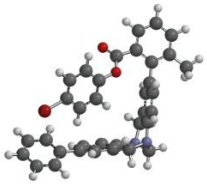

Unfolded

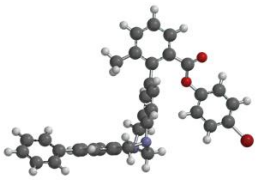

A.7.3 **1Br** at ωB97X-D

Folded

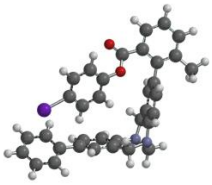

Unfolded

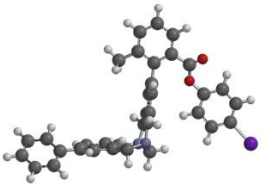

A.7.4 **1I** at ωB97X-D

Folded

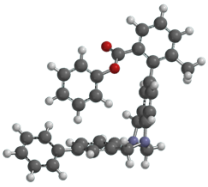

Unfolded

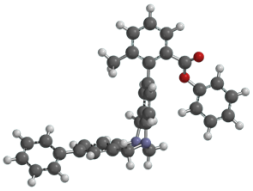

A.7.5 **1H** at ωB97X-D

Folded

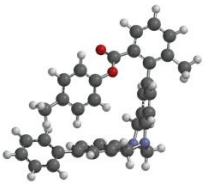

Unfolded

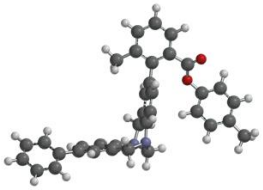

A.7.6 1Me at ωB97X-D

A.8 SAPT calculations

A.8.1 SAPT computational methodologies

SAPT calculations pertaining to halogen···arene interactions in the minimized balance **1** structure were conducted based using truncated versions of the ωB97X-D/6-311G* minimized geometries. Calculations were conducted using the Psi4 software package.

Angular geometry SAPT calculations were conducted using a simplified model of the system based on the truncated model. Starting models were fixed at bond distances of, 4.0 Å, 3.9 Å and 3.7 Å for the Me, Br and Cl systems respectively. C_1-X···Y (Y = atom, bond or centroid) angles were initially set to 180^o and systematically reduced by 10^o increments down to 90^o. Accounting for interaction between the two aromatic rings was done by repeating the calculations by with the X moiety replaced by a hydrogen. Energies from this exercise were then subtracted to give corrected values for all the systems. All calculations were conducted using the Psi4 software package using the manually defined 6-311G* basis set.

Due to the inclusion of iodine atoms in computational studies; the 6-311G* basis set was manually defined for Psi4 calculations as shown below. Basis set provided by https://www.basissetexchange.org/. 6-311G* basis set was last updated 19/02/2015 at time of writing.

```
****
H     0
S    3   1.00
     33.86500                0.0254938
      5.094790               0.190373
      1.158790               0.852161
S    1   1.00
      0.325840               1.000000
S    1   1.00
      0.102741               1.000000
****
C     0
S    6   1.00
   4563.240                 0.00196665
    682.0240                0.0152306
    154.9730                0.0761269
     44.45530               0.2608010
     13.02900               0.6164620
      1.827730              0.2210060
SP   3   1.00
     20.96420                0.114660              0.0402487
      4.803310               0.919999              0.237594
      1.459330              -0.00303068            0.815854
```

```
SP   1   1.00
      0.4834560             1.000000              1.000000
SP   1   1.00
      0.1455850             1.000000              1.000000
D    1   1.00
      0.626                 1.000000
****
N     0
S    6   1.00
   6293.480                 0.00196979
    949.0440                0.0149613
    218.7760                0.0735006
     63.69160               0.2489370
     18.82820               0.6024600
      2.720230              0.2562020
SP   3   1.00
     30.63310                0.111906              0.0383119
      7.026140               0.921666              0.237403
      2.112050              -0.00256919            0.817592
SP   1   1.00
      0.684009              1.000000              1.000000
SP   1   1.00
      0.200878              1.000000              1.000000
D    1   1.00
      0.913                 1.000000
****
O     0
S    6   1.00
   8588.500                 0.00189515
   1297.230                 0.0143859
    299.2960                0.0707320
     87.37710               0.2400010
     25.67890               0.5947970
      3.740040              0.2808020
SP   3   1.00
     42.11750                0.113889              0.0365114
      9.628370               0.920811              0.237153
      2.853320              -0.00327447            0.819702
SP   1   1.00
      0.905661              1.000000              1.000000
SP   1   1.00
      0.255611              1.000000              1.000000
D    1   1.00
      1.292                 1.000000
****
F     0
S    6   1.00
  11427.10                  0.00180093
   1722.350                 0.0137419
    395.7460                0.0681334
    115.1390                0.2333250
     33.60260               0.5890860
      4.919010              0.2995050
SP   3   1.00
     55.44410                0.114536              0.0354609
     12.63230                0.920512              0.237451
      3.717560              -0.00337804            0.820458
SP   1   1.00
      1.165450              1.000000              1.000000
SP   1   1.00
```

```
      0.321892               1.000000               1.000000
D    1   1.00
      1.750                  1.000000
****
Cl     0
S    6   1.00
 105819.0                    0.000738
  15872.00                   0.005718
   3619.650                  0.029495
   1030.800                  0.117286
    339.9080                 0.362949
    124.5380                 0.584149
S    3   1.00
    124.5380                 0.134177
     49.51350                0.624250
     20.80560                0.291756
S    1   1.00
      6.583460               1.000000
S    1   1.00
      2.564680               1.000000
S    1   1.00
      0.559763               1.000000
S    1   1.00
      0.183273               1.000000
P    5   1.00
    589.7760                 0.002391
    139.8490                 0.018504
     45.14130                0.081377
     16.87330                0.221552
      6.741100               0.772569
P    2   1.00
      6.741100              -1.572244
      2.771520               0.992389
P    1   1.00
      1.023870               1.000000
P    1   1.00
      0.381368               1.000000
P    1   1.00
      0.109437               1.000000
D    1   1.00
      0.7500000              1.0000000
****
Br     0
S    6   1.00
 439700.0                    0.0008130
  66030.00                   0.0062850
  15140.00                   0.0319200
   4317.000                  0.1288000
   1414.000                  0.3946000
    523.9000                 0.5413000
S    3   1.00
    523.9000                 0.1831
    207.7000                 0.6176
     86.54000                0.2538
S    1   1.00
     30.52                   1.000000
S    1   1.00
     12.98                   1.000000
S    1   1.00
      4.412                  1.000000
```

```
S    1   1.00
      1.862                    1.000000
S    1   1.00
      0.3932                   1.000000
S    1   1.00
      0.1400                   1.000000
P    3   1.00
   2957.000                    0.02226
    700.3000                   0.18020
    224.6000                   0.86240
P    3   1.00
     82.59                     0.3440
     33.19                     0.5071
     14.20                     0.2590
P    3   1.00
     14.20                     0.07965
      7.438                    0.3734
      3.526                    0.6049
P    1   1.00
      1.595000                 1.000000
P    1   1.00
      0.846200                 1.000000
P    1   1.00
      0.318600                 1.000000
P    1   1.00
      0.109600                 1.000000
D    4   1.00
    134.8                      0.01831
     36.39                     0.13500
     12.16                     0.42610
      4.341                    0.60430
D    1   1.00
      1.535000                 1.000000
D    1   1.00
      0.451000                 1.000000
****
I     0
S    5   1.00
 444750.0                      0.00089
  66127.00                     0.00694
  14815.00                     0.03609
   4144.900                    0.13568
   1361.200                    0.33878
S    2   1.00
S   1  1.00    508.4400                 0.43659
    209.5900                   0.18375
S    1   1.00
     81.959                    1.00000

     36.805                    1.00000
S    1   1.00
     13.495                    1.00000
S    1   1.00
      6.8859                   1.00000
S    1   1.00
      2.5520                   1.00000
S    1   1.00
      1.2088                   1.00000
S    1   1.00
      0.2734                   1.00000
```

```
S    1   1.00
      0.1009                1.00000
P    4   1.00
   2953.600                 0.01221
    712.6100                0.08587
    236.7100                0.29493
     92.63100               0.47849
P    1   1.00
     39.73200                1.00000
P    1   1.00
     17.27300                1.000000
P    1   1.00
      7.957000               1.000000
P    1   1.00
      3.152900               1.000000
P    1   1.00
      1.332800               1.000000
P    1   1.00
      0.494700               1.000000
P    1   1.00
      0.216000               1.000000
P    1   1.00
      0.082930               1.000000
D    3   1.00
    261.9500                0.03144
     76.73400                0.19028
     27.55100                0.47247
D    1   1.00
     10.60600                1.000000
D    1   1.00
      3.421700               1.000000
D    1   1.00
      1.137000               1.000000
D    1   1.00
      0.302000               1.000000
****
```

A.8.2 Tabulated truncated ωB97X-D geometry SAPT2 energies

Balance System	Electrostatic (kJ mol^{-1})	Exchange (kJ mol^{-1})	Induction (kJ mol^{-1})	Dispersion (kJ mol^{-1})	SAPT2 Total (kJ mol^{-1})
F	-4.484	11.417	-1.245	-7.800	-2.111
Cl	-5.663	17.830	-2.182	-13.049	-3.064
Br	-5.931	19.724	-2.320	-15.166	-3.693
I	-7.498	22.299	-2.528	-17.330	-5.057
H	-8.962	16.007	-1.678	-11.756	-6.388
Me	-12.881	25.165	-2.712	-18.704	-9.132

A.8.3 Cartesian coordinates for truncated ωB97X-D geometries

A.8.3.1 Iodine system

```
0 1
I        4.070616      2.395661     -0.646632
C       -0.760540      2.019959     -0.167707
C       -0.192616      3.274193     -0.335879
C        1.184879      3.385114     -0.465104
C        1.975532      2.242291     -0.422325
C        1.399924      0.990733     -0.242524
C        0.021215      0.876789     -0.118417
H        2.023552      0.090778     -0.193694
H       -0.453829     -0.102467      0.010454
H       -1.847086      1.878657     -0.141877
H       -0.825246      4.168796     -0.361948
H        1.637406      4.373817     -0.602591
--
0 1
C        4.001706     -1.696525      0.780211
C        4.942412     -1.908311     -0.230477
C        6.191960     -1.305622     -0.175526
C        6.526859     -0.484188      0.894199
C        5.598157     -0.260636      1.902756
C        4.346333     -0.855958      1.842592
H        3.608330     -0.641905      2.624096
H        5.844083      0.402553      2.739963
H        7.514414     -0.010919      0.938575
H        6.918314     -1.488412     -0.975659
H        4.700782     -2.579098     -1.062869
H        3.012427     -2.167028      0.745999
```

A.8.3.2 Bromine system

```
0 1
Br      -3.963980      3.540135     -1.471417
C       -1.469283      1.239605      1.709076
```

```
C       -2.418659      2.161085      2.127041
C       -3.155497      2.856193      1.178972
C       -2.931068      2.618077     -0.170172
C       -1.973069      1.704453     -0.585652
C       -1.234705      1.008010      0.362855
H       -2.584588      2.338930      3.195711
H       -3.911712      3.583054      1.496821
H       -1.795818      1.533759     -1.653669
H       -0.479094      0.274164      0.059974
H       -0.928409      0.609342      2.424227
--
0 1
C       -1.012109      2.243782     -4.250462
C       -1.990493      1.871075     -5.175270
C       -2.864476      2.811643     -5.702510
C       -2.773072      4.144415     -5.318229
C       -1.805357      4.527352     -4.398630
C       -0.936282      3.585102     -3.866484
H       -0.203248      3.891294     -3.111419
H       -0.328461      1.501876     -3.822191
H       -2.051535      0.828104     -5.506482
H       -3.622014      2.500265     -6.430793
H       -3.463161      4.887070     -5.734710
H       -1.737559      5.571922     -4.073833
```

A.8.3.3 Chlorine system

```
Cl      -3.746192      3.596020     -1.370705
C       -1.413372      1.302210      1.716446
C       -1.199797      1.042705      0.371696
C       -1.916030      1.756109     -0.580880
C       -2.829420      2.715131     -0.170108
C       -3.035775      2.979147      1.176282
C       -2.322503      2.266083      2.128464
H       -1.759372      1.566126     -1.648860
H       -0.477392      0.274319      0.073484
H       -0.889394      0.663337      2.436519
```

```
H       -2.473937      2.464222      3.195715
H       -3.759499      3.742431      1.484239
--
0 1
C       -1.056011      2.184601     -4.282677
C       -2.021190      1.801971     -5.217505
C       -2.903037      2.732705     -5.748928
C       -2.833694      4.064664     -5.357321
C       -1.878207      4.457469     -4.428862
C       -0.999533      3.525213     -3.894228
H       -1.827253      5.501551     -4.099448
H       -3.531477      4.799240     -5.775308
H       -3.650339      2.414389     -6.484747
H       -2.065958      0.758926     -5.551075
H       -0.369988      1.448813     -3.847699
H       -0.276006      3.837801     -3.132642
```

A.8.3.4 Fluorine system

```
0 1
F        0.970708      1.816312      4.334021
C        1.840414      1.840337      0.344955
C        2.403085      2.804169      1.169677
C        2.107649      2.789637      2.525840
C        1.257742      1.815997      3.018599
C        0.691469      0.852298      2.204477
C        0.990684      0.866523      0.848755
H        3.079407      3.561466      0.756997
H        1.983545      1.845919     -0.741644
H        0.557969      0.124439      0.168103
H        0.020515      0.095772      2.627214
H        2.535816      3.532988      3.207983
--
0 1
C       -2.035173     -1.013413      4.591146
C       -2.176426     -2.219776      5.281425
C       -1.928899     -2.289401      6.645420
```

```
C       -1.533990     -1.153501      7.342828
C       -1.389378      0.051358      6.666375
C       -1.640790      0.121236      5.302614
H       -1.490348      1.068929      4.773028
H       -2.507756     -3.114083      4.741377
H       -2.052198     -3.242514      7.172287
H       -1.335041     -1.208938      8.419193
H       -1.063618      0.949618      7.203242
H       -2.217920     -0.960846      3.511768
```

A.8.3.5 Hydrogen system

```
0 1
C       -1.866172     -1.571032      0.512184
C       -1.137527     -0.487491      0.977965
C       -0.967459     -0.332704      2.347965
C       -2.410459     -2.507400      1.378940
C       -1.512276     -1.254283      3.233823
C       -2.228222     -2.341206      2.745963
H       -1.943079     -1.679363     -0.575734
H       -0.707662      0.219889      0.259601
H       -0.396643      0.521272      2.730205
H       -1.371338     -1.120008      4.312398
H       -2.659170     -3.073006      3.438761
H       -2.984776     -3.353977      0.985642
--
0 1
C        1.928917      0.746089      4.445948
C        1.182784      0.577143      7.141581
C        1.582970      1.793595      6.601304
C        1.524194     -0.471399      4.999997
C        1.952605      1.876804      5.265340
C        1.155925     -0.555467      6.336354
H        2.195148      0.809128      3.384645
H        1.467525     -1.360435      4.361546
H        0.834292     -1.517716      6.750897
H        0.890397      0.511740      8.195833
```

```
H        1.613905      2.690247      7.230808
H        2.287884      2.834615      4.851333
```

A.8.3.6 Methyl system

```
0 1
C        3.052386     -2.154678      2.750378
C        4.413480     -1.860999      2.864217
C        5.372304     -2.850515      2.688659
C        4.987405     -4.155566      2.405097
C        3.636631     -4.460637      2.289895
C        2.679626     -3.468751      2.452572
H        1.619991     -3.710953      2.312117
H        3.322408     -5.482969      2.050484
H        5.743997     -4.936796      2.269212
H        6.434866     -2.600401      2.786745
H        4.726598     -0.842166      3.119469
H        2.290815     -1.374797      2.864449
--
0 1
C        0.008327     -1.122860     -2.129759
C        0.413344     -2.186808     -2.923856
C        1.551073     -2.896067     -2.570706
C        2.297438     -2.557288     -1.441005
C        1.859812     -1.488598     -0.665036
C        0.716885     -0.769057     -0.995183
C        3.539032     -3.327315     -1.075139
H       -0.163648     -2.462134     -3.814076
H       -0.833990     -0.481769     -2.413873
H        0.373389      0.070898     -0.380609
H        2.426846     -1.209495      0.230392
H        1.869639     -3.737081     -3.197147
H        3.299716     -4.366922     -0.823820
H        4.251726     -3.346838     -1.907546
H        4.042315     -2.890901     -0.204814
```

A.8.4 Tabulated angular geometry SAPT2 energies

A.8.4.1 Iodine over bond system (η2)

A.8.4.1.1 Halogen···arene system

C1-I···bond	Electrostatic (kJ mol^{-1})	Exchange (kJ mol^{-1})	Induction (kJ mol^{-1})	Dispersion (kJ mol^{-1})	SAPT2 Total (kJ mol^{-1})
180	-5.27355351	8.07453743	-1.49805337	-9.05046067	-7.74753011
170	-5.66926158	8.13797663	-1.4264074	-8.9967931	-7.95448545
160	-5.87394084	8.68224812	-1.35157366	-9.0422103	-7.58547668
150	-5.86150827	9.61524843	-1.29716335	-9.18150493	-6.72492812
140	-5.62982753	10.78626891	-1.27372595	-9.41061068	-5.52789525
130	-5.19779611	12.01381602	-1.27674774	-9.72648598	-4.18721382
120	-4.60309905	13.11173784	-1.29309729	-10.1297799	-2.9142384
110	-3.90409559	13.91171961	-1.31021735	-10.63840951	-1.94100285
100	-3.19396532	14.30041041	-1.3218459	-11.32433411	-1.53973491
90	-2.6429934	14.34281953	-1.3306545	-12.39530616	-2.02613453

A.8.4.1.2 Arene···arene system

C1-H···bond	Electrostatic (kJ mol^{-1})	Exchange (kJ mol^{-1})	Induction (kJ mol^{-1})	Dispersion (kJ mol^{-1})	SAPT2 Total (kJ mol^{-1})
180	-0.76209259	0.00558103	-0.04141623	-0.73350175	-1.53142955
170	-0.7940095	0.00603043	-0.03955472	-0.71254173	-1.54007551
160	-0.82357914	0.00740397	-0.03913247	-0.72185101	-1.57715866
150	-0.85332559	0.01018848	-0.04014624	-0.76280352	-1.64608686
140	-0.88449461	0.01560776	-0.04289471	-0.84215814	-1.7539397
130	-0.91678014	0.02665673	-0.04814644	-0.97443107	-1.91270092
120	-0.94754603	0.05132283	-0.05764618	-1.18772661	-2.14159599
110	-0.97186088	0.11309668	-0.0754584	-1.53715289	-2.47137549
100	-0.99122365	0.28521559	-0.11197954	-2.13577444	-2.95376204
90	-1.06635015	0.8050975	-0.19587169	-3.22483858	-3.68196291

A.8.4.1.3 Corrected halogen···arene system

C1-I···bond	Electrostatic (kJ mol^{-1})	Exchange (kJ mol^{-1})	Induction (kJ mol^{-1})	Dispersion (kJ mol^{-1})	SAPT2 Total (kJ mol^{-1})
180	-4.51146092	8.0689564	-1.45663714	-8.31695892	-6.21610056
170	-4.87525208	8.1319462	-1.38685268	-8.28425137	-6.41440994
160	-5.0503617	8.67484415	-1.31244119	-8.32035929	-6.00831802
150	-5.00818268	9.60505995	-1.25701711	-8.41870141	-5.07884126
140	-4.74533292	10.77066115	-1.23083124	-8.56845254	-3.77395555
130	-4.28101597	11.98715929	-1.2286013	-8.75205491	-2.2745129
120	-3.65555302	13.06041501	-1.23545111	-8.94205329	-0.77264241
110	-2.93223471	13.79862293	-1.23475895	-9.10125662	0.53037264
100	-2.20274167	14.01519482	-1.20986636	-9.18855967	1.41402713
90	-1.57664325	13.53772203	-1.13478281	-9.17046758	1.65582838

A.8.4.2 Bromine over bond system (η2)

A.8.4.2.1 Halogen···arene system

C1-Br···bond	Electrostatic (kJ mol^{-1})	Exchange (kJ mol^{-1})	Induction (kJ mol^{-1})	Dispersion (kJ mol^{-1})	SAPT2 Total (kJ mol^{-1})
180	-2.18844372	4.42214624	-0.80800641	-6.35458152	-4.92888542
170	-2.51716635	4.49829521	-0.78292821	-6.31729577	-5.11909511
160	-2.64229061	4.82819204	-0.75771974	-6.33564803	-4.90746633
150	-2.54914918	5.35350589	-0.74473807	-6.41006408	-4.35044544
140	-2.24162575	5.98450673	-0.75063506	-6.54493342	-3.5526875
130	-1.7460354	6.61796997	-0.7731495	-6.74846491	-2.64967983
120	-1.11871313	7.15280885	-0.80284013	-7.03749075	-1.80623516
110	-0.454072	7.50858913	-0.82824495	-7.45356608	-1.2272939
100	0.11498134	7.66569613	-0.84231865	-8.09925403	-1.1608952
90	0.40121751	7.78785693	-0.85176057	-9.21311225	-1.87579838

A.8.4.2.2 Arene···arene system

C1-H···bond	Electrostatic (kJ mol^{-1})	Exchange (kJ mol^{-1})	Induction (kJ mol^{-1})	Dispersion (kJ mol^{-1})	SAPT2 Total (kJ mol^{-1})
180	-0.80630921	0.01539818	-0.05178895	-0.88986643	-1.73256641
170	-0.85648034	0.01649869	-0.04965719	-0.86879186	-1.75843069
160	-0.89916393	0.01953495	-0.04915374	-0.88199833	-1.81078105
150	-0.93778648	0.02543504	-0.05029198	-0.93147179	-1.89411521
140	-0.97412551	0.03637882	-0.05346428	-1.02528818	-2.01649915
130	-1.00812255	0.05743028	-0.05969623	-1.18042433	-2.19081283
120	-1.0375308	0.10127651	-0.07131583	-1.42941548	-2.4369856
110	-1.05967314	0.20186086	-0.0937263	-1.8349876	-2.78652619
100	-1.0852066	0.45467703	-0.14006693	-2.5215944	-3.29219088
90	-1.19930433	1.13557269	-0.24323775	-3.7419452	-4.04891458

A.8.4.2.3 Corrected halogen···arene system

C1-Br···bond	Electrostatic (kJ mol^{-1})	Exchange (kJ mol^{-1})	Induction (kJ mol^{-1})	Dispersion (kJ mol^{-1})	SAPT2 Total (kJ mol^{-1})
180	-1.38213451	4.40674806	-0.75621746	-5.46471509	-3.19631901
170	-1.66068601	4.48179652	-0.73327102	-5.44850391	-3.36066442
160	-1.74312668	4.80865709	-0.708566	-5.4536497	-3.09668528
150	-1.6113627	5.32807085	-0.69444609	-5.47859229	-2.45633023
140	-1.26750024	5.94812791	-0.69717078	-5.51964524	-1.53618835
130	-0.73791285	6.56053969	-0.71345327	-5.56804058	-0.458867
120	-0.08118233	7.05153234	-0.7315243	-5.60807527	0.63075044
110	0.60560114	7.30672827	-0.73451865	-5.61857848	1.55923229
100	1.20018794	7.2110191	-0.70225172	-5.57765963	2.13129568
90	1.60052184	6.65228424	-0.60852282	-5.47116705	2.1731162

A.8.4.3 Chlorine over bond system (η2)

A.8.4.3.1 Halogen···arene system

C1-Cl···bond	Electrostatic (kJ mol^{-1})	Exchange (kJ mol^{-1})	Induction (kJ mol^{-1})	Dispersion (kJ mol^{-1})	SAPT2 Total (kJ mol^{-1})
180	-2.71491984	5.28133528	-0.81485345	-6.13192674	-4.38036475
170	-3.06009179	5.36273476	-0.8056701	-6.08954109	-4.59256822
160	-3.07512852	5.68721687	-0.79880954	-6.09139901	-4.27812021
150	-2.81729269	6.19885976	-0.8003843	-6.14083022	-3.55964744
140	-2.37683743	6.80905787	-0.81354123	-6.25012434	-2.63144513
130	-1.83631176	7.41423962	-0.83531316	-6.44183801	-1.69922331
120	-1.27859482	7.91613621	-0.85784842	-6.75724329	-0.97755032
110	-0.79667031	8.25754406	-0.87348431	-7.27923284	-0.6918434
100	-0.51921393	8.51851113	-0.88365737	-8.18185109	-1.06621125
90	-0.74271075	9.20012387	-0.92067067	-9.83054439	-2.29380194

A.8.4.3.2 Arene···arene system

C1-H···bond	Electrostatic (kJ mol^{-1})	Exchange (kJ mol^{-1})	Induction (kJ mol^{-1})	Dispersion (kJ mol^{-1})	SAPT2 Total (kJ mol^{-1})
180	-0.94046115	0.05494369	-0.08344709	-1.27002187	-2.23898642
170	-1.00822917	0.0579758	-0.08056629	-1.24154501	-2.27236468
160	-1.06404172	0.06679789	-0.08005095	-1.26118625	-2.33848103
150	-1.11213418	0.08376054	-0.08193797	-1.33219294	-2.44250454
140	-1.15449015	0.11448493	-0.08693051	-1.46698345	-2.59391918
130	-1.19114044	0.17199769	-0.09686471	-1.69174311	-2.80775057
120	-1.22253001	0.28793494	-0.11605036	-2.05700441	-3.10764983
110	-1.26158378	0.5438476	-0.15469792	-2.65979455	-3.53222865
100	-1.37938663	1.15977435	-0.23765304	-3.68824481	-4.14551012
90	-1.85579494	2.76432212	-0.42794701	-5.51212461	-5.03154444

A.8.4.3.3 Corrected halogen···arene system

C1-Cl···bond	Electrostatic (kJ mol^{-1})	Exchange (kJ mol^{-1})	Induction (kJ mol^{-1})	Dispersion (kJ mol^{-1})	SAPT2 Total (kJ mol^{-1})
180	-1.77445869	5.22639159	-0.73140636	-4.86190487	-2.14137833
170	-2.05186262	5.30475896	-0.72510381	-4.84799608	-2.32020354
160	-2.0110868	5.62041898	-0.71875859	-4.83021276	-1.93963918
150	-1.70515851	6.11509922	-0.71844633	-4.80863728	-1.1171429
140	-1.22234728	6.69457294	-0.72661072	-4.78314089	-0.03752595
130	-0.64517132	7.24224193	-0.73844845	-4.7500949	1.10852726
120	-0.05606481	7.62820127	-0.74179806	-4.70023888	2.13009951
110	0.46491347	7.71369646	-0.71878639	-4.61943829	2.84038525
100	0.8601727	7.35873678	-0.64600433	-4.49360628	3.07929887
90	1.11308419	6.43580175	-0.49272366	-4.31841978	2.7377425

A.8.4.4 Iodine over atom system (η1)

A.8.4.4.1 Halogen···arene system

C1-I···atom	Electrostatic (kJ mol^{-1})	Exchange (kJ mol^{-1})	Induction (kJ mol^{-1})	Dispersion (kJ mol^{-1})	SAPT2 Total (kJ mol^{-1})
180	-4.35173135	6.34215037	-1.25518209	-7.68581981	-6.95058289
170	-4.86961028	6.38544309	-1.21618652	-7.64080933	-7.34116304
160	-5.18747621	6.86098767	-1.15977791	-7.67799669	-7.16426315
150	-5.26501875	7.68865657	-1.10647237	-7.79119667	-6.47403123
140	-5.09131251	8.73342574	-1.07176647	-7.97544336	-5.4050966
130	-4.68388408	9.83128507	-1.06050577	-8.22794333	-4.14104812
120	-4.0859256	10.81455823	-1.06759099	-8.54990437	-2.88886274
110	-3.36351244	11.53233178	-1.08312131	-8.95481671	-1.86911869
100	-2.60936449	11.87409921	-1.09784139	-9.49131658	-1.32442324
90	-1.96914494	11.83731156	-1.10718834	-10.29587932	-1.53490104

A.8.4.4.2 Arene···arene system

C1-H···atom	Electrostatic (kJ mol^{-1})	Exchange (kJ mol^{-1})	Induction (kJ mol^{-1})	Dispersion (kJ mol^{-1})	SAPT2 Total (kJ mol^{-1})
180	-0.67073463	0.00513694	-0.03374792	-0.65749357	-1.35683918
170	-0.71302727	0.00542263	-0.03177868	-0.63727	-1.37665333
160	-0.75194456	0.00641537	-0.03098328	-0.64308294	-1.41959541
150	-0.79118075	0.00847118	-0.03132983	-0.67573061	-1.48977
140	-0.83350278	0.01245899	-0.03303773	-0.74036542	-1.59444694
130	-0.88092438	0.02045291	-0.03671747	-0.8482094	-1.74539834
120	-0.93464338	0.03780506	-0.04376231	-1.02072932	-1.96132995
110	-0.99555248	0.07969942	-0.05739828	-1.29892595	-2.27217729
100	-1.06992158	0.19174896	-0.08545727	-1.76376739	-2.72739727
90	-1.19879925	0.51475421	-0.14780963	-2.58101033	-3.41286499

A.8.4.4.3 Corrected halogen···arene system

C1-I···atom	Electrostatic (kJ mol^{-1})	Exchange (kJ mol^{-1})	Induction (kJ mol^{-1})	Dispersion (kJ mol^{-1})	SAPT2 Total (kJ mol^{-1})
180	-3.68099672	6.33701343	-1.22143417	-7.02832624	-5.59374371
170	-4.15658301	6.38002046	-1.18440784	-7.00353933	-5.96450971
160	-4.43553165	6.8545723	-1.12879463	-7.03491375	-5.74466774
150	-4.473838	7.68018539	-1.07514254	-7.11546606	-4.98426123
140	-4.25780973	8.72096675	-1.03872874	-7.23507794	-3.81064966
130	-3.8029597	9.81083216	-1.0237883	-7.37973393	-2.39564978
120	-3.15128222	10.77675317	-1.02382868	-7.52917505	-0.92753279
110	-2.36795996	11.45263236	-1.02572303	-7.65589076	0.4030586
100	-1.53944291	11.68235025	-1.01238412	-7.72754919	1.40297403
90	-0.77034569	11.32255735	-0.95937871	-7.71486899	1.87796395

A.8.4.5 Iodine over centroid system (η6)

A.8.4.5.1 Halogen···arene system

C1-I···atom	Electrostatic (kJ mol^{-1})	Exchange (kJ mol^{-1})	Induction (kJ mol^{-1})	Dispersion (kJ mol^{-1})	SAPT2 Total (kJ mol^{-1})
180	-5.18308596	7.47001339	-1.2504435	-9.0304233	-7.99393938
170	-5.07391000	7.65547431	-1.2664512	-9.08209966	-7.76698655
160	-4.75990267	8.18654503	-1.30614935	-9.23824038	-7.11774738
150	-4.2793358	8.98177092	-1.34960321	-9.50007377	-6.14724186
140	-3.68354722	9.91904112	-1.37618731	-9.86866844	-5.00936184
130	-3.03117821	10.85305103	-1.37618496	-10.35241124	-3.90672338
120	-2.38968119	11.64363337	-1.35568339	-10.99327096	-3.09500217
110	-1.85077929	12.23461883	-1.33377537	-11.9294686	-2.87940443
100	-1.61165258	12.91819521	-1.34571109	-13.53241754	-3.571586
90	-2.42091234	15.30467811	-1.50649188	-16.69477535	-5.31750146

A.8.4.5.2 Arene···arene system

C1-H···atom	Electrostatic (kJ mol^{-1})	Exchange (kJ mol^{-1})	Induction (kJ mol^{-1})	Dispersion (kJ mol^{-1})	SAPT2 Total (kJ mol^{-1})
180	-0.86324266	0.00459432	-0.04612922	-0.75777325	-1.66255081
170	-0.86300179	0.00508694	-0.04694309	-0.77479453	-1.67965246
160	-0.86118578	0.0068497	-0.04957539	-0.82881407	-1.73272554
150	-0.85482523	0.01101223	-0.05458951	-0.92971167	-1.04884698
140	-0.83736491	0.02101037	-0.06325119	-1.09813671	-1.97774244
130	-0.79619679	0.0479718	-0.07834281	-1.3748402	-2.201408
120	-0.71217164	0.13033261	-0.10655463	-1.8429907	-2.53138436
110	-0.57953517	0.40271713	-0.16635532	-2.68221614	-3.02538951
100	-0.52866923	1.34202019	-0.31308221	-4.29329995	-3.7930312
90	-1.36920520	4.72086094	-0.718514	-7.57097036	-4.93782863

A.8.4.5.3 Corrected halogen···arene system

C1-I···atom	Electrostatic (kJ mol^{-1})	Exchange (kJ mol^{-1})	Induction (kJ mol^{-1})	Dispersion (kJ mol^{-1})	SAPT2 Total (kJ mol^{-1})
180	-4.31984330	7.46541907	-1.20431428	-8.27265005	-6.33138857
170	-4.21090821	7.65038737	-1.21950811	-8.30730513	-6.08733409
160	-3.89871689	8.17969533	-1.25657396	-8.40942631	-5.38502184
150	-3.42451057	8.97075869	-1.2950137	-8.5703621	-5.09839488
140	-2.84618231	9.89803075	-1.31293612	-8.77053173	-3.0316194
130	-2.23498142	10.80507923	-1.29784215	-8.97757104	-1.70531538
120	-1.67750955	11.51330076	-1.24912876	-9.15028026	-0.56361781
110	-1.27124412	11.8319017	-1.16742005	-9.24725246	0.14598508
100	-1.08298335	11.57617502	-1.03262888	-9.23911759	0.2214452
90	-1.05170714	10.58381717	-0.78797788	-9.12380499	-0.37967283

A.9 Multiple linear regression analysis

Values for ΔG_{Eqn} were obtained from equation S1. Coefficients a, b and c were determined by fitting experimental ΔG values measured from balance series 1 to equation 2.4 using the solver plugin for Microsoft Excel. In equation A1, ced refers to cohesive energy density and P refers to bulk polarizability with values for both being obtained from literature

$$\Delta G_{\mathrm{Eqn}} = \mathrm{a}(ced) + \mathrm{b}(P) + \mathrm{c} \qquad \text{(Equation 2.4)}$$

A.9.1 Free energies calculated from multiple linear regression analysis

Solvent	ced / cal cm^{-3}	P	ΔG_{EqnI} /kJ mol^{-1}	$\Delta G_{\mathrm{EqnBr}}$ /kJ mol^{-1}	$\Delta G_{\mathrm{EqnCl}}$ /kJ mol^{-1}	ΔG_{EqnF} /kJ mol^{-1}	ΔG_{EqnH} /kJ mol^{-1}	$\Delta G_{\mathrm{EqnMe}}$ /kJ mol^{-1}
CCl_4	73.6	0.274	-1.2	-1.3	-1.5	-1.5	-1.4	-2.0
C_6D_6	83.7	0.296	-1.2	-1.3	-1.5	-1.5	-1.3	-1.9

$CDCl_3$	85.4	0.267	-1.3	-1.4	-1.6	-1.5	-1.5	-2.2
CD_2Cl_2	93.7	0.257	-1.4	-1.5	-1.7	-1.6	-1.6	-2.3
C_5D_5N	112.4	0.300	-1.4	-1.5	-1.7	-1.6	-1.4	-2.0
DMSO-d_6	168.6	0.285	-1.8	-1.9	-2.1	-2.0	-1.7	-2.5
CS_2	100.0	0.356	-1.0	-1.2	-1.4	-1.5	-1.0	-1.5
THF-d_8	86.9	0.248	-1.4	-1.5	-1.7	-1.6	-1.6	-2.3
9% v/v D_2O / THF	128.6	0.245	-1.7	-1.8	-2.0	-1.8	-1.8	-2.6
15% v/v D_2O / THF	156.4	0.244	-1.9	-2.0	-2.1	-2.0	-1.9	-2.7
20% v/v D_2O / THF	179.6	0.243	-2.0	-2.1	-2.3	-2.1	-2.0	-2.9
25% v/v D_2O / THF	202.7	0.241	-2.1	-2.3	-2.4	-2.2	-2.1	-3.0
35% v/v D_2O / THF	249.1	0.238	-2.4	-2.6	-2.7	-2.5	-2.3	-3.3
40% v/v D_2O / THF	272.2	0.236	-2.6	-2.8	-2.9	-2.6	-2.4	-3.4
9% v/v CD_3OD / THF	97.9	0.244	-1.5	-1.6	-1.8	-1.6	-1.7	-2.4
15% v/v CD_3OD / THF	105.2	0.241	-1.6	-1.7	-1.8	-1.7	-1.8	-2.5
20% v/v CD_3OD / THF	111.3	0.239	-1.6	-1.7	-1.9	-1.7	-1.8	-2.5
25% v/v CD_3OD / THF	117.4	0.237	-1.7	-1.8	-1.9	-1.8	-1.8	-2.6
35% v/v CD_3OD / THF	129.6	0.232	-1.8	-1.8	-2.0	-1.8	-1.9	-2.7
40% v/v CD_3OD / THF	135.7	0.230	-1.8	-1.9	-2.0	-1.9	-1.9	-2.7

In all cases THF refers to THF-d_8. Samples in CS_2 and CCl_4 were locked using a sealed internal standard of C_6D_6.

A.9.2 Multiple linear regression coefficients

Coefficient	Eqn I	Eqn Br	Eqn Cl	Eqn F	Eqn H	Eqn Me
ced coefficient (a)	–0.0059	–0.0064	–0.0064	–0.0054	–0.0036	–0.0053
P coefficent (b)	4.3221	3.3610	3.1608	1.4064	6.3641	8.4261
solvent-independent constant (c)	–1.9928	–1.9778	–1.9078	–1.4533	–2.9043	–3.9620

A.10 Plots of ΔG_{Eqn} against ΔG_{Exp}

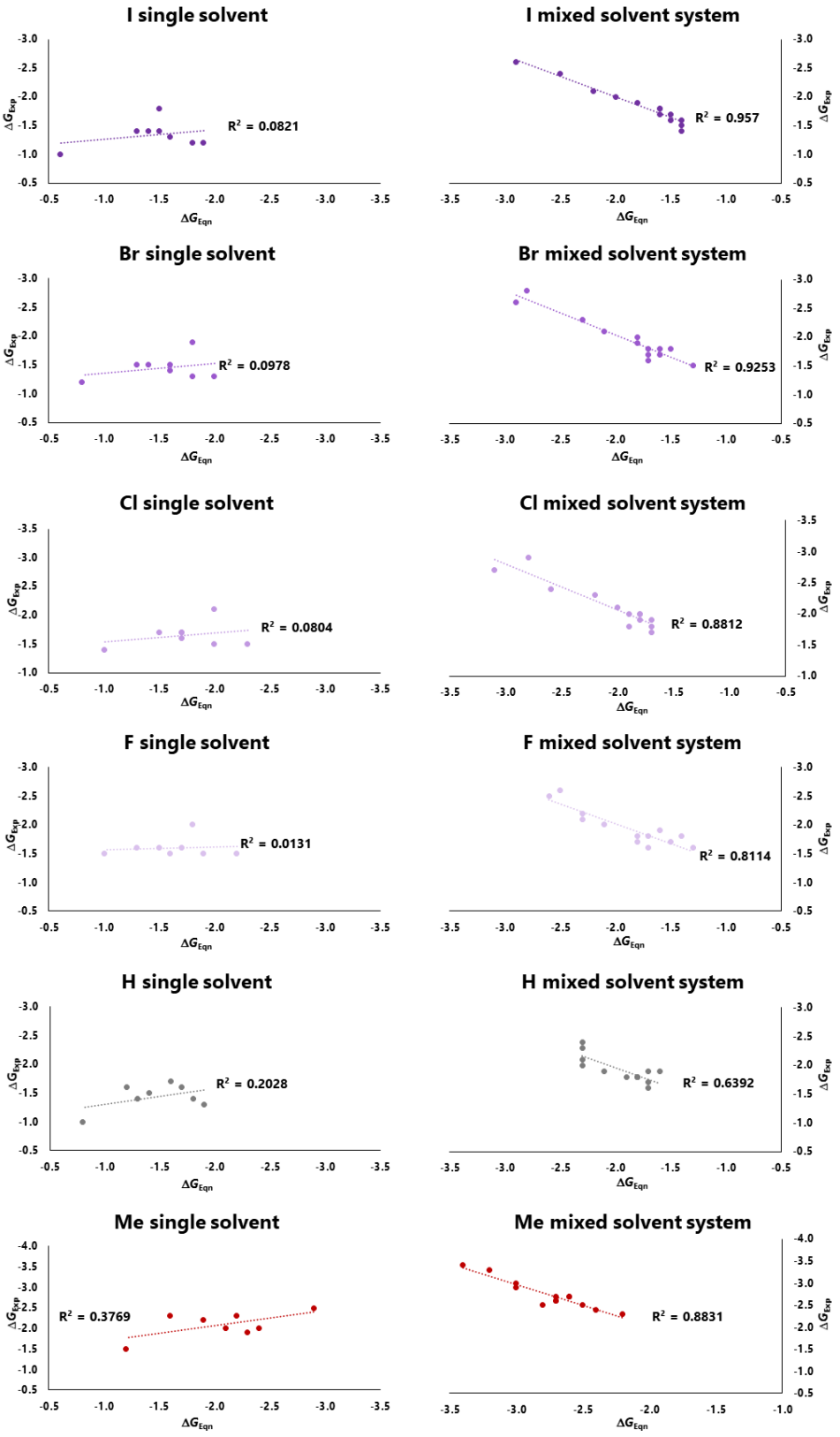

A.11 General experimental practices

Unless stated otherwise all synthetic procedures reported were conducted used reagents purchased from commercial sources and used without additional purification.

Solvents listed as *dry* were either purchased as anhydrous or were purified using a Glass Contour brand solvent purification system. In addition, reactions requiring *dry* conditions used oven dried glassware (130-140^{o}C overnight). Nitrogen gas for inert atmospheres was provided via in house supply.

Analytical TLC was conducted on aluminium backed silica gel 60 F254 plates and visualised under UV (254 nm) light. Flash chromatography was carried out using Geduran 60 (40 – 63 µm) silica gel eluting with the specified solvents/solvent mixtures. In all cases "petroleum either" refers to 40-60^{o}C boiling point range grade.

NMR spectra were recorded using either a 500 MHz Bruker Ultrashield equipped with a prodigy cryoprobe, or a 600 MHz Bruker Ultrashield spectrometer equipped with a TCI cryoprobe. All NMR analysis was conducted using standard Pyrex tubes, ambered tubes were used for analysis of photoreactive iodine species. Chemical shifts are reported in parts per million (ppm) coupling constants are reported in Hertz. High resolution mass spectroscopy was conducted using a Bruker micrOTOF II. Dr Logan Mackay of the University of Edinburgh is thanked for this service.

A.12 Synthesis and characterisation of balance series 1

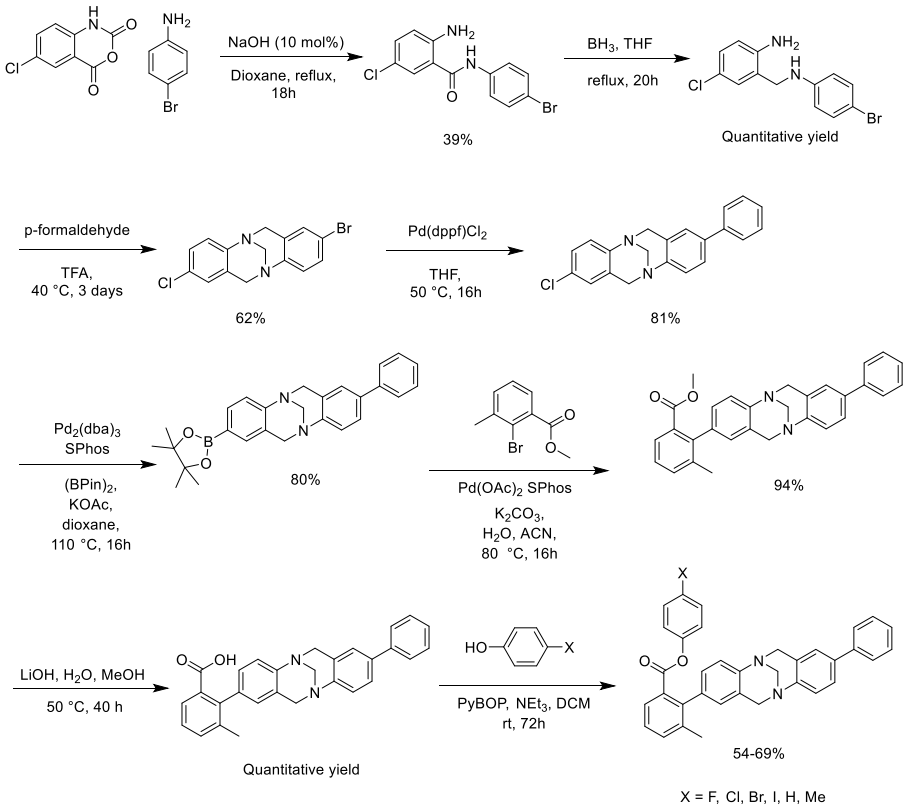

Step I. 2-Amino-*N*-(4-bromophenyl)-5-chloro-benzamide

4-Bromoaniline (1 Eq, 45.2 mmol, 7.77 g), 5-Chloroisatoic anhydride (1.1 Eq, 49.7 mmol, 9.82 g) and sodium hydroxide (0.1 Eq, 4.51 mmol, 0.18 g) were combined under an inert nitrogen atmosphere. Dioxane (anhydrous grade, 94 mL) was added and the mixture heated to reflux for 18 h. The reaction mixture was allowed to cool to room temperature, filtered and concentrated under reduced pressure. The residue was triturated from ethanol and dried under vacuum to yield 2-amino-*N*-(4-bromophenyl)-5-chloro-benzamide (5.74 g, 39%).

^{1}H NMR (500 MHz, DMSO-d_6) δ 10.19 (s, 1H), 7.71 – 7.66 (m, 3H), 7.56 – 7.49 (m, 2H), 7.24 (dd, J = 8.8, 2.5 Hz, 1H), 6.79 (d, J = 8.8 Hz, 1H), 6.47 (s, 2H).

^{13}C NMR (126 MHz, DMSO-d_6) δ 166.6, 148.7, 138.4, 132.0, 131.3, 127.8, 122.5, 118.1, 117.8, 115.6, 115.3.

HRMS (ESI) obtained m/z 346.9538, 348.9531 (M+Na+). Expected 346.9557, 348.9535.

^{1}H NMR

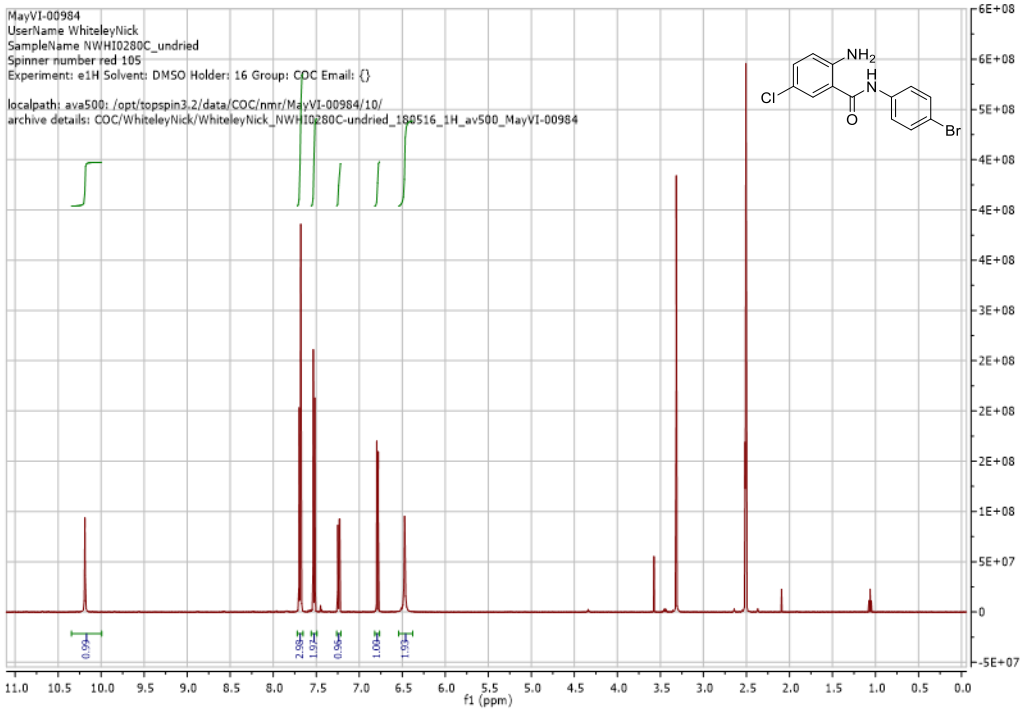

^{13}C NMR

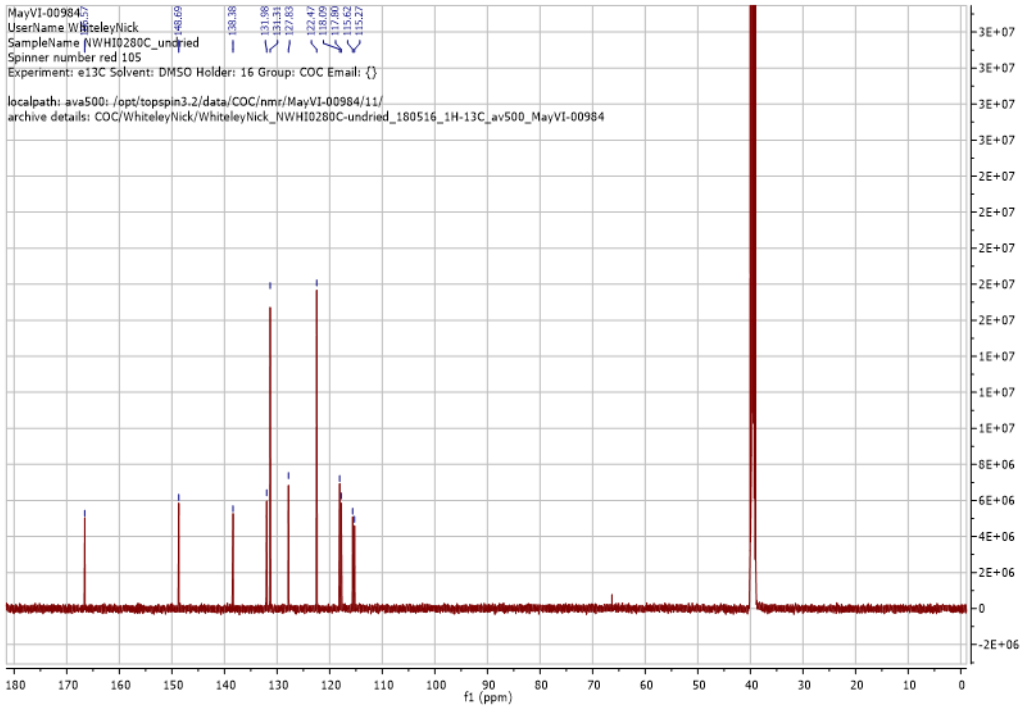

Steps II-III. 2-Bromo-8-chloro-6H,12H-5,11-methanodibenzo[b,f][1,5]diazocine

2-amino-4-bromo-*N*-(4-chlorophenyl)benzamide (1 Eq, 14.3 mmol, 4.65 g) was dissolved in THF (24 mL) and cooled to 0 °C. BH_3.THF (5.8 Eq, 1.0 M in THF, 82.9 mmol, 83 mL) was added slowly and the mixture stirred at 0 °C for 30 minutes. The reaction was then slowly heated to reflux and refluxed for 20 h. The solution was then added slowly to 1.0 M aqueous sodium hydroxide (200 mL) at 0°C. The resulting mixture was extracted with ethyl acetate (3 x 150 mL). Combined organics were washed with brine (150 mL), dried over magnesium sulfate and solvents removed under reduced pressure to yield crude (~90% pure) 2-[(4-bromoanilino)methyl]-4-chloro-aniline in quantitative yield (4.17 g).

2-[(4-bromoanilino)methyl]-4-chloro-aniline (1 Eq, 21.1 mmol, 6.59 g) and paraformaldehyde (6 Eq, 126.9 mmol, 3.81 g) were combined in TFA (350 mL) under an inert nitrogen atmosphere. The reaction was stirred at room temperature for 30 minutes and then heated to 40 °C for 24 h. The reaction mixture was added dropwise to 35% aqueous ammonia (500 mL) at 0 °C and extracted with DCM (3 x 300 mL). Combined organics dried over magnesium sulfate and solvents removed under reduced pressure. The residue was purified by flash chromatography (10-40% ethyl acetate in petroleum ether gradient) to yield 2-Bromo-8-chloro-6H,12H-5,11-methanodibenzo[b,f][1,5]diazocine (4.40 g, 62%).

^{1}H NMR (500 MHz, $CDCl_3$) δ 7.27 (dd, J = 8.6, 2.4 Hz, 1H), 7.13 (dd, J = 8.6, 2.4 Hz, 1H), 7.06 – 7.04 (m, 2H), 7.00 (d, J = 8.6 Hz, 1H), 6.90 (d, J = 2.4 Hz, 1H), 4.64 (app dd, J = 16.8, 0.8 Hz, 2H), 4.25 (app t, J = 1.2 Hz, 2H), 4.09 (app d, J = 16.8 Hz, 2H).

^{13}C NMR (126 MHz, $CDCl_3$) δ 147.0, 146.4, 130.8, 129.9, 129.8, 129.3, 129.3, 127.9, 126.9, 126.5, 116.9, 66.7, 58.6, 58.5. Two peaks appear to coalesce at 129.9 ppm.

HRMS (ESI) obtained m/z 334.9948, 336.9931 (M+H+). Expected 334.9945, 336.9923.

^{1}H NMR

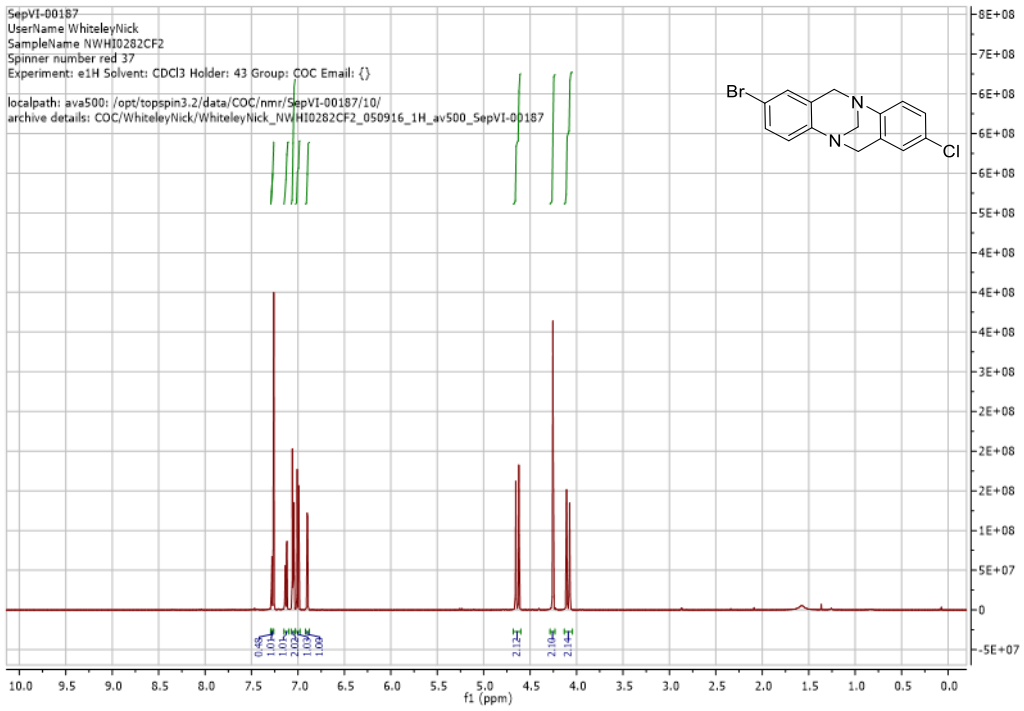

^{13}C NMR

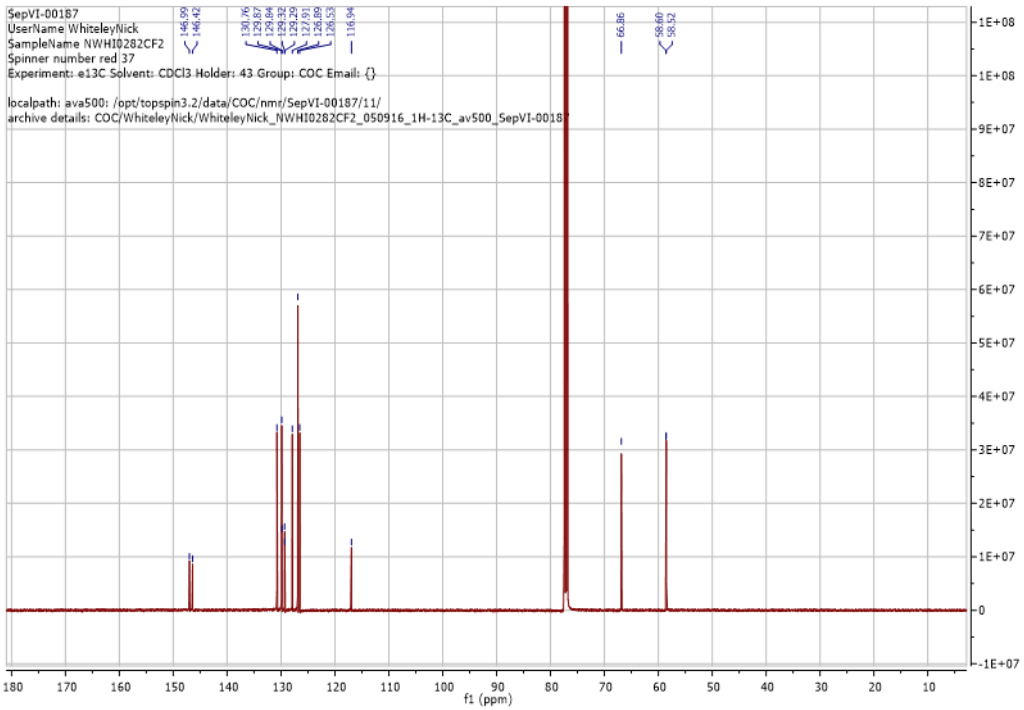

Step IV: 2-Chloro-8-phenyl-6H,12H-5,11-methanodibenzo[b,f][1,5]diazocine

2-Bromo-8-chloro-6H,12H-5,11-methanodibenzo[b,f][1,5]diazocine (1 Eq, 13.1 mmol, 4.40 g), phenylboronic acid (1.5 Eq, 20.0 mmol, 2.40 g), Pd(dppf)Cl_2.DCM (0.04 Eq, 0.524 mmol, 0.43 g), K_3PO_4 (2 Eq, 26.2 mmol, 5.56 g) and water (10 Eq, 131 mmol, 2.10 g, 2.1 mL) were combined in THF (65 mL) under an inert nitrogen atmosphere. The mixture was heated to 50 °C for 24 h. The reaction mixture was filtered through kieselguhr eluting with ethyl acetate (250 mL). Organics were washed with sodium bicarbonate (100 mL), brine (100 mL), dried over magnesium sulfate and solvents removed under reduced pressure. The residue was purified by flash chromatography (10-20%) ethyl acetate in petroleum ether gradient to yield 2-Chloro-8-phenyl-6H,12H-5,11-methanodibenzo[b,f][1,5]diazocine (3.53 g, 81%) and further crude product (0.80 g).

^{1}H NMR (500 MHz, $CDCl_3$) δ 7.50 – 7.47 (m, 2H), 7.42 – 7.36 (m, 3H), 7.32 – 7.27 (m, 1H), 7.19 (app d, J = 8.3 Hz, 1H), 7.15 – 7.11 (m, 2H), 7.09 (app d, J = 8.6 Hz, 1H), 6.93 (d, J = 1.9 Hz, 1H), 4.75 (d, J = 16.7 Hz, 1H), 4.69 (d, J = 16.7 Hz, 1H), 4.33 (app q, J = 12.9 Hz, 2H), 4.19 (app d, J = 16.7 Hz, 2H).

^{13}C NMR (126 MHz, $CDCl_3$) δ 147.3, 146.8, 140.8, 137.4, 129.7, 129.1, 128.9, 127.9, 127.8, 127.2, 127.0, 126.9, 126.6, 126.5, 125.7, 125.5, 67.1, 59.0, 58.6.

HRMS (ESI) obtained m/z 333.1145 (M+H+). Expected 333.1153.

^{1}H NMR

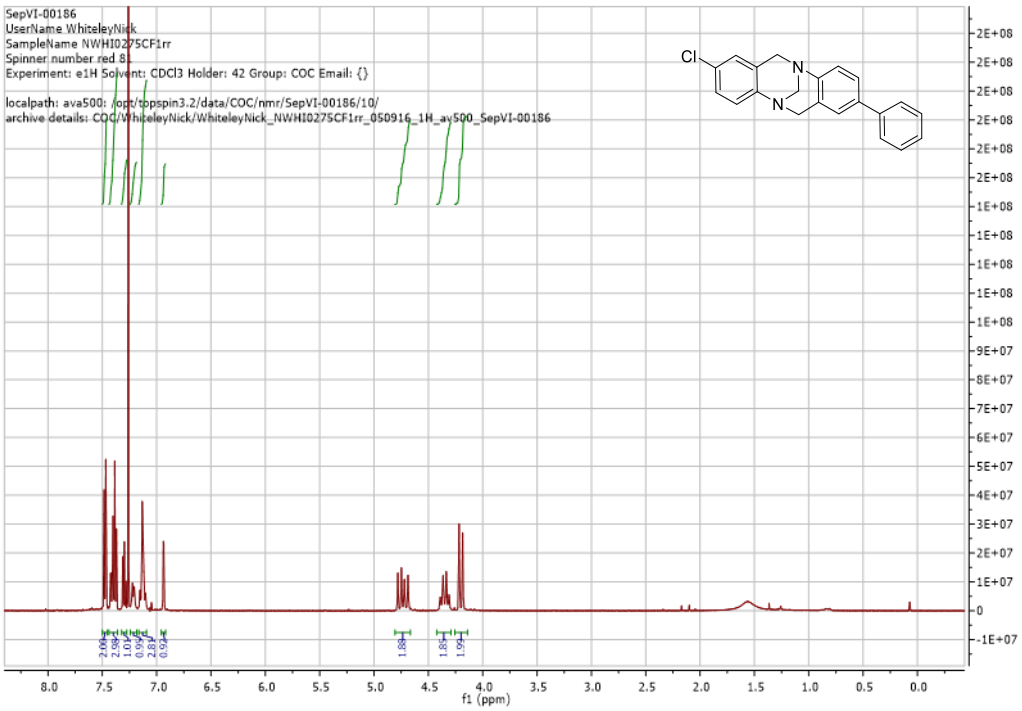

^{13}C NMR

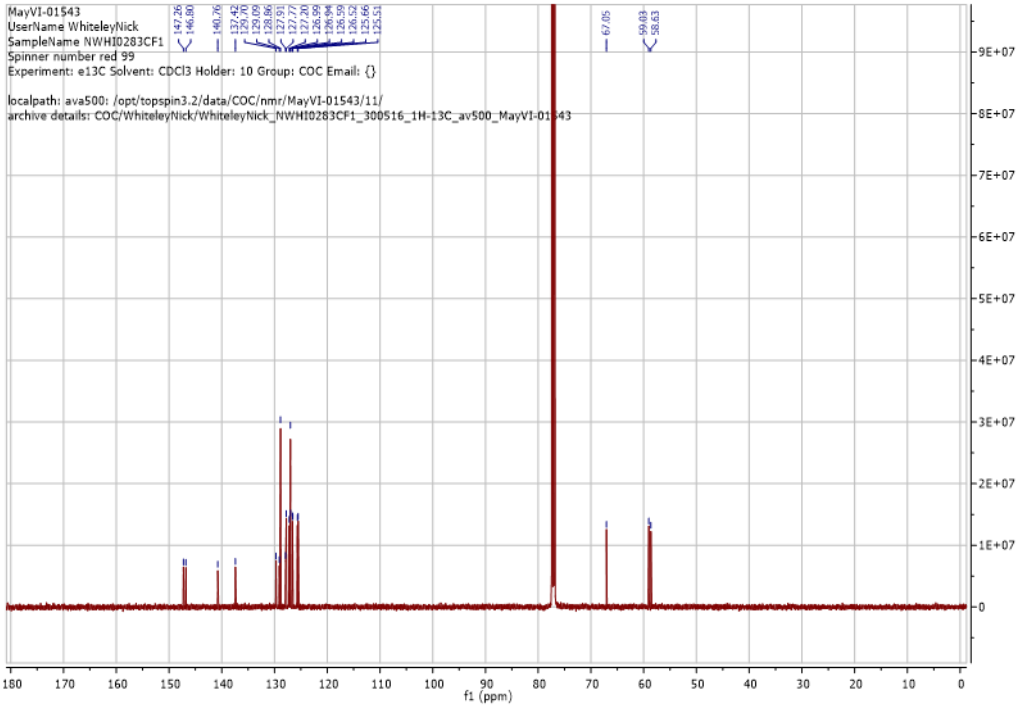

Step V. 2-(Bispinacolatodiboron)-8-phenyl-6H,12H-5,11-methanodibenzo[b,f][1,5]diazocine

2-Chloro-8-phenyl-6H,12H-5,11-methanodibenzo[b,f][1,5]diazocine (1 Eq, 10.4 mmol, 3.50 g), $(BPin)_2$ (3 Eq, 31.1 mmol, 7.90 g), $Pd_2(dba)_3$ (0.02 Eq, 0.21 mmol, 0.19 g), SPhos (0.04 Eq, 0.41 mmol, 0.17 g) and potassium acetate (3 Eq, 31.1 mmol, 3.05 g) were combined in degassed dioxane (7.3 mL) under an inert nitrogen atmosphere. The reaction was heated to reflux for 16 h. The reaction mixture was cooled and filtered through kieselguhr eluting with ethyl acetate (200 mL). Organics were washed with saturated sodium bicarbonate (150 mL), brine (50 mL) and then dried over magnesium sulfate. Solvents were removed under reduced pressure and the residue purified by flash chromatography (10-25% ethyl acetate in petroleum ether) to yield 2-(Bispinacolatodiboron)-8-phenyl-6H,12H-5,11-methanodibenzo[b,f][1,5]diazocine (3.50 g, 80%).

^{1}H NMR (500 MHz, $CDCl_3$) δ 7.62 (dd, J = 8.0, 1.1 Hz, 1H), 7.48 – 7.44 (m, 2H), 7.43 (s, 1H), 7.39 – 7.35 (m, 3H), 7.30 – 7.26 (m, 1H), 7.17 (app dd, J = 12.9, 8.2 Hz, 2H), 7.10 (d, J = 2.0 Hz, 1H), 4.80 – 4.69 (m, 2H), 4.36 (s, 2H), 4.26 (app t, J = 16.9 Hz, 2H), 1.29 (s, 12H).

^{13}C NMR (126 MHz, $CDCl_3$) δ 151.3, 147.4, 140.9, 137.2, 134.1, 133.9, 128.8, 128.1, 127.3, 127.1, 127.0, 126.4, 125.7, 125.5, 124.5, 83.8, 67.1, 59.0, 58.8, 25.0. No peak observed for boron bound carbon.

HRMS (ESI) obtained m/z 447.2197 (M+Na+). Expected 447.2219.

^{1}H NMR

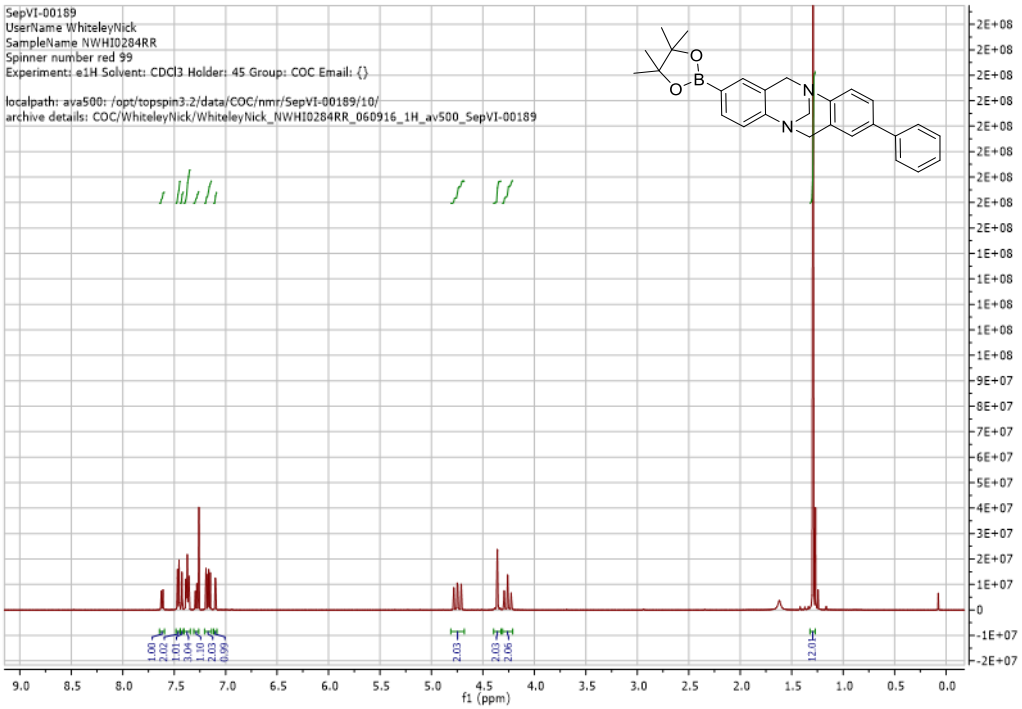

^{13}C NMR

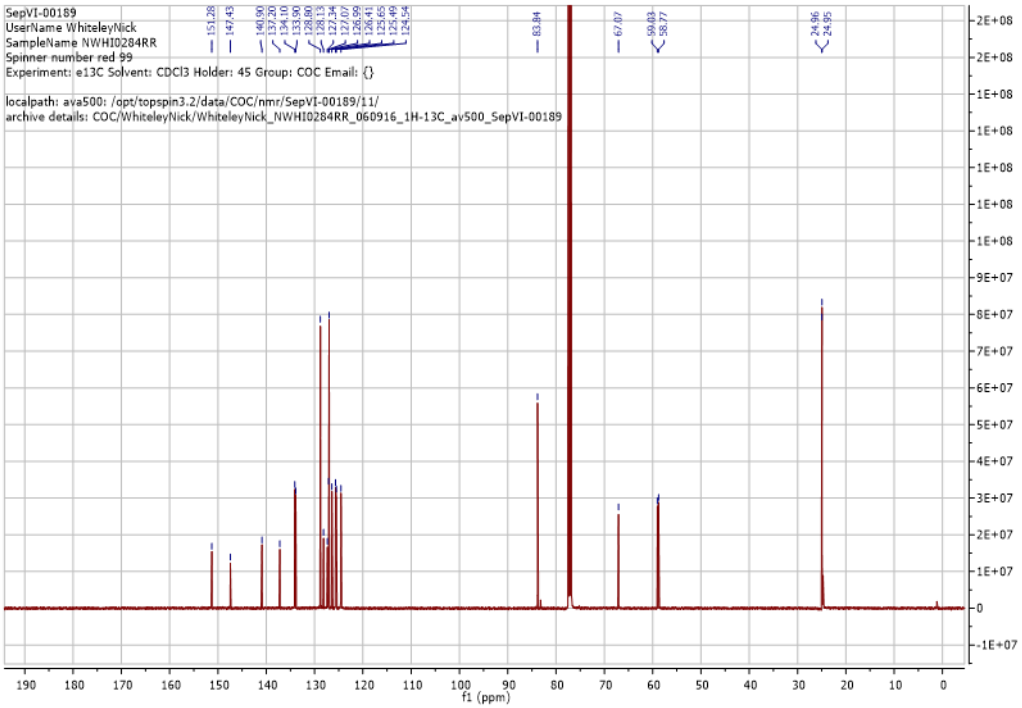

Step VI- VII. 3-methyl-2-[8-(phenyl)-6H,12H-5,11-methano dibenzo[b,f][1,5]diazocin-2-yl]benzoic acid

2-(Bispinacolatodiboron)-8-phenyl-6H,12H-5,11-methanodibenzo[b,f][1,5]diazocine (1 Eq, 8.09 mmol, 3.43 g), methyl 2-bromo-3-methyl-benzoate (1.5 Eq, 12.1 mmol, 2.78 g), $Pd(OAc)_2$ (0.02 Eq, 0.162 mmol, 0.036 g) and SPhos (0.04 Eq, 0.323 mmol, 0.13 g) were combined in acetonitrile (27 mL). Aqueous potassium carbonate solution (2 M, 2.5 Eq, 20.2 mmol, 10 mL) was added and the reaction heated to reflux under an inert nitrogen atmosphere for 16 h. The reaction mixture was diluted with ethyl acetate (250 mL), washed with saturated aqueous sodium bicarbonate (2 x 150 mL) and then brine (2 x 100 mL). Organics were dried over magnesium sulfate and solvents removed under reduced pressure. The residue was purified by flash chromatography (10-40% ethyl acetate in petroleum ether) to yield product which was further purified by trituration from methanol to yield methyl 3-methyl-2-[8-(phenyl)-6H,12H-5,11-methano dibenzo[b,f][1,5]diazocin-2-yl]benzoate (3.40 g, 94%).

Methyl 3-methyl-2-[8-(trifluoromethyl)-6H,12H-5,11-methano dibenzo[b,f][1,5]diazocin-2-yl]benzoate (1 Eq, 0.208 mmol, 1.31 g) and lithium hydroxide (17 Eq, 49.8 mmol, 2.10 g) were combined in methanol (44 mL), THF (44 mL) and water (0.4 mL) and heated to 50 °C for 40 h. Solvents were removed under reduced pressure and the residue taken up in saturated aqueous ammonium chloride (100 mL). 1 M Hydrochloric acid (17 Eq, 49.8 mmol, 48 mL) was added to neutralise and the mixture was extracted with ethyl acetate (3 x 100 mL). Organics were washed with brine (50 mL), dried over magnesium sulfate and solvents were removed under reduced pressure to give 3 methyl-2-[8-(phenyl)-6H,12H-5,11-methano dibenzo[b,f][1,5]diazocin-2-yl]benzoic acid in quantitative yield (1.30 g).

^{1}H NMR (500 MHz, $CDCl^{3}$) δ 7.64 (d, J = 7.1 Hz, 1H), 7.50 (app d, J = 7.5 Hz, 2H), 7.46 (app d, J = 6.9 Hz, 1H), 7.42 – 7.37 (m, 3H), 7.35 – 7.27 (m, 3H), 7.24 – 7.12 (m, 3H), 6.85 (s, 1H), 4.80 (app d, J = 16.8 Hz, 1H), 4.52 (app d, J = 17.0 Hz, 1H), 4.32 – 4.14 (m, 3H), 3.86 (app d, J = 12.8 Hz, 1H), 2.07 (s, 3H).

^{13}C NMR (126 MHz, $CDCl_3$) δ 172.2, 145.6, 145.1, 140.4, 139.9, 138.2, 137.8, 136.9, 134.1, 132.6, 129.1, 129.0, 127.7, 127.4, 127.4, 127.3, 127.0, 126.7, 126.6, 126.5, 125.7, 125.5, 124.4, 65.8, 58.1, 57.8, 20.9.

HRMS (ESI) obtained m/z 455.1740 (M+Na+). Expected 455.1730.

^{1}H NMR

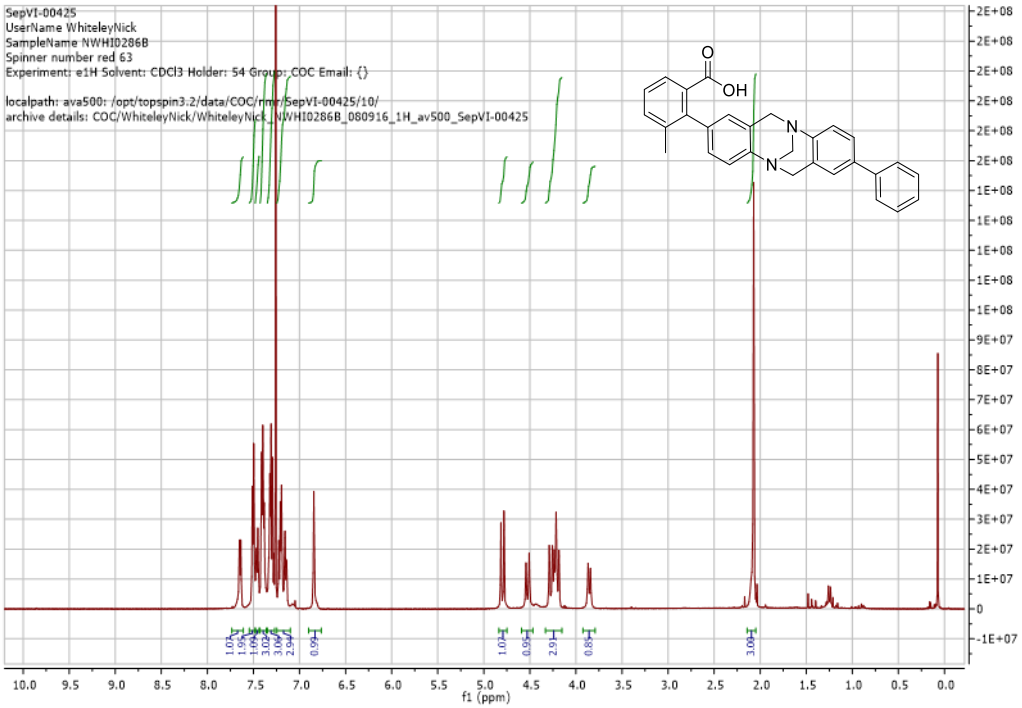

^{13}C NMR

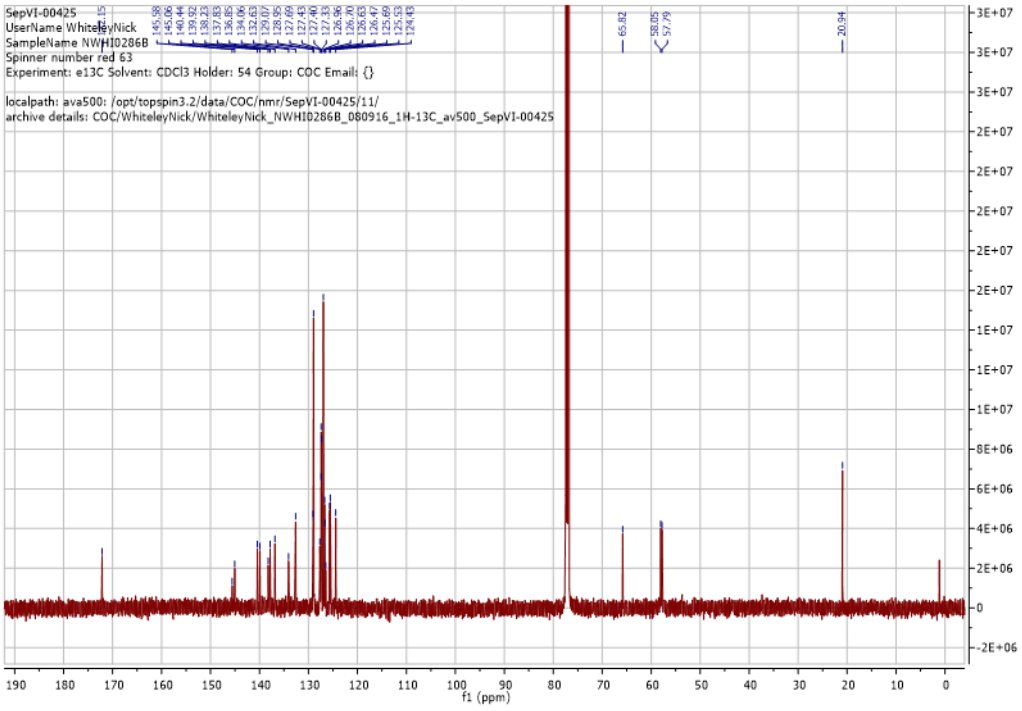

Step VIII (1F). 4-Fluorophenyl 3-methyl-2-[8-(phenyl)-6H,12H-5,11-methano dibenzo[b,f][1,5]diazocin-2-yl]benzoate

3 Methyl-2-[8-(phenyl)-6H,12H-5,11-methano dibenzo[b,f][1,5]diazocin-2-yl]benzoic acid (1 Eq, 0.462 mmol, 0.20 g), 4-fluorophenol (3 Eq, 1.39 mmol, 0.16 g) and PyBOP (2 Eq, 0.924 mmol, 0.48 g) were combined in DCM (11 mL). Triethylamine (8 Eq, 3.70 mmol, 0.37 g, 0.515 mL) was added and the stirred at room temperature for 48 h. Further DCM was added (50 mL) and the solution washed with saturated aqueous sodium bicarbonate (40 mL). Organics were dried over magnesium sulfate and solvents removed under reduced pressure. The residue was purified by flash chromatography (20-40% ether in hexane) to yield 4-fluorophenyl 3-methyl-2-[8-(phenyl)-6H,12H-5,11-methano dibenzo[b,f][1,5]diazocin-2-yl]benzoate (0.14 mg, 55%).

^{1}H NMR (600 MHz, $CDCl_3$) δ 7.74 (d, J = 7.5 Hz, 0.3H, minor conformer), 7.65 (d, J = 7.6 Hz, 0.6H, major conformer), 7.57 – 7.51 (m, 2H), 7.49 – 7.38 (m, 4H), 7.34 (app. t, J = 7.5 Hz, 1.6H), 7.30 (app. t, J = 7.4 Hz, 0.4H), 7.24 – 7.19 (m, 3H), 7.12 (app. dd, J = 8.2, 1.5 Hz, 0.6H, major conformer), 7.09 (app. d, J = 8.2 Hz, 0.4H, minor conformer), 6.99 (app. t, J = 8.5 Hz, 0.7H, minor conformer), 6.84 (app. d, J = 0.8 Hz, 0.7H, major conformer), 6.80 (app. s, 0.3H, minor conformer), 6.74 – 6.71 (m, 0.6H, minor conformer), 6.41 (app. t, J = 8.6 Hz, 1.3H, major conformer), 6.08 – 6.04 (m, 1.2H, major conformer), 4.86 – 4.76 (m, 1.7H), 4.69 (d, J = 16.8 Hz, 0.4H, minor conformer), 4.42 – 4.18 (m, 4H), 2.16 (s, 2H, major conformer), 2.09 (s, 1H, minor conformer).

^{13}C NMR (126 MHz, $CDCl_3$) δ 168.2, 167.6, 160.3 (d, J = 244.4 Hz), 159.9 (d, J = 244.4 Hz), 147.7, 147.6, 147.4, 146.6 (d, J = 2.5 Hz), 146.0 (d, J = 2.6 Hz), 141.2, 140.7, 140.5, 137.7, 137.5 , 137.1, 136.2, 135.9, 133.7, 133.5, 131.9, 131.8, 129.0, 128.9, 128.6, 128.3, 128.3, 128.1, 127.7, 127.5, 127.3, 127.3, 127.2, 127.1, 127.1, 126.9, 126.5, 126.3, 125.9, 125.7, 125.6, 125.5, 125.0, 122.8 (d, J = 8.4 Hz), 122.2 (d, J = 8.5 Hz), 116.0 (d, J = 23.8 Hz), 115.8 (d, J = 23.7 Hz), 67.1, 67.0, 58.8, 58.7, 58.6, 58.5, 21.0, 20.9. Two conformers. Some aryl conformer peaks occluded.

^{19}F NMR (376 MHz, 1H decoupled, $CDCl_3$) δ -116.80 (s, 0.7F), -117.08 (s, 0.3F).

HRMS (ESI) obtained m/z 549.1935 (M+Na+). Expected 549.1949.

^{1}H NMR

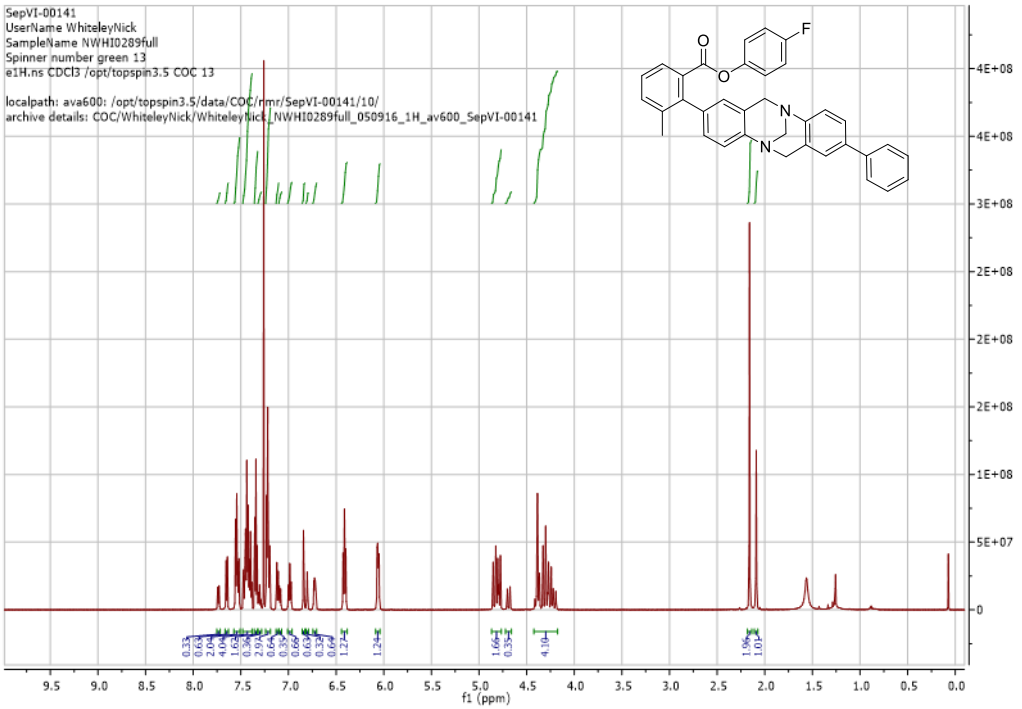

^{13}C NMR

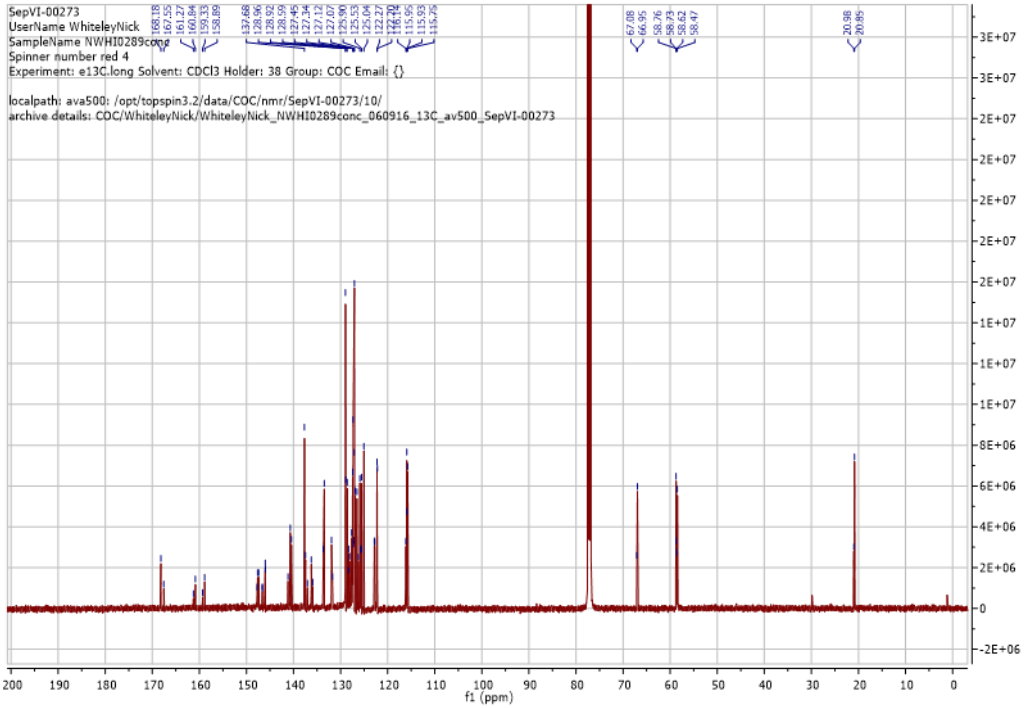

Step VIII (1Cl). 4-Chlorophenyl 3-methyl-2-[8-(phenyl)-6H,12H-5,11-methano dibenzo[b,f][1,5]diazocin-2-yl]benzoate

3 Methyl-2-[8-(phenyl)-6H,12H-5,11-methano dibenzo[b,f][1,5]diazocin-2-yl]benzoic acid (1 Eq, 0.391 mmol, 0.17 g), 4-chlorophenol (3 Eq, 1.17 mmol, 0.15 g) and PyBOP (2 Eq, 0.781 mmol, 0.41 g) were combined in DCM (11 mL). Triethylamine (8 Eq, 3.70 mmol, 0.37 mg, 0.515 mL) was added and the reaction stirred at room temperature for 48 h. Further DCM was added (50 mL) and the solution washed with saturated aqueous sodium bicarbonate 40 mL). Organics were dried over magnesium sulfate and solvents removed under reduced pressure. The residue was purified by flash chromatography (20-50% ether in hexane) to yield 4-chlorophenyl 3-methyl-2-[8-(phenyl)-6H,12H-5,11-methano dibenzo[b,f][1,5]diazocin-2-yl]benzoate (0.13 mg, 59%).

^{1}H NMR (500 MHz, $CDCl_3$) δ 7.76 (d, J = 7.5 Hz, 0.3H, minor conformer), 7.68 (d, J = 7.6 Hz, 0.7H, major conformer), 7.61 (app d, J = 7.6 Hz, 1.4H, major confomer), 7.55 (app d, J = 7.6 Hz, 1.4H, major conformer), 7.52 (dd, J = 8.3, 1.7 Hz, 0.7H), 7.48 – 7.40 (m, 3.5H), 7.39 – 7.30 (m, 2.5H), 7.27 – 7.20 (m, 2.4H), 7.15 – 7.09 (m, 1H), 6.84 (app d, J = 21.3 Hz, 1H), 6.73 (d, J = 8.7 Hz, 2H), 6.07 (app d, J = 8.7 Hz, 1.3H), 4.89 – 4.77 (m, 1.7H), 4.70 (app d, J = 16.8 Hz, 0.3H), 4.45 – 4.20 (m, 4H), 2.19 (s, 2H), 2.12 (s, 1H).

^{13}C NMR (126 MHz, $CDCl_3$) δ 168.2, 167.5, 149.5, 148.9, 147.9, 147.7, 141.5, 141.0, 140.5, 138.0, 137.6, 137.3, 136.4, 136.1, 134.0, 133.8, 132.0, 131.9, 131.5, 131.3, 129.7, 129.5, 129.3, 129.2, 128.8, 128.6, 128.5, 128.3, 128.0, 127.9, 127.7, 127.6, 127.5, 127.3, 127.1, 126.7, 126.5, 126.1, 126.0, 125.9, 125.6, 125.3, 123.0, 122.5, 67.3, 67.2, 59.0, 58.9, 58.8, 21.2, 21.1. Two conformers, some aromatic and one Tröger's base bridgehead conformer peaks occluded.

HRMS (ESI) obtained m/z 543.1819 (M+H+). Expected 543.1834.

^{1}H NMR

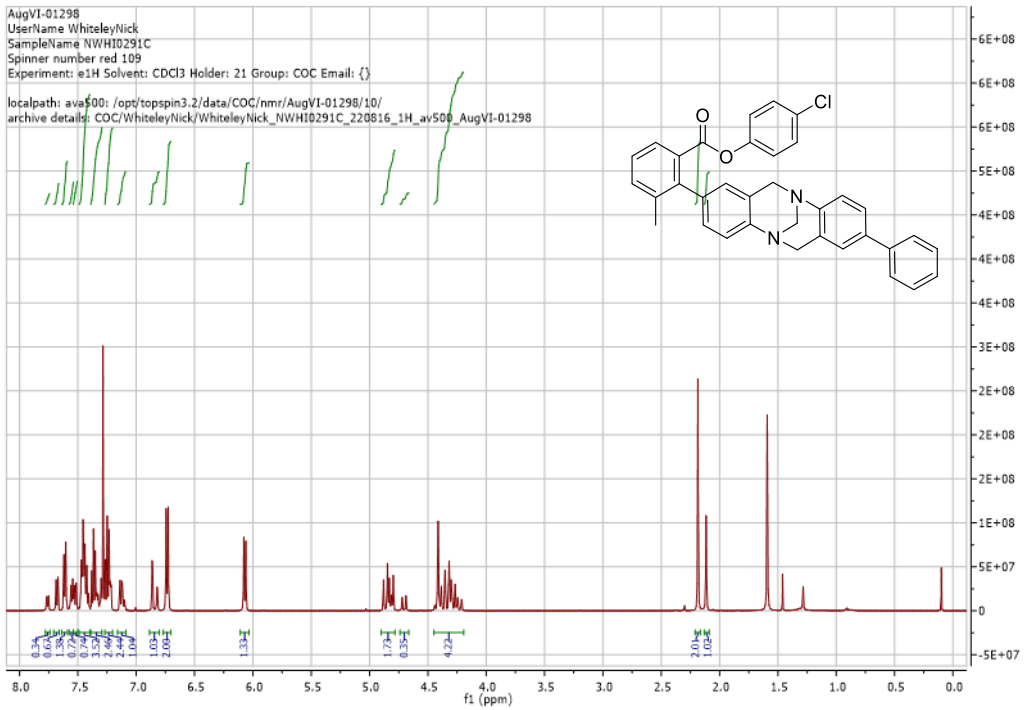

^{13}C NMR

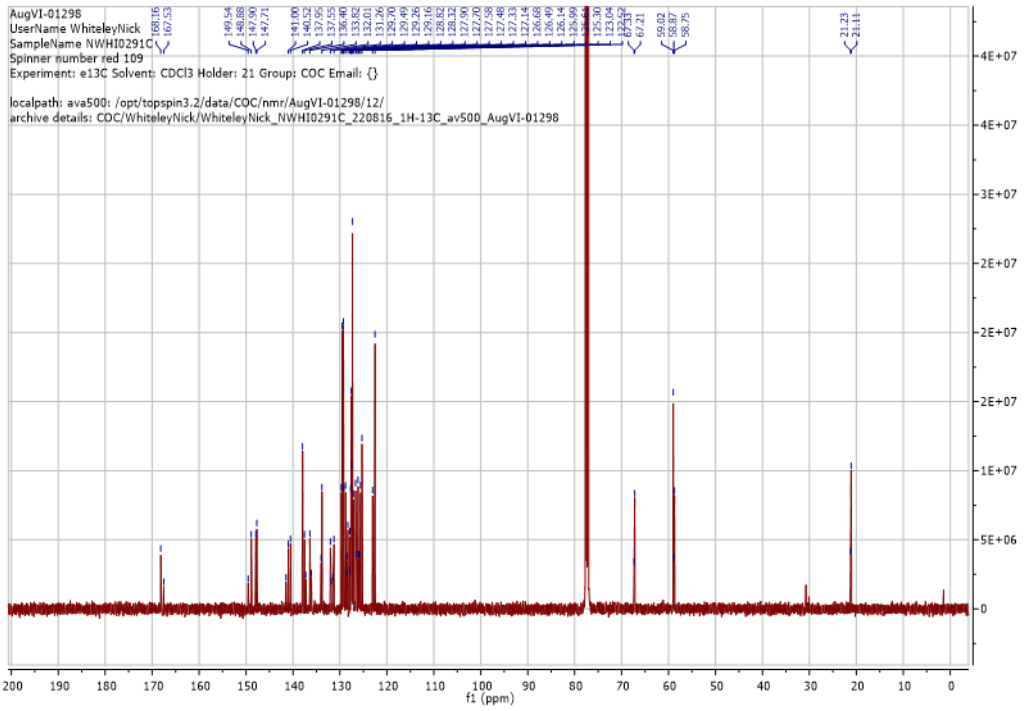

Step VIII (1Br). 4-Bromophenyl 3-methyl-2-[8-(phenyl)-6H,12H-5,11-methano dibenzo[b,f][1,5]diazocin-2-yl]benzoate

3 Methyl-2-[8-(phenyl)-6H,12H-5,11-methano dibenzo[b,f][1,5]diazocin-2-yl]benzoic acid (1 Eq, 0.462 mmol, 0.20 g), 4-bromophenol (3 Eq, 0.924 mmol, 0.48 g) and PyBOP (2 Eq, 0.924 mmol, 0.48 g) were combined in DCM (11 mL). Triethylamine (8 Eq, 3.70 mmol, 0.37 g, 0.515 mL) was added and the stirred at room temperature for 48 h. Further DCM was added (50 mL) and the solution washed with saturated aqueous sodium bicarbonate 40 mL). Organics were dried over magnesium sulfate and solvents removed under reduced pressure. The residue was purified by flash chromatography (20-40% ether in hexane) to yield 4-bromophenyl 3-methyl-2-[8-(phenyl)-6H,12H-5,11-methano dibenzo[b,f][1,5]diazocin-2-yl]benzoate (0.16 g, 59%).

^{1}H NMR (600 MHz, $CDCl_3$) δ 7.73 (d, J = 7.6 Hz, 0.3H, minor conformer), 7.65 (d, J = 7.5 Hz, 0.6H, major conformer), 7.60 (d, J = 7.4 Hz, 1.3H), 7.54 – 7.49 (m, 1.3H), 7.46 – 7.38 (m, 4H), 7.36 – 7.29 (m, 2H), 7.28 – 7.26 (m, 0.7H), 7.25 – 7.18 (m, 2.3H), 7.13 – 7.06 (m, 1H), 6.86 (d, J = 8.7 Hz, 1.3H, major conformer), 6.84 (d, J = 1.1 Hz, 0.6H, major conformer), 6.79 (app. s, 0.3H, minor conformer) ,6.65 (d, J = 8.7 Hz, 0.7H, minor conformer), 5.99 (d, J = 8.7 Hz, 1.2H, major conformer), 4.87 – 4.76 (m, 1.7H), 4.68 (app. d, J = 16.8 Hz, 0.3H, minor conformer), 4.43 – 4.17 (m, 4H), 2.16 (s, 2H, major conformer), 2.09 (s, 1H, minor conformer).

^{13}C NMR (126 MHz, $CDCl_3$) δ 167.8, 167.2, 149.9, 149.2, 147.8, 147.8, 147.6, 147.4, 141.2, 140.8, 140.7, 140.7, 140.2, 137.7, 137.3, 137.0, 136.1, 135.9, 133.8, 133.6, 132.4, 132.2, 131.7, 131.6, 129.1, 128.9, 128.6, 128.4, 128.3, 128.1, 127.7, 127.6, 127.5, 127.3, 127.3, 127.1, 126.9, 126.4, 126.2, 125.9, 125.7, 125.6, 125.3, 125.1, 123.2, 122.7, 119.0, 118.8, 67.1, 67.0, 58.8, 58.6, 58.5, 21.0, 20.9. Two conformers, some aromatic and one Tröger's base bridgehead conformer peaks occluded.

HRMS (ESI) obtained m/z 609.1101, 611.1086 (M+Na+). Expected 609.1148, 611.1134.

^{1}H NMR

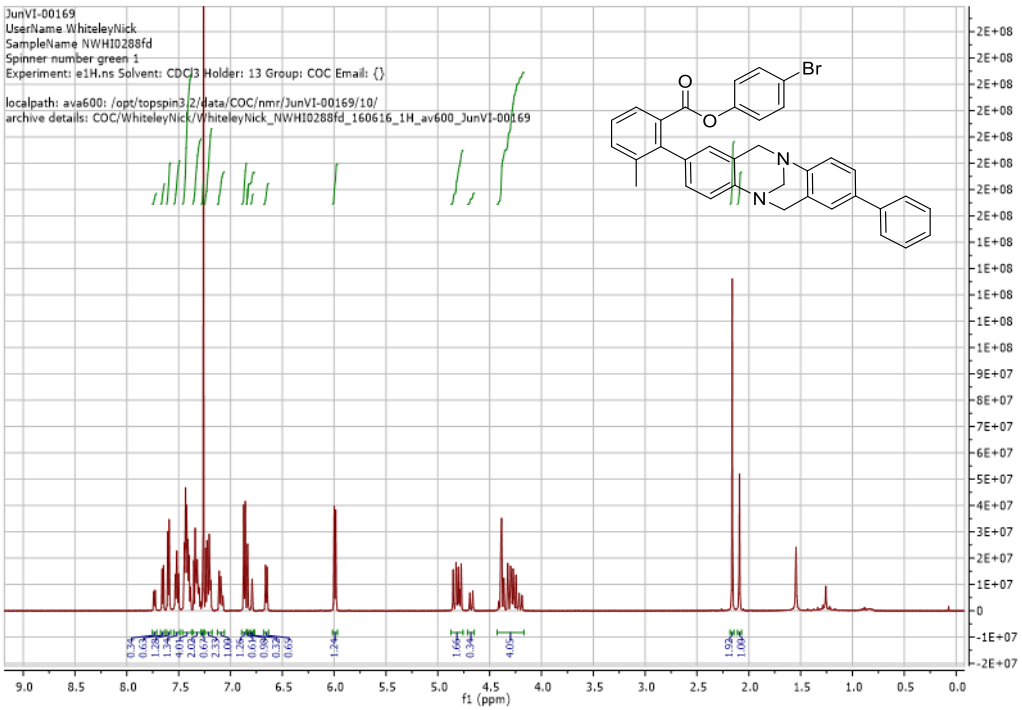

^{13}C NMR

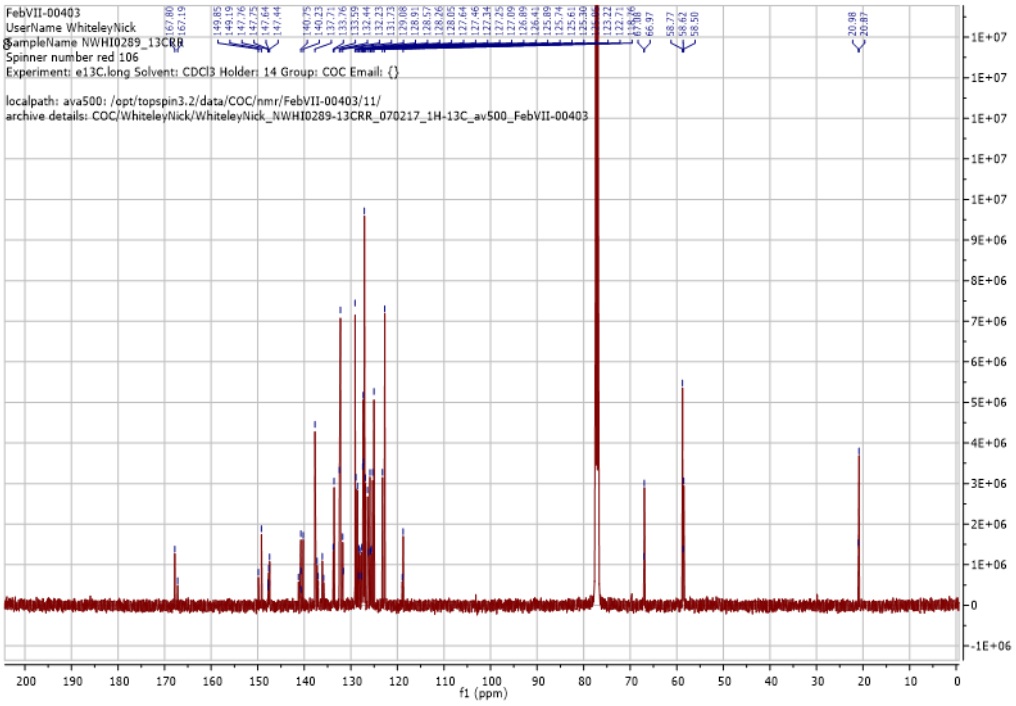

Step VIII (1I). 4-Iodophenyl 3-methyl-2-[8-(phenyl)-6H,12H-5,11-methano dibenzo[b,f][1,5]diazocin-2-yl]benzoate

3 Methyl-2-[8-(phenyl)-6H,12H-5,11-methano dibenzo[b,f][1,5]diazocin-2-yl]benzoic acid (1 Eq, 0.201 mmol, 0.087 g), 4-iodophenol (3 Eq, 0.603 mmol, 0.13 g) and PyBOP (2 Eq, 0.402 mmol, 0.21 g) were combined in DCM (5 mL). Triethylamine (8 Eq, 1.61 mmol, 0.16 g, 0.225 mL) was added and the reaction stirred at room temperature for 72 h. Further DCM was added (50 mL) and the solution washed with saturated aqueous sodium bicarbonate (30 mL) and brine (2 x 30 mL). Organics were dried over magnesium sulfate and solvents removed under reduced pressure. The residue was purified by flash chromatography (20-40% ethyl acetate in petroleum ether) to yield 4-iodophenyl 3-methyl-2-[8-(phenyl)-6H,12H-5,11-methano dibenzo[b,f][1,5]diazocin-2-yl]benzoate (0.067 g, 54%).

^{1}H NMR (601 MHz, $CDCl_3$) δ 7.75 (d, J = 7.6 Hz, 0.3H, minor conformer), 7.68 (d, J = 7.5 Hz, 0.7H, major conformer), 7.65 – 7.61 (m, 2H), 7.56 – 7.53 (m, 1.3H), 7.49 – 7.40 (m, 3.5H), 7.38 – 7.29 (m, 2.7H), 7.27 – 7.20 (m, 2.4H), 7.14 – 7.08 (m, 2.3H), 6.86 (d, J = 1.3 Hz, 0.6H, major conformer), 6.81 (app. s, 0.3H, minor conformer), 6.56 (app d, J = 8.7 Hz, 0.7H, minor conformer), 5.90 (app. d, J = 8.7 Hz, 1.3H, major conformer), 4.88 – 4.78 (m, 1.7H), 4.70 (d, J = 16.8 Hz, 0.3H, minor conformer), 4.44 – 4.19 (m, 4H), 2.18 (s, 2H, major conformer), 2.11 (s, 1H, minor conformer).

^{13}C NMR (126 MHz, $CDCl_3$) δ 167.6, 167.0, 150.5, 149.9, 147.6, 147.5, 147.3, 141.1, 140.6, 140.6, 140.1, 138.3, 138.1, 137.6, 137.0, 136.9, 136.0, 135.7, 133.6, 133.5, 131.6, 131.5, 129.1, 128.8, 128.4, 128.2, 128.1, 127.9, 127.6, 127.5, 127.3, 127.2, 127.2, 127.1, 127.1, 127.0, 126.8, 126.2, 126.1, 125.7, 125.6, 125.5, 125.1, 124.9, 123.5, 123.0, 89.7, 89.5, 66.9, 66.8, 58.6, 58.5, 58.4, 20.8, 20.7. Two conformers, some aromatic and one Tröger's base bridgehead conformer peaks occluded.

HRMS (ESI) obtained m/z 635.1179 (M+H+). Expected 635.1190.

^{1}H NMR

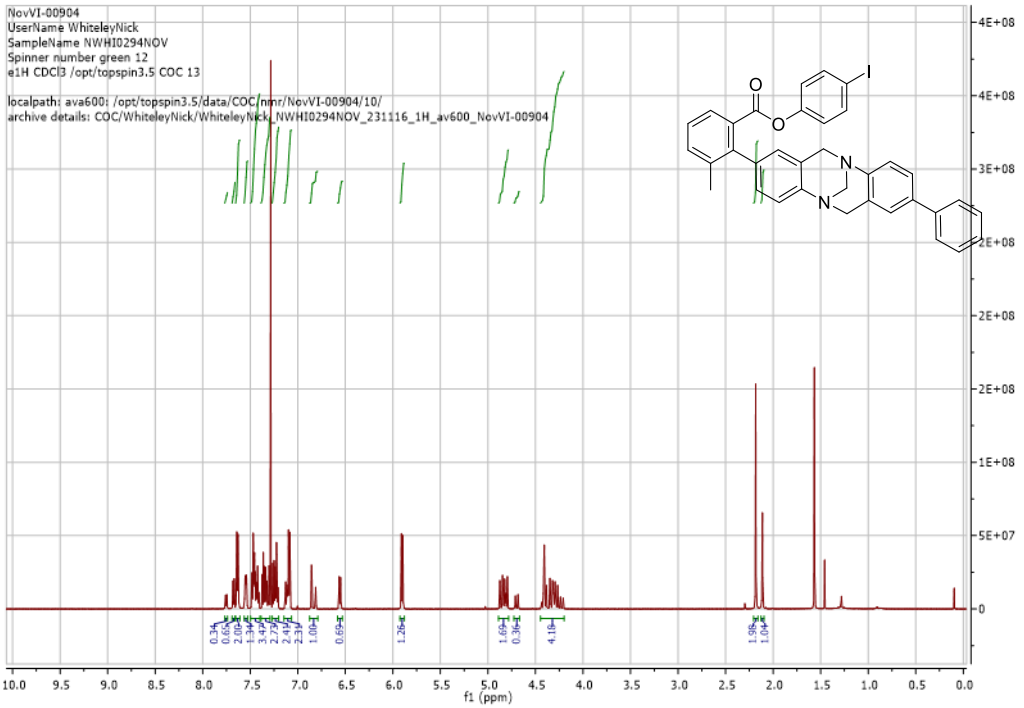

^{13}C NMR

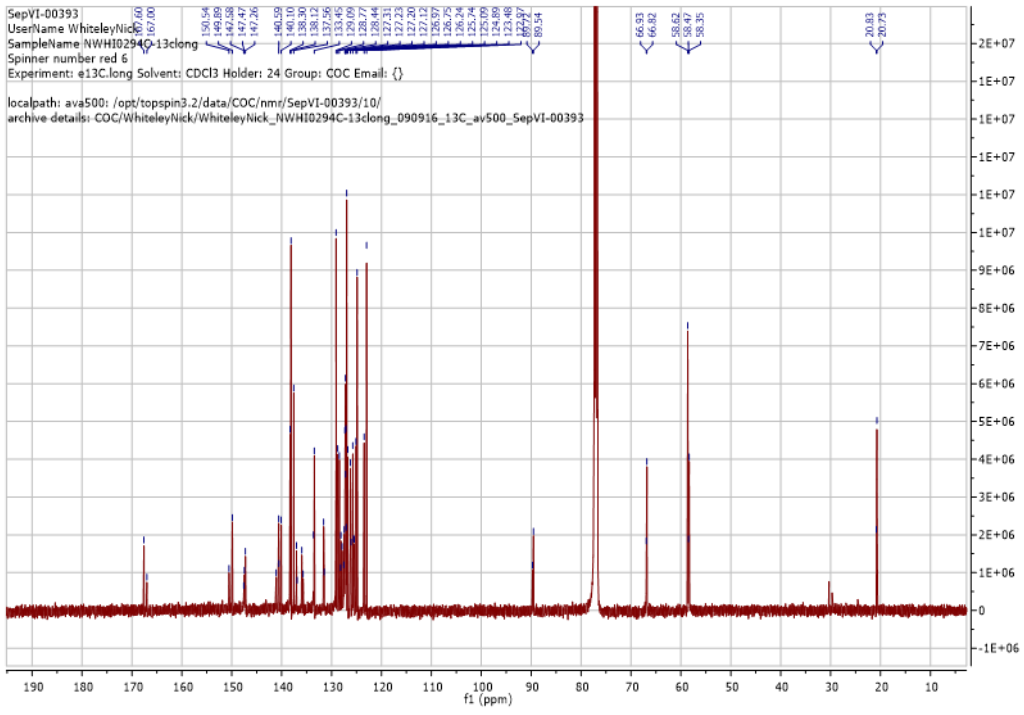

Step VIII (1H). Phenyl 3-methyl-2-[8-(phenyl)-6H,12H-5,11-methano dibenzo[b,f][1,5]diazocin-2-yl]benzoate

3 Methyl-2-[8-(phenyl)-6H,12H-5,11-methano dibenzo[b,f][1,5]diazocin-2-yl]benzoic acid (1 Eq, 0.430 mmol, 0.19 g), phenol (3 Eq, 1.29 mmol, 0.12 g) and PyBOP (2 Eq, 1.29 mmol, 0.12 g) were combined in DCM (10 mL). Triethylamine (8 Eq, 3.44 mmol, 0.35 g, 0.480 mL) was added and the stirred at room temperature for 72 h. Further DCM was added (50 mL) and the solution washed with saturated aqueous sodium bicarbonate 40 mL). Organics were dried over magnesium sulfate and solvents removed under reduced pressure. The residue was purified by flash chromatography (20-40% ether in hexane) to yield phenyl 3-methyl-2-[8-(phenyl)-6H,12H-5,11-methano dibenzo[b,f][1,5]diazocin-2-yl]benzoate (0.12 g, 55%).

^{1}H NMR (500 MHz, $CDCl_3$) δ 7.75 (d, J = 7.6 Hz, 0.4H, minor conformer), 7.66 (d, J = 7.6 Hz, 0.7H, major conformer), 7.56 – 7.50 (m, 2H), 7.48 – 7.37 (m, 4H), 7.37 – 7.28 (m, 2.6H), 7.24 – 7.15 (m, 3.3H), 7.15 – 7.08 (m, 1H), 6.85 (s, 0.6H, major conformer), 6.82 (s, 0.4H, minor conformer), 6.77 (app d, J = 7.9 Hz, 0.7H, minor conformer), 6.75 – 6.70 (m, 1.3H, major conformer), 6.69 – 6.65 (m, 0.6H, minor conformer), 6.11 (d, J = 7.9 Hz, 1.2H, major conformer), 4.86 – 4.75 (m, 1.6H), 4.69 (app d, J = 16.8 Hz, 0.4H, minor conformer), 4.43 – 4.17 (m, 4H), 2.16 (s, 1.9H, major conformer), 2.10 (s, 1.1H, minor conformer).

^{13}C NMR (126 MHz, $CDCl_3$) δ 168.2, 167.6, 150.9, 150.2, 147.8, 147.7, 147.4, 147.4, 141.1, 140.8, 140.7, 137.6, 137.3, 137.0, 136.2, 135.9, 133.5, 133.3, 132.2, 132.1, 129.4, 129.2, 128.9, 128.6, 128.4, 128.3, 128.1, 127.7, 127.4, 127.3, 127.2, 127.2, 127.1, 127.0, 126.9, 126.5, 126.2, 125.9, 125.8, 125.6, 125.5, 125.0, 121.4, 120.8, 67.0, 67.0, 58.8, 58.7, 58.7, 58.5, 21.0, 20.8. Two conformers, some peaks occluded.

HRMS (ESI) obtained m/z 509.2185 (M+H+). Expected 509.2224. Significant dimer signal also observed in mass spec m/z 1017.4278.

^{1}H NMR

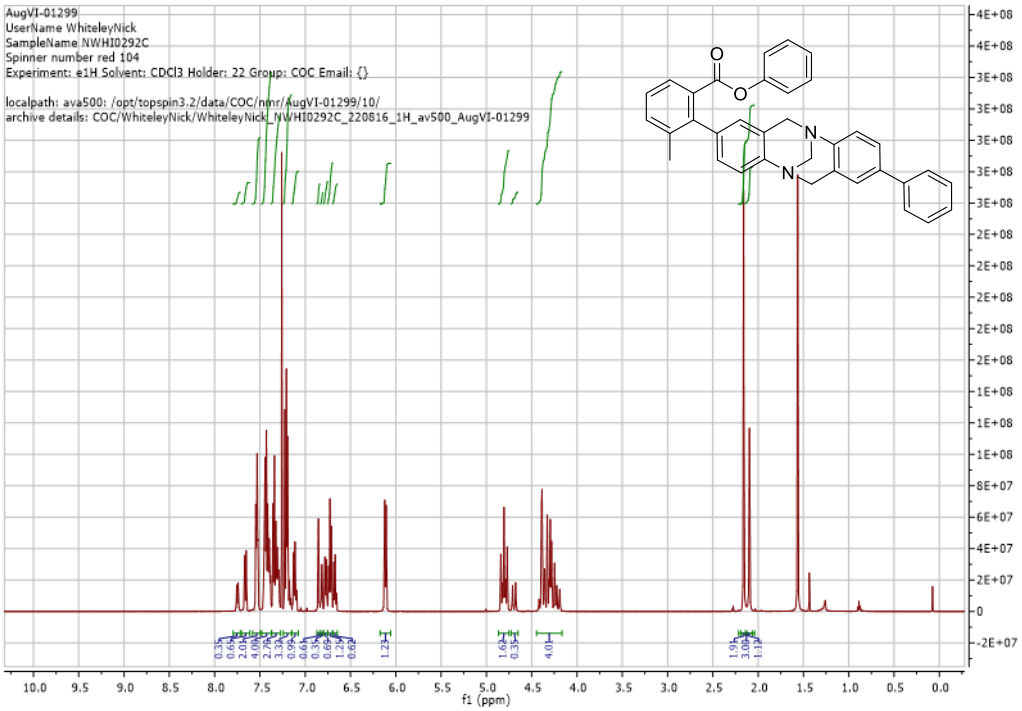

^{13}C NMR

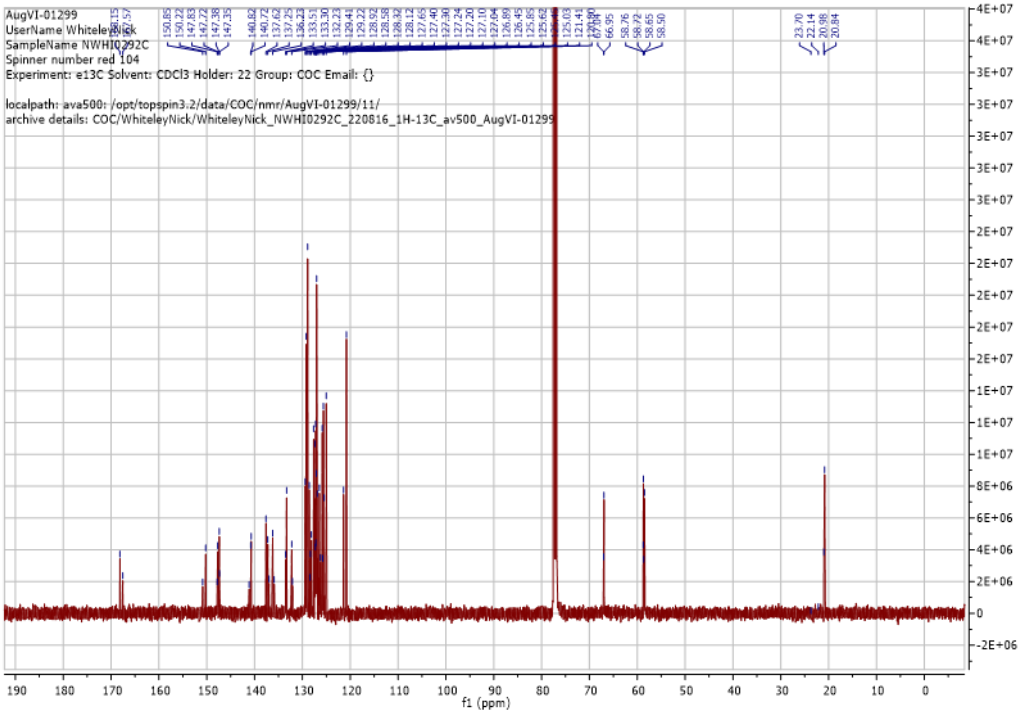

Step VIII (1Me) 4-methylphenyl 3-methyl-2-[8-(phenyl)-6H,12H-5,11-methano dibenzo[b,f][1,5]diazocin-2-yl]benzoate

3 methyl-2-[8-(phenyl)-6H,12H-5,11-methano dibenzo[b,f][1,5]diazocin-2-yl]benzoic acid (1 Eq, 0.417 mmol, 0.18 g), 4-methylphenol (3 Eq, 1.24 mmol, 0.14 g) and PyBOP (2 Eq, 0.832 mmol, 0.43 g) were combined in DCM (10 mL). Triethylamine (8 Eq, 3.32 mmol, 0.34 g, 0.465 mL) was added and the reaction stirred at room temperature for 96 h. Further DCM was added (50 mL) and the solution washed with saturated aqueous sodium carbonate (30 mL), bicarbonate (30 mL) and brine (30 mL). Organics were dried over magnesium sulfate and solvents removed under reduced pressure. The residue was purified by flash chromatography (20-40% ether in hexane) to yield 4-methylphenyl 3-methyl-2-[8-(phenyl)-6H,12H-5,11-methano dibenzo[b,f][1,5]diazocin-2-yl]benzoate (0.14 g, 62%).

^{1}H NMR (601 MHz, $CDCl_3$) δ 7.73 (d, J = 7.5 Hz, 0.3H, minor conformer), 7.64 (d, J = 7.5 Hz, 0.7H, major conformer), 7.58 (app. d, J = 7.3 Hz, 1.4H), 7.53 (app. d, J = 7.5 Hz, 0.6H), 7.49 (dd, J = 8.3, 1.9 Hz, 0.7H), 7.45 – 7.38 (m, 3.3H), 7.35 – 7.28 (m, 2H), 7.25 – 7.18 (m, 2.3H), 7.27 (app. s, obscured by solvent peak, 0.7H) 7.13 – 7.08 (m, 1.6H), 6.84 (d, J = 1.1 Hz, 0.7H, major conformer), 6.81 (app. s, 0.3H, minor conformer), 6.64 (d, J = 8.3 Hz, 0.6H, minor conformer), 6.52 (d, J = 8.2 Hz, 1.3H, major conformer), 5.95 (d, J = 8.4 Hz, 1.3H, major conformer), 4.86 – 4.76 (m, 1.7H), 4.69 (d, J = 16.7 Hz, 0.3H, minor conformer), 4.43 – 4.18 (m, 4H), 2.31 (s, 1H, minor conformer), 2.16 (s, 2H, major conformer), 2.09 (s, 1H, minor conformer), 1.72 (s, 2H, major conformer).

^{13}C NMR (126 MHz, $CDCl_3$) δ 168.4, 167.8, 148.6, 147.9, 147.8, 147.8, 147.3, 141.1, 140.7, 140.6, 140.5, 137.5, 137.0, 136.9, 136.3, 135.9, 135.9, 135.5, 135.2, 133.4, 133.2, 132.4, 132.3, 129.9, 129.7, 129.0, 128.9, 128.7, 128.4, 128.4, 128.3, 128.2, 127.6, 127.4, 127.4, 127.4, 127.3, 127.2, 127.2, 127.1, 127.0, 126.9, 126.3, 126.2, 125.9, 125.8, 125.6, 125.4, 125.0, 121.1, 120.5, 67.1, 67.0, 58.8, 58.7, 58.6, 30.5, 21.0, 20.8, 20.3. Two conformers, one aromatic and one Tröger's base bridgehead conformer peaks occluded.

HRMS (ESI) obtained m/z 523.2356 (M+H+). Expected 523.2380.

^{1}H NMR

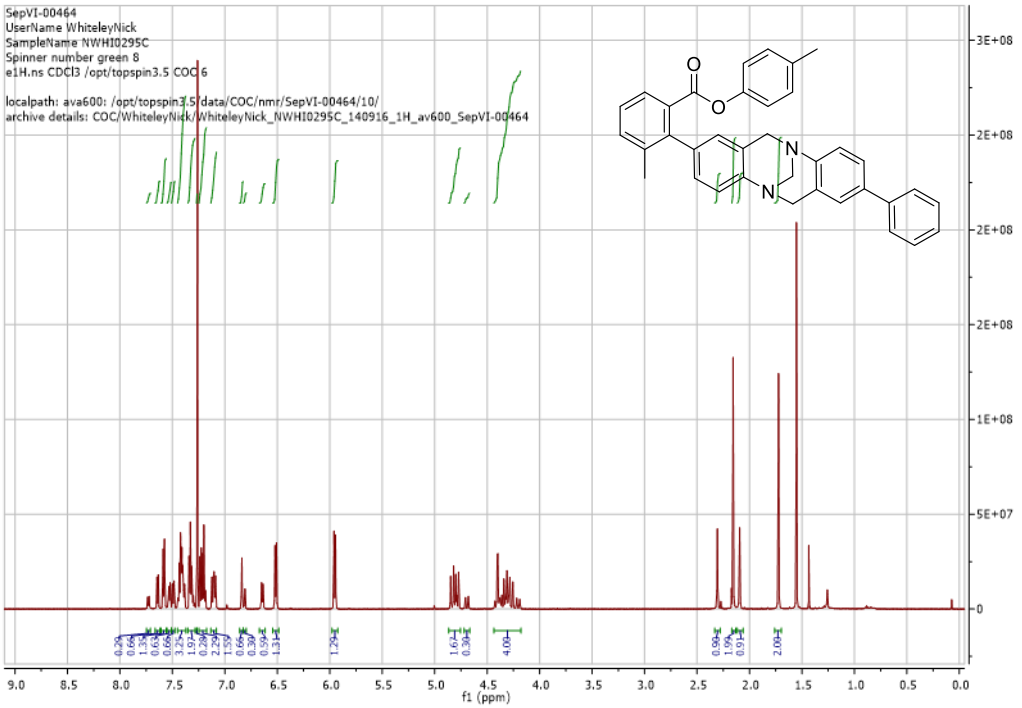

^{13}C NMR

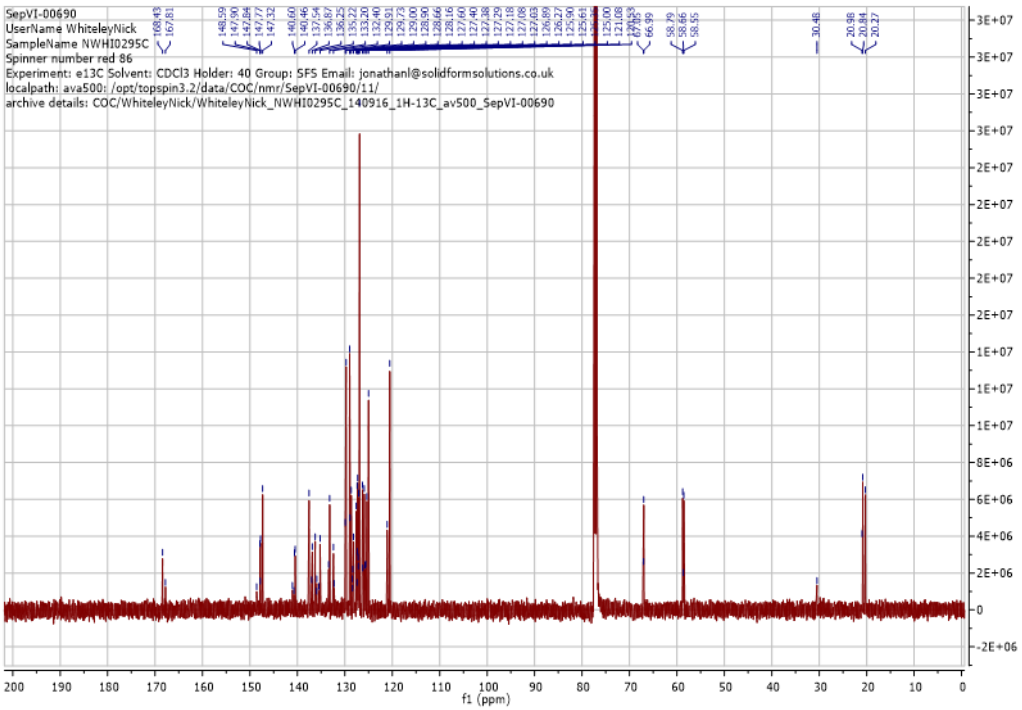

A.13 Synthesis of balance series 2

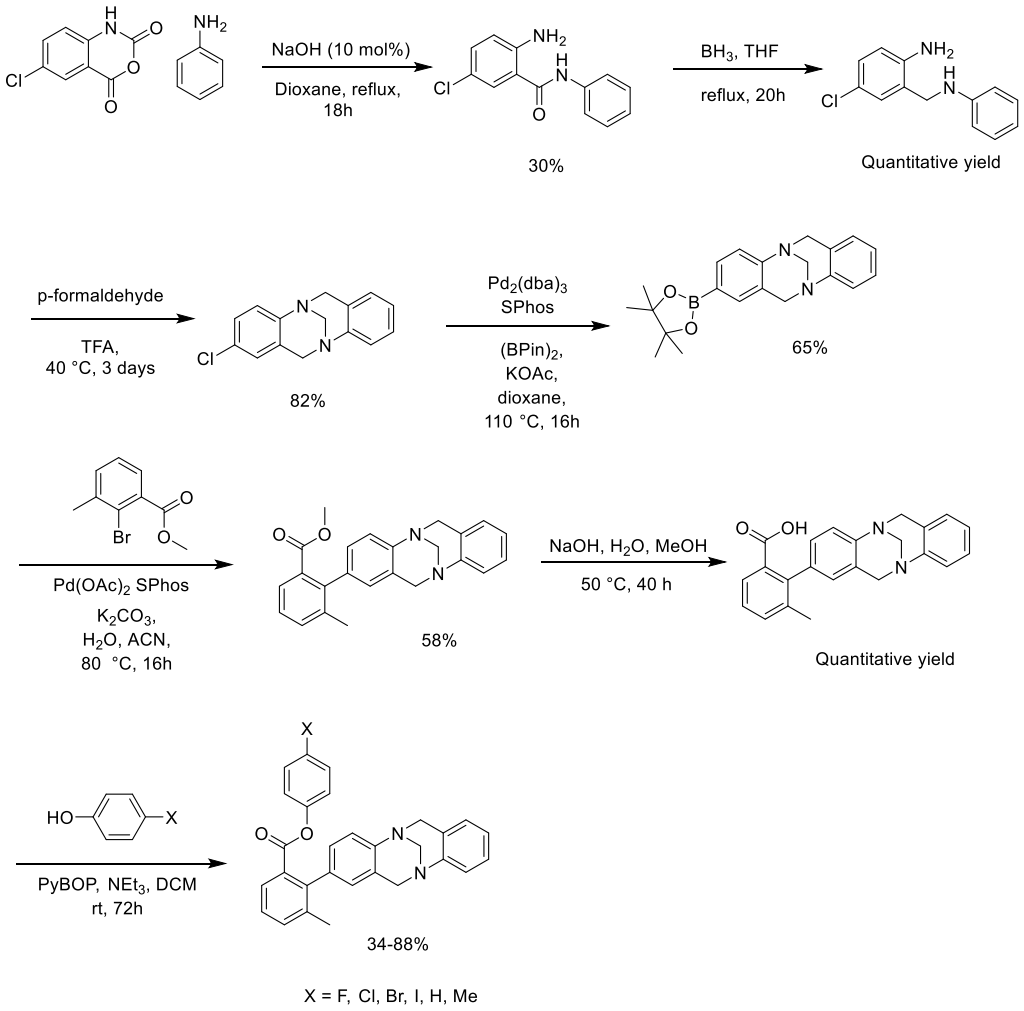

Step I. 2-Amino-5-chlorobenzanilide

5-Chloroisatoic anhydride (1.1 Eq, 15.00 g), aniline (1 Eq, 6.23 mL) and sodium hydroxide (0.1 Eq, 0.30 g) were dissolved in dioxane (anhydrous grade, 150 mL) under an inert nitrogen atmosphere. The mixture was then heated to reflux and refluxed for 48 hours. Reaction mixture was cooled to room temperature, filtered and concentrated under reduced pressure before being diluted with ethyl acetate (50 mL) and washed with water (2 x 50 mL). Organics were dried with magnesium sulfate before solvent was removed under reduced pressure. The residue was then trituration from ethanol and dried under vacuum to yield 2-amino-5-chlorobenzanilide (6.33 g, 30%).

^{1}H NMR (500 MHz, $CDCl_3$) δ 7.71 (s, 1H), δ 7.59 - 7.57 (dd, 2H), δ 7.47 - 7.46 (d, J = 2.4 Hz, 1H), δ 7.42 – 7.38 (m, 2H), δ 7.24 – 7.22 (dd, J = 8.8, 2.4 Hz, 1H), δ 7.21 – 7.17 (m, 1H), δ 6.70 – 6.68 (d, J = 8.8 Hz, 1H), δ 5.50 (s, 2H).

^{13}C NMR (126 MHz, DMSO-d_6) δ 167.0, 149.1, 139.5, 132.3, 129.0, 128.4, 124.1, 121.1, 118.5, 118.3, 116.6.

HRMS (ESI) obtained m/z 269.0452, 271.0426 (M+Na+). Expected 269.0452, 271.0423.

^{1}H NMR

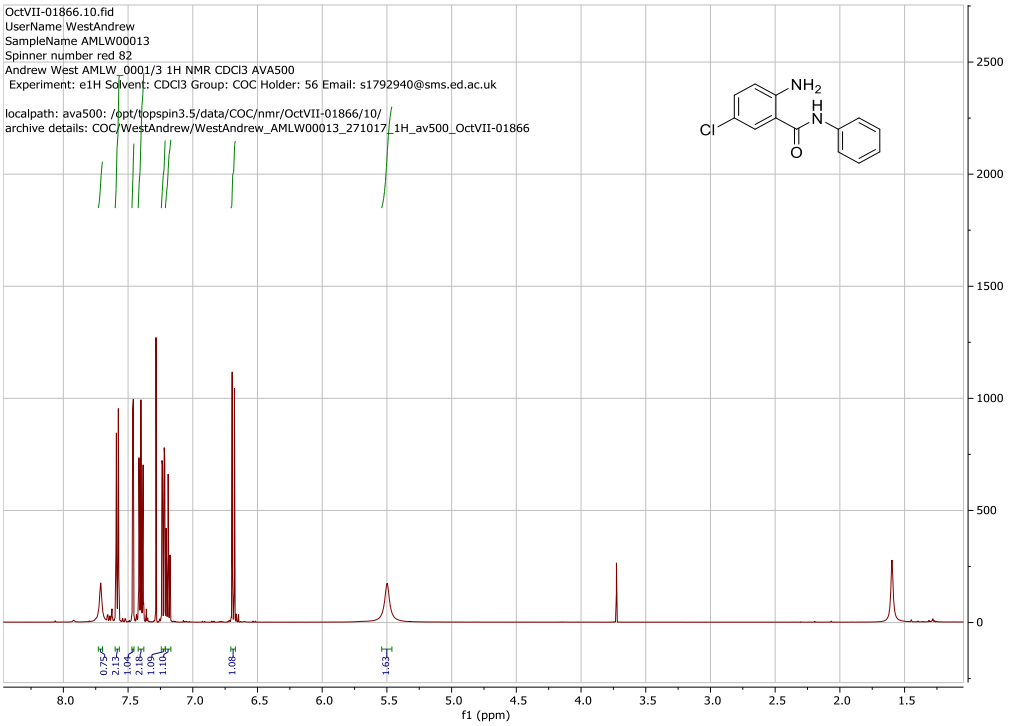

^{13}C NMR

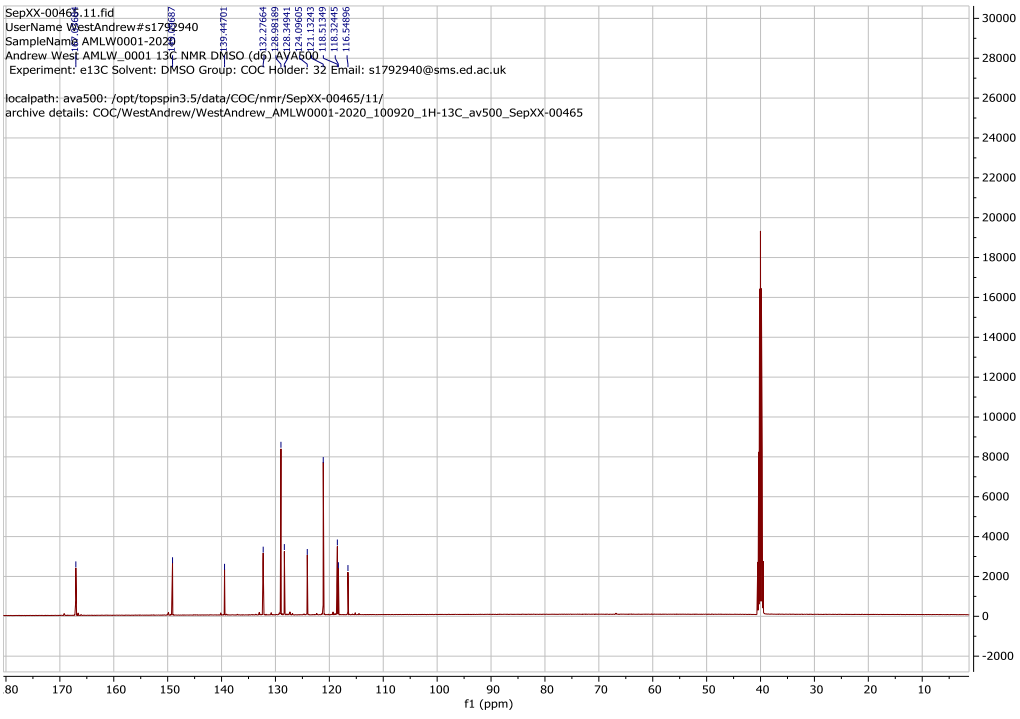

Step II-III. 2-chloro-6H,12H-5,11-Methanodibenzo[b,f][1,5]diazocine

2-Amino-5-chlorobenzanilide (1 Eq, 6.00 g) was dissolved in THF (38 mL) at 0 °C under an inert nitrogen atmosphere. BH_3.THF (5.8 Eq, 1.0 M in THF, 142 mL), was added slowly and stirred at 0 °C for 30 minutes. The reaction mixture was then slowly heated to reflux and refluxed for 18 hours. The reaction mixture was then slowly added to a 1.0 M aqueous sodium hydroxide (200 mL) at 0 °C. The reaction mixture was then extracted with ethyl acetate (3 x 150 mL) before organics were washed with brine (150 mL) and dried over magnesium sulfate. Solvent was then removed under reduced pressure to yield crude (~95% pure) 2-Amino-5-chloro-*N*-phenyl-benzenemethanamine in quantitative yields (5.25 g,).

2-Amino-5-chloro-*N*-phenyl-benzenemethanamine (1 Eq, 5.00 g) and p-formaldehyde (6 Eq, 3.91 g) were dissolved in TFA (500 mL) under an inert nitrogen atmosphere. The resultant mixture was then stirred at room temperature for 30 minutes before being heated to 40 °C and stirred for 72 hours. The reaction mixture was then added dropwise to a 0 °C 35% aqueous ammonia solution (700 mL) before extraction with DCM (3 x 300 mL). Combined organics dried over magnesium sulfate and solvents removed under reduced pressure. Resultant residue was purified by flash chromatography (10-40% ethyl acetate in petroleum ether) to yield 2-chloro-6H,12H-5,11-Methanodibenzo[b,f][1,5]diazocine (4.59 g, 81.8%).

^{1}H NMR (500 MHz, $CDCl_3$) δ 7.20 – 7.15 (m, 1H), δ 7.13 -7.10 (m, 2H), δ 7.08 – 7.05 (d, J = 8.6 Hz, 1H), δ 7.02 – 6.97 (td, J = 7.4, 1.4 Hz, 1H), δ 6.92 – 6.89 (m, 2H), δ 4.73 – 4.62 (app dd, J = 18.0, 2.7 Hz, 2H), δ 4.36 – 4.24 (app m, 2H), δ 4.19 – 4.08 (app t J = 15.5 Hz, 2H).

^{13}C NMR (126 MHz, $CDCl_3$) δ 147.8, 146.7, 129.6, 128.9, 127.6, 127.5, 127.0, 126.8, 126.4, 125.1, 124.2, 66.8, 58.8, 58.5.

HRMS (ESI) obtained m/z 257.0840, 259.0814 (M+H+). Expected 257.0840, 259.0811.

^{1}H NMR

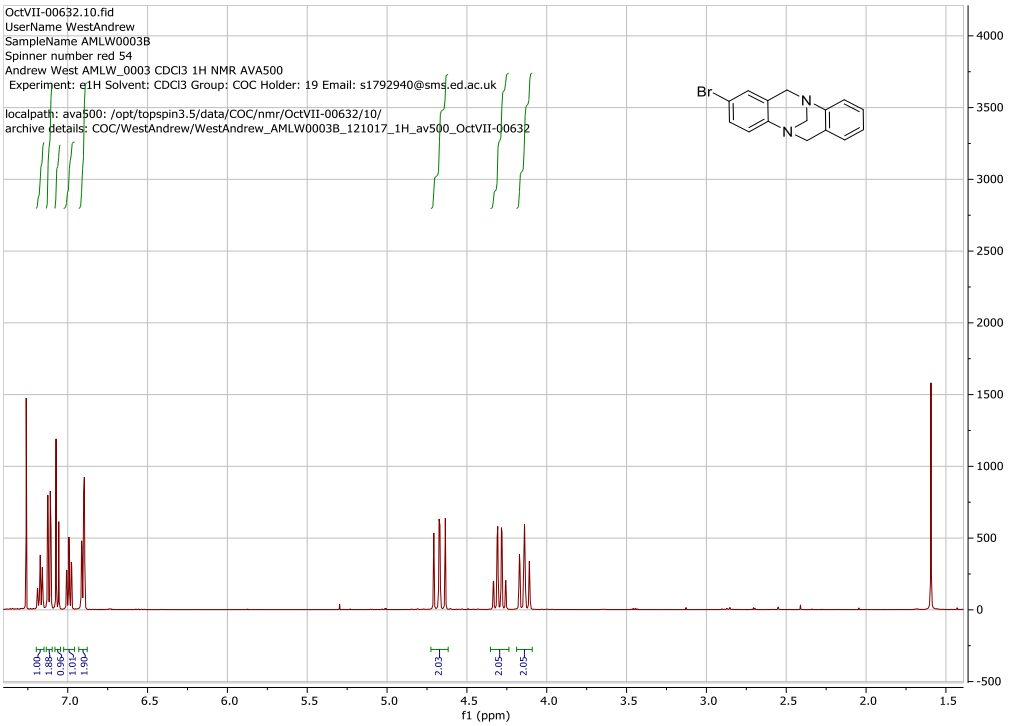

^{13}C NMR

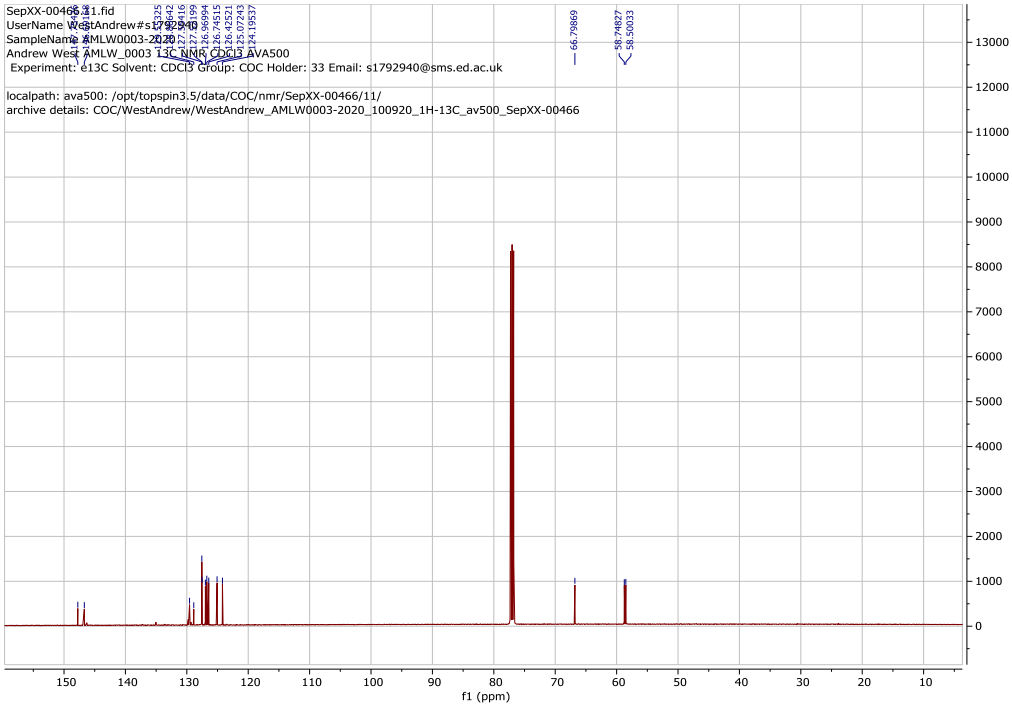

Step IV. 2-(4,4,5,5-Tetramethyl-1,3,2-dioxaborolan-2-yl)-6H,12H-5,11-methanodibenzo[b,f][1,5]diazocine

2-chloro-6H,12H-5,11-Methanodibenzo[b,f][1,5]diazocine (1 Eq, 4.50 g), bis(pinacolato)diboron (3 Eq, 13.35 g), tris(dibenzylideneacetone)dipalladium (0.02 Eq, 0.32 g), SPhos (0.04 Eq, 0.29 g) and $Pd(OAc)_2$ (3 Eq, 5.16 g) were dissolved in degassed dioxane (anhydrous grade, 14 mL). The reaction mixture was then heated to reflux and refluxed for 16 hours. The reaction mixture was then cooled and filtered through kieselguhr with ethyl acetate. Organics were washed with saturated sodium bicarbonate solution (150 mL), brine (50 mL) and dried over magnesium sulfate before the solvent was removed under vacuum and purified via flash chromatography (40% ethyl acetate in petroleum ether) to yield 2-(4,4,5,5-Tetramethyl-1,3,2-dioxaborolan-2-yl)-6H,12H-5,11-methanodibenzo[b,f][1,5]diazocine (3.94 g, 65%).

^{1}H NMR (500 MHz, $CDCl_3$) δ 7.62 – 7.57 (d, J = 8.0 Hz, 1H), δ 7.39 (s, 1H), δ 7.17 – 7.08 (m, 3H), δ 6.98 – 6.91 (td, J = 1.6, 7.3, 6.9 Hz, 1H), δ 6.90 – 6.85 (d, J = 7.3 Hz, 1H), δ 4.74 – 4.66 (app dd, J = 6.6, 16.6 Hz, 2H), δ 4.35 – 4.31 (app s, 2H), δ 4.24 – 4.17 (app d, J = 16.6, 2H), δ 1.29 (s, 12H).

^{13}C NMR (126 MHz, $CDCl_3$) δ 151.2, 148.0, 133.9, 133.7, 127.8, 127.4, 127.2, 126.9, 83.7, 66.8, 58.8, 58.6, 24.8, 24.8.

HRMS (ESI) obtained m/z 349.2064 (M+H+). Expected 349.2082.

^{1}H NMR

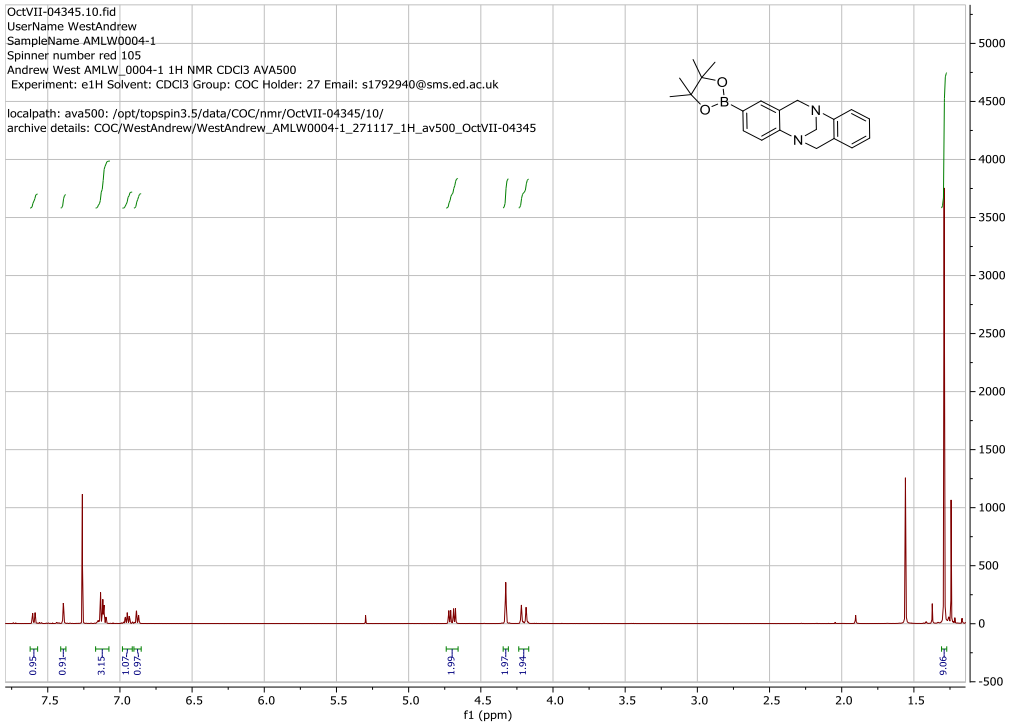

^{13}C NMR

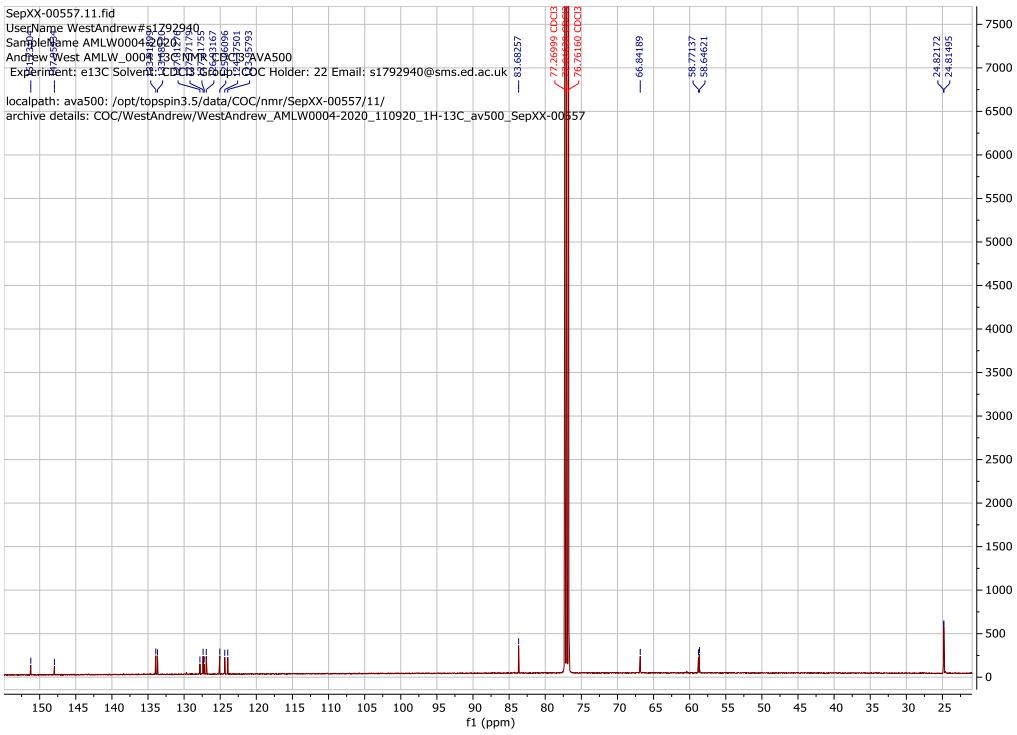

Step V. Benzoic acid, 2-(6H,12H-5,11-methanodibenzo[b,f][1,5]diazocin-2-yl)-3-methyl-, methyl ester

2-(4,4,5,5-Tetramethyl-1,3,2-dioxaborolan-2-yl)-6H,12H-5,11-methanodibenzo[b,f][1,5]diazocine (1 Eq, 2.00 g) palladium(II)acetate (0.02 Eq, 0.026 g), SPhos (0.04 Eq, 0.094 g) and methyl 2-bromo-3methyl-benzoate (1.5 Eq, 1.97 g) were dissolved in acetonitrile. To the resultant mixture, 2 M potassium carbonate solution (2.5 Eq, 7.2 mL) was added before the reaction mixture was heated to reflux under a nitrogen atmosphere and allowed to react for 16 hours. The reaction mixture was then diluted with ethyl acetate (250 mL) and washed with sodium bicarbonate solution (2 x 150 mL) and brine (100 mL) before the organics were dried with magnesium sulfate before solvent was removed under reduced pressure. The crude reaction mixture was then purified by flash chromatography (10-14% ethyl acetate in petroleum ether) to yield Benzoic acid, 2-(6H,12H-5,11-methanodibenzo[b,f][1,5]diazocin-2-yl)-3-methyl-, methyl ester (1.25 g, 58%).

^{1}H NMR (500 MHz, $CDCl_3$) δ 7.62 – 7.49 (dd, J = 7.7, 33.8 Hz, 1H), δ 7.39 – 7.30 (dd, J = 7.8, 13.97 Hz, 1H) δ 7.29 – 7.23 (m, 1H), δ 7.22 – 7.10 (m, 3H), δ 7.05 – 6.92 (m, 2H), 6.92 – 9.87 (d, J = 7.6 Hz, 1H), 6.73 – 6.63 (m, 1H), δ 4.79 – 4.68 (app m, 2H), δ 4.50 – 4.30 (app m, 2H), δ 4.21 – 4.08 (app m, 2H), δ 3.58 (s, 1.2H, minor conformer), δ 2.78 (s, 1.8H, major conformer), δ 2.18 (s, 1.8H, major conformer), δ 2.02 (s, 1.2H, minor conformer).

13C NMR (126 MHz, $CDCl_3$) δ 169.7, 169.1, 143.3, 147.9, 146.9, 146.7, 136.8, 135.9, 132.9, 132.8, 128.1, 127.9, 127.4, 127.3, 127.0, 126.9, 126.8, 126.7, 125.3, 124.9, 124.6, 124.2, 123.8, 67.4, 67.0, 59.3, 59.2, 58.6, 51.9, 50.9, 20.8, 20.7.

HRMS (ESI) obtained m/z 393.1572 (M+Na+). Expected 393.1573.

^{1}H NMR

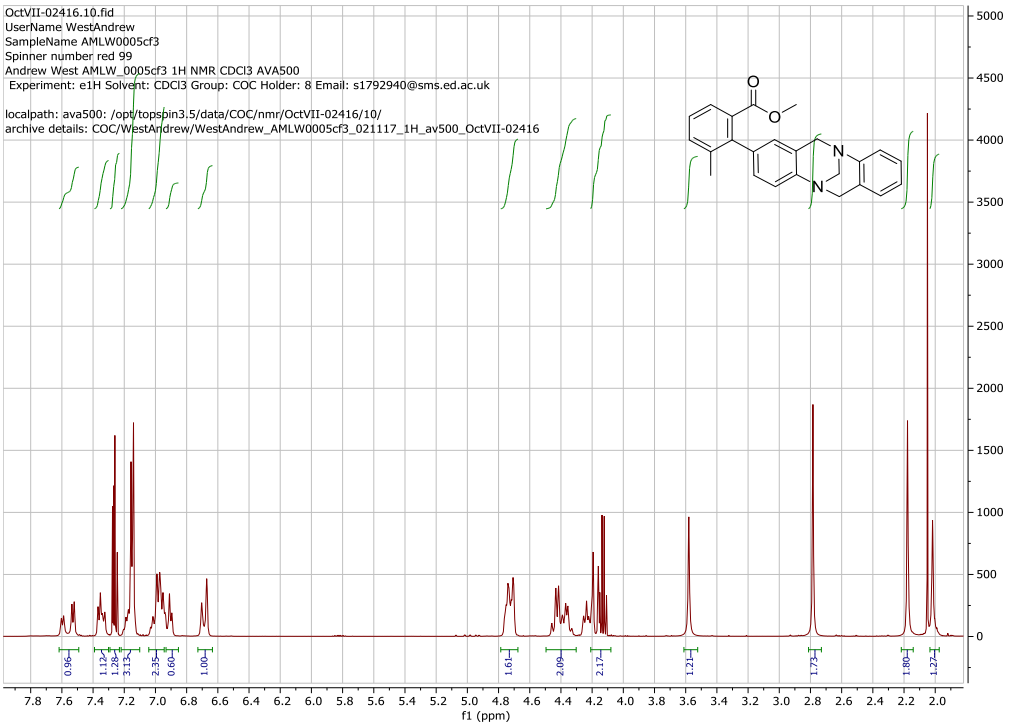

^{13}C NMR

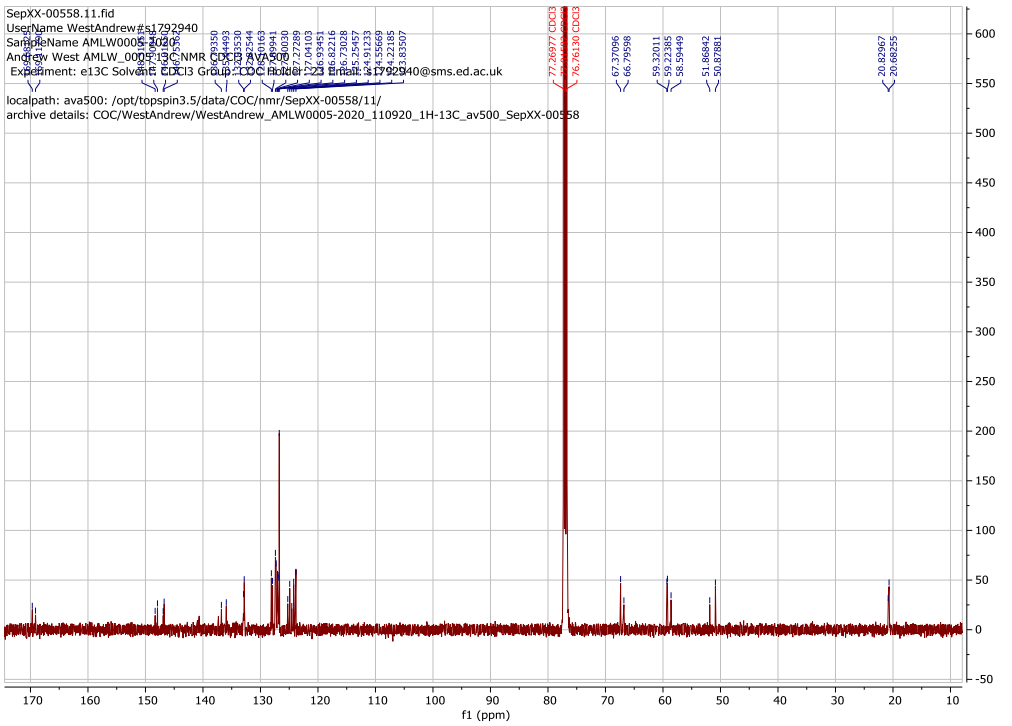

Step VI. 2-(6H,12H-5,11-methanodibenzo[b,f][1,5]diazocin-2-yl)-3-methyl-benzoic acid.

A solution of methanol (44 mL), tetrahydrofuran (44 mL) and water (0.4 mL) was prepared and used to dissolve benzoic acid, 2-(6H,12H-5,11-methanodibenzo[b,f][1,5]diazocin-2-yl)-3-methyl-, methyl ester (1 Eq, 0.57 g) and sodium hydroxide (17 Eq, 1.1 g) were added before the reaction mixture was heated to 55 °C and allowed to react for 40 hours. The reaction mixture was then cooled to room temperature before 1 M hydrochloride acid (1.67 mL) was added dropwise. Phases were then separated and solvent removed under reduced pressure yielding 2-(6H,12H-5,11-methanodibenzo[b,f][1,5]diazocin-2-yl)-3-methyl-benzoic acid. (0.55 g) in quantitative yield.

^{1}H NMR (500 MHz, DMSO-d_6) δ 12.41 (s, 1H), δ 7.48 – 7.44 (bs, 1H) δ 7.40 – 7.36 (bs, 1H), δ 7.34 – 7.27 (t, J = 7.6 Hz, 1H), δ 7.20 – 7.16 (m, 2H), δ 7.14 – 7.10 (d, J = 5.7 Hz, 1H), δ 7.04 – 6.93 (m, 3H), δ 6.79 – 6.75 (d, J = 2.02, 1H), δ 4.71 – 4.64 (app d, J = 16.8 Hz, 1H), δ 4.33 – 4.05 (app m, 4H), δ 3.66 – 3.59 (app m, 1H), δ 2.10 – 1.90 (d, J = 28.8 Hz, 3H).

^{13}C NMR (126 MHz, DMSO-d_6) δ 170.1, 148.8, 147.3, 140.0, 135.1, 132.4, 128.6, 128.2, 127.6, 127.5, 127.4, 127.3, 125.5, 124.7, 123.9, 66.5, 58.4, 20.9.

HRMS (ESI) obtained m/z 379.4139. (M+Na+). Expected 379.4142.

^{1}H NMR

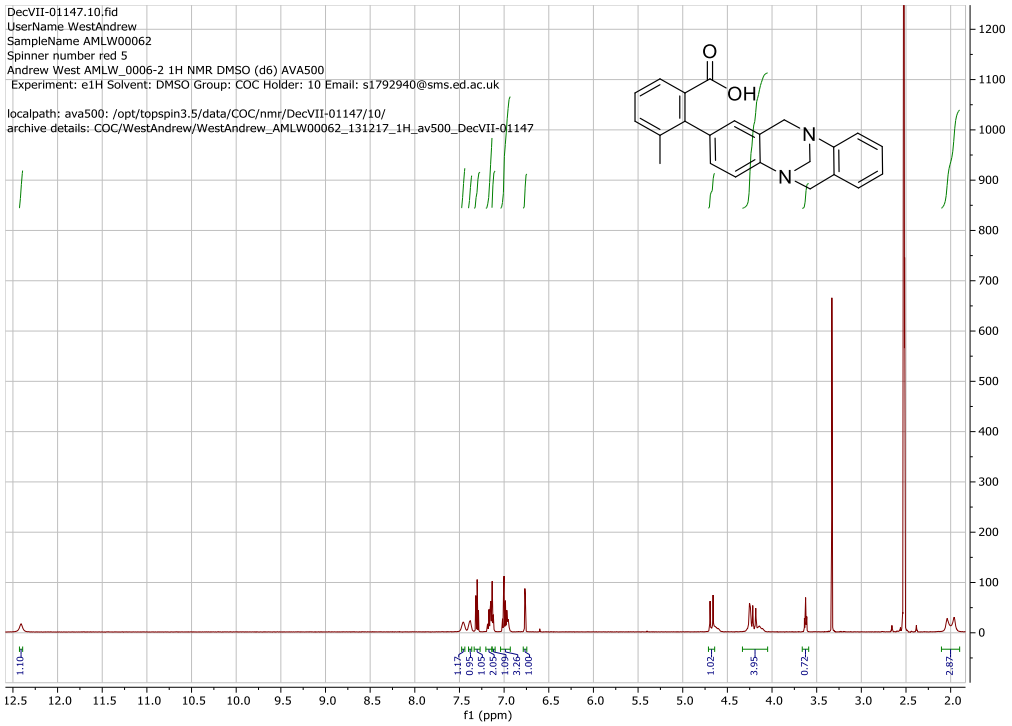

^{13}C NMR

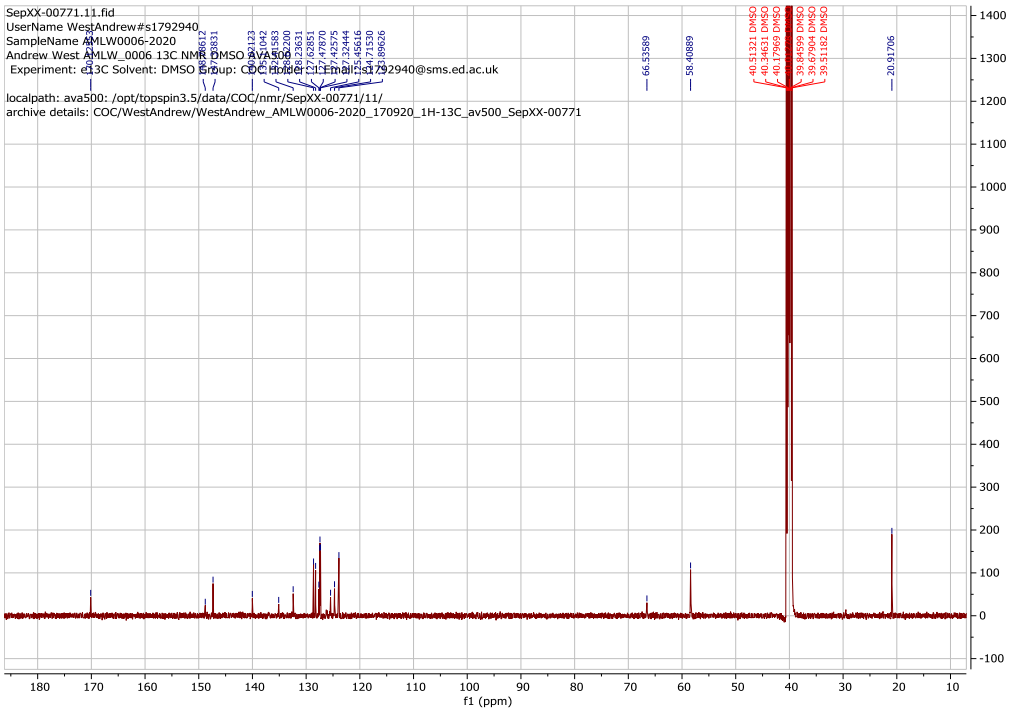

Step VII (2F). 4-Fluorophenyl 3-methyl-2-[6H,12H-5,11-methano dibenzo[b,f][1,5]diazocin-2-yl]benzoate

To a solution of 2-(4,4,5,5-Tetramethyl-1,3,2-dioxaborolan-2-yl)-6H,12H-5,11-methanodibenzo[b,f][1,5]diazocine (1 Eq, 0.50 g) desolved in acetonitrile (10 mL), $Pd(OAc)_2$ (0.02 Eq, 0.0065 g), SPhos (0.04 Eq, 0.024 g) and methyl 2-bromo-3-(4-fluorophenol)-benzoate (1.5 Eq, 0.66 g) were added. To the resultant solution, 2 M potassium carbonate solution (2.5 Eq, 1.44 mL) was added before the mixture was heated to reflux under an inert nitrogen atmosphere and refluxed for 16 hours. The reaction mixture was then diluted with ethyl acetate (250 mL) and washed with saturated sodium bicarbonate solution (2 x 150 mL) and brine (100 mL) before organics were dried over magnesium sulfate and the solvent was removed under reduced pressure. The crude reaction mixture was then purified by flash chromatography (30% ethyl acetate in petroleum ether) yielding 4-Fluorophenyl 3-methyl-2-[6H,12H-5,11-methano dibenzo[b,f][1,5]diazocin-2-yl]benzoate (0.38 g, 58%).

^{1}H NMR (500 MHz, $CDCl_3$) δ 7.75 (d, J = 7.6 Hz, 0.3H, minor conformer), 7.67 (d, J = 7.7 Hz, 0.6H major conformer), 7.44 (t, 1H), 7.36 (t, 1H), 7.27-7.07 (m, 5H), 7.07-6.96 (m, 2H), 6.84 (d, J = 1.9 Hz, 0.7H major conformer), 6.80 (d, J = 1.9 Hz, 0.3H, minor conformer), 6.77-6.70 (m, 0.6H, minor conformer), 6.56 (m, 1H), 6.11-6.05 (m, 1.3H, major conformer), 4.78 (m, J = 16.8 Hz, 1.7H, major conformer), 4.68 (m, J = 16.8 Hz, 0.3H, minor conformer), 4.43-4.33 (m, 2H), 4.31-4.15 (m, 2H), 2.18 (s, 2H, major conformer), 2.11 (s, 1H minor conformer).

^{13}C NMR (126 MHz, $CDCl_3$) δ 168.0, 167.4, 160.7, 158.8, 148.2, 147.3, 145.9, 141.0, 140.6, 137.5, 136.0, 135.7, 133.5, 133.3, 131.8, 131.6, 129.7, 128.3, 128.1, 127.7, 127.6, 127.3, 127.2, 127.0, 127.0, 125.4, 125.3, 124.9, 124.3, 123.9, 122.7, 122.6, 122.1, 122.0, 116.0, 115.9, 115.8, 115.7, 66.8, 66.7, 58.5, 58.4, 20.8, 20.7. Two conformers. Some peaks occluded.

HRMS (ESI) obtained m/z 473.1637. (M+Na+). Expected 473.1641.

^{1}H NMR

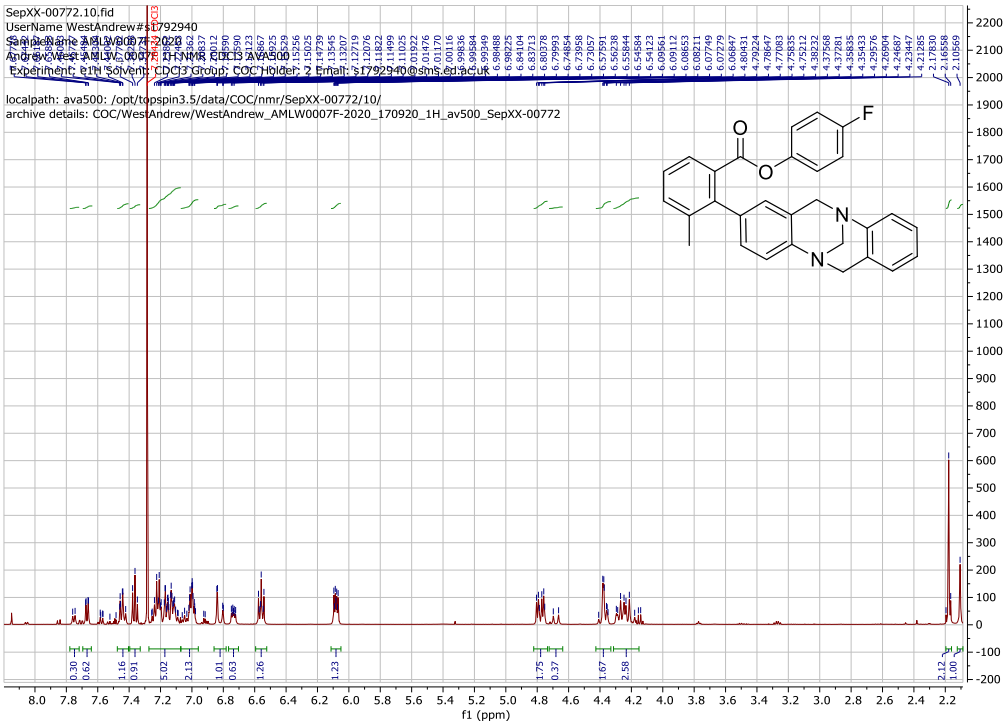

^{13}C NMR

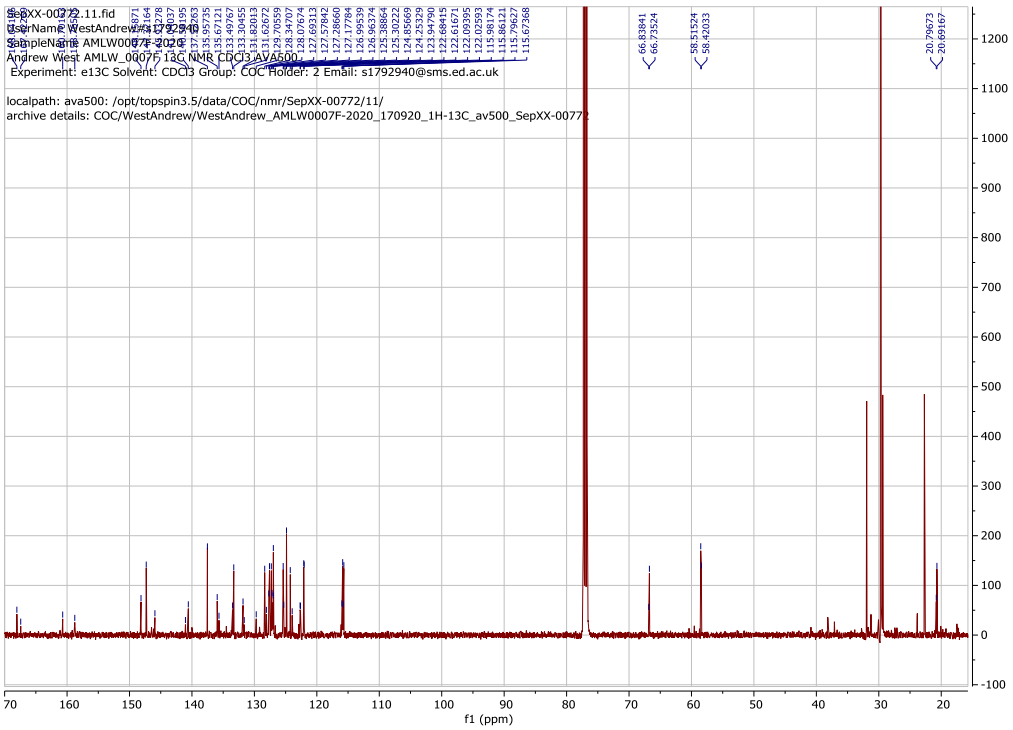

Step VII (2Cl). 4-Chlorophenyl 3-methyl-2-[6H,12H-5,11-methano dibenzo[b,f][1,5]diazocin-2-yl]benzoate

2-(6H,12H-5,11-methanodibenzo[b,f][1,5]diazocin-2-yl)-3-methyl-benzoic acid (1 Eq, 0.099 g), 4-chlorophenol (3 Eq, 0.11 g), and PyBOP (2 Eq, 0.29 g) were dissolved in DCM (5 mL). To the resultant mixture, triethylamine (8 Eq, 0.726 mL) was added before the solution was stirred at room temperature for 72 hours. Additional DCM (50 mL) was added to the reaction mixture before the mixture was washed with saturated aqueous sodium bicarbonate solution (30 mL) and brine (2 x 30 mL). Organics were then dried on magnesium sulfate before the solvent was removed under reduced pressure and the resultant residue was purified by flash chromatography (20% ethyl acetate in petroleum ether). 4-Chlorophenyl 3-methyl-2-[6H,12H-5,11-methano dibenzo[b,f][1,5]diazocin-2-yl]benzoate was isolated as a while solid (0.090 g, 67%).

^{1}H NMR (500 MHz, $CDCl_3$) δ 7.73 (d, J = 7.6 Hz, 0.3H, minor conformer), 7.64 (d, J = 7.5 Hz, 0.7H, major conformer), 7.42 (t, 1H), 7.34 (t, 1H), 7.28-7.15 (m, 4H), 7.13 (m, 2H), 7.09 (dd, 1H), 6.98 (d, 1H), 6.81-676 (m, 2H), 6.70 (d, J = 8.8 Hz, 0.5H, minor conformer) 6.05 (d, J = 8.8 Hz, 0.7H), 4.75 (dd, J = 16.8 Hz, 1.7H, major conformer), 4.65 (d, J = 16.7 Hz, 0.3H, minor conformer), 4.38-4.33 (m, 2H), 4.26-4.15 (m, 2H), 2.15 (s, 2H, major conformer), 2.08 (2, 1H, minor conformer).

^{13}C NMR (126 MHz, $CDCl_3$) δ 168.06, 167.76, 148.60, 148.11, 147.36, 136.07, 133.38, 129.42, 129.42, 129.18, 128.31, 127.60, 127.30, 127.00, 126.92, 125.36, 124.86, 124.32, 122.63, 122.00, 66.83, 66.73, 58.52, 58.41, 37.11, 36.66, Two conformers. Some peaks occluded.

HRMS (ESI) obtained m/z 489.1301, 489.1429. (M+Na+). Expected 489.1346, 489.1316.

^{1}H NMR

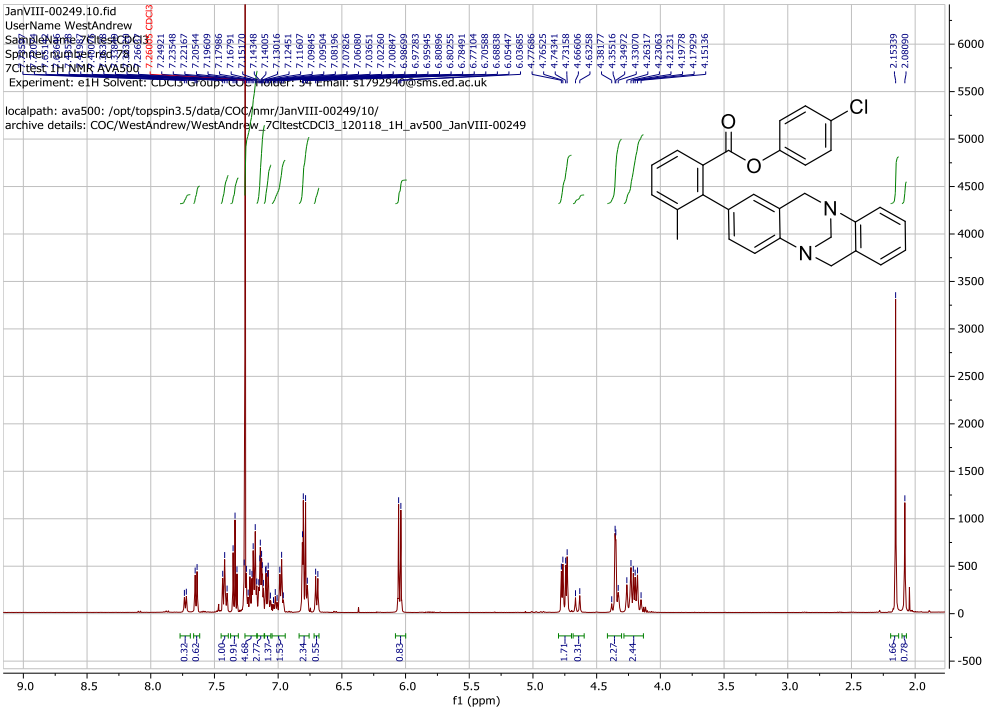

^{13}C NMR

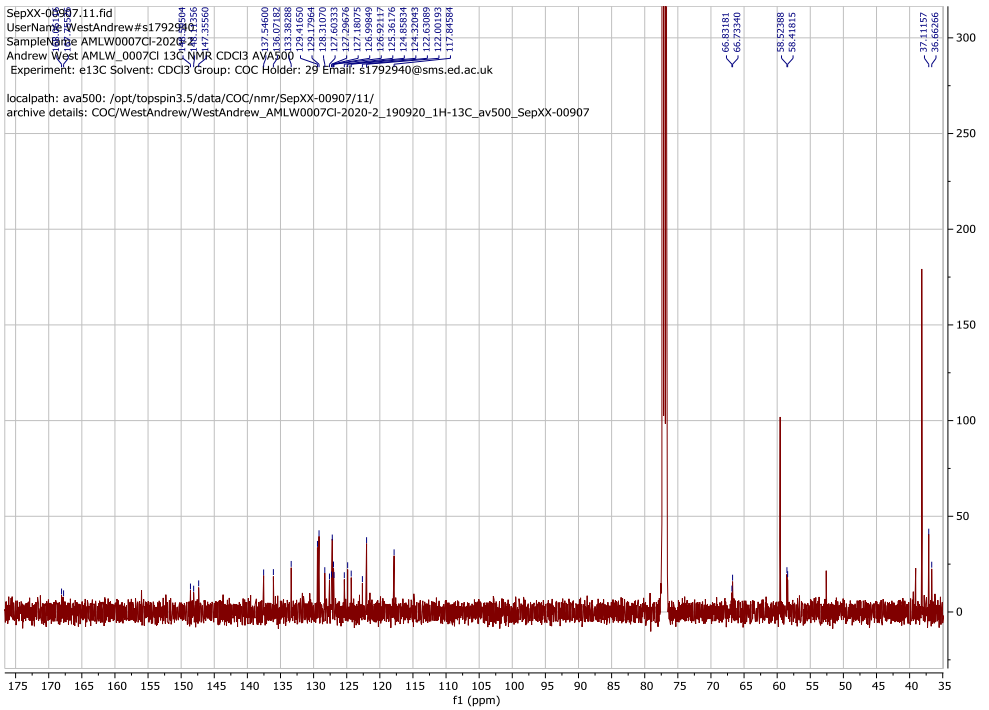

Step VII (2Br). 4-Brorophenyl 3-methyl-2-[6H,12H-5,11-methano dibenzo[b,f][1,5]diazocin-2-yl]benzoate

2-(6H,12H-5,11-methanodibenzo[b,f][1,5]diazocin-2-yl)-3-methyl-benzoic acid (1 Eq, 0.087 g), 4-bromophenol (3 Eq, 0.13 g), and PyBOP (2 Eq, 0.26 g) were dissolved in DCM (5 mL). To the resultant mixture, triethylamine (8 Eq, 0.73 mL) was added before the solution was stirred at room temperature for 72 hours. Additional DCM (50 mL) was added to the reaction mixture before the mixture was washed with saturated aqueous sodium bicarbonate solution (30 mL) and brine (2 x 30 mL). Organics were then dried on magnesium sulfate before the solvent was removed under reduced pressure and the resultant residue was purified by flash chromatography (20% ethyl acetate in petroleum ether). 4-Brorophenyl 3-methyl-2-[6H,12H-5,11-methano dibenzo[b,f][1,5]diazocin-2-yl]benzoate was isolated as a while solid (0.11 g, 86%).

^{1}H NMR (500 MHz, $CDCl_3$) δ 7.75 (d, J = 7.7 Hz, 0.3 H, minor conformer), 7.67 (d, J = 7.7 Hz, 0.7H, major conformer), 7.44 (t, 1H), 7.36 (t, 1H), 7.27-7.14 (m, 4H), 7.13-6.98 (m, 3H), 6.95 (m, 1H), 6.83 (d, J = 2.0 Hz, 0.7H, major conformer), 6.79 (d, J = 1.9 Hz, 0.3H, minor conformer), 6.67 (m, 0.6H, minor conformer), 6.01 (m, 1.3H, major conformer), 4.77 (dt, J = 16.8 Hz, 1.7H, major conformer), 4.67 (d, J = 16.8 Hz, 0.3H, minor conformer), 4.42-4.33 (m, 2H), 4.30-4.16 (m, 2H), 2.18 (s, 2H, major conformer), 2.11 (s, 1H, minor conformer).

^{13}C NMR (126 MHz, $CDCl_3$) δ 167.7, 167.1, 149.7, 149.1, 148.2, 148.1, 147.4, 141.1, 140.6, 137.5, 135.9, 135.6, 133.6, 133.4, 132.3, 132.2, 131.7, 131.5, 128.3, 128.1, 128.0, 127.7, 127.6, 127.6, 127.3, 127.2, 127.2, 127.0, 126.9, 125.4, 125.3, 124.9, 124.9, 124.4, 123.9, 123.1, 122.4, 118.8, 118.4, 66.8, 66.7, 58.5, 58.4, 20.8, 20.7. Two conformers. Some peaks occluded.

HRMS (ESI) obtained m/z 533.7021, 535.0831 (M+Na+). Expected 533.0835, 535.0815.

^{1}H NMR

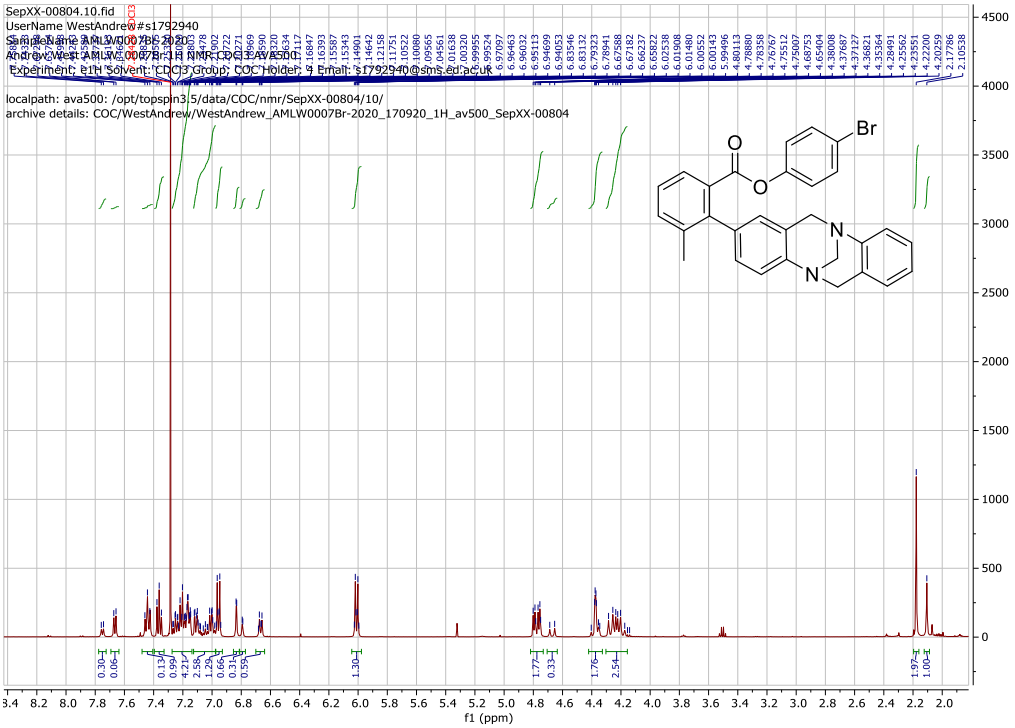

^{13}C NMR

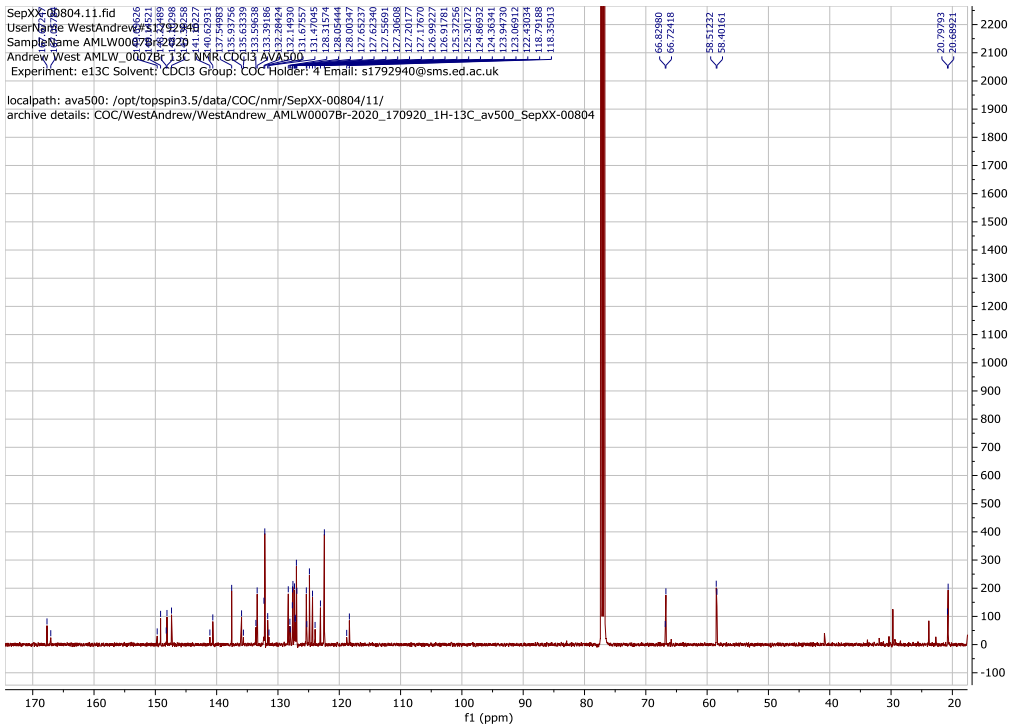

Step VII (2I). 4-Iodophenyl 3-methyl-2-[6H,12H-5,11-methano dibenzo[b,f][1,5]diazocin-2-yl]benzoate

2-(6H,12H-5,11-methanodibenzo[b,f][1,5]diazocin-2-yl)-3-methyl-benzoic acid (1 Eq, 0.070 g), 4-iododphenol (3 Eq, 0.13 g), and PyBOP (2 Eq, 0.21 g) were dissolved in DCM (5 mL). To the resultant mixture, triethylamine (8 Eq, 0.73 mL) was added before the solution was stirred at room temperature for 72 hours. Additional DCM (50 mL) was added to the reaction mixture before the mixture was washed with saturated aqueous sodium bicarbonate solution (30 mL) and brine (2 x 30 mL). Organics were then dried on magnesium sulfate before the solvent was removed under reduced pressure and the resultant residue was purified by flash chromatography (20% ethyl acetate in petroleum ether). 4-Iodophenyl 3-methyl-2-[6H,12H-5,11-methano dibenzo[b,f][1,5]diazocin-2-yl]benzoate was isolated as a while solid (0.13 g, 88%).

^{1}H NMR (500 MHz, $CDCl_3$) δ 7.75 (d, J = 7.2 Hz, 0.5H, minor conformer), 7.66 (d, J = 7.6, 0.6H, major conformer), 7.44 (t, 1H), 7.36 (t, 1H), 7.27-7.23 (m, 1H), 7.23-7.06 (m, 5H), 7.06-6.96 (m, 2H), 6.84-6.81 (m, 0.7H major conformer), 6.80-6.78 (m, 0.4H minor conformer), 6.55 (d, J = 8.7 Hz, 0.6H minor conformer), 5.88 (d, J = 8.8 Hz, 1.3H, major conformer), 4.43-4.32 (m, 1.5H, major conformer), 4.70-4.60 (m, 0.5H, minor conformer), 4.43-4.32 (m, 2H), 4.31-4.15 (m, 2H), 2.17 (s, 2H, major conformer), 2.10 (s, 1H, minor conformer).

^{13}C NMR (126 MHz, $CDCl_3$) δ 167.65, 167.29, 149.98, 148.11, 147.38, 145.97, 144.54, 143.4, 138.29, 138.11, 137.54, 135.95, 135.79, 133.38, 132.16, 131.69, 128.34, 128.32, 127.65, 127.63, 127.56, 127.31, 127.13, 126.99, 126.96, 126.92, 126.90, 126.22, 125.53, 125.39, 125.31, 124.87, 124.39, 67.99, 66.71, 58.49, 58.37, 22.70, 20.68. Two conformers. Some peaks occluded.

HRMS (ESI) obtained m/z 581.3996. (M+Na+). Expected 581.4087.

^{1}H NMR

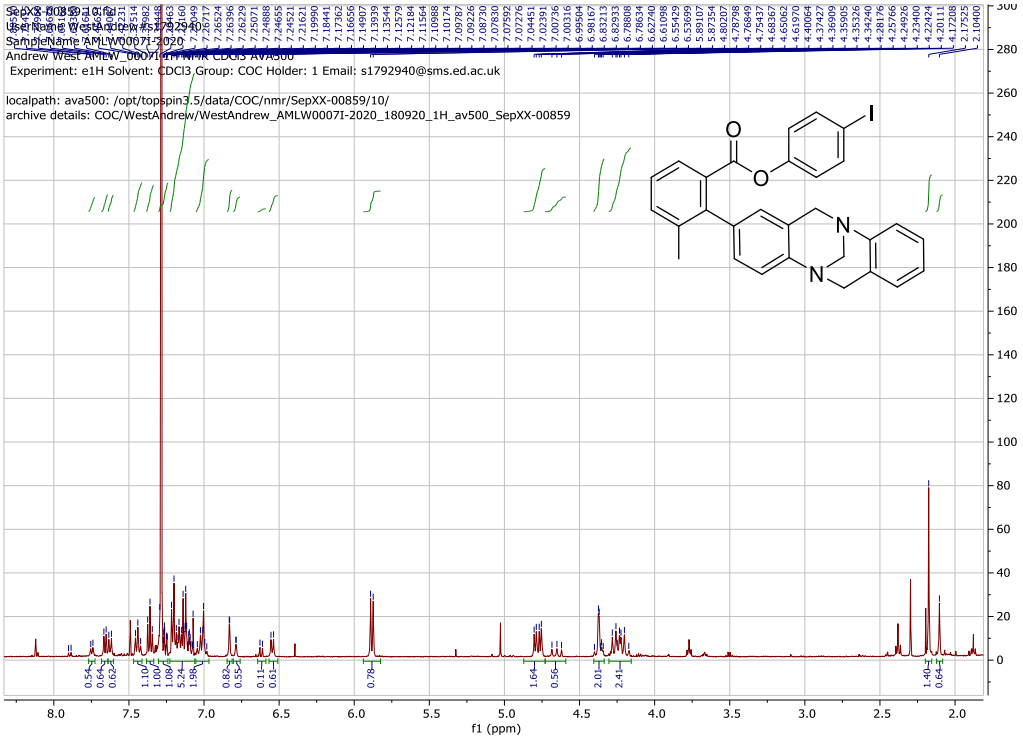

^{13}H NMR

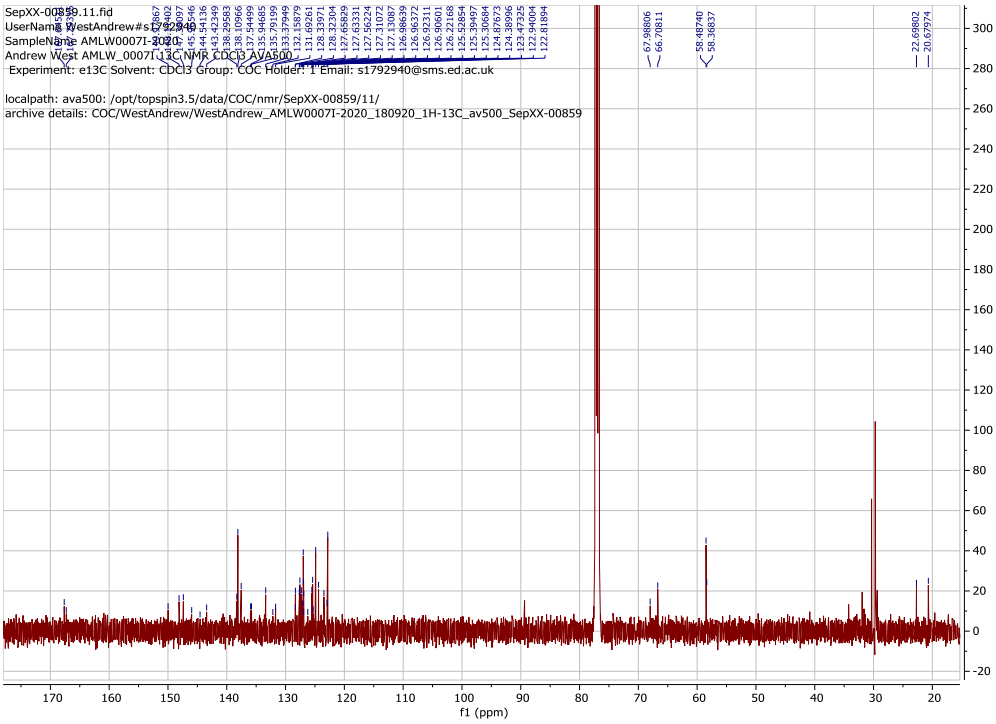

Step VII (2H). Phenyl 3-methyl-2-[6H,12H-5,11-methano dibenzo[b,f][1,5]diazocin-2-yl]benzoate

To a solution of 2-(4,4,5,5-Tetramethyl-1,3,2-dioxaborolan-2-yl)-6H,12H-5,11-methanodibenzo[b,f][1,5]diazocine (1 Eq, 0.50 g) dissolved in acetonitrile (10 mL), Pd(OAc)2 (0.02 Eq, 0.0065 g), SPhos (0.04 Eq, 0.024 g) and methyl 2-bromo-3-phenol benzoate (1.5 Eq, 0.69 g) were added. To the resultant solution, 2 M potassium carbonate solution (2.5 Eq, 1.44 mL) was added before the mixture was heated to reflux under an inert nitrogen atmosphere and refluxed for 16 hours. The reaction mixture was diluted with ethyl acetate (250 mL) and washed with saturated sodium bicarbonate solution (2 x 150 mL) and brine (100 mL) before organics were dried over magnesium sulfate before solvent was removed under reduced pressure. The crude reaction mixture was then purified by flash chromatography (30% ethyl acetate in petroleum ether) yielding Phenyl 3-methyl-2-[6H,12H-5,11-methano dibenzo[b,f][1,5]diazocin-2-yl]benzoate (0.34 g, 54%).

^{1}H NMR (500 MHz, $CDCl_3$) δ 7.77 (d, J = 7.6 Hz, 0.4H, minor conformer), 7.69 (d, J = 7.6 Hz, 0.6H, major conformer), 7.44 (m, 1H), 7.34 (m, 1H), 7.26-7.09 (m, 5H), 7.07-6.97 (m, 2H), 6.92 (t, 1H), 6.86 (s, 0.6H, major conformer), 6.82 (s, 0.4H, minor conformer), 6.79 (d, J = 7.9 Hz, 0.8H, minor conformer), 6.17 (d, J = 7.8 Hz, 1.1 H, major conformer), 4.78 (dd, J = 16.8 Hz, 1.6H, major conformer), 4.69 (d, J = 16.7 Hz, 0.4H minor conformer), 4.44-4.34 (m, 2H), 4.33-4.19 (m, 2H), 2.18 (s, 1.9H, major conformer), 2.11 (s, 1.1H minor conformer).

^{13}C NMR (126 MHz, $CDCl_3$) δ 168.0, 167.4, 150.7, 150.2, 148.3, 148.1, 147.2, 141.0, 140.6, 137.5, 135.9, 135.7, 133.4, 133.2, 132.1, 132.0, 129.7, 129.3, 129.2, 128.4, 128.1, 127.9, 127.7, 127.5, 127.2, 127.1, 127.0, 125.7, 125.3, 125.3, 124.9, 124.2, 123.9, 121.5, 121.3, 120.8, 66.8, 66.7, 58.5, 58.4, 29.7, 29.7. Two conformers. Some peaks occluded.

HRMS (ESI) obtained m/z 433.1671. (M+H+). Expected 433.1911.

^{1}H NMR

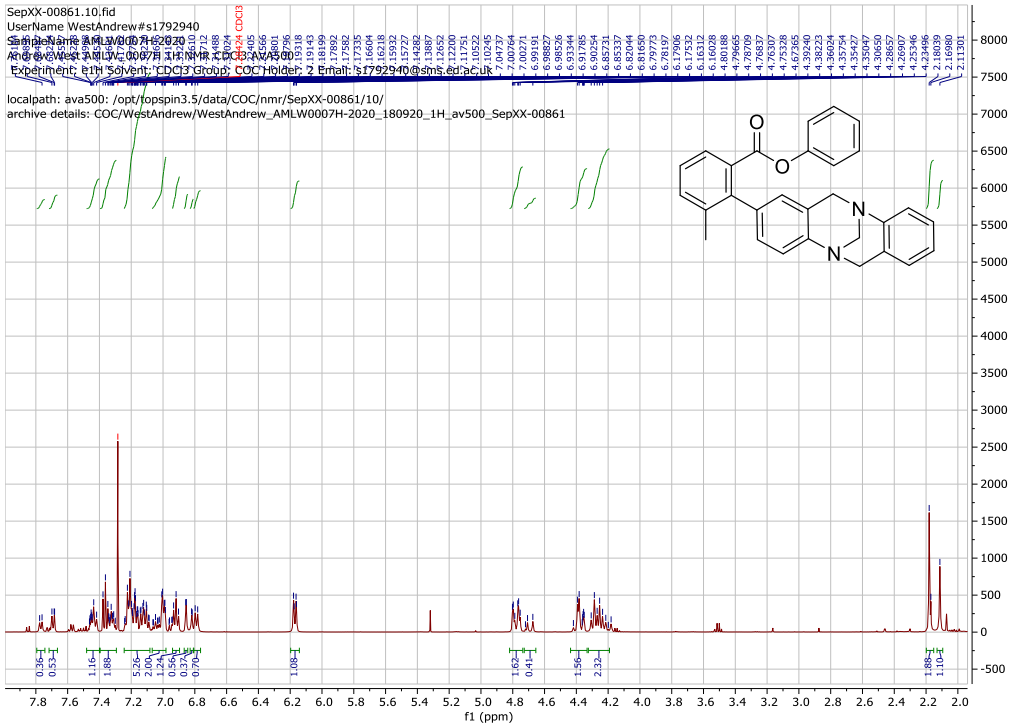

^{13}C NMR

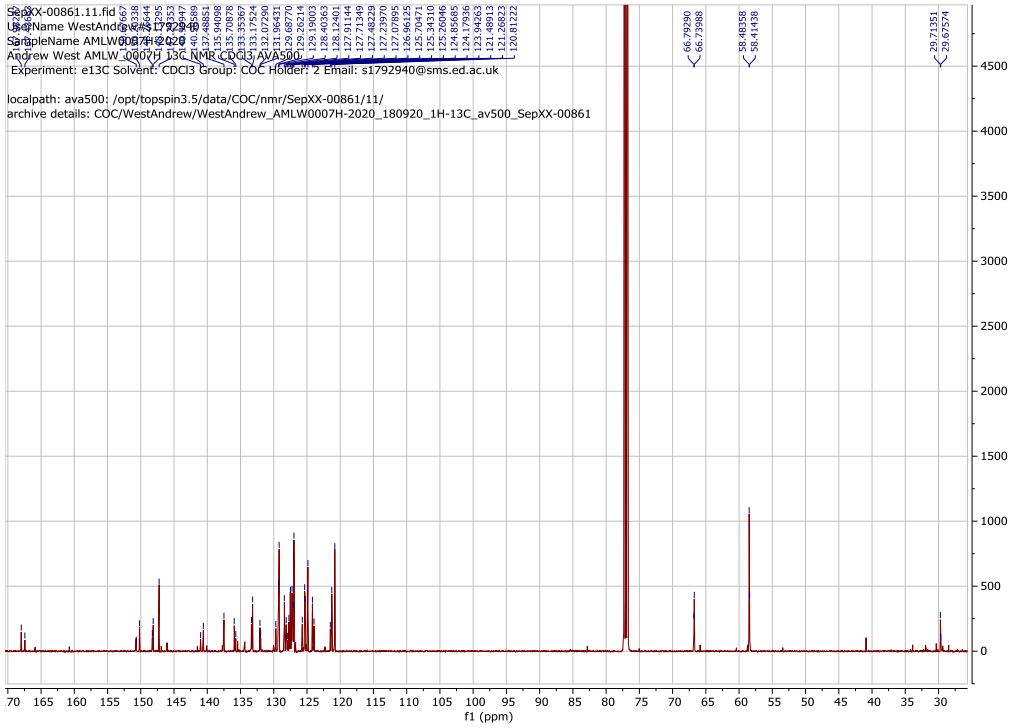

Step VII (2Me). 4-Methylphenyl 3-methyl-2-[6H,12H-5,11-methano dibenzo[b,f][1,5]diazocin-2-yl]benzoate

To a solution of 2-(4,4,5,5-Tetramethyl-1,3,2-dioxaborolan-2-yl)-6H,12H-5,11-methanodibenzo[b,f][1,5]diazocine (1 Eq, 0.50 g) dissolved in acetonitrile (10 mL), palladium(II)acetate (0.02 Eq, 0.0065 g), SPhos (0.04 Eq, 0.024 g) and methyl 2-bromo-3-(4-methyl phenol)-benzoate (1.5 Eq, 0.72 g) were added. To the resultant solution, 2 M potassium carbonate solution (2.5 Eq, 1.44 mL) was added before the mixture was heated to reflux under an inert nitrogen atmosphere and refluxed for 16 hours. The reaction mixture was diluted with ethyl acetate (250 mL) and washed with saturated sodium bicarbonate solution (2 x 150 mL) and brine (100 mL) before organics were dried over magnesium sulfate before solvent was removed under reduced pressure. The crude reaction mixture was then purified by flash chromatography (30% ethyl acetate in petroleum ether) yielding 4-Methylphenyl 3-methyl-2-[6H,12H-5,11-methano dibenzo[b,f][1,5]diazocin-2-yl]benzoate (0.22 g, 34%).

^{1}H NMR (500 MHz, $CDCl_3$) δ 7.75 (d, J = 7.6 Hz, 0.4H, minor conformer), d, J = 7.6 Hz, 0.6H, major conformer), 7.44 (t, 1H), 7.35 (t, 1H), 7.26-7.09 (m, 6H), 7.07-6.98 (m, 1H), 6.85 (s, 0.6H, major conformer), 6.81 (s, 0.4H, minor conformer), 6.67 (dd, 2H), 6.04 (d, 1H), 4.78 (dt, J = 16.7 Hz, 1.6H, major conformer), 4.69 (d, J = 16.8 Hz, 0.6H, minor conformer), 4.42-4.14 (m, 4H), 2.32 (s, 1.2H, minor conformer), 2.23 (s, 1.8H, major conformer), 2.17 (s, 1.8H, major conformer), 2.11 (s, 1.2H, minor conformer).

^{13}C NMR (126 MHz, $CDCl_3$) δ 168.2, 167.7, 148.4, 148.3, 148.2, 148.0, 147.3, 140.9, 140.5, 137.4, 137.4, 136.0, 135.7, 135.3, 134.8, 133.2, 133.1, 132.3, 132.1, 129.8, 129.7, 128.4, 128.1, 128.1, 127.8, 127.5, 127.5, 127.2, 127.0, 126.8, 125.4, 125.3, 124.8, 124.1, 123.9, 121.1, 120.9, 120.4, 66.8, 66.7, 58.5, 58.5, 58.4, 58.3, 20.8, 20.8, 20.7, 20.7. Two conformers. Some peaks occluded.

HRMS (ESI) obtained m/z 447.1886. (M+H+). Expected 447.2017.

^{1}H NMR

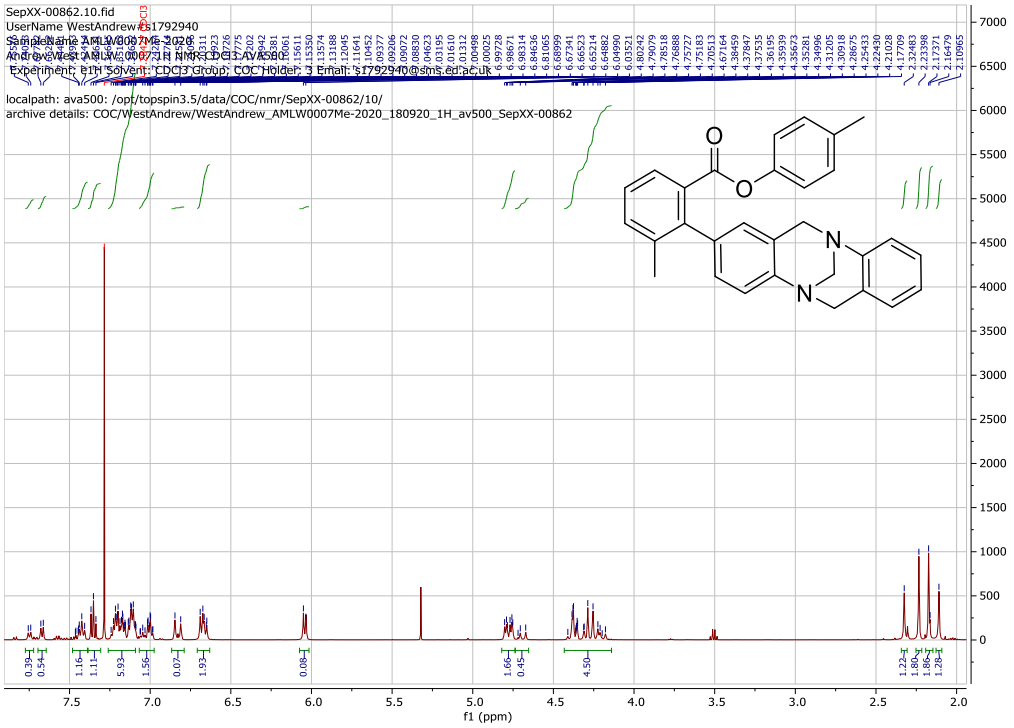

^{13}C NMR

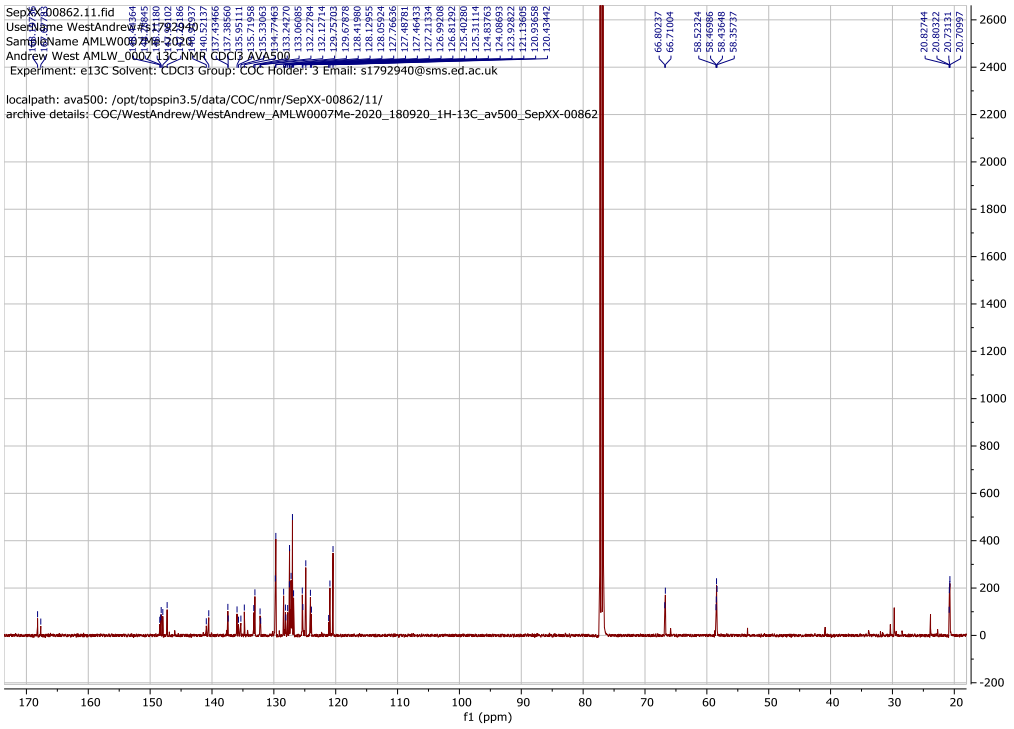

A.14 Appendix A references

1 Gung, B. W., Emenike, B. U., Lewis, M. & Kirschbaum, K. Quantification of CH···π Interactions: Implications on How Substituent Effects Influence Aromatic Interactions. *Chem. Eur. J.* **16**, 12357 – 12362 (2010).

2 Bauer, M., Bertario, A., Boccardi, G., Fontaine, X., Rao, R. & Verrier, D. Reproducibility of ^{1}H-NMR integrals: a collaborative study. *J. Pharma. Biomed. Anal.* **17**, 419-425 (1998).

Appendix B

Supporting information for chapter 3

Contents

B.1 Titration methodology

Host species were prepared as 0.1 M solutions in fresh benzene-d_6 before 500 μL of the resultant solution was transferred to a capped NMR tube. Guest species were prepared as 1.0 M solutions dissolved in 0.1 M solutions of the relevant host species in fresh benzene (d_6) and as 5.0 M solutions for partially weakly bound complexes. Such preparation affording a constant host species concentration throughout the experiment.

^{1}H NMR spectra were recorded of a Bruker AVA-400 spectrometer operating at 400 MHz equipped with a BBFO± room temperature probe both initially for just the host solution and then after each subsequent injection.

B.2 Tabulated values from fitting of titration data

Guest	Host	% bound	LogK global	K global	ΔG (kJ/mol)	mean ΔG	SD	% error	δ Free H	δ HG	Δδ H_a
C_6F_5I	Pyridine	63	-0.06	0.87	0.35	0.25	0.10	1.75	8.53	8.25	-0.28
C_6F_5I	Pyridine	65	-0.03	0.94	0.15	-	-	1.18	8.53	8.26	-0.26
C_6F_5I	1,8-Naphthyridine	56	0.26	1.83	-1.52	-1.68	0.16	1.19	8.88	8.77	-0.11
C_6F_5I	1,8-Naphthyridine	60	0.32	2.08	-1.84	-	-	0.81	8.88	8.77	-0.11
C_6F_5I	1,10-Phenanthroline	68	0.78	6.08	-4.55	-4.95	0.40	3.01	9.03	9.05	0.02
C_6F_5I	1,10-Phenanthroline	72	0.92	8.36	-5.35	-	-	1.73	9.02	9.05	0.03
C_6F_5I	1,2-Pyrazine	48	0.10	1.27	-0.60	-0.48	0.12	0.87	8.69	8.55	-0.14
C_6F_5I	1,2-Pyrazine	46	0.06	1.16	-0.37	-	-	1.00	8.68	8.54	-0.14
C_6F_5I	TEA	63	0.39	2.43	-2.23	-1.94	0.29	0.87	2.43	2.38	-0.05
C_6F_5I	TEA	58	0.28	1.92	-1.65	-	-	1.40	2.43	2.38	-0.05
C_6F_5I	TMEDA	80	0.77	5.85	-4.45	-4.75	0.30	1.36	2.36	2.29	-0.07
C_6F_5I	TMEDA	84	0.87	7.41	-5.05	-	-	1.81	2.36	2.29	-0.07
C_6F_5I	1,4,7-Triazacyclononane	91	1.16	14.60	-6.75	-6.10	0.65	0.71	2.57	2.30	-0.28
C_6F_5I	1,4,7-Triazacyclononane	86	0.94	8.70	-5.45	-	-	1.17	2.56	2.29	-0.27
N-Butylacetamide	Pyridine	46	0.11	1.30	-0.65	-0.60	0.05	1.22	8.53	8.30	-0.22
N-Butylacetamide	Pyridine	47	0.09	1.24	-0.54	-	-	1.63	8.52	8.31	-0.22
N-Butylacetamide	1,8-Naphthyridine	86	0.98	9.61	-5.70	-5.79	0.09	4.05	8.87	8.73	-0.14

N-Butylacetamide	1,8-Naphthyridine	87	1.01	10.29	-5.87	-	-	3.91	8.87	8.74	-0.13
N-Butylacetamide	1,10-Phenanthroline	76	0.96	9.20	-5.59	-5.38	0.21	0.63	9.03	8.80	-0.23
N-Butylacetamide	1,10-Phenanthroline	73	0.89	7.77	-5.16	-	-	2.50	9.02	8.79	-0.23
N-Butylacetamide	1,2-Pyrazine	48	1.02	10.53	-5.93	-5.94	0.01	5.25	8.68	8.67	-0.01
N-Butylacetamide	1,2-Pyrazine	48	1.03	10.63	-5.95	-	-	9.16	8.68	8.67	-0.01
N-Butylacetamide	TEA	9	-0.81	0.15	4.72	4.96	0.24	2.85	0.97	0.35	-0.62
N-Butylacetamide	TEA	8	-0.90	0.13	5.21	-	-	3.02	0.97	0.22	-0.75
N-Butylacetamide	TMEDA	22	-0.37	0.43	2.12	2.05	0.07	2.57	2.35	1.96	-0.40
N-Butylacetamide	TMEDA	23	-0.34	0.46	1.98	-	-	0.88	2.35	1.97	-0.39
N-Butylacetamide	1,4,7-Triazacyclononane	43	0.33	2.14	-1.92	-2.13	0.21	4.43	2.56	2.32	-0.24
N-Butylacetamide	1,4,7-Triazacyclononane	47	0.40	2.54	-2.35	-	-	3.30	2.56	2.34	-0.23
N,N'-Dibutylurea	Pyridine	7	-0.27	0.54	1.57	0.43	1.14	3.61	8.52	8.07	-0.45
N,N'-Dibutylurea	Pyridine	17	0.12	1.33	-0.71	-	-	2.80	8.52	8.33	-0.19
N,N'-Dibutylurea	1,8-Naphthyridine	78	1.39	24.53	-8.06	-7.62	0.44	1.54	8.87	8.72	-0.15
N,N'-Dibutylurea	1,8-Naphthyridine	70	1.24	17.34	-7.19	-	-	4.01	8.87	8.70	-0.16
N,N'-Dibutylurea	1,10-Phenanthroline	68	1.13	11.76	-6.21	-6.51	0.30	2.56	9.02	8.86	-0.17
N,N'-Dibutylurea	1,10-Phenanthroline	68	1.17	14.96	-6.82	-	-	2.23	9.02	8.88	-0.14
N,N'-Dibutylurea	1,2-Pyrazine	49	1.31	20.31	-7.59	-8.52	0.93	7.42	8.68	8.64	-0.04
N,N'-Dibutylurea	1,2-Pyrazine	65	1.63	42.66	-9.46	-	-	10.06	8.68	10.06	-0.03
N,N'-Dibutylurea	TEA	2	-0.90	0.13	5.20	5.22	0.02	6.87	2.40	1.70	-0.70
N,N'-Dibutylurea	TEA	2	-0.90	0.13	5.23	-	-	9.86	2.40	1.66	-0.74
N,N'-Dibutylurea	TMEDA	31	0.47	2.97	-2.74	-3.33	0.59	1.23	2.12	1.68	-0.44
N,N'-Dibutylurea	TMEDA	41	0.68	4.75	-3.93	-	-	1.70	2.12	1.79	-0.33
N,N'-Dibutylurea	1,4,7-Triazacyclononane	74	1.31	20.24	-7.58	-7.29	0.29	3.05	2.58	2.54	-0.03
N,N'-Dibutylurea	1,4,7-Triazacyclononane	70	1.21	16.07	-7.00	-	-	3.20	2.57	2.54	-0.04
N,N'-Dibutylthiourea	Pyridine	30	0.27	1.86	-1.57	-1.91	0.35	0.70	8.52	8.14	-0.39
N,N'-Dibutylthiourea	Pyridine	36	0.39	2.45	-2.26	-	-	3.35	8.52	8.19	-0.33
N,N'-Dibutylthiourea	1,8-Naphthyridine	92	1.73	53.58	-10.03	-8.66	1.37	1.25	8.87	8.60	-0.27

N,N'-Dibutylthiourea	1,8-Naphthyridine	80	1.26	18.12	-7.30	-	-	2.94	8.87	8.73	-0.14
N,N'-Dibutylthiourea	1,10-Phenanthroline	91	1.68	47.53	-9.73	-9.89	0.16	0.86	9.02	8.72	-0.30
N,N'-Dibutylthiourea	1,10-Phenanthroline	92	1.73	53.97	-10.05	-	-	2.04	9.02	8.72	-0.29
N,N'-Dibutylthiourea	1,2-Pyrazine	81	1.27	18.72	-7.38	-7.58	0.20	2.06	8.69	8.55	-0.14
N,N'-Dibutylthiourea	1,2-Pyrazine	83	1.34	21.99	-7.79	-	-	2.34	8.69	8.56	-0.13
N,N'-Dibutylthiourea	TEA	5	-0.64	0.23	3.71	5.11	1.40	5.26	0.96	0.35	-0.62
N,N'-Dibutylthiourea	TEA	2	-1.12	0.08	6.50	-	-	2.75	0.97	0.48	-1.95
N,N'-Dibutylthiourea	TMEDA	48	0.60	3.99	-3.49	-2.97	0.52	0.61	2.12	1.84	-0.28
N,N'-Dibutylthiourea	TMEDA	38	0.42	2.64	-2.45	-	-	1.27	2.12	1.76	-0.36
N,N'-Dibutylthiourea	1,4,7-Triazacyclononane	83	1.34	22.04	-7.79	-7.79	0.00	0.86	2.56	2.45	-0.11
N,N'-Dibutylthiourea	1,4,7-Triazacyclononane	83	1.34	22.06	-7.79	-	-	0.88	2.56	2.45	-0.11

B.3 Binding isotherm plots for HG systems

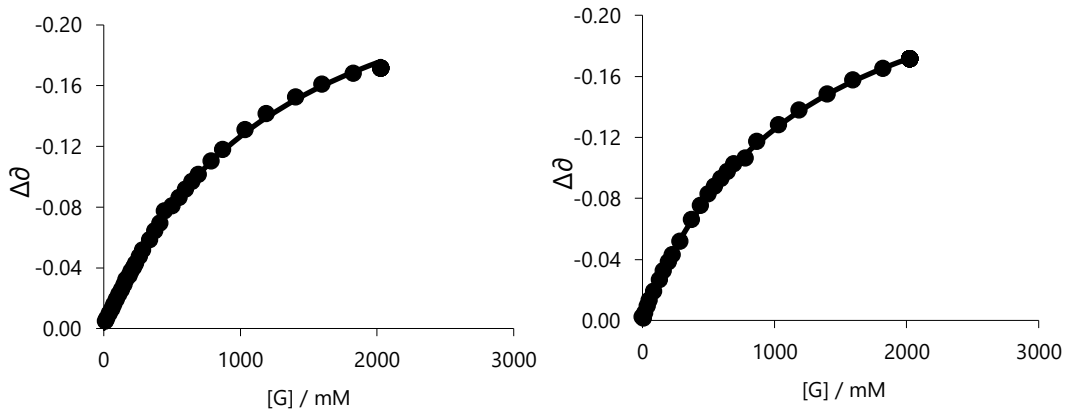

B.3.1 Titrations of C_6F_5I : Pyridine in benzene-d_6

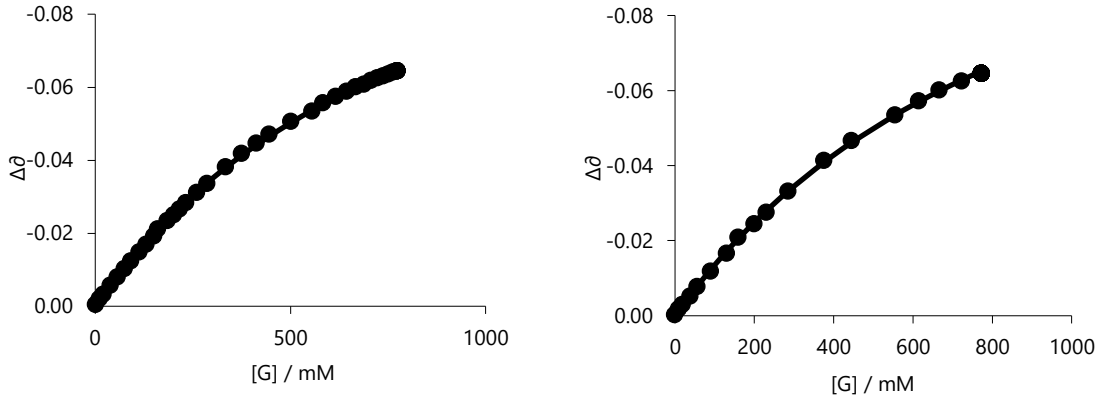

B.3.2 Titrations of C_6F_5I : 1,2-Pyrazine in benzene-d_6

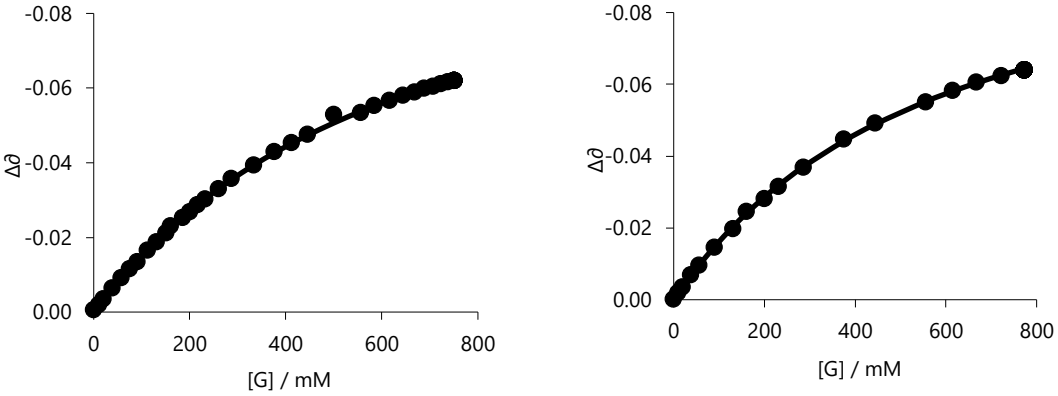

B.3.3 Titrations of C_6F_5I : 1,8-Naphthyridine in benzene-d_6

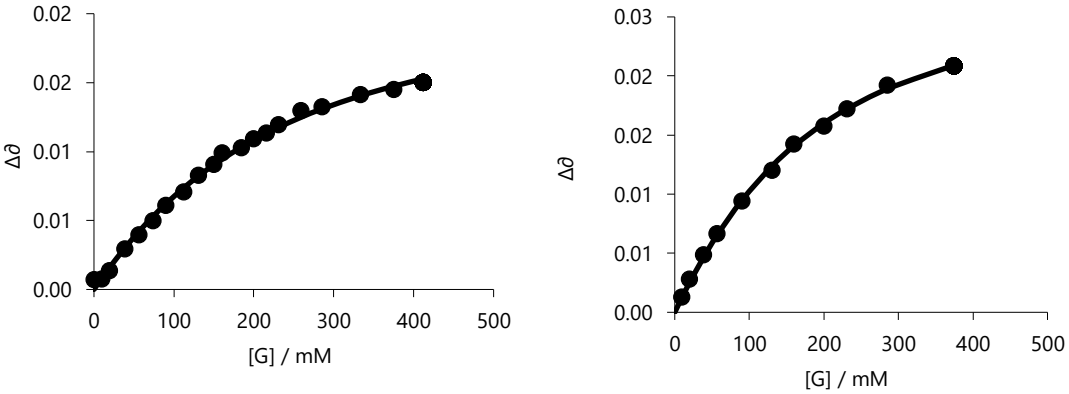

B.3.4 Titrations of C_6F_5I : 1,10-Phenanthroline in benzene-d_6

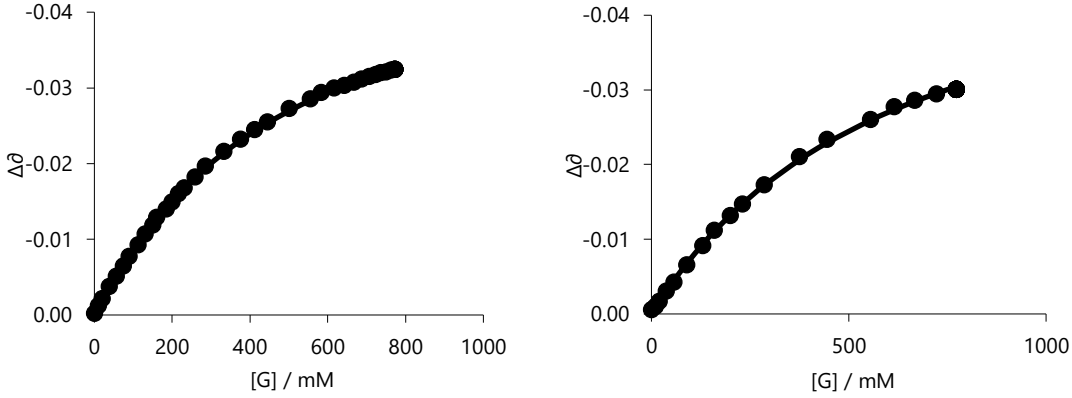

B.3.5 Titrations of C6F5I : Triethylamine in benzene-d6

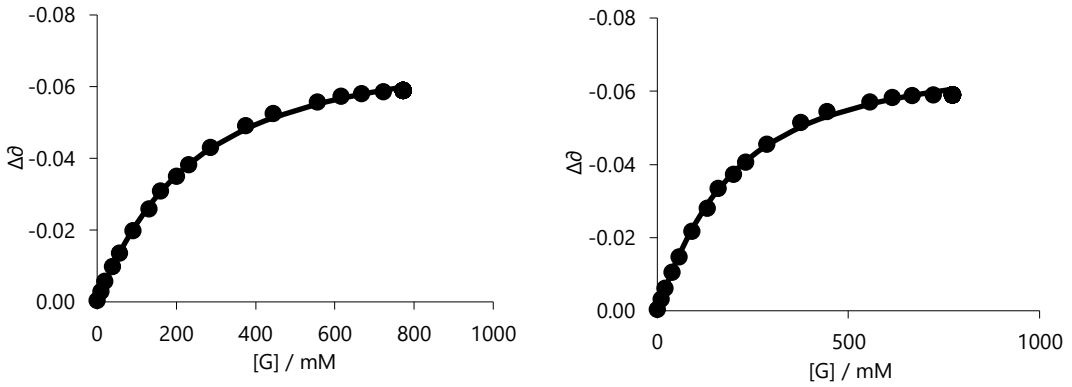

B.3.6 Titrations of C_6F_5I : Tetramethylethylenediamine in benzene-d_6

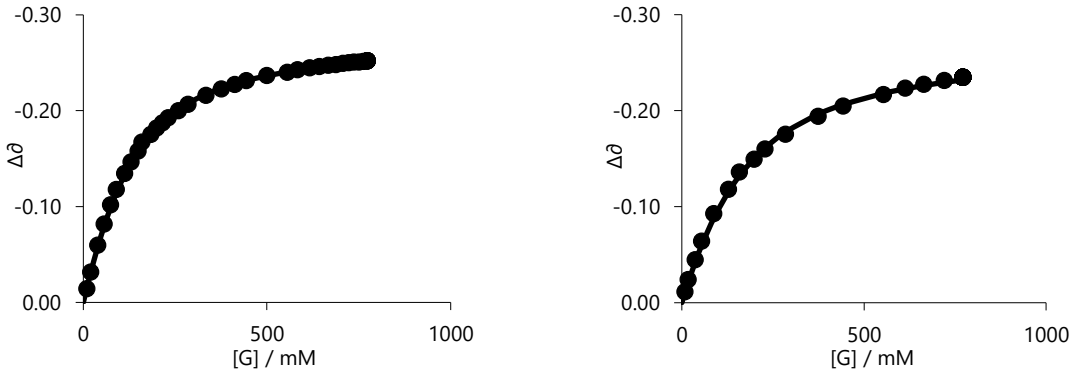

B.3.7 Titrations of C_6F_5I : 1,4,7-triazacyclononane in benzene-d_6

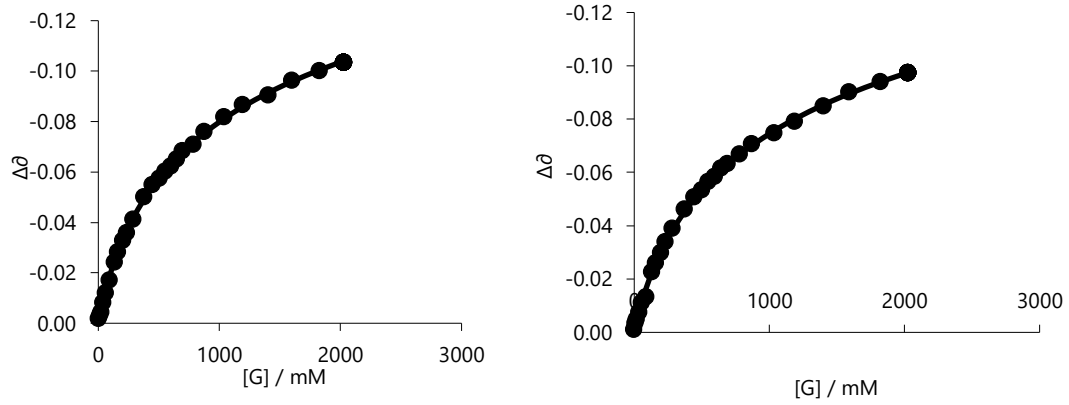

B.3.8 Titrations of Butylacetamide : Pyridine in benzene-d_6

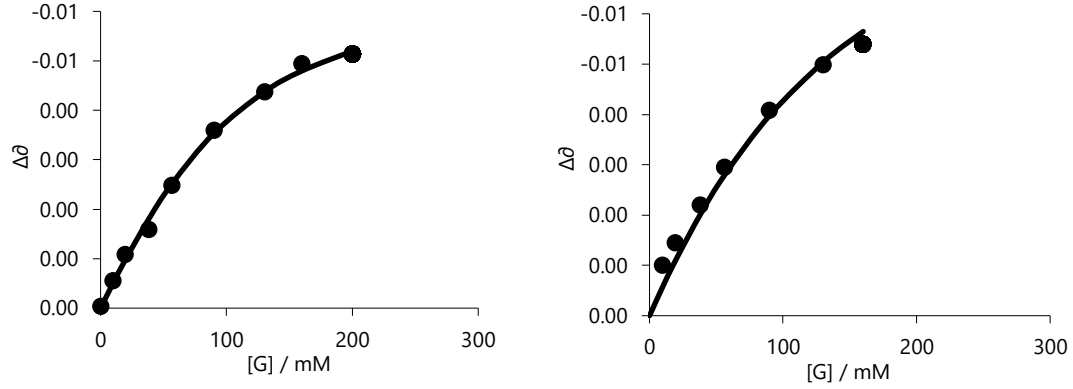

B.3.9 Titrations of Butylacetamide : 1,2-Pyrazine in benzene-d_6

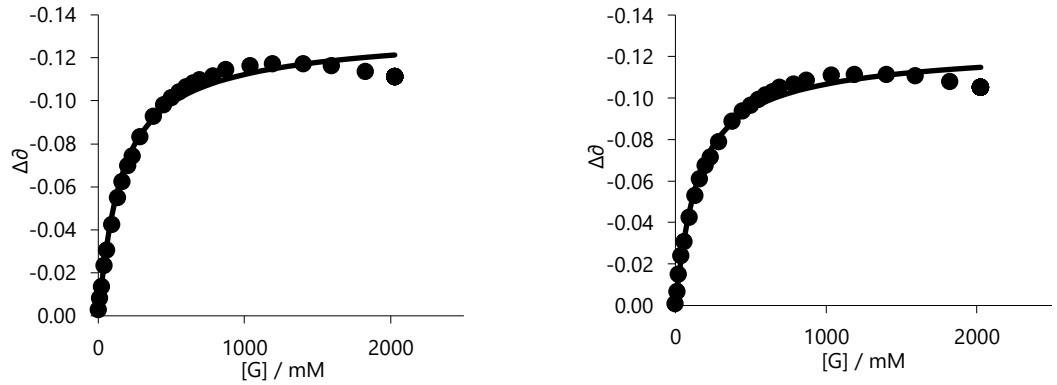

B.3.10 Titrations of Butylacetamide : 1,8-Naphthyridine in benzene-d_6

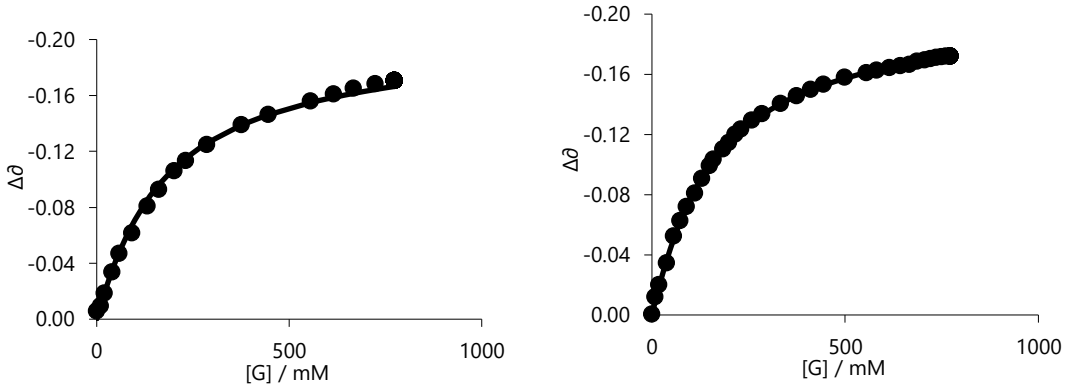

B.3.11 Titrations of Butylacetamide : 1,10-Phenanthroline in benzene-d_6

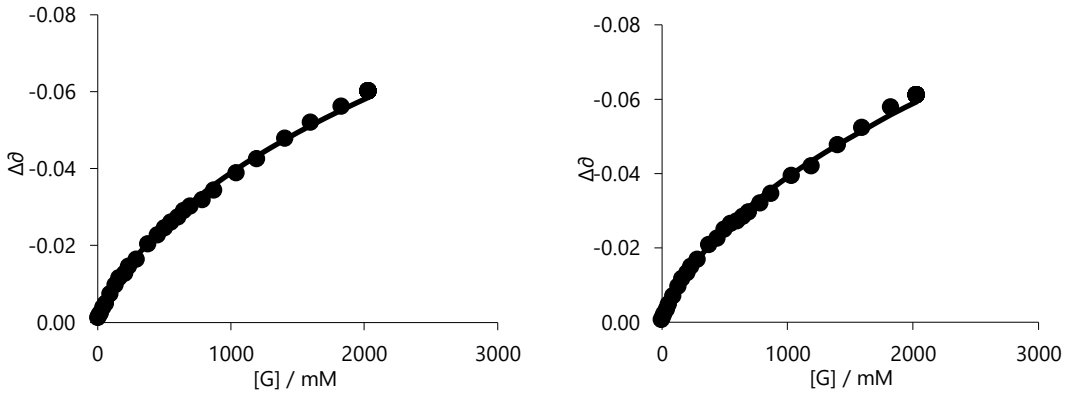

B.3.12 Titrations of Butylacetamide : Triethylamine in benzene-d_6

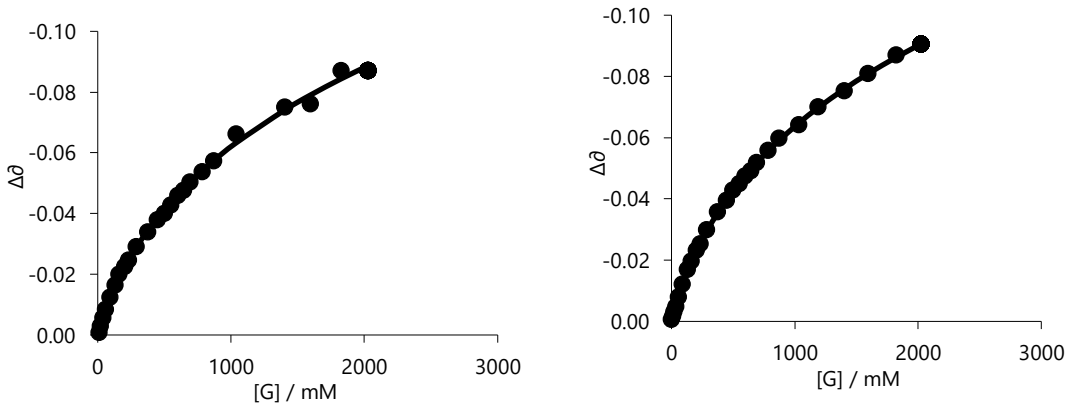

B.3.13 Titrations of Butylacetamide : Tetramethylethylenediamine in benzene-d_6

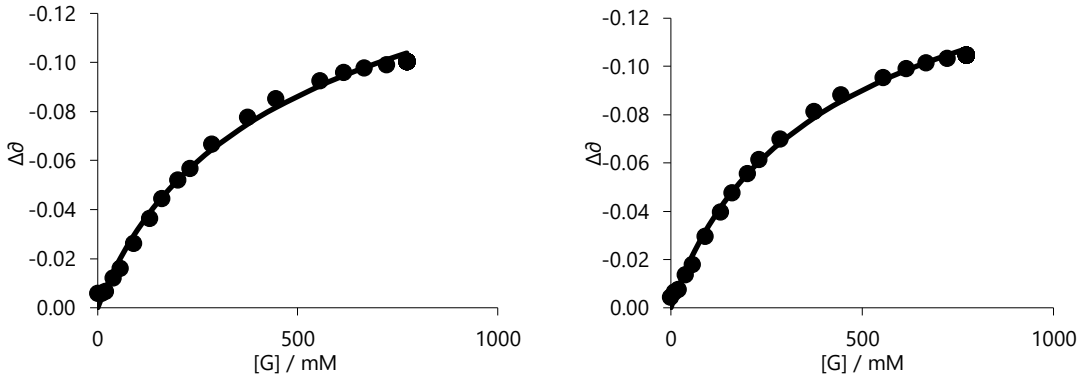

B.3.14 Titrations of Butylacetamide : 1,4,7-triazacyclononane in benzene-d_6

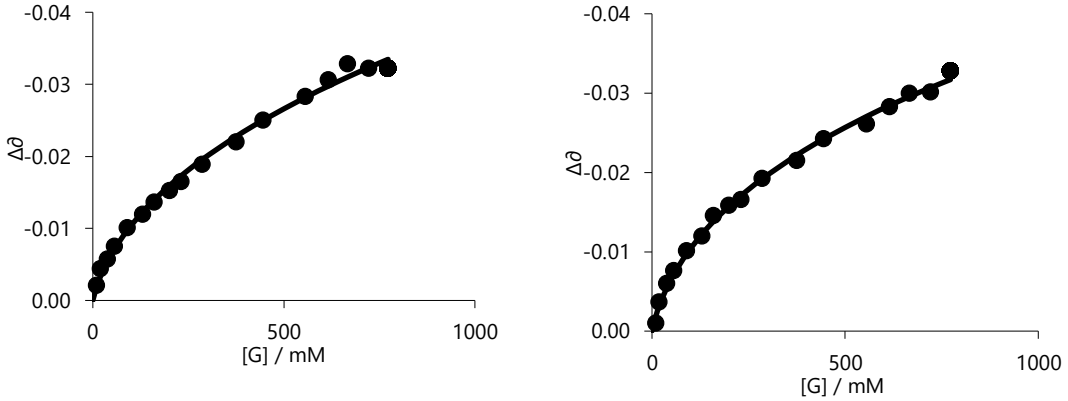

B.3.15 Titrations of *N*,*N*'-Dibutylurea : Pyridine in benzene-d_6

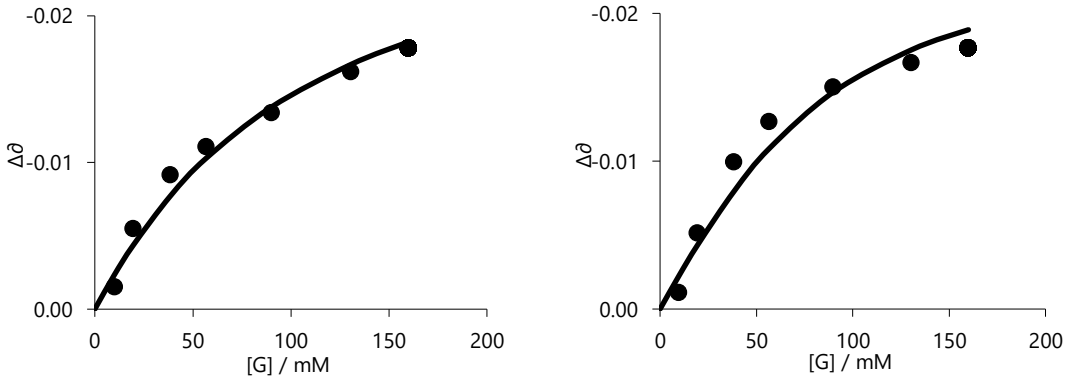

B.3.16 Titrations of *N*,*N*'-Dibutylurea : 1,2-Pyrazine in benzene-d_6

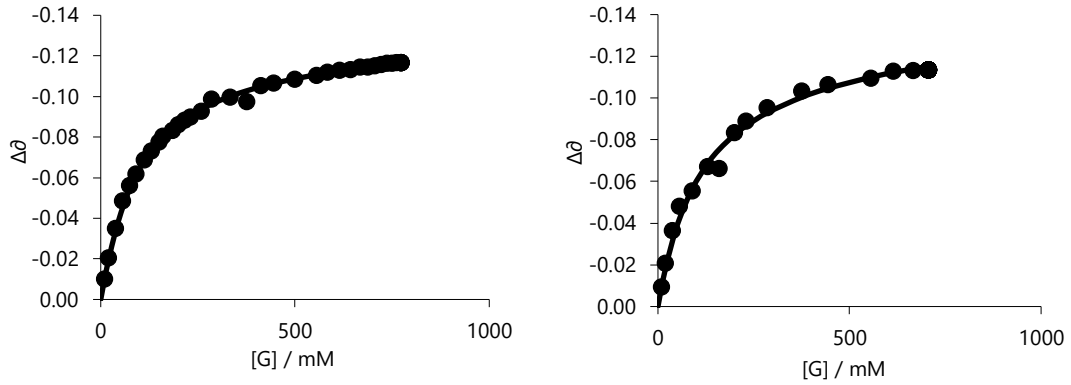

B.3.17 Titrations of *N*,*N*'-Dibutylurea : 1,8-Naphthyridine in benzene-d_6

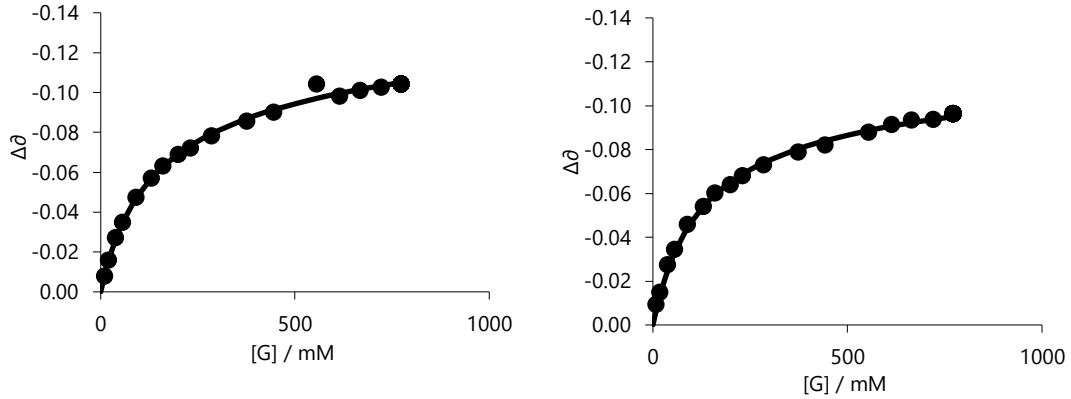

B.3.18 Titrations of *N*,*N*'-Dibutlyurea : 1,10-Phenanthroline in benzene-d_6

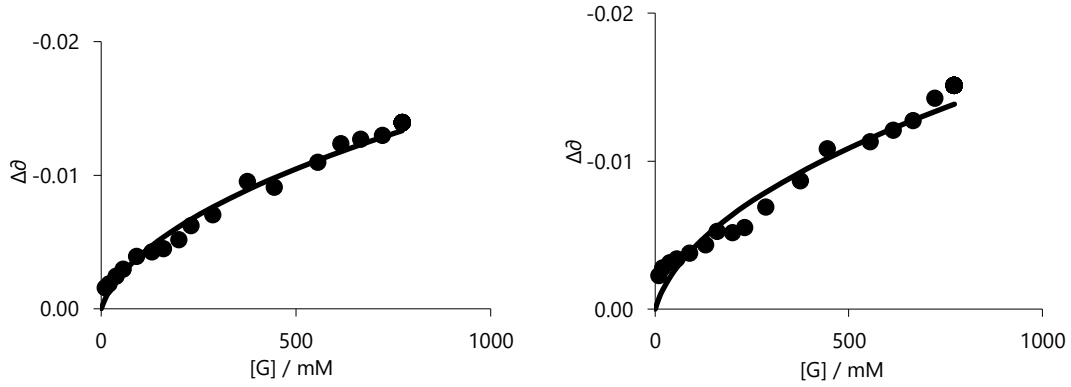

B.3.19 Titrations of N,N'-Dibutylurea : Triethylamine in benzene-d_6

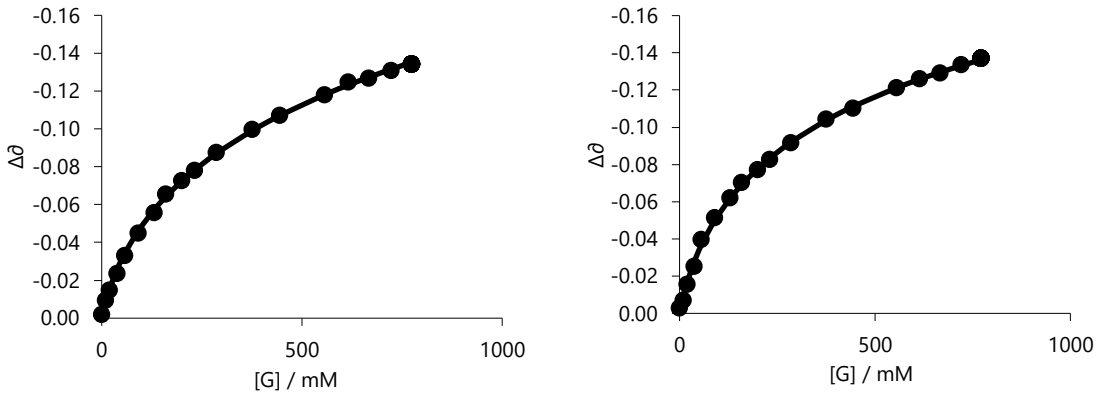

B.3.20 Titrations of N,N'-Dibutylurea : Tetramethylethylenediamine in benzene-d6

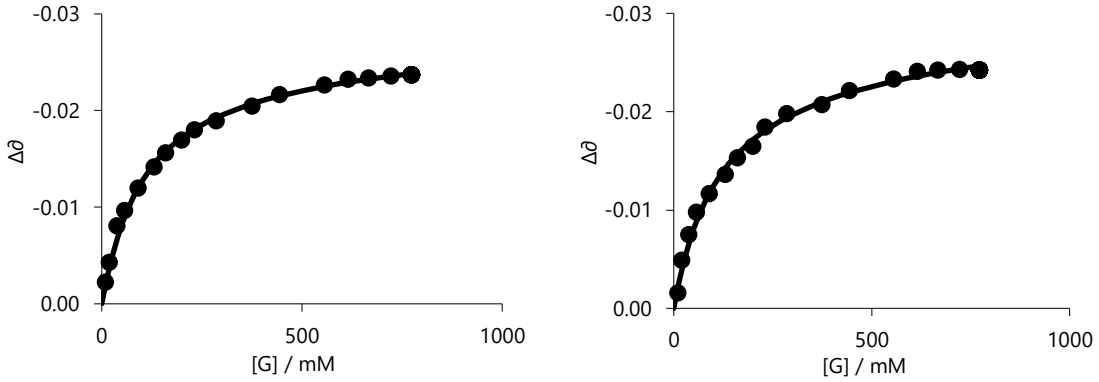

B.3.21 Titrations of *N*,*N*'-Dibutylurea : 1,4,7-triazacyclononane in benzene-d_6

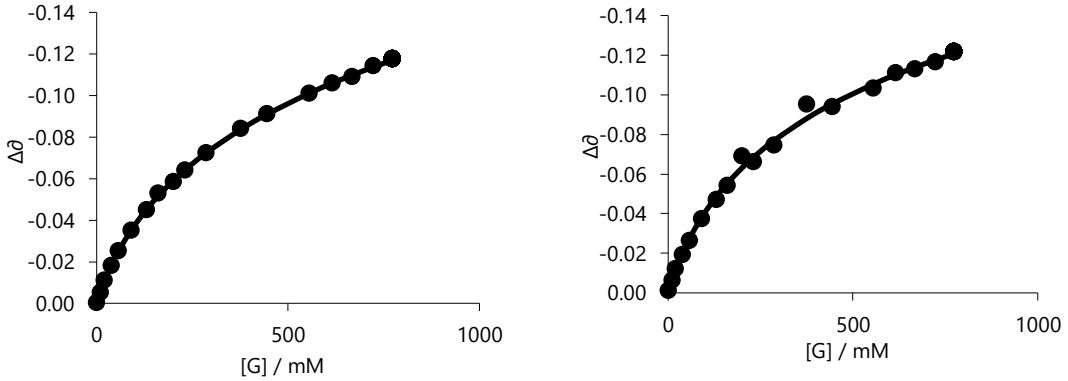

B.3.22 Titrations of *N*,*N*'-Dibutylthiourea : Pyridine in benzene-d_6

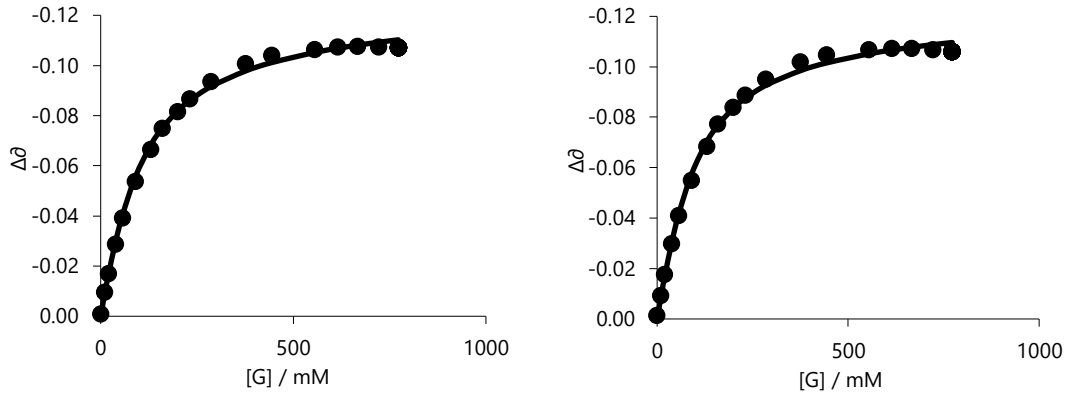

B.3.23 Titrations of N,N'-Dibutylthiourea : 1,2-Pyrazine in benzene-d_6

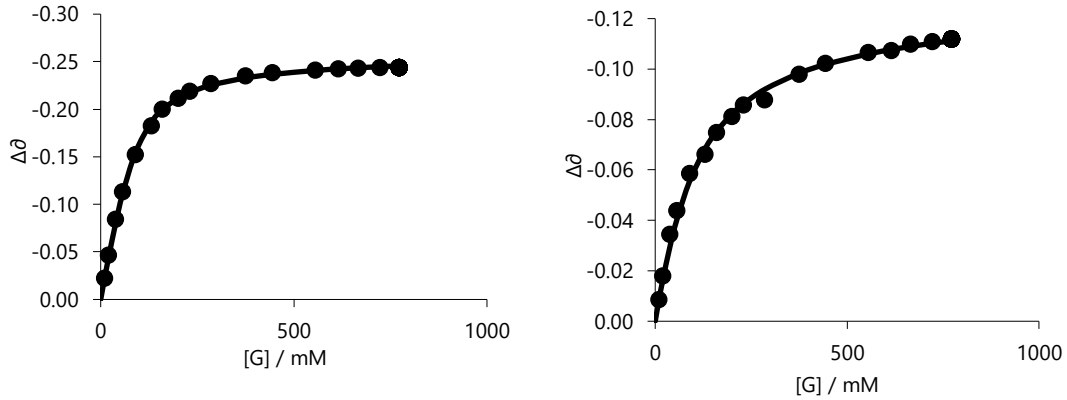

B.3.24 Titrations of *N,N*'-Dibutylthiourea : 1,8-Naphthyridine in benzene-d_6

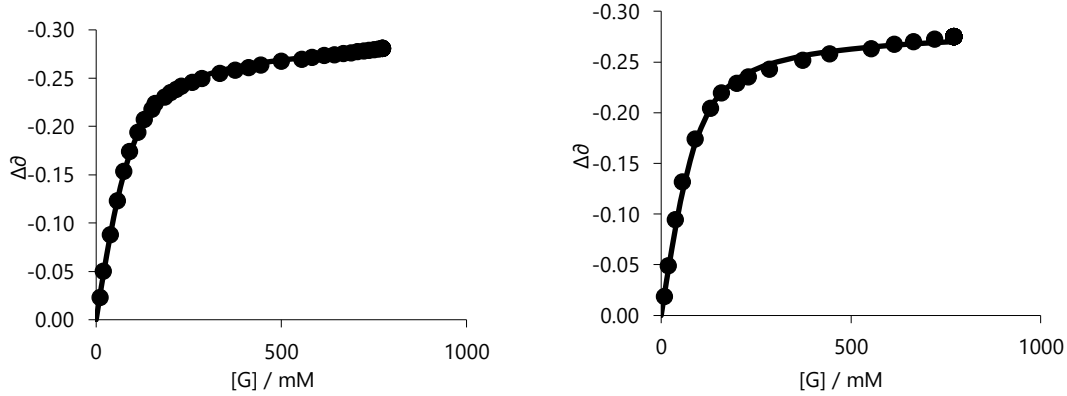

B.3.25 Titrations of N,N'-Dibutylthiourea : 1,10-Phenanthroline in benzene-d_6

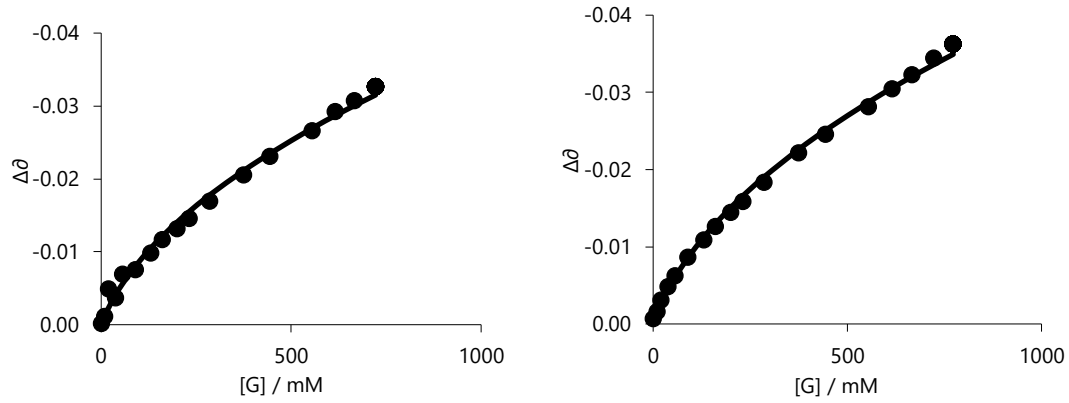

B.3.26 Titrations of N,N'-Dibutylthiourea : Triethylamine in benzene-d_6

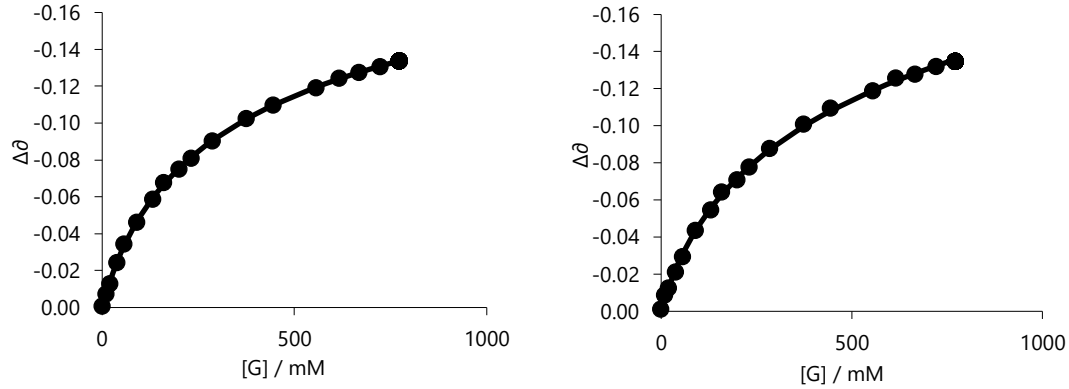

B.3.27 Titrations of *N,N*'-Dibutylthiourea : Tetramethylethylenediamine in benzene-d_6

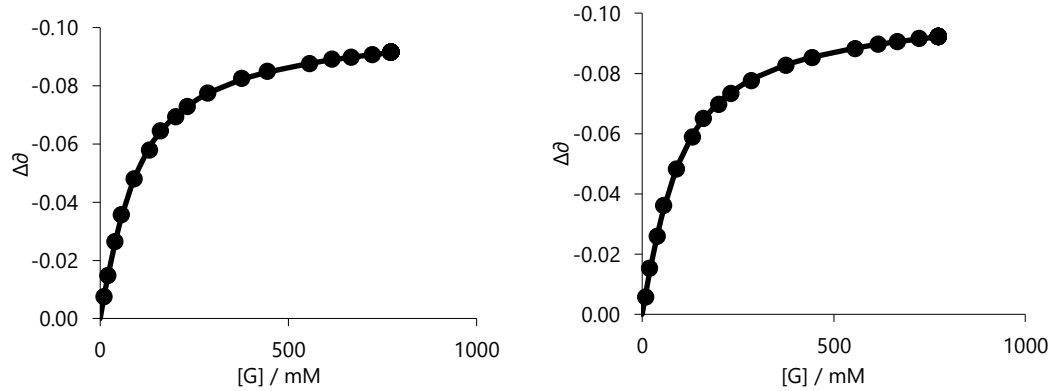

B.3.28 Titrations of *N,N*'-Dibutylthiourea : 1,4,7-triazacyclononane in benzene-d_6

B.4 Computational methodologies

All geometry minimizations were concluded using the Spartan ’14 program using either the B3LYP or ωB97X-D methods were appropriate and the 6-311G* basis set. Counterpoise corrected BSSE calculations and all SAPT calculations were conducted using the Psi4 software package.

Due to the inclusion of iodine atoms in computational studies; the 6-311G* basis set was manually defined for Psi4 calculations as shown below. Basis set provided by https://www.basissetexchange.org/. 6-311G* basis set was last updated 19/02/2015 at time of writing.

```
****
H     0
S    3   1.00
     33.86500               0.0254938
      5.094790              0.190373
      1.158790              0.852161
S    1   1.00
      0.325840              1.000000
S    1   1.00
      0.102741              1.000000
****
C     0
S    6   1.00
   4563.240                 0.00196665
    682.0240                0.0152306
    154.9730                0.0761269
     44.45530               0.2608010
     13.02900               0.6164620
      1.827730              0.2210060
SP   3   1.00
     20.96420               0.114660              0.0402487
      4.803310              0.919999              0.237594
      1.459330             -0.00303068            0.815854
SP   1   1.00
      0.4834560             1.000000              1.000000
SP   1   1.00
      0.1455850             1.000000              1.000000
D    1   1.00
      0.626                 1.000000
****
N     0
S    6   1.00
   6293.480                 0.00196979
    949.0440                0.0149613
    218.7760                0.0735006
     63.69160               0.2489370
     18.82820               0.6024600
      2.720230              0.2562020
SP   3   1.00
     30.63310               0.111906              0.0383119
      7.026140              0.921666              0.237403
```

```
      2.112050              -0.00256919             0.817592
SP    1   1.00
      0.684009               1.000000               1.000000
SP    1   1.00
      0.200878               1.000000               1.000000
D     1   1.00
      0.913                  1.000000
****
O     0
S     6   1.00
   8588.500                  0.00189515
   1297.230                  0.0143859
    299.2960                 0.0707320
     87.37710                0.2400010
     25.67890                0.5947970
      3.740040               0.2808020
SP    3   1.00
     42.11750                0.113889               0.0365114
      9.628370               0.920811               0.237153
      2.853320              -0.00327447             0.819702
SP    1   1.00
      0.905661               1.000000               1.000000
SP    1   1.00
      0.255611               1.000000               1.000000
D     1   1.00
      1.292                  1.000000
****
F     0
S     6   1.00
  11427.10                   0.00180093
   1722.350                  0.0137419
    395.7460                 0.0681334
    115.1390                 0.2333250
     33.60260                0.5890860
      4.919010               0.2995050
SP    3   1.00
     55.44410                0.114536               0.0354609
     12.63230                0.920512               0.237451
      3.717560              -0.00337804             0.820458
SP    1   1.00
      1.165450               1.000000               1.000000
SP    1   1.00
      0.321892               1.000000               1.000000
D     1   1.00
      1.750                  1.000000
****
S     0
S     6   1.00
  93413.4                    0.000743
  13961.7                    0.005793
   3169.91                   0.029954
    902.456                  0.119028
    297.158                  0.368432
    108.702                  0.577299
S     3   1.00
    108.702                  0.143186
     43.1553                 0.624465
     18.1079                 0.283366
S     1   1.00
      5.56009                1.000000
```

```
S    1   1.00
      2.13183                1.000000
S    1   1.00
      0.420403               1.000000
S    1   1.00
      0.136045               1.000000
P    4   1.00
    495.040                 0.008309
    117.221                 0.064024
     37.7749                0.277614
     14.0584                0.745076
P    2   1.00
      5.56574                0.613712
      2.26297                0.443818
P    1   1.00
      0.807994               1.000000
P    1   1.00
      0.277460               1.000000
P    1   1.00
      0.077141               1.000000
D    1   1.00
      0.6500000              1.0000000
****
Cl     0
S    6   1.00
 105819.0                   0.000738
  15872.00                  0.005718
   3619.650                 0.029495
   1030.800                 0.117286
    339.9080                0.362949
    124.5380                0.584149
S    3   1.00
    124.5380                0.134177
     49.51350               0.624250
     20.80560               0.291756
S    1   1.00
      6.583460               1.000000
S    1   1.00
      2.564680               1.000000
S    1   1.00
      0.559763               1.000000
S    1   1.00
      0.183273               1.000000
P    5   1.00
    589.7760                0.002391
    139.8490                0.018504
     45.14130               0.081377
     16.87330               0.221552
      6.741100              0.772569
P    2   1.00
      6.741100              -1.572244
      2.771520               0.992389
P    1   1.00
      1.023870               1.000000
P    1   1.00
      0.381368               1.000000
P    1   1.00
      0.109437               1.000000
D    1   1.00
      0.7500000              1.0000000
```

```
****
Br     0
S    6   1.00
 439700.0                    0.0008130
  66030.00                   0.0062850
  15140.00                   0.0319200
   4317.000                  0.1288000
   1414.000                  0.3946000
    523.9000                 0.5413000
S    3   1.00
    523.9000                 0.1831
    207.7000                 0.6176
     86.54000                0.2538
S    1   1.00
     30.52                   1.000000
S    1   1.00
     12.98                   1.000000
S    1   1.00
      4.412                  1.000000
S    1   1.00
      1.862                  1.000000
S    1   1.00
      0.3932                 1.000000
S    1   1.00
      0.1400                 1.000000
P    3   1.00
   2957.000                  0.02226
    700.3000                 0.18020
    224.6000                 0.86240
P    3   1.00
     82.59                   0.3440
     33.19                   0.5071
     14.20                   0.2590
P    3   1.00
     14.20                   0.07965
      7.438                  0.3734
      3.526                  0.6049
P    1   1.00
      1.595000               1.000000
P    1   1.00
      0.846200               1.000000
P    1   1.00
      0.318600               1.000000
P    1   1.00
      0.109600               1.000000
D    4   1.00
    134.8                    0.01831
     36.39                   0.13500
     12.16                   0.42610
      4.341                  0.60430
D    1   1.00
      1.535000               1.000000
D    1   1.00
      0.451000               1.000000
****
I     0
S    5   1.00
 444750.0                    0.00089
  66127.00                   0.00694
  14815.00                   0.03609
```

```
   4144.900                  0.13568
   1361.200                  0.33878
S    2   1.00
    508.4400                 0.43659
    209.5900                 0.18375
S    1   1.00
     81.959                  1.00000
S    1   1.00
     36.805                  1.00000
S    1   1.00
     13.495                  1.00000
S    1   1.00
      6.8859                 1.00000
S    1   1.00
      2.5520                 1.00000
S    1   1.00
      1.2088                 1.00000
S    1   1.00
      0.2734                 1.00000
S    1   1.00
      0.1009                 1.00000
P    4   1.00
   2953.600                  0.01221
    712.6100                 0.08587
    236.7100                 0.29493
     92.63100                0.47849
P    1   1.00
     39.73200                1.00000
P    1   1.00
     17.27300                1.000000
P    1   1.00
      7.957000               1.000000
P    1   1.00
      3.152900               1.000000
P    1   1.00
      1.332800               1.000000
P    1   1.00
      0.494700               1.000000
P    1   1.00
      0.216000               1.000000
P    1   1.00
      0.082930               1.000000
D    3   1.00
    261.9500                 0.03144
     76.73400                0.19028
     27.55100                0.47247
D    1   1.00
     10.60600                1.000000
D    1   1.00
      3.421700               1.000000
D    1   1.00
      1.137000               1.000000
D    1   1.00
      0.302000               1.000000
****
```

B.5 Tabulated B3LYP/6-311G* (BSSE=CP) calculated energies and interaction energies

Bond Donor	Bond Acceptor	Complex energy (kJ/mol)	Donor energy (kJ/mol)	Acceptor energy (kJ/mol)	ΔE (kJ/mol)
C_6F_5I	Pyridine	-20725028.0	-20072635.7	-652365.1	-20.9
C_6F_5I	1,8-Naphthyridine	-21170840.5	-20072635.7	-1098178.5	-20.9
C_6F_5I	1,10-Phenanthroline	-21574567.3	-20072635.7	-1501903.3	-23.0
C_6F_5I	1,2--Pyrazine	-20767043.5	-20072635.7	-694382.8	-19.7
C_6F_5I	TEA	-20840976.3	-20072635.7	-768316.9	-21.0
C_6F_5I	TMEDA	-20986325.6	-20072635.7	-913667.3	-19.4
C_6F_5I	1,4,7-Triazacyclononane	-21128514.8	-20072635.7	-1055839.8	-29.3
N-Butylacetamide	Pyridine	-1615222.9	-962829.2	-652365.1	-24.0
N-Butylacetamide	1,8-Naphthyridine	-2061040.0	-962829.2	-1098178.5	-28.6
N-Butylacetamide	1,10-Phenanthroline	-2464769.5	-962829.2	-1501903.3	-32.9
N-Butylacetamide	1,2-Pyrazine	-1657239.7	-962829.2	-694382.8	-24.5
N-Butylacetamide	TEA	-1731159.1	-962829.2	-768316.9	-11.9
N-Butylacetamide	TMEDA	-1876519.4	-962829.2	-913667.3	-20.0
N-Butylacetamide	1,4,7-Triazacyclononane	-2018706.9	-962829.2	-1055839.8	-24.8
N,N'-Dibutylurea	Pyridine	-2070558.0	-1418160.4	-652365.1	-28.4
N,N'-Dibutylurea	1,8-Naphthyridine	-2516382.7	-1418160.4	-1098178.5	-40.2
N,N'-Dibutylurea	1,10-Phenanthroline	-2920108.5	-1418160.4	-1501903.3	-42.9
N,N'-Dibutylurea	1,2-Pyrazine	-2112582.0	-1418160.4	-694382.8	-34.2
N,N'-Dibutylurea	TEA	-2186491.6	-1418160.4	-768316.9	-18.2
N,N'-Dibutylurea	TMEDA	-2331863.6	-1418160.4	-913667.3	-32.6
N,N'-Dibutylurea	1,4,7-Triazacyclononane	-2474089.5	-1418160.4	-1055839.8	-36.3
N,N'-Dibutylthiourea	Pyridine	-2918013.0	-2265610.8	-652365.1	-32.5
N,N'-Dibutylthiourea	1,8-Naphthyridine	-3363838.6	-2265610.8	-1098178.5	-45.8
N,N'-Dibutylthiourea	1,10-Phenanthroline	-3767568.3	-2265610.8	-1501903.3	-52.9
N,N'-Dibutylthiourea	1,2-Pyrazine	-2960037.4	-2265610.8	-694382.8	-38.4
N,N'-Dibutylthiourea	TEA	-3033938.8	-2265610.8	-768316.9	-11.1
N,N'-Dibutylthiourea	TMEDA	-3179320.0	-2265610.8	-913667.3	-40.7
N,N"-Dibutylthiourea	1,4,7-Triazacyclononane	-3321541.3	-2265610.8	-1055839.8	-45.6

B.6 Tabulated ωB97X-D/6-311G* (BSSE=CP) calculated energies and interaction energies

Bond Donor	Bond Acceptor	Complex energy (kJ/mol)	Donor energy (kJ/mol)	Acceptor energy (kJ/mol)	Δ*E* (kJ/mol)
C_6F_5I	Pyridine	-20723611.1	-20071473.1	-652103.6	-29.2
C_6F_5I	1,8-Naphthyridine	-21169256.7	-20071473.1	-1097747.9	-31.4
C_6F_5I	1,10-Phenanthroline	-21572836.4	-20071473.1	-1501321.1	-38.5
C_6F_5I	1,2--Pyrazine	-20765609.8	-20071473.1	-694105.3	-27.1
C_6F_5I	TEA	-20839579.5	-20071473.1	-768060.8	-40.1
C_6F_5I	TMEDA	-20984881.6	-20071473.1	-913365.3	-43.0
C_6F_5I	1,4,7-Triazacyclononane	-21127037.3	-20071473.1	-1055502.6	-53.4
N-Butylacetamide	Pyridine	-1614641.1	-962496.2	-652103.6	-36.9
N-Butylacetamide	1,8-Naphthyridine	-2060288.8	-962496.2	-1097747.9	-42.2
N-Butylacetamide	1,10-Phenanthroline	-2463875.6	-962496.2	-1501321.1	-56.6
N-Butylacetamide	1,2-Pyrazine	-1656639.4	-962496.2	-694105.3	--34.9
N-Butylacetamide	TEA	-1730605.0	-962496.2	-768060.8	-51.7
N-Butylacetamide	TMEDA	-1875900.4	-962496.2	-913365.3	-48.2
N-Butylacetamide	1,4,7-Triazacyclononane	-2018068.7	-962496.2	-1055502.6	-55.1
N,N'-Dibutylurea	Pyridine	-2069837.4	-1417683.3	-652103.6	-47.2
N,N'-Dibutylurea	1,8-Naphthyridine	-2515493.9	-1417683.3	-1097747.9	-59.5
N,N'-Dibutylurea	1,10-Phenanthroline	-2919075.1	-1417683.3	-1501321.1	-71.6
N,N'-Dibutylurea	1,2-Pyrazine	-2111839.9	-1417683.3	-694105.3	-46.3
N,N'-Dibutylurea	TEA	-2185791.7	-1417683.3	-768060.8	-55.8
N,N'-Dibutylurea	TMEDA	-2331125.6	-1417683.3	-913365.3	-79.0
N,N'-Dibutylurea	1,4,7-Triazacyclononane	-2473311.4	-1417683.3	-1055502.6	-76.6
N,N'-Dibutylthiourea	Pyridine	-2917216.3	-2265058.1	-652103.6	-49.7
N,N'-Dibutylthiourea	1,8-Naphthyridine	-3362880.7	-2265058.1	-1097747.9	-71.4
N,N'-Dibutylthiourea	1,10-Phenanthroline	-3766459.6	-2265058.1	-1501321.1	-81.7
N,N'-Dibutylthiourea	1,2-Pyrazine	-2959224.2	-2265058.1	-694105.3	-57.4
N,N'-Dibutylthiourea	TEA	-3033178.8	-2265058.1	-768060.8	-63.5
N,N'-Dibutylthiourea	TMEDA	-3178505.9	-2265058.1	-913365.3	-89.6
N,N'-Dibutylthiourea	1,4,7-Triazacyclononane	-3320695.2	-2265058.1	-1055502.6	-89.4

B.7 Correlations of computational and experimental energies

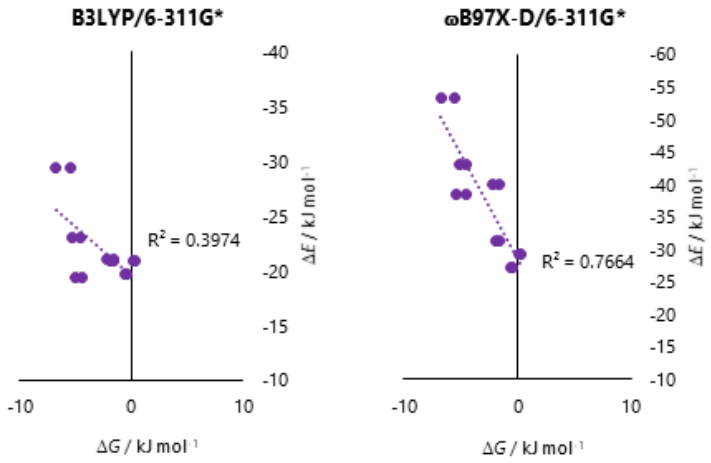

B.7.1 Plots of experimental against computational energies for C6F5I (G1) complexes

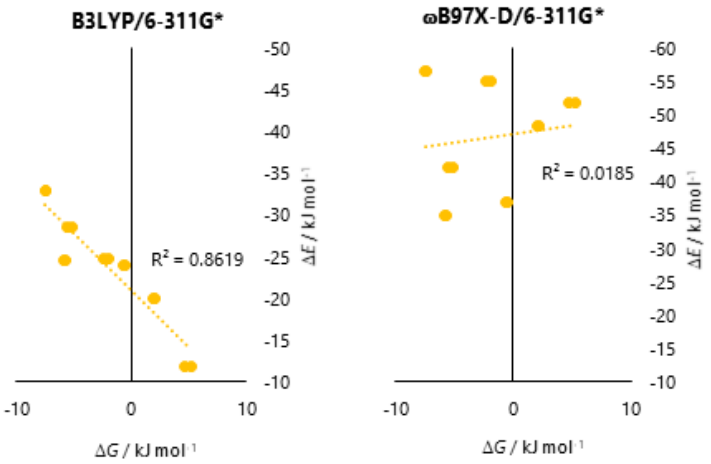

B.7.2 Plots of experimental against computational energies for Butylacetamide (G2) complexes

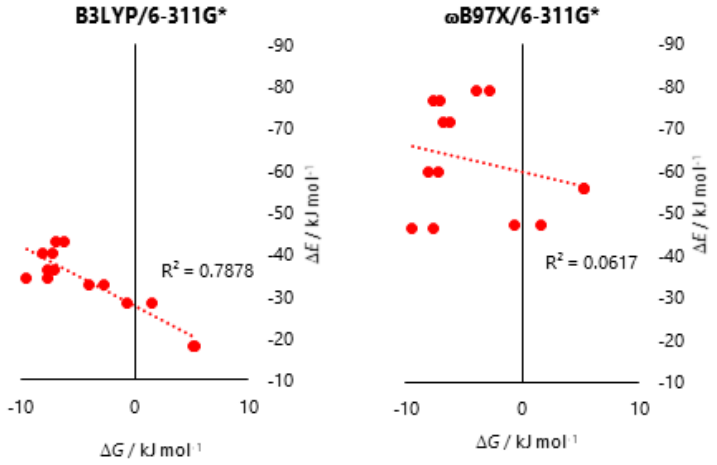

B.7.3 Plots of experimental against computational energies for *N*,*N*'-Dibutylurea (G3) complexes.

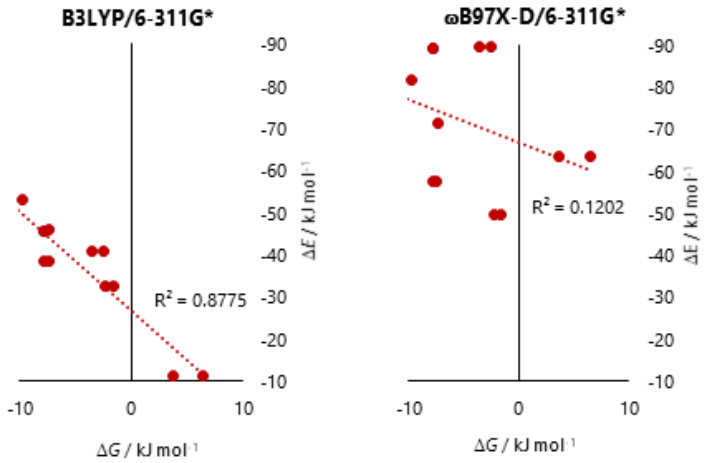

B.7.3 Plots of experimental against computational energies for *N*,*N*'-Dibutylthiourea (G4) complexes.

B.8 Tabulated SAPT2 terms (B3LYP/6-311G* minimised geometries)

Bond Donor	Bond Acceptor	Electrostatic (kJ/mol)	Exchange (kJ/mol)	Induction (kJ/mol)	Dispersion (kJ/mol)	SAPT2 Total (kJ/mol)
C_6F_5I	Pyridine	-76.6	91.6	-27.3	-20.5	-32.8
C_6F_5I	1,8-Naphthyridine	-60.7	71.1	-23.8	-20.6	-34.1
C_6F_5I	1,10-Phenanthroline	-59.2	65.5	-22.2	-24.4	-40.3
C_6F_5I	1,2-Pyrazine	-65.2	75.7	-23.2	-18.3	-31.1
C_6F_5I	TEA	-94.4	114.8	-30.4	-31.2	-41.1

C_6F_5I	TMEDA	-80.9	99.5	-27.1	-31.8	-40.3
C_6F_5I	1,4,7-Triazacyclononane	-89.1	101.3	-31.4	-31.1	-50.4
N-Butylacetamide	Pyridine	-46.9	42.6	-13.4	-14.2	-32.0
N-Butylacetamide	1,8-Naphthyridine	-46.6	37.6	-13.9	-15.6	-38.4
N-Butylacetamide	1,10-Phenanthroline	-52.0	38.1	-14.4	-21.2	-49.6
N-Butylacetamide	1,2-Pyrazine	-43.7	36.3	-12.3	-12.2	-31.9
N-Butylacetamide	TEA	-37.0	40.2	-9.9	-22.9	-29.6
N-Butylacetamide	TMEDA	-50.4	50.8	-14.3	-25.6	-39.5
N-Butylacetamide	1,4,7-Triazacyclononane	-56.3	54.9	-16.4	-21.9	-39.6
N,N'-Dibutylurea	Pyridine	-51.7	42.6	-12.8	-17.3	-39.1
N,N'-Dibutylurea	1,8-Naphthyridine	-67.5	55.8	-20.4	-21.7	-53.8
N,N'-Dibutylurea	1,10-Phenanthroline	-69.8	54.9	-20.4	-26.3	-61.5
N,N'-Dibutylurea	1,2-Pyrazine	-59.1	48.6	-16.6	-17.1	-44.2
N,N'-Dibutylurea	TEA	-49.2	51.1	-14.4	-24.1	-36.7
N,N'-Dibutylurea	TMEDA	-79.7	79.6	-23.7	-34.7	-58.4
N,N'-Dibutylurea	1,4,7-Triazacyclononane	-91.3	93.5	-27.2	-32.2	-57.2
N,N'-Dibutylthiourea	Pyridine	-58.2	48.5	-15.8	-19.8	-45.3
N,N'-Dibutylthiourea	1,8-Naphthyridine	-75.7	62.9	-24.0	-26.5	-63.3
N,N'-Dibutylthiourea	1,10-Phenanthroline	-81.7	62.1	-25.5	-28.9	-74.0
N,N'-Dibutylthiourea	1,2-Pyrazine	-67.7	57.0	-20.5	-22.1	-53.3
N,N'-Dibutylthiourea	TEA	-33.5	33.8	-7.5	-26.8	-34.0
N,N'-Dibutylthiourea	TMEDA	-88.0	84.5	-27.8	-36.0	-67.4
N,N'-Dibutylthiourea	1,4,7-Triazacyclononane	-102.8	101.2	-32.6	-35.7	-70.0

B.9 Full graphical presentation of hydrogen bonded SAPT2 terms

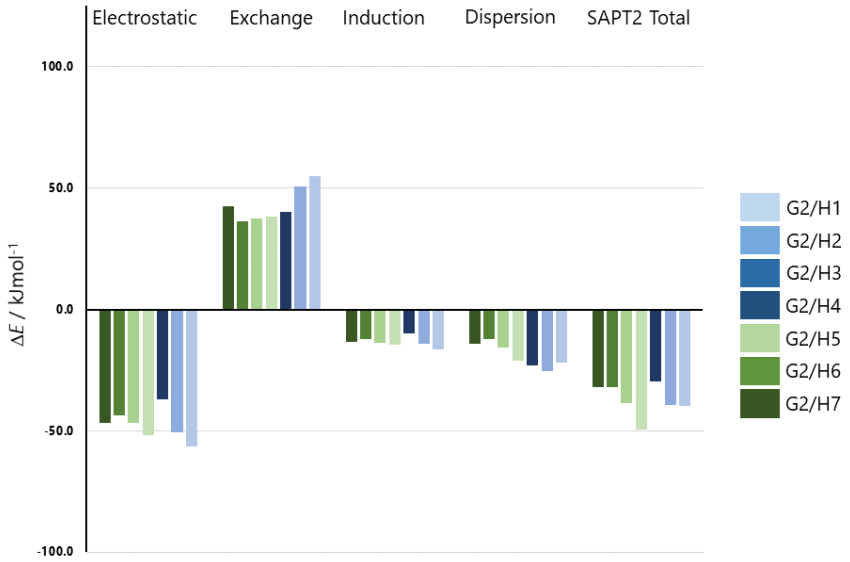

B.9.1 Energetic terms of SAPT2 data for *N*-Butylacetamide (G2) host guest complexes based on B3LYP/6-311G* minimised geometries.

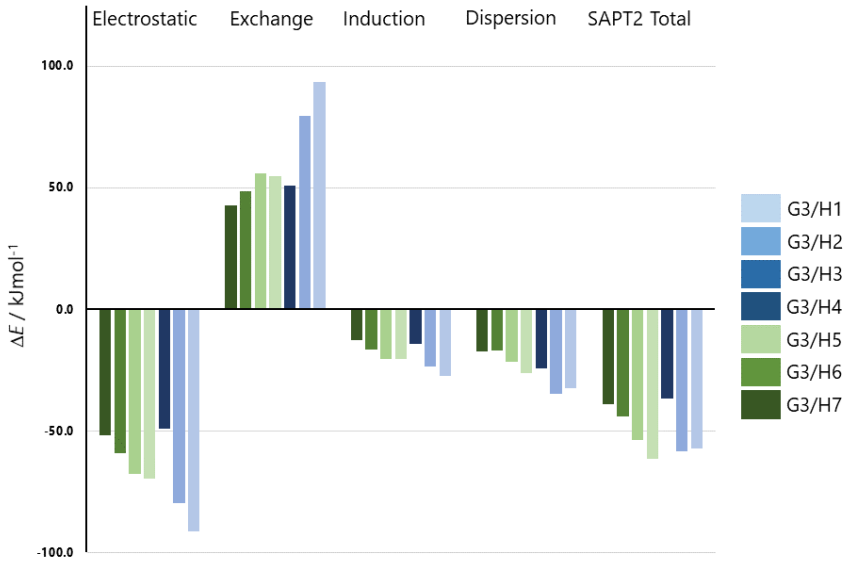

B.9.2 Energetic terms of SAPT2 data for *N,N'*-Dibutylurea (G3) host guest complexes based on B3LYP/6-311G* minimised geometries.

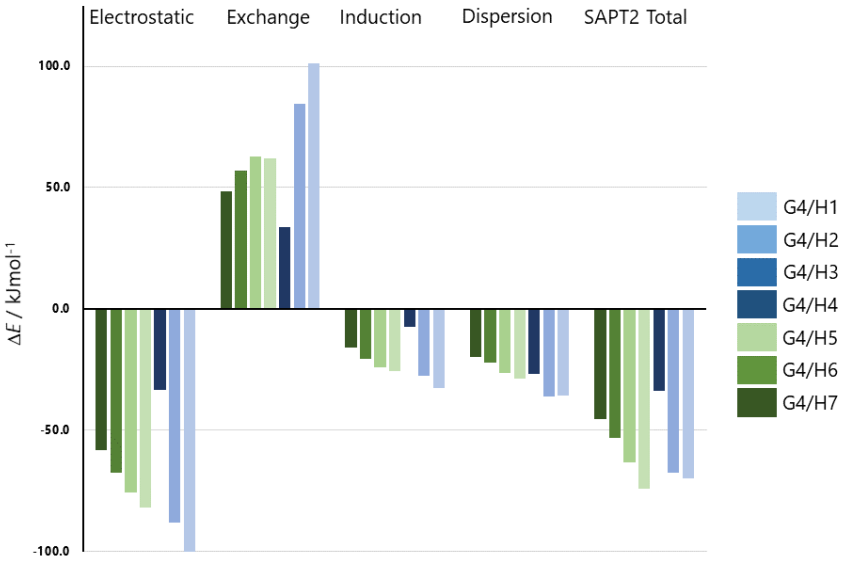

B.9.1 Energetic terms of SAPT2 data for *N,N'*-Dibutylthiourea (G4) host guest complexes based on B3LYP/6-311G* minimised geometries.

B.10 Tabulated SAPT2 terms (ωB97X-D/6-311G* minimised geometries)

Bond Donor	Bond Acceptor	Electrostatic (kJ/mol)	Exchange (kJ/mol)	Induction (kJ/mol)	Dispersion (kJ/mol)	SAPT2 Total (kJ/mol)
C_6F_5I	Pyridine	-71.6	84.6	-24.9	-19.6	-31.4
C_6F_5I	1,8-Naphthyridine	-62.3	74.4	-24.5	-21.3	-33.7
C_6F_5I	1,10-Phenanthroline	-62.9	72.0	-23.6	-25.7	-40.3
C_6F_5I	1,2-Pyrazine	-62.8	72.4	-21.7	-17.8	-29.9
C_6F_5I	TEA	-101.2	126.0	-32.4	-32.9	-40.5
C_6F_5I	TMEDA	-87.4	111.8	-28.7	-35.0	-39.3
C_6F_5I	1,4,7-Triazacyclononane	-94.6	111.5	-33.4	-33.5	-50.0
N-Butylacetamide	Pyridine	-52.9	58.5	-14.7	-20.6	-29.7
N-Butylacetamide	1,8-Naphthyridine	-56.1	58.9	-16.2	-21.9	-35.3
N-Butylacetamide	1,10-Phenanthroline	-66.0	69.8	-20.0	-32.6	-48.9
N-Butylacetamide	1,2-Pyrazine	-50.3	51.1	-14.7	-16.9	-30.8

N-Butylacetamide	TEA	-66.1	96.3	-19.0	-39.4	-28.3
N-Butylacetamide	TMEDA	-61.3	96.6	-17.3	-41.5	-23.5
N-Butylacetamide	1,4,7-Triazacyclononane	-71.9	90.0	-21.2	-34.2	-37.4
N,N'-Dibutylurea	Pyridine	-60.3	66.8	-14.7	-28.8	-37.1
N,N'-Dibutylurea	1,8-Naphthyridine	-79.1	85.3	-24.4	-32.4	-50.7
N,N'-Dibutylurea	1,10-Phenanthroline	-74.0	95.3	-22.3	-56.4	-57.4
N,N'-Dibutylurea	1,2-Pyrazine	-65.4	62.3	-18.9	-20.7	-42.7
N,N'-Dibutylurea	TEA	-64.6	86.1	-17.7	-39.5	-35.7
N,N'-Dibutylurea	TMEDA	-108.5	139.6	-34.3	-51.2	-54.4
N,N'-Dibutylurea	1,4,7-Triazacyclononane	-124.7	152.9	-39.1	-45.7	-56.7
N,N'-Dibutylthiourea	Pyridine	-65.1	61.5	-17.7	-20.8	-42.0
N,N'-Dibutylthiourea	1,8-Naphthyridine	-87.9	82.2	-30.1	-23.8	-59.7
N,N'-Dibutylthiourea	1,10-Phenanthroline	-96.1	92.4	-33.8	-30.8	-68.3
N,N'-Dibutylthiourea	1,2-Pyrazine	-77.0	68.1	-23.9	-18.8	30.5
N,N'-Dibutylthiourea	TEA	-67.8	94.0	-16.3	-46.7	-36.8
N,N'-Dibutylthiourea	TMEDA	-118.9	153.9	-39.2	-58.4	-62.6
N,N'-Dibutylthiourea	1,4,7-Triazacyclononane	-138.2	164.3	-46.2	-49.5	-69.6

B.11 Tabulated SAPT2+(ccd) terms (B3LYP/6-311G* minimised geometries)

Bond Donor	Bond Acceptor	Electrostatic (kJ/mol)	Exchange (kJ/mol)	Induction (kJ/mol)	Dispersion (kJ/mol)	SAPT2+ Total (kJ/mol)
C_6F_5I	Pyridine	-76.6	91.6	-27.3	-18.6	-30.8
C_6F_5I	1,8-Naphthyridine	-60.7	71.1	-23.8	-18.4	-31.8
C_6F_5I	1,10-Phenanthroline	-52.0	38.1	-14.4	-20.2	-48.6
C_6F_5I	1,2-Pyrazine	-59.1	48.6	-16.6	-17.2	-44.3
C_6F_5I	TEA	-94.4	114.8	-30.4	-28.8	-38.7
C_6F_5I	TMEDA	-50.4	50.8	-14.3	-26.0	-39.9
C_6F_5I	1,4,7-Triazacyclononane	-89.1	101.3	-31.4	-28.5	-47.8
N-Butylacetamide	Pyridine	-46.9	42.6	-13.4	-14.3	-32.0
N-Butylacetamide	1,8-Naphthyridine	-46.6	37.6	-13.9	-15.2	-38.1
N-Butylacetamide	1,10-Phenanthroline	-52.0	38.1	-14.4	-20.2	-48.6
N-Butylacetamide	1,2-Pyrazine	-43.7	36.3	-12.3	-12.1	-31.8

N-Butylacetamide	TEA	-37.0	40.2	-9.9	-23.3	-30.0
N-Butylacetamide	TMEDA	-50.4	50.8	-14.3	-26.0	-39.9
N-Butylacetamide	1,4,7-Triazacyclononane	-56.3	54.9	-16.4	-22.7	-40.5
N,N'-Dibutylurea	Pyridine	-51.7	42.6	-12.8	-17.2	-39.0
N,N'-Dibutylurea	1,8-Naphthyridine	-67.5	55.8	-20.4	-21.9	-54.0
N,N'-Dibutylurea	1,10-Phenanthroline	-	-	-	-	-
N,N'-Dibutylurea	1,2-Pyrazine	-59.1	48.6	-16.6	-17.2	-44.3
N,N'-Dibutylurea	TEA	-49.2	51.1	-14.4	-24.7	-37.3
N,N'-Dibutylurea	TMEDA	-79.7	79.6	-23.7	-35.3	-59.0
N,N'-Dibutylurea	1,4,7-Triazacyclononane	-91.3	93.5	-27.2	-33.7	-58.7
N,N'-Dibutylthiourea	Pyridine	-58.2	48.5	-15.8	-19.3	-44.8
N,N'-Dibutylthiourea	1,8-Naphthyridine	-51.9	41.6	-16.3	-19.5	-46.1
N,N'-Dibutylthiourea	1,10-Phenanthroline	-	-	-	-	-
N,N'-Dibutylthiourea	1,2-Pyrazine	-67.7	57.0	-20.5	-22.0	-53.2
N,N'-Dibutylthiourea	TEA	-33.5	33.8	-7.5	-27.0	-34.2
N,N'-Dibutylthiourea	TMEDA	-88.0	84.5	-27.8	-36.4	-67.8
N,N'-Dibutylthiourea	1,4,7-Triazacyclononane	-102.8	101.2	-32.6	-36.8	-71.0

B.12 Renderings of NBOs involved in inter-unit donation > 4 kJ mol^{-1}

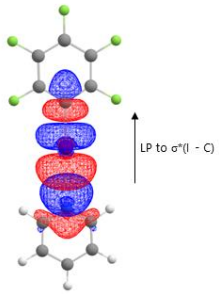

B.12.1 C_6F_5I/Pyridine (G1/H1)

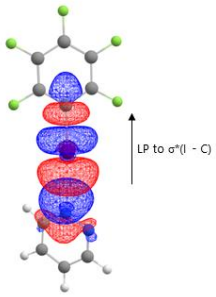

B.12.2 C_6F_5I/1,2-Pyrazine (G1/H2)

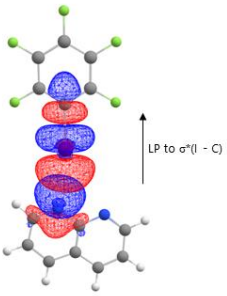

B.12.3 C_6F_5I/1,8-Naphthyridine (G1/H3)

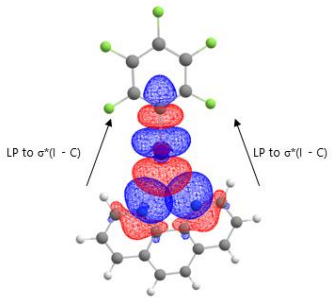

B.12.4 C_6F_5I/1,10-Phenanthroline (G1/H4)

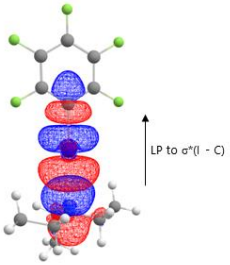

B.12.5 C_6F_5I/TEA (G1/H5)

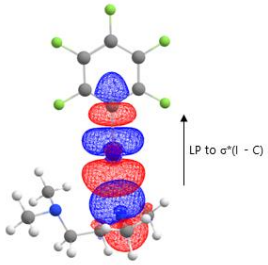

B.12.6 C_6F_5I/TMEDA (G1/H6)

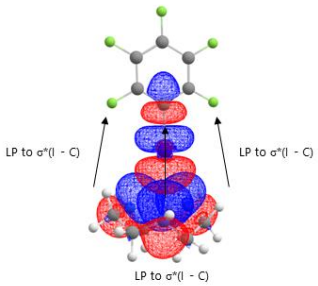

B.12.7 C_6F_5I/1,4,7-Triazacyclononane (G1/H7)

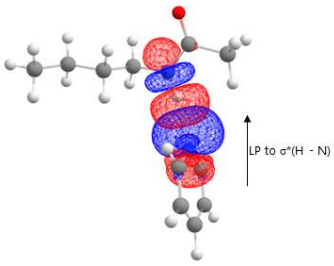

B.12.8 Butylacetamide/Pyridine (G2/H1)

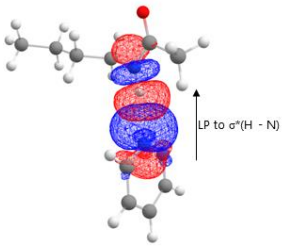

B.12.9 Butylacetamide/1,2-Pyrazine (G2/H2)

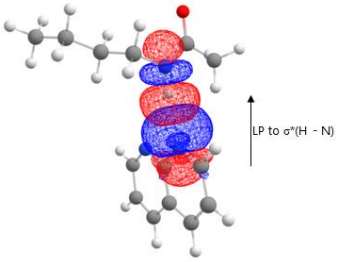

B.12.10 Butylacetamide/1,8-Naphthyridine (G2/H3)

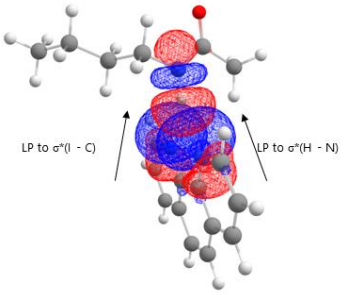

B.12.11 Butylacetamide/1,10-Phenanthroline (G2/H4)

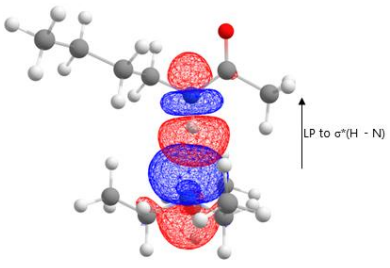

B.12.12 Butylacetamide/TEA (G2/H5)

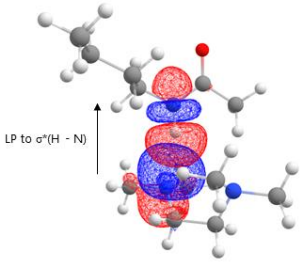

B.12.13 Butylacetamide/TMEDA (G2/H6)

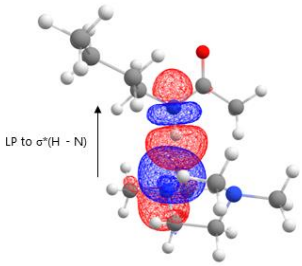

B.12.14 Butylacetamide/1,4,7-Triazacyclononane (G2/H7)

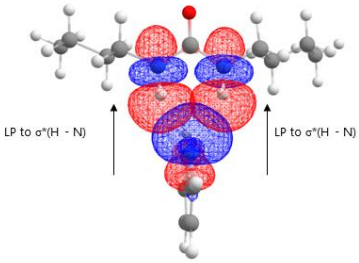

B.12.15 *N,N'*-Dibutylurea/Pyridine (G3/H1)

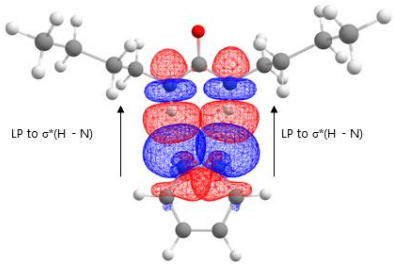

B.12.16 *N,N'*-Dibutylurea/1,2-Pyrazine (G3/H2)

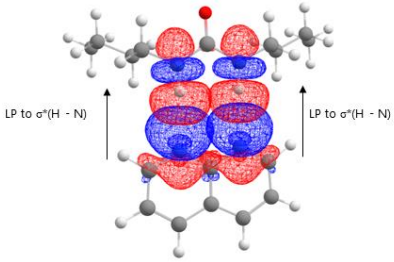

B.12.17 *N,N'*-Dibutylurea/1,8-Naphthyridine (G3/H3)

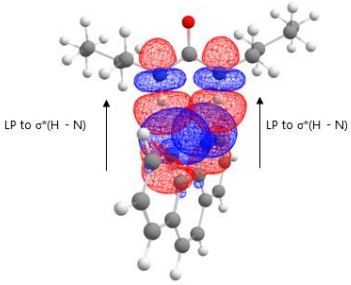

B.12.18 *N,N'*-Dibutylurea/1,10-Phenanthroline (G3/H4)

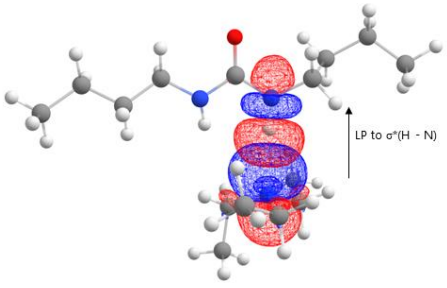

B.12.19 *N,N'*-Dibutylurea/TEA (G3/H5)

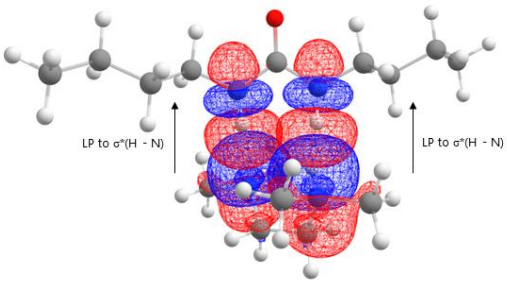

B.12.20 *N,N'*-Dibutylurea/TMEDA (G3/H6)

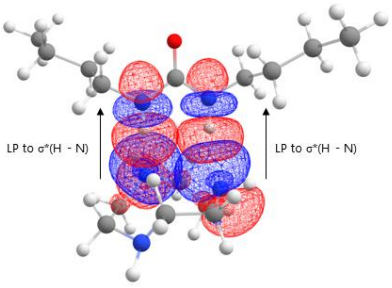

B.12.21 *N,N'*-Dibutylurea/1,4,7-Triazacyclononane (G3/H7)

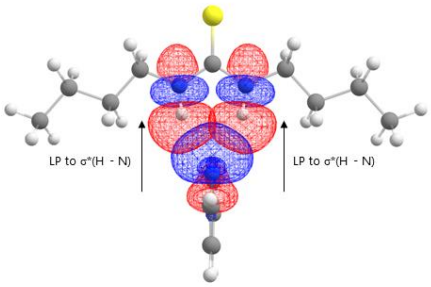

B.12.22 *N,N'*-Dibutylthiourea/Pyridine (G4/H1)

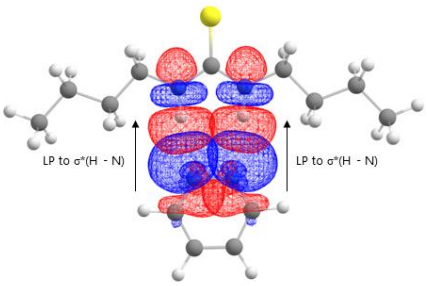

B.12.23 *N,N'*-Dibutylthiourea/1,2-Pyrazine (G4/H2)

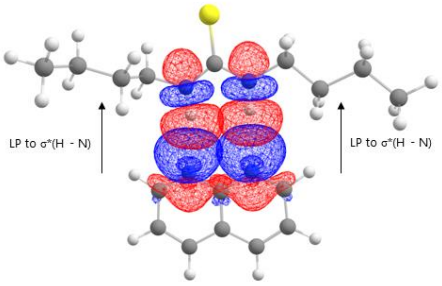

B.12.24 *N,N'*-Dibutylthiourea/1,8-Naphthyridine (G4/H3)

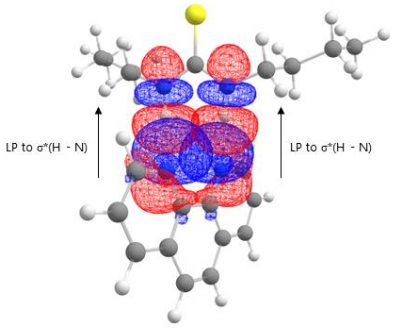

B.12.25 *N,N'*-Dibutylthiourea/1,10-Phenanthroline (G4/H4)

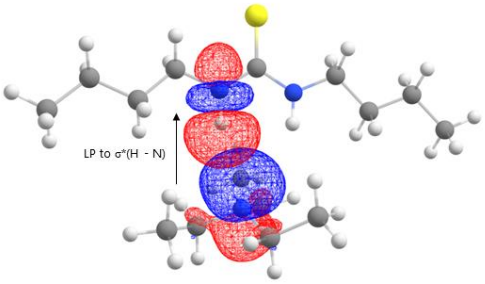

B.12.26 *N,N'*-Dibutylthiourea/TEA (G4/H5)

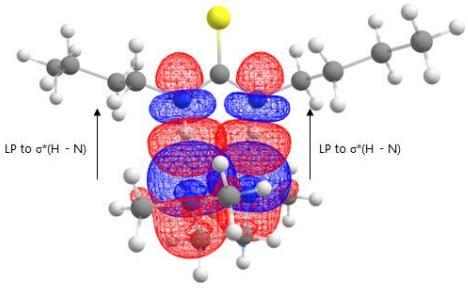

B.12.27 *N,N'*-Dibutylthiourea/TMEDA (G4/H5)

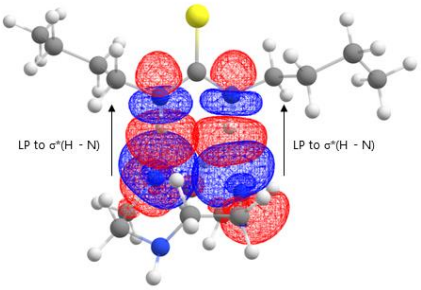

B.12.28 *N,N'*-Dibutylthiourea/1,4,7-Triazacyclononane (G4/H7)

B.13 Tabulated Σ E^2 = >4 kJ/mol (B3LYP/6-311G* minimised geometries)

Bond Donor	Bond Acceptor	Σ NBO > 4 kJ mol^{-1} ($kJ\ mol^{-1}$)
C_6F_5I	Pyridine	39.0
C_6F_5I	1,8-Naphthyridine	31.5
C_6F_5I	1,10-Phenanthroline	25.6
C_6F_5I	1,2-Pyrazine	33.7
C_6F_5I	TEA	38.8
C_6F_5I	TMEDA	30.4
C_6F_5I	1,4,7-Triazacyclononane	29.8
N-Butylacetamide	Pyridine	34.2
N-Butylacetamide	1,8-Naphthyridine	28.0
N-Butylacetamide	1,10-Phenanthroline	37.4
N-Butylacetamide	1,2-Pyrazine	30.3
N-Butylacetamide	TEA	17.1
N-Butylacetamide	TMEDA	25.1
N-Butylacetamide	1,4,7-Triazacyclononane	38.3

N,N'-Dibutylurea	Pyridine	20.3
N,N'-Dibutylurea	1,8-Naphthyridine	42.5
N,N'-Dibutylurea	1,10-Phenanthroline	31.6
N,N'-Dibutylurea	1,2-Pyrazine	38.0
N,N'-Dibutylurea	TEA	28.6
N,N'-Dibutylurea	TMEDA	52.0
N,N'-Dibutylurea	1,4,7-Triazacyclononane	66.2
N,N'-Dibutylthiourea	Pyridine	28.3
N,N'-Dibutylthiourea	1,8-Naphthyridine	47.8
N,N'-Dibutylthiourea	1,10-Phenanthroline	38.5
N,N'-Dibutylthiourea	1,2-Pyrazine	48.6
N,N'-Dibutylthiourea	TEA	5.4
N,N'-Dibutylthiourea	TMEDA	58.2
N,N'-Dibutylthiourea	1,4,7-Triazacyclononane	72.9

B.14 Synthesis of G2

For general synthetic procedure see section A.11.

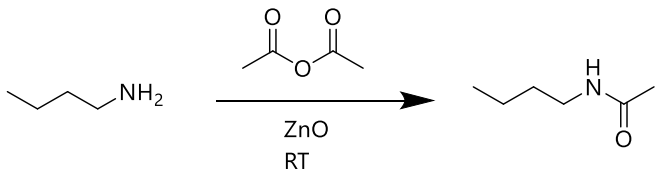

A solution of butylamide (0.1 mol, 1.00 mL) and acetic anhydride (0.1 mol, 0.94 mL) was prepared at room temperature. Zinc oxide (0.005 mol, 0.41 g) was added. Reaction progress was monitored by TLC until completion. Reaction mixture was subsequently diluted with 20 mL of DCM before the reaction mixture was washed with an aqueous bicarbonate solution and dried over anhydrous sodium sulphate. Products were clean by NMR so no further purification was needed (0.87 g, 7.578 mmol, 76 % yield).

^{1}H NMR (500 MHz, $CDCl_3$) δ, 5.47 (bs, 1H), 3.24 (q, 2H, J = 6.9 Hz), 1.96 (s, 3H), 1.47 (m, 2H), 1.34 (m, 2H), 0.92 (t, 3H, J = 7.4 Hz).

^{13}C NMR (126 MHz, $CDCl_3$) δ 170.03, 39.41, 31.68, 23.35, 20.06, 13.73

HRMS (ESI) obtained m/z: 115.09996 Expected: 115.09917

^{1}H NMR

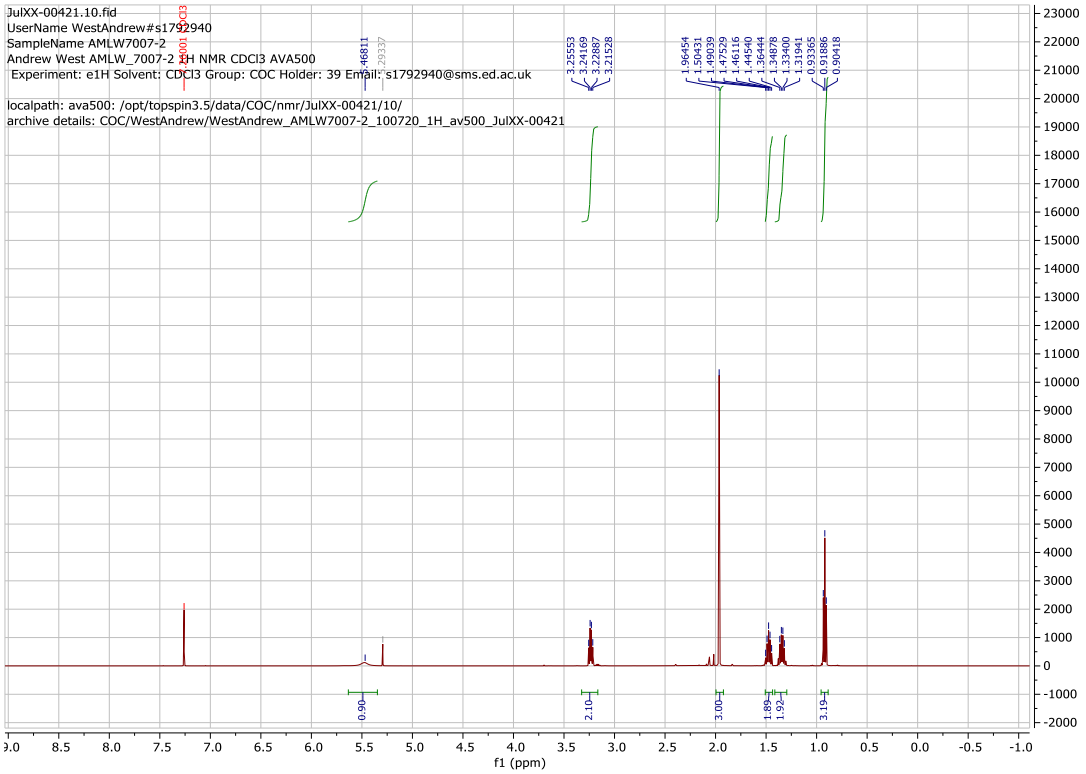

^{13}C NMR

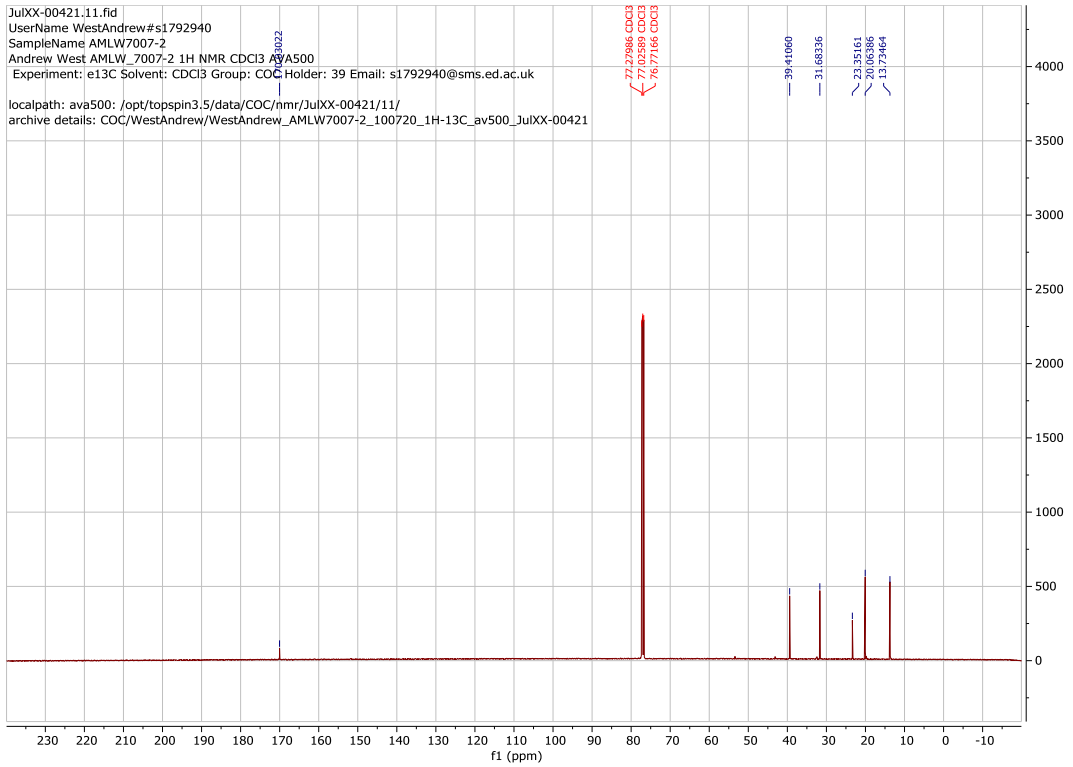

B.15 Alternative G1/H4 geometries

Face to Face

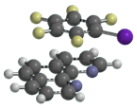

Face to Edge

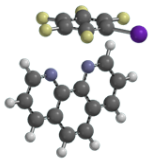

Bond Donor	Bond Acceptor	Complex energy (kJ/mol)	Donor energy (kJ/mol)	Acceptor energy (kJ/mol)	ΔE (kJ/mol)
C6F5I	XB	-21579617.5	-20078514.3	-1501068.2	-35.0
C6F5I	Face to Edge	-21176132.8	-20078514.3	-1097598.6	-19.9
C6F5I	Face to Face	-21176120.8	-20078514.3	-1097598.6	-7.9

B.16 Tabulated B3LYP/6-311G* (BSSE=CP) calculated energies and interaction energies for Syn- and Anti- dibutylthiourea (G4) complexes

Bond Donor	Bond Acceptor	*Syn*-complex Δ*E* (kJ/mol)	*Syn*- apparent bonding mode	*Anti*-complex Δ*E* (kJ/mol)	*Anti*- apparent bonding mode
N,N'-Dibutylthiourea	Pyridine	-32.5	D2•A	-26.0	Single
N,N'-Dibutylthiourea	1,8-Naphthyridine	-45.8	Dual	-25.1	Single
N,N'-Dibutylthiourea	1,10-Phenanthroline	-52.9	Dual	-36.0	Single
N,N'-Dibutylthiourea	1,2-Pyrazine	-38.4	Dual	-25.7	D•A2
N,N'-Dibutylthiourea	TEA	-11.1	Single	-2.4	Single
N,N'-Dibutylthiourea	TMEDA	-40.7	Dual	-12.7	Single
N,N'-Dibutylthiourea	1,4,7-Triazacyclononane	-45.6	Dual	-22.4	Single

B.17 Hydrogen bond donor guest species dimerization

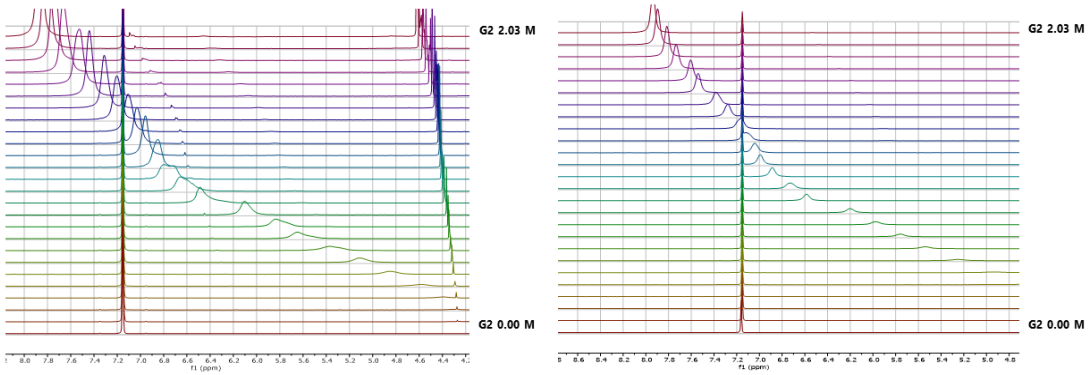

B.17.1 Stacked spectra for G2 titrations; left G2 alone (dimerization); right G2/H1 titration

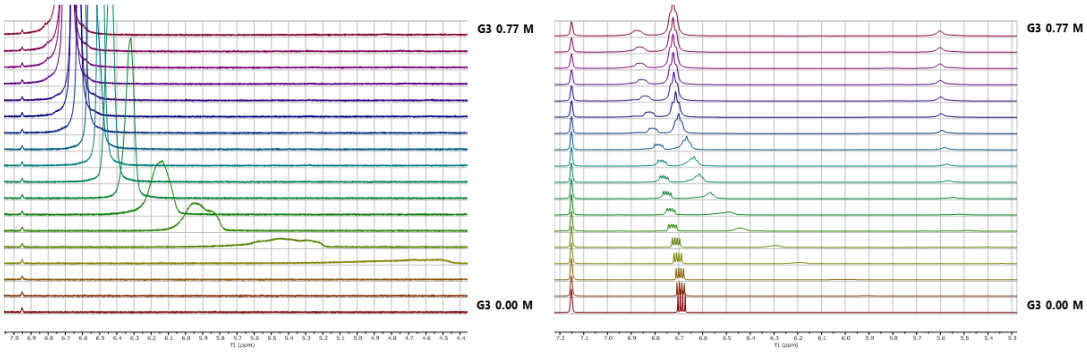

B.17.2 Stacked spectra for G3 titrations; left, G3 alone (dimerization); right, G3/H1 titration.

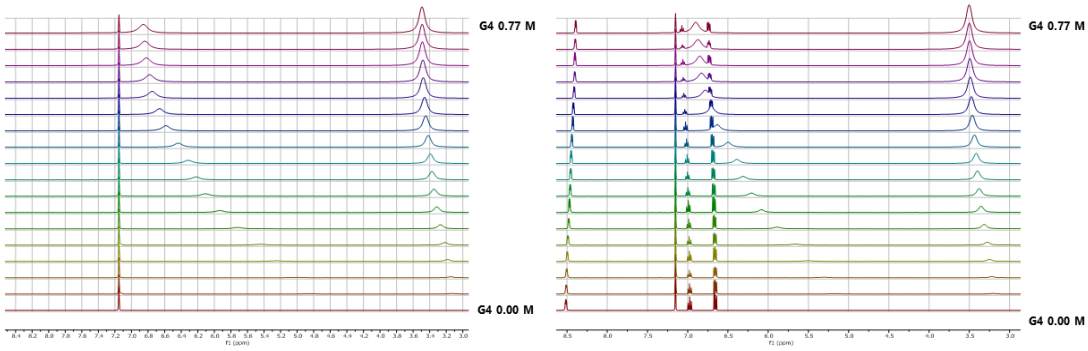

B.17.3 Stacked spectra for G4 titrations; left, G4 alone (dimerization); right, G4/H1 titration.

B.18 Dispersion corrected minimized geometries (ωB97X-D/6-311G*)

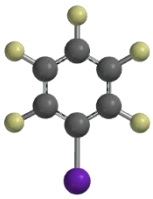

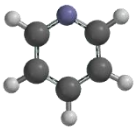

B.18.1 C_6F_5I/Pyridine (G1/H1)

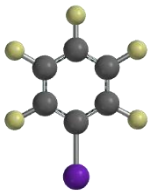

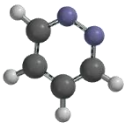

B.18.2 C_6F_5I/1,2-Pyrazine (G1/H2)

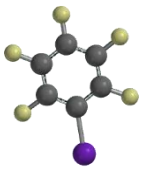

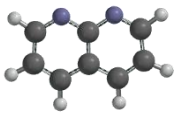

B.18.3 C_6F_5I/1,8-Naphthyridine (G1/H3)

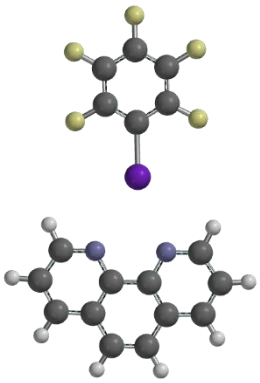

B.18.4 C_6F_5I/1,10-Phenanthroline (G1/H4)

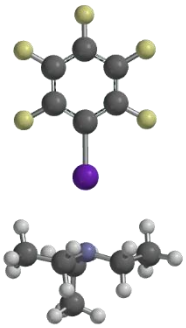

B.18.5 C_6F_5I/TEA (G1/H5)

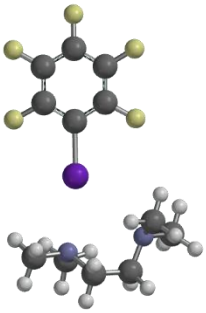

B.18.6 C_6F_5I/TMEDA (G1/H6)

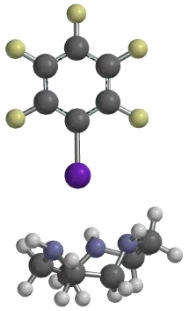

B.18.7 C_6F_5I/1,4,7-Triazacyclononane (G1/H7)

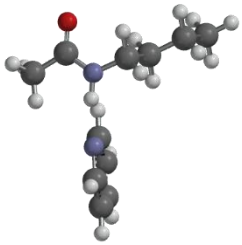

B.18.8 Butylacetamide/Pyridine (G2/H1)

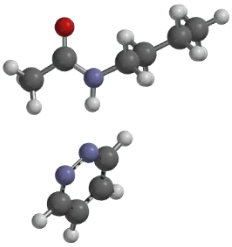

B.18.9 Butylacetamide/1,2-Pyrazine (G2/H2)

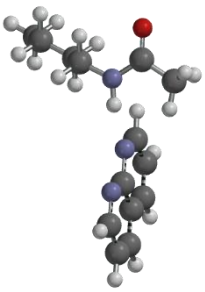

B.18.10 Butylacetamide/1,8-Naphthyridine (G2/H3)

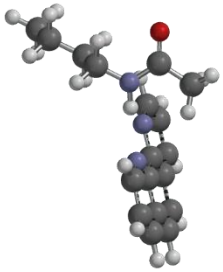

B.18.11 Butylacetamide/1,10-Phenanthroline (G2/H4)

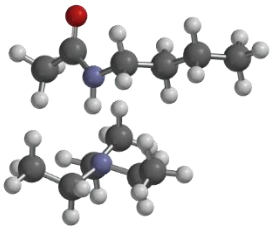

B.18.12 Butylacetamide/TEA (G2/H5)

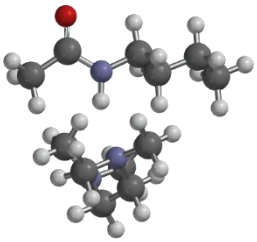

B.18.13 Butylacetamide/TMEDA (G2/H6)

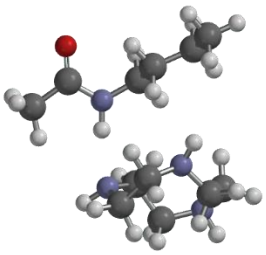

B.18.14 Butylacetamide/1,4,7-Triazacyclononane (G2/H7)

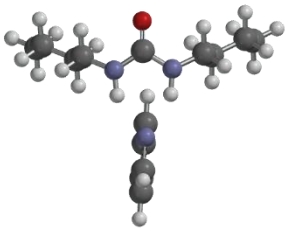

B.18.15 *N,N'*-Dibutylurea/Pyridine (G3/H1)

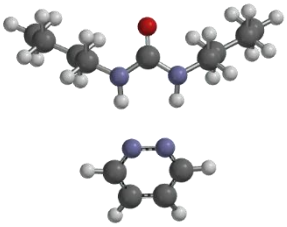

B.18.16 *N,N'*-Dibutylurea/1,2-Pyrazine (G3/H2)

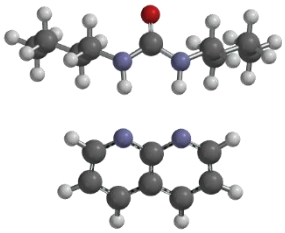

B.18.17 *N,N'*-Dibutylurea/1,8-Naphthyridine (G3/H3)

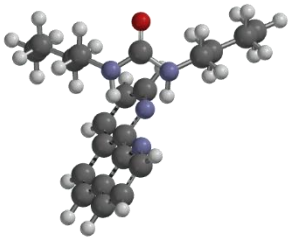

B.18.18 *N,N'*-Dibutylurea/1,10-Phenanthroline (G3/H4)

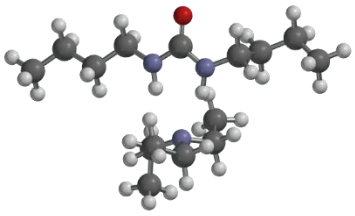

B.18.19 *N,N'*-Dibutylurea/TEA (G3/H5)

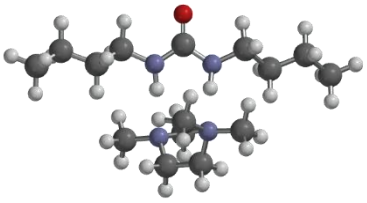

B.18.20 *N,N'*-Dibutylurea/TMEDA (G3/H6)

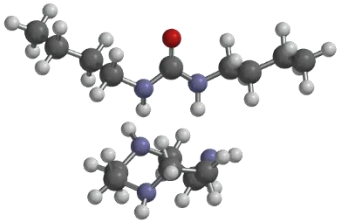

B.18.21 *N,N'*-Dibutylurea/1,4,7-Triazacyclononane (G3/H7)

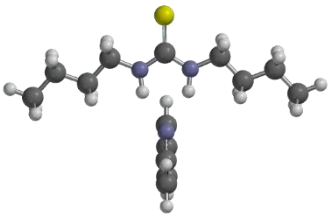

B.18.22 *N,N'*-Dibutylthiourea/Pyridine (G4/H1)

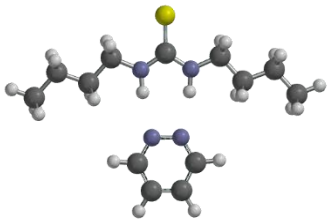

B.18.23 *N,N'*-Dibutylthiourea/1,2-Pyrazine (G4/H2)

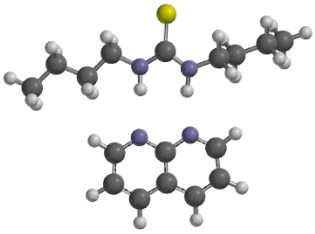

B.18.24 *N,N'*-Dibutylthiourea/1,8-Naphthyridine (G4/H3)

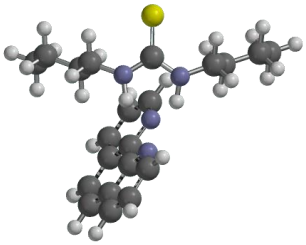

B.18.25 *N,N'*-Dibutylthiourea/1,10-Phenanthroline (G4/H4)

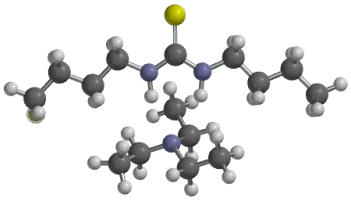

B.18.26 *N,N'*-Dibutylthiourea/TEA (G4/H5)

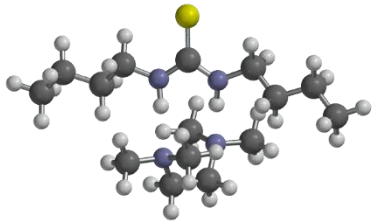

B.18.27 *N,N'*-Dibutylthiourea/TMEDA (G4/H5)

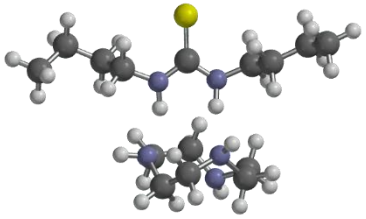

B.18.28 *N,N'*-Dibutylthiourea/1,4,7-Triazacyclononane (G4/H7)